Development and Mechanistic Investigation of Chimeric Molecules for the Degradation of Intra- and Extracellular Proteins

By

Yaxian Zhou

A dissertation submitted in partial fulfillment of the requirements for the degree of

Doctor of Philosophy

(Pharmaceutical Sciences)

at the

UNIVERSITY OF WISCONSIN–MADISON

2024

Date of final oral examination: 12/05/2024

The dissertation is approved by the following members of the Final Oral Committee:

Weiping Tang, Professor, Pharmaceutical Sciences

Cody James Wenthur, Associate Professor, Pharmaceutical Sciences

Qquanyin Hu, Assistant Professor, Pharmaceutical Sciences

Deric L Wheeler, Professor, Human Oncology

Development and Mechanistic Investigation of Chimeric Molecules for the Degradation of Intra- and Extracellular Proteins

Abstract

Targeted protein degradation (TPD) has rapidly emerged as a transformative therapeutic modality and a powerful tool for selectively depleting various protein targets. Proteolysis Targeting Chimeras (PROTACs) are the most advanced, with dozens of PROTAC molecules currently in clinical trials. However, traditional PROTAC synthesis methods are stepwise, time-consuming, and unsuitable for high-throughput screening. In this thesis, we introduce Rapid-TAC, a rapid synthesis platform employing a traceless OPA-amine coupling reaction to enables high-throughput synthesis of PROTACs for direct screening without requiring additional purification steps. Using Rapid-TAC platform, we successfully identified PROTACs targeting the androgen receptor (AR) and bromodomain-containing protein 4 (BRD4), demonstrating the feasibility and efficiency of this platform.

Complementing PROTACs, Lysosome Targeting Chimeras (LYTACs) expand TPD to include extracellular secreted and membrane-bound proteins. The first LYTACs, which recruit cation-independent mannose-6-phosphate receptors (CI-M6PR), can induce protein degradation across various tissues due to CI-M6PR's ubiquitous expression. However, this widespread expression raises concerns about on-target/off-tissue toxicity. Additionally, the complex synthesis and high multivalency required for CI-M6PR ligands have hindered their broader application. To address these limitations, we developed

structurally well-defined M6Pn-peptide ligands with a simplified synthesis process and demonstrated its ability to mediate internalization of soluble proteins and degradation of membrane proteins. To minimize on-target/off-tissue toxicity, we developed triantennary *N*-acetylgalactosamine (tri-GalNAc)-attached conjugates that interact with asialoglycoprotein receptor (ASGPR) for selective degradation of target proteins in liver cells. To broaden the scope of TPD for cancer-related targets, we developed two novel platforms: integrin-targeting chimeras (ITACs) and Folate Receptor Targeting Chimeras (FRTACs). These platforms leverage cancer-overexpressing receptors, integrin and folate receptor (FR), respectively, to specifically induce protein degradation in cancer cells. Notably, FRTACs targeting PD-L1 exhibit significant anti-tumor effects by promoting the infiltration of cytotoxic T cells into tumors. Lastly, we explored the potential of developing catalytic degraders using transferrin and its receptor, transferrin receptor (TfR). This innovative approach demonstrated the feasibility of recycling degraders to enhance catalytic efficiency. In summary, this thesis presents advancements in TPD through innovative platforms that improve the selectivity, efficiency, and therapeutic potential of TPD strategies.

Table of Contents

Table of Figures

Acknowledgements

This thesis represents the culmination of years of study and research, made possibly by the support and encouragement of many people who have helped me along the way.

I would like to extend my heartfelt gratitude to my advisor, Prof. Weiping Tang, for his support and guidance throughout my doctoral journey. His insightful mentorship and deep expertise have been instrumental in shaping my research, from tackling complex scientific questions to developing innovative approaches. Through his encouragement, I have grown into a more independent and confident researcher, equipped with the skills to navigate challenges and contribute meaningfully to our field. I am incredibly grateful for the countless hours he devoted to discussions, reviews, and encouragement.

I am also deeply indebted to my thesis committee members, Prof. Cody Wenthur, Prof. Quanyin Hu, and Prof. Deric Wheeler, for their insightful feedback, constructive criticism, and encouragement. Their guidance challenged me to think critically and enriched this research in ways I could not have achieved on my own. I truly appreciate the time and effort they invested in helping me succeed in this endeavor.

I would like to extend my sincere appreciation to my current and previous lab members, whose friendship and expertise have deeply enriched my journey. They are not only exceptional biologists and chemists but also generous colleagues who provided invaluable insights and suggestions from both disciplines, allowing me to approach my work from new perspectives. I am especially grateful to Dr. Jin Liu, Dr. Ka Yang, and Dr. Haibo Xie for their mentorship when I first joined the lab, helping me navigate the early stages of my research. I would also like to thank Dr. Peng Teng, Dr. Le Guo, Dr.

Christopher Stevens, Dr. Yu Zhao, and Dr. Deqin Cai for synthesizing all the compounds used in my studies. A special thanks goes to Dr. Chunrong Li for conducting the in vivo studies, which were essential to my research, and to Dr. Xiaolei Li, Wenxin Wu, Penghsuan Huang for performing numerous MALDI-MASS analyses. I also appreciate the efforts of Yuan Zhao, Yaxian Liao, and Xuankun Chen, who generously contributed their time and skills to support data collection for my work.

I also want to express my appreciation for my previous advisors, Dr. Wan-Ju Li, Dr. Anil K. Ghosh, and Dr. Leslie S. Itsara. Their mentorship provided a solid foundation for my journey in scientific research, equipping me with essential skills and confidence. Their early encouragement and support not only shaped my abilities but also ignited my passion for scientific inquiry, which continues to inspire me throughout my career.

Finally, to my family—thank you for your endless patience, love, and understanding. To my parents, who instilled in me the values of hard work and perseverance; to my husband, Jifan Gao, whose support has been my anchor throughout this process; and to my son, Benyu Gao, for being my source of joy and motivation. Your belief in me has been my greatest strength, and I am grateful beyond words for the sacrifices you have made to help me reach this milestone.

Chapter 1

Introduction

1.1. Inhibition vs Targeted protein degradation

Traditional therapeutic drugs based on occupancy-driven pharmacology predominantly exert their effects by inhibiting active sites to modulate the activity of target proteins, which primarily include enzymes, receptors, and ion channels. However, many important targets, such as non-enzymatic proteins, scaffolding proteins, and transcription factors, lack accessible functional binding pockets for conventional inhibitors, which results in a category of proteins referred to as “undruggable” targets[1]. Currently, it is estimated that approximately 85% of the human proteome remains undruggable, leaving a significant gap in effective therapeutics for disease-relevant proteins within this category[2]. Some druggable proteins exhibit multiple functions. However, traditional drugs primarily inhibit enzymatic activities without influencing non-enzymatic roles, such as scaffolding. Furthermore, in cases where druggable proteins possess multiple active sites, conventional inhibitors often engage with only one active domain, leaving other functional domains unaffected. Traditional drugs require high dosage to maintain sufficient inhibition, which may lead to off-target toxicity. Moreover, prolonged exposure may result in mutations or overexpression of targets, which can diminish the inhibitory efficacy and ultimately contribute to drug resistance[3,4].

Targeted protein degradation (TPD), an emerging strategy within event-driven pharmacology, represents a novel therapeutic modality. It relies on the application of bifunctional molecules to capture and selectively remove proteins of interest (POIs) by exploiting cells’ own degradation machinery[5]. The chimeric molecules for TPD require only a binder of the target, which enables the depletion of targets that are inaccessible to the traditional therapeutic drugs. Another advantage of TPD is its ability to remove

entire proteins, thereby abolishing all their functions, providing a more sustained reduction in downstream signaling and prolonging the duration of the therapeutic response[6]. Moreover, degraders have the potential to overcome drug resistance caused by mutations or upregulation of target proteins[7]. Over the past decade, various platforms have been developed for degrading POIs, including proteolysis-targeting chimeras (PROTACs)[8], molecular glues[9], specific and nongenetic IAP-dependent protein erasers (SNIPERs)[10], degradation tags (dTAGs)[11], autophagy-targeting chimeras (AUTACs)[12], and autophagosome-tethering compounds (ATTECs)[13]. However, many therapeutic targets are secreted proteins or transmembrane proteins that lack cytosolic binding domains, which cannot be targeted by these platforms. To address this limitation, the recent development of Lysosomal Targeting Chimeras (LYTACs) has expanded the scope of TPD to include extracellular proteins, which constitute approximately 40% of the proteome[14]. Following this advancement, several additional platforms have emerged, such as antibody-based PROTACs (AbTACs)[15], proteolysis-targeting antibodies (PROTABs)[16], and GlueBody Chimeras (GlueTACs)[17], all built upon the principles established by LYTACs. TPD strategies fundamentally leverage the cell's intrinsic degradation pathways, specifically the ubiquitin-proteasome system (UPS) and the lysosomal degradation pathway, to effectively eliminate pathogenic or unwanted proteins. In TPD, small molecules or engineered antibodies/proteins play a crucial role in directing target proteins to these degradation mechanisms. This is typically achieved by marking the proteins for destruction, either through the recruitment of endogenous E3 ubiquitin ligases for proteasome-mediated degradation or through the use of lysosome-targeting molecules to facilitate lysosomal

degradation. By harnessing these natural pathways, TPD strategies offer a promising approach for the selective removal of detrimental proteins, paving the way for novel therapeutic interventions (Fig. 1.1).

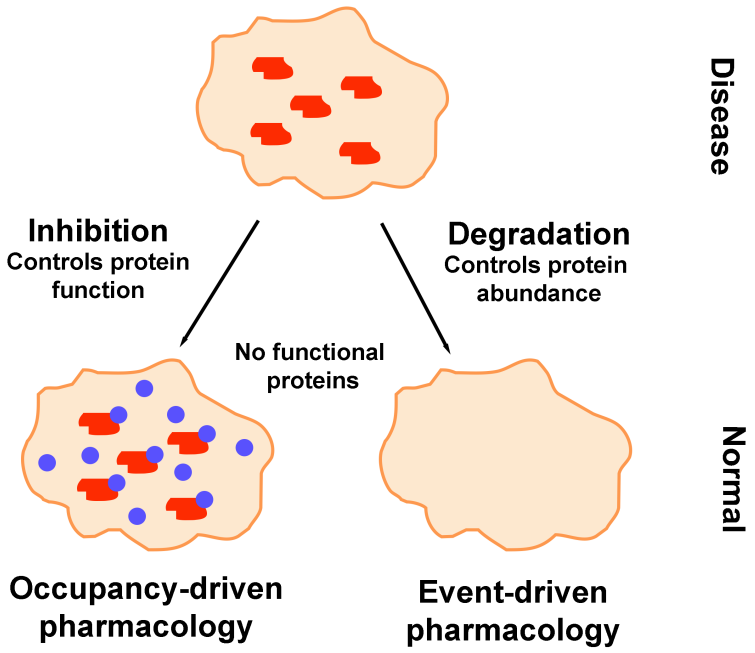

Figure 1.1. Occupancy-and event-driven pharmacology models.

1.2. Mechanisms of naturally occurring protein degradation pathways

1.2.1. Ubiquitin-proteasome system (UPS)

The ubiquitin-proteasome system (UPS) is a highly conserved and fundamental pathway responsible for the regulated degradation of intracellular proteins, which plays a critical role in protein quality control and protein homeostasis maintenance. By targeting a wide array of short-lived proteins, such as cell cycle regulators, misfolded proteins, and mutated proteins, the UPS controls multiple essential cellular functions. These functions include cell signaling, apoptosis, protein processing, immune response, and DNA repair[18].

UPS mediates protein degradation through two main steps: ubiquitination and proteasomal degradation. Ubiquitination is a tightly regulated process, which occurs via a cascade of three enzymatic steps in an ATP-dependent manner. First, ubiquitin-activating enzyme (E1) uses ATP energy to activate ubiquitin, a conserved protein with 76 amino acids, by forming the thioester bond between the C-terminal glycine residue of ubiquitin and the cysteine at the active site of E1. This activation allows the transfer of ubiquitin from E1 to the cysteine at the active site of ubiquitin-conjugating enzyme (E2) sequentially. Lastly, ubiquitin ligases (E3) catalyze the transfer of ubiquitin from E2 to the lysine residues on the protein substrates through different mechanisms, depending on the types of E3 ligases[18,19]. Really interesting new gene (RING) E3s function by bringing protein substrates into close proximity to E2 in order to directly transfer ubiquitin from E2 to the substrate, while homologous to E6-AP C terminus (HECT) E3s form a thioester intermediate with ubiquitin before transferring to protein substrates[20,21]. RING-between-RING (RBR) E3s use a sequential mechanism, wherein the first RING domain binds to the E2, which enable the ubiquitin being transferred to the second RING domain before attachment to the substrate[22]. Human genome encodes two E1s, around 40 E2s, and more than 600 E3s[23]. The substrate specificity is largely determined by E3 ligases, which identify specific motifs in the protein substrates, known as degron[24]. Individual protein substrates may be targeted by multiple E3 ligases, and conversely, a single E3 ligase may regulate the degradation of numerous protein substrates. E3 ligases can recognize degrons in the native state of the substrate or following post-translational modifications (PTMs) of either the substrate or the E3 ligase

itself. These modifications often modulate degron exposure or formation, allowing for precise control over protein turnover[25,26].

Once the first ubiquitin is attached to the protein substrate, additional activated ubiquitin is successively conjugated to the previously attached ubiquitin to generate the polyubiquitin chain on the protein substrates. Ubiquitin contains seven lysine residues (K6, K11, K27, K29, K33, K48, and K63), which facilitate the elongation of the ubiquitin chain, a process catalyzed by E3 ligases. Among these, K48-linked polyubiquitin chains are the most abundant and serve as the canonical signal for protein degradation via the 26S proteasome[27]. The 26S proteasome consists of two distinct subcomplexes: the 19S regulatory particle (RP), which is responsible for the recognition, unfolding, and translocation of polyubiquitin-tagged protein substrates, and the 20S core particle (CP), which is responsible for proteolysis[28]. Specifically, the conjugated polyubiquitin chains bind to the ubiquitin receptors on the 19S RP, which leads to the removal of ubiquitin chains by deubiquitinating enzymes (DUBs). The protein substrates are further unfolded by the ATPase subunits of the 19S RP, which use ATP hydrolysis to linearize the protein to translocate the substrates into the 20S CP. Once inside the 20S CP, the substrate is cleaved by the proteolytic active sites into small peptide fragments, which are subsequently degraded into individual amino acids by cytosolic peptidases. Detached ubiquitin molecules and amino acids are recycled and reused to maintain efficient and sustained protein homeostasis within the cell[29-31] (Fig. 1.2).

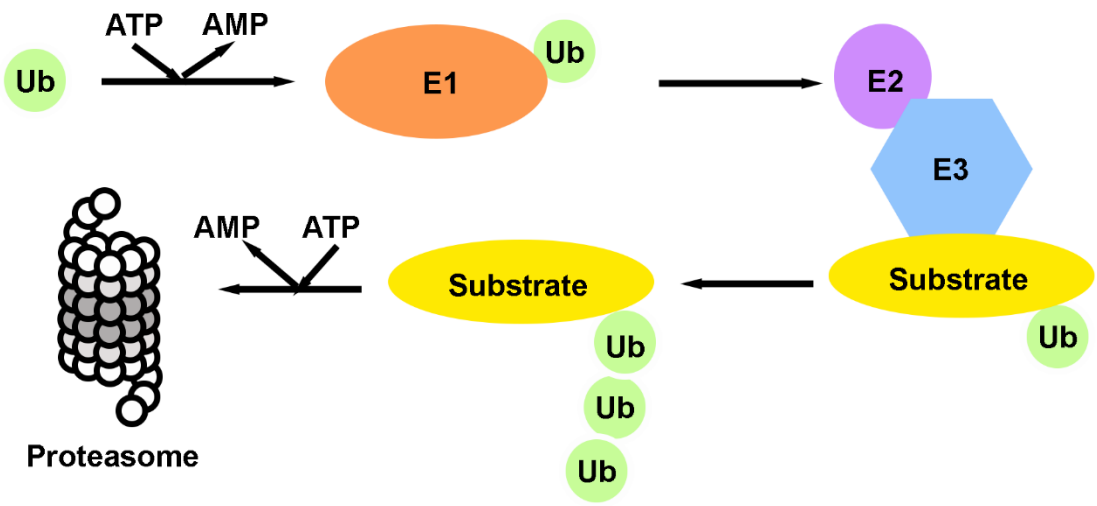

Figure 1.2. Overview of ubiquitin-proteasome system (UPS).

1.2.2. Lysosomal degradation pathway

The lysosome is another major proteolytic compartment in mammalian cells, responsible for the degradation and recycling of both extracellular and intracellular macromolecules. Lysosomes are membrane-bound organelles enclosed by a single phospholipid bilayer and have an acidic internal environment (pH ~4.5–5.0). The acidic luminal pH is regulated by vacuolar-type proton adenosine triphosphatase (v-ATPase) by pumping protons into the lysosome across the membrane[32]. Other key proteins on the lysosomal membrane include soluble N-ethylmaleimide-sensitive factor attachment protein receptors (SNAREs) and RAB GTPases involved in membrane fusion and vesicular trafficking, as well as Lysosomal-associated membrane protein 1 (LAMP1), a lysosomal marker that constitutes about half of the lysosomal membrane[33,34]. Newly synthesized lysosomal membrane proteins are delivered to the lysosome via the endoplasmic reticulum (ER), trans-Golgi network (TGN), and are either directly trafficked through the endosome to the lysosome or indirectly transported to the plasma membrane, where they are delivered into the lysosome via endocytosis (as discussed

below)[35]. The lysosomal membrane prevents the uncontrolled degradation of the cytosolic compartment and maintains the acidic internal pH, which is essential for the optimal activity of hydrolytic enzymes within the lysosomal lumen. The lysosome contains nearly 70 soluble hydrolytic enzymes, including proteases, lipases, glycosidases, nucleases, phosphatases, and sulfatases, all of which function to degrade various macromolecules[36]. The precursors of lysosomal hydrolases are synthesized and tagged with oligosaccharides chains in ER. After transporting from ER through Golgi apparatus to the TGN, mannose residues in the oligosaccharide chain are phosphorylated to form mannose-6-phosphate (M6P) and recognized by mannose-6-phosphate receptor (M6PR) in TGN. The clathrin-coated vesicles are then budded from TGN and transport hydrolases-M6PR complex to early and late endosomes. The acidic pH in late endosome causes the dissociation of M6P-attached hydrolases from M6RP, allowing the hydrolases to be transported into the lysosome[37].

Unlike UPS, the lysosome plays a crucial role in the removal of long-lived, insoluble protein aggregates, and organelles through the autophagy-lysosome pathway, including three main processes: macroautophagy, microautophagy, and chaperone-mediated autophagy (CMA). Macroautophagy, the predominant pathway, begins with the formation of a double-membrane structure, phagophore, which is tightly regulated by the ULK1/Atg1 complex and the class III PI3K complex (Beclin-1/Atg6)[38]. The phagophore elongates and engulfs cytoplasmic cargo, such as damaged organelles or protein aggregates, to form an enclosed vesicle called the autophagosome. This elongation process is mediated by the lipidation of microtubule-associated protein 1 light chain 3 (LC3), a critical marker of autophagosome maturation[39]. Once fully formed, the

autophagosome fuses with the lysosome, a step mediated by fusion proteins such as the SNARE family and the small GTPase Rab7, resulting in the formation of an autophagolysosome. Within the autophagolysosome, the lysosomal enzymes degrade the cargo, recycling essential macromolecules back into the cytosol[40]. In microautophagy, the lysosome directly engulfs small portions of the cytoplasm by invaginating its own membrane, allowing for the direct internalization and degradation of intracellular components[41]. Chaperone-mediated autophagy (CMA) is a selective process that specifically targets proteins containing the KFERQ-like motif. These proteins are recognized by cytosolic chaperones, such as Hsc70, and are translocated directly across the lysosomal membrane via the LAMP-2A receptor[42,43].

Extracellular and membrane-bound proteins can be also delivered to the lysosome for degradation via the endocytosis and endosome-lysosome pathway. Multiple endocytic mechanisms mediate the internalization of extracellular materials, with the clathrin-mediated endocytosis (CME) pathway being the most common. Transmembrane cargo molecules bearing short linear sequence motifs or specific covalent modifications, such as phosphorylation or ubiquitylation, in their cytosolic regions can trigger the sequential recruitment of clathrin-adaptor proteins and scaffold proteins to the membrane[44]. Most of the adaptor proteins could also directly attach to the membrane to form the clathrin coat first followed by recruiting cargos into the coat[45]. Adaptor proteins, such as AP2 complex, clathrin assembly lymphoid myeloid leukaemia protein (CALM), F-BAR domain only protein 1 (FCHO1), and FCHO2, along with scaffold proteins, including clathrin, epidermal growth factor receptor substrate 15 (EPS15), epidermal growth factor receptor substrate 15-like 1 (EPS15R), and intersectins form a pioneer module at

the endocytic site to initiate the endocytosis process[46-49]. Clathrin, together with the actin cytoskeleton, promotes membrane bending to generate clathrin-coated pits (60–120 nm in diameter), which then undergo a series of well-defined morphological transitions to form clathrin-coated vesicles (CCVs)[50]. The large GTPase dynamin catalyzes the scission of membrane invagination, severing the CCVs from the plasma membrane[51]. Finally, the heat shock cognate 71 kDa protein (HSC70), recruited by auxilin, facilitates the disassembly of the clathrin polymer on CCVs. The dephosphorylation of phosphatidylinositol 4,5-bisphosphate (PI(4,5)P2) may also contribute to the uncoating process[52]. The uncoating process disassembles endocytic protein machinery on CCVs which enables their subsequent fusion with early endosomes for further intracellular transport.

Clathrin-independent endocytosis (CIE) pathways represent a minor fraction of endocytic routes in mammalian cells and are relatively less well understood compared to clathrin-mediated endocytosis. Caveolae-dependent endocytosis is one of CIE pathways that involves the formation of caveolae and the subsequent fission of these invaginations from the plasma membrane. Caveolae are flask-shaped membrane invaginations with the diameter of 50-80 nm[53]. The main structural components of caveolae are proteins from the caveolin family, including caveolin-1, along with caveolin-2 and caveolin-3[54]. Unlike clathrin, a cytosolic protein, caveolin-1 is an integral membrane protein that cooperates with peripheral membrane proteins cavins to form caveolae coat. Cavins not only stabilize caveolae but also modulate their morphology and functions[55]. Moreover, caveolin binds to cholesterol- and sphingolipid-rich membrane domains to recruit additional proteins and lipids to caveolae for their

assembly and function[56]. Caveolin, cavin, and lipid can recognize and cluster specific receptors into caveolae and the ligand-receptor interaction triggers the signaling for internalization[57]. Caveolins are capable of oligomerization (caveolin-1 and caveolin-2) on membranes, which could further potentiate membrane curvature[58]. Actin cytoskeleton also play a role in caveolae internalization[59]. Although dynamin was initially thought to promote caveolae scission in a way similarly to CCVs, recent studies suggest that it may function more like another important protein, Eps15 homology domain-containing protein 2 (EHD2), which is now understood to prevent premature fission of caveolae[60,61]. This action helps maintain caveolae stability at the membrane until signaling events trigger their internalization.

Another dynamin-dependent CIE pathway is RhoA-dependent interleukin 2 receptor beta (IL-2Rβ) endocytosis, shared by many cytokine receptors undergoing endocytosis via this route. It requires activation of RhoA, Rac1, and p21-activated kinase 1 (Pak1) signaling cascade to facilitates the formation of vesicles ranging from 50 to 100 nm in diameter[62,63]. Several endocytosis pathways are vesicle coat- and dynamin-independent, such as The Clathrin-Independent Carrier/Glycosylphosphatidylinositol (GPI)-Anchored Protein (AP)-Enriched Endosomal Compartments (CLIC/GEEC) pathway endocytosis, flotillin-dependent endocytosis, and Arf6-dependent endocytosis. The CLIC/GEEC pathway primarily mediates the transport of GPI-anchored proteins and fluid-phase contents into the cell via GPI-AP-enriched early endosomal compartments (GEECs), which form via the fusion of Clathrin-Independent Carriers (CLICs)[64]. The internalization process begins with the recruitment of the guanine nucleotide exchange factor (GEF) GBF1, followed by activation of GTP-binding protein

ADP-ribosylation factor 1 (Arf1)[65]. Subsequently, actin-driven membrane dynamics mediated by Cdc42 promote the formation of CLICs and the enrichment of CLICs in GEECs is regulated by the recruitment of GTPase regulator associated with focal adhesion kinase1 (GRAF1)[54,66]. Additionally, other CIE pathways have been reported to require flotillin proteins and the small GTPase ADP-ribosylation factor 6 (Arf6)[67,68].

The aforementioned pathways are mediated by vesicles less than 100 nm in diameter, which are classified as forms of micropinocytosis. In contrast, bulk endocytic processes, such as phagocytosis and macropinocytosis, facilitate the internalization of significantly larger particles. Phagocytosis, employed by specialized cells including macrophages, neutrophils, monocytes, and dendritic cells, is responsible for engulfing particles larger than 0.5 μm. Specific receptors, such as Fc receptors and complement receptors, recognize these particles, initiating signaling cascades that lead to actin cytoskeletal rearrangements, ultimately resulting in the formation of large vesicles known as phagosomes[69]. Macropinocytosis, distinct from receptor-mediated endocytosis, allows for the rapid internalization of substantial amounts of plasma membrane and extracellular fluid, along with pathogens such as bacteria, viruses, protozoa, and prions. This process begins with actin polymerization at the plasma membrane, forming membrane ruffles that engulf extracellular solutes into large vesicles termed macropinosomes, which range in size from 0.2 to 5 μm in diameter[70].

After internalization, uncoated vesicles, which are pinched off from the plasma membrane via endocytic pathways, fuse with early endosomes (EEs). EEs, marked by the presence of Rab5, form in the peripheral cytoplasm and maintain a slightly acidic intraluminal pH (pH ~6.5), which facilitates the dissociation of cargo from receptors[71].

These EEs serve as critical sorting stations, where cargo is processed and directed toward distinct intracellular fates, including recycling pathways or degradation. Vacated receptors may be recycled back to the plasma membrane either directly via Rab4 GTPase-positive tubular-vesicular structures originating from EEs or transferred to recycling endosomes, which are regulated by Rab11, before being returned to the cell surface[72,73]. Additionally, the retromer complex can assemble on early endosomes to recognize specific cargos and mediate their retrograde transport from early endosomes to the TGN, enabling subsequent recycling back to the plasma membrane[74]. In the process leading to degradation, cargo proteins modified by ubiquitination are recognized by the endosomal sorting complex required for transport (ESCRT) machinery, which facilitates their sorting into multivesicular bodies (MVBs). Recent studies have shown that even integral membrane proteins and soluble cargoes lacking ubiquitin modification can still be internalized into multivesicular endosomes (MVEs) in an ESCRT-dependent manner[75]. Then, intraluminal vesicles (ILVs) bud inward from the endosomal membrane, and as the resulting multivesicular bodies (MVBs) containing these ILVs detach from early endosomes (EEs), they progressively mature into late endosomes (LEs, pH ~5.5)[76]. This maturation process is characterized by the replacement of Rab5 with Rab7, a gradual acidification of the lumen due to the assembly of the vacuolar-type H+-ATPase complex on the endosomal membrane, and migration along microtubules toward the perinuclear region, driven by the coordinated actions of dynein and kinesin motor proteins[77,78]. Finally, late endosomes or MVBs fuse with lysosomes, leading to the degradation of cargo proteins and intraluminal vesicles.

Alternatively, MVBs can fuse with the plasma membrane and release their ILVs into the extracellular space as exosomes[79] (Fig. 1.3).

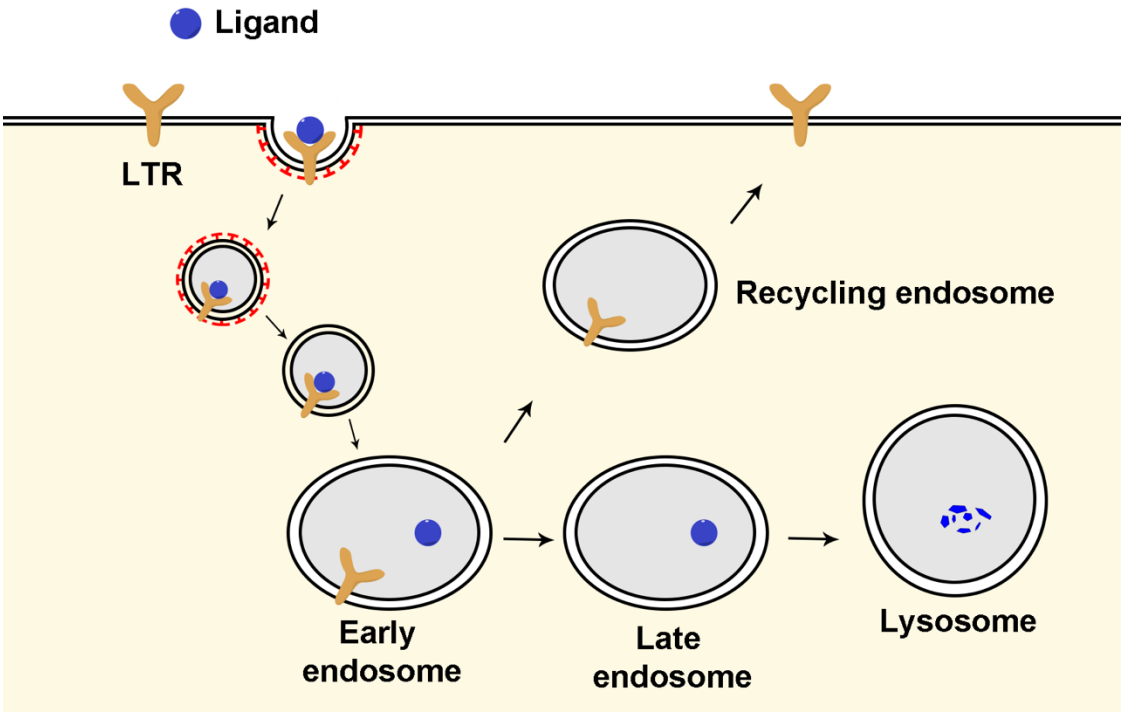

Figure 1.3. Overview of endosome/lysosome degradation pathway.

1.3. Target protein degradation hijacking UPS

Proteolysis-targeting chimeras (PROTACs) represent the most well-developed class of TPD modality utilizing the UPS. PROTACs are bifunctional molecules composed of an E3 ligase ligand and a binder for the POI, connected by a linker. The interaction of a PROTAC with both the target protein and the E3 ubiquitin ligase leads to the formation of a ternary complex. This proximity promotes the polyubiquitination of the POI by the E3 ligase, marking it for degradation by the proteasome. Notably, PROTACs act catalytically, meaning they dissociate from the POI after ubiquitination, allowing them to be recycled to engage additional POI molecules for multiple rounds of protein

degradation (Fig. 1.4). The first PROTAC, Protac-1, was reported in 2001 by Crews and Deshaies groups. Protac-1 consists of the antiangiogenic drug Ovalicin which targets methionine aminopeptidase-2 (MetAP-2), and a phosphopeptide derived from IkBα (IPP) that binds to Skp1-Cullin-F-box (SCF) ubiquitin ligase complex[80]. This approach was subsequently expanded to degrade another two different proteins, the estrogen (ER) and androgen (AR) receptors, which drive the progression of breast and prostate cancer, respectively[81]. In 2008, Crews group developed the first small molecule-based PROTAC containing the ligand of ubiquitin ligase murine double minute 2 (MDM2), a PEG-based linker, and the ligand of a non-steroidal androgen receptor ligand (SARM)[82]. Small molecule PROTACs exhibit improved cell permeability and stability compared to peptide-based PROTACs, as well as the advantage of oral bioavailability. However, the degradation of AR target requires high concentration of the PROTAC molecule and the mechanism of this PROTAC was not fully investigated. Subsequently, additional E3 ligases were investigated for PROTAC development, with cereblon (CRBN) and von Hippel-Lindau (VHL) becoming the most widely used ligases[83]. PROTAC has been developed to target a wide range of diseases, including cancer, neurodegenerative diseases, autoimmune and inflammatory diseases[84-87]. According to the open-access database that compiles PROTAC information (PROTAC-DB), 6111 PROTACs have been developed to target 442 different POIs through the recruitment of 20 distinct E3 ligases[88]. Currently, over 20 PROTACs are in clinical trials, with ARV-471, which targets the estrogen receptor (ER), showing promising results and advancing to phase III clinical studies[89].

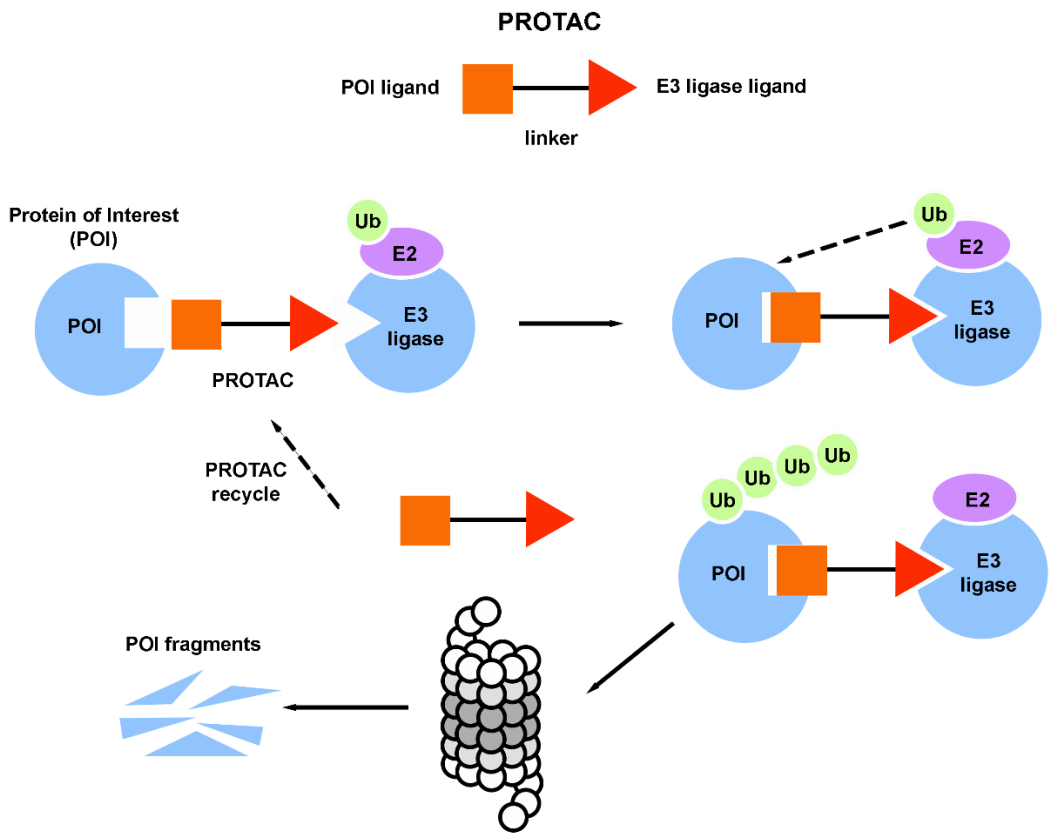

Figure 1.4. The degradation mechanism of POI by PROTACs.

Despite the significant advancements in PROTAC development, there remain challenges, particularly the potential for on-target but off-tissue toxicity due to systemic application. To address this issue, efforts are being made to enhance the tissue- or cancer-selectivity of PROTACs through rational design. One interesting approach is the development of spatiotemporally controllable PROTACs through photochemical modulation. Photo-caged PROTACs (pc-PROTACs) represent one such strategy. These molecules utilize photo-removable blocking groups, such as 4,5-dimethoxy-2-nitrobenzyl (DMNB) or diethylamino coumarin (DEACM), attached to either the ligand for the protein of interest (POI) or the E3 ligase ligand[90,91]. The presence of a photolabile caging group renders the PROTAC inactive until it is exposed to ultraviolet

(UV) light, at which point the blocking group is removed, and the PROTAC regains its activity. Building on this concept, photoswitchable PROTACs (ps-PROTACs) have been developed, incorporating photoswitchable linker moieties between the POI and E3 ligase ligands. These linkers enable the reversible on/off switching of protein degradation in response to specific wavelengths of light, offering a more refined control over PROTAC activity in both time and space[92]. In addition to photochemical modulation, various targeting molecules have been conjugated to PROTACs via cleavable linkers to enable tissue-specific delivery and controlled release upon hydrolysis. The therapeutic antibody trastuzumab, which targets HER2, has been conjugated to an MZ1-based BRD4 degrader to form an Antibody–PROTAC Conjugate (Ab-PROTAC), facilitating the targeted delivery of PROTACs to HER2-positive breast cancer cells[15]. Aptamers, single-stranded DNA or RNA oligonucleotides typically shorter than 100 nucleotides, have also been employed as targeting agents. Nucleolin-targeting aptamers allow PROTACs to be specifically delivered to breast cancer cells while sparing normal breast cells[93]. Additionally, studies have demonstrated that conjugating folate to PROTACs promotes the selective degradation of cytosolic proteins in cancer cells that overexpress folate receptors, further enhancing the specificity of PROTAC-based therapies[94].

Beyond PROTACs, other platforms leveraging the ubiquitin-proteasome system (UPS) have also been developed. Molecular glues, which are monovalent small molecules typically with molecular weight of less than 500 Da, function similarly to PROTACs. Molecular glue degraders interact with ubiquitin ligases and target proteins to promote the formation of novel protein-protein interactions (PPIs) or enhance pre-existing PPIs,

leading to the target's degradation[95]. Thalidomide and its analogs lenalidomide (Revlimid) and pomalidomide (Pomalyst) are the only FDA-approved molecular glue degraders, which interact with CRBN to induce the degradation of its transcription factor substrates IKZF1/3[96]. Additionally, Nabet et al. reported a degradation tag (dTAG) system as a powerful tool for rapid target validation. In this system, the POI is fused with $FKBP12^{F36V}$ via transgene expression or CRISPR-mediated locus-specific knock-in. The mutation is introduced to FKBP12 to avoid degradation of endogenous FKBP12. $FKBP12^{F36V}$-fused POI works in conjunction with a PROTAC specific to $FKBP12^{F36V}$, which recruits CRBN to induce the rapid degradation of the tagged POI.

1.4. Target protein degradation hijacking lysosome degradation pathway

TPD strategies that utilize the UPS are restricted to degrading intracellular, soluble, and short-lived proteins, which hinders their effectiveness in addressing diseases caused by extracellular proteins and protein aggregates, as seen in conditions like Huntington's and Alzheimer's disease. Therefore, incorporating lysosomal degradation of biomolecules can significantly enhance the repertoire of TPD methods, broadening their applicability in treating various human diseases.

1.4.1. Degrading intracellular proteins via autophagy-lysosome pathway

To complement PROTAC and expand the scope of TPD beyond intracellular proteins, several novel platforms leveraging the autophagy-lysosome degradation pathways have been developed. One such platform, the autophagy-targeting chimera (AUTAC), utilizes a modified guanine tag, p-fluorobenzylguanine (FBnG), which induces S-guanylation and subsequent K63 polyubiquitination on POIs. This modification allows POIs to be recognized by autophagy and transported into lysosomal for degradation. AUTACs have

been shown to effectively degrade intracellular proteins such as methionine aminopeptidase 2 (MetAP2) and FK506-binding protein (FKBP12), as well as mitochondria[12]. Another platform, autophagosome-tethering compounds (ATTECs), recruits key autophagosome protein LC3 to route the POIs into autophagy-lysosome degradation pathway[13]. In addition to proteins, such as mutant Huntington (HTT) and BRD4, ATTECs have recently demonstrated the feasibility of degrading non-protein biomolecules lipid droplets, which cannot be targeted by PROTACs and AUTACs[97,98]. Moreover, autophagy-targeting chimera (AUTOTAC) consists of an autophagy cargo receptor p62-binding ligand and a target binding ligand. P62 self-polymerization, along with its interaction with LC3, directs POIs to autophagic membranes for lysosomal degradation. AUTOTACs can clear not only monomeric proteins but also ubiquitin-conjugated, aggregation-prone proteins that are inaccessible to the proteasome[99]. However, the generality of these strategies has not been demonstrated and their clinical applications remained to be unexplored.

1.4.2. Degrading intracellular proteins via endosome-lysosome pathway

The concept of lysosome-targeting chimeras (LYTACs) was first introduced by the Bertozzi group in 2020. LYTACs are bifunctional molecules composed of a target protein binder and a lysosome-targeting receptor (LTR) binder, connected by a linker. These molecules bind extracellular or membrane proteins at their extracellular binding domain and form a ternary complex upon interaction with an LTR. This interaction triggers internalization of the ternary complex, which then directs the protein to the lysosomal degradation pathway. Once internalized, the complex enters the early endosome, where the LTR dissociates from its ligand due to the drop in pH. The target protein is

subsequently transported to the late endosome and then to the lysosome for degradation. Meanwhile, the LTR is recycled back to the cell membrane to mediate the internalization of another ternary complex (Fig. 1.5). The first LYTAC was developed using the ubiquitously expressed cation-independent mannose 6-phosphate receptor (CI-M6PR) as the LTR. CI-M6PR has been widely used in delivering recombinant hydrolases for lysosomal enzyme replacement therapy due to its lysosomal shuttling function. The polymeric glycopeptide bearing multiple mannose-6-phosphonate (M6Pn) motifs was chemically synthesized as the ligand to recruit CI-M6PR. This ligand was then conjugated to antibodies targeting distinct soluble and membrane proteins, such as apolipoprotein E4, epidermal growth factor receptor (EGFR), CD71, and programmed death-ligand 1 (PD-L1), generating various LYTACs to induce protein degradation[14]. In 2021, lysosome targeting degraders leveraging the pair of asialoglycoprotein receptor (ASGPR)/ triantennary N-acetylgalactosamine (tri-GalNAc) were reported by three groups including ours to induce protein degradation specifically in liver. ASGPR is primarily and highly expressed in hepatocytes responsible for clearing glycoproteins via clathrin-mediated endocytosis and lysosomal degradation. Tri-GalNAc, the ligand of ASPGR with well-defined structure, has been widely applied in ASGPR-mediated drug delivery. Similar to the first LYTAC, Bertozzi and Tang groups generated small molecule/antibody or small molecule/peptide conjugates as the tissue-selective degraders to target disease-causing proteins such as EGFR, human epidermal growth factor receptor 2 (HER2), and integrins, while Spiegel group synthesized bifunctional small molecule degraders, named MoDE-As (Molecular Degraders of Extracellular

proteins through the Asialoglycoprotein receptor (ASGPR)), for the depletion of cytokines and antibodies[100-102].

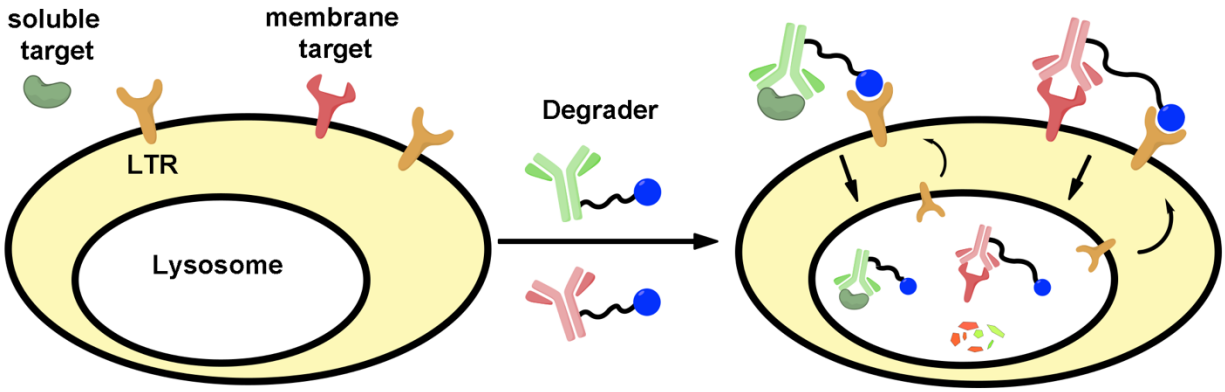

Figure 1.5. The degradation mechanism of POI by LYTACs.

Subsequent research has focused on improving the ligand/LTR binding and generating homogeneous degraders for both CI-M6PR and ASGPR. The initial LYTACs employed large multivalent M6Pn structures without well-defined configurations, which posed challenges for quality control in drug development. To address this, the Tang group developed structurally well-defined CI-M6PR glycopeptide ligands by using a library of oligopeptides with varying numbers of cysteine residues (e.g., 1, 2, 3, 4, and 6) and employing a highly efficient thiol-ene reaction to couple the alkene-containing M6Pn to the cysteine residues. They demonstrated that degraders bearing glycopeptides with four units of M6Pn efficiently promoted the degradation of therapeutically relevant EGFR in cancer cells[103]. While antibody conjugates that recruit CI-M6PR and ASGPR were initially generated through lysine-NHS reactions, resulting in heterogeneous mixtures with variable ligand-to-antibody ratios, the Wang group recently developed a homogeneous antibody conjugate for both CI-M6PR- and ASGPR-mediated degradation. They employed a chemoenzymatic method using endoglycosidases

(Endo-S, Endo-S2) to convert diverse N-glycans on a mixture of antibodies into a homogenous product with a GlcNAc residue (with or without fucosylation). This product was then modified using glycosyltransferases to attach oligosaccharides with an oxazoline motif to the antibody[104,105]. In addition to small molecules, peptides, and antibodies, aptamers have emerged as another modality for targeting either LTRs or proteins, offering advantages such as higher binding affinity and better tissue penetration[106,107]. Furthermore, polypeptide-modified GalNAc self-assembled into nanospheres that could bind ASGPR has been used to generate Nano-LYTACs[108]. Recently, Novartis developed lysosome targeting degraders using both antibodies and cyclic peptides as binders of proprotein convertase subtilisin/kexin type 9 (PCSK9), reporting in vivo activity for ASGPR-recruiting degraders that can accelerate the clearance of secreted PCSK9, with potential for treating hyperlipidemia[109].

Liver-specific degraders based on ASGPR/tri-GalNAc pair restrict degradation to liver tissue, thereby reducing unwanted exposure of degraders to other organs. However, except for liver cancers, most of the membrane-bound cancer-related POIs cannot be targeted by these types of degraders. To improve the therapeutic efficacy and safety of LYTACs, there is a need for lysosome-targeting degraders that selectively deplete tumorigenic POIs in cancer cells, while sparing healthy tissues. An ideal approach to achieve this selectivity is to leverage lysosome-targeting receptors (LTRs) that are overexpressed on cancer cells. Integrin αvβ3, along with its recognition motif, the Arg-Gly-Asp (RGD) sequence, has been widely used to deliver therapeutic agents to tumors. A novel strategy called integrin-facilitated lysosomal degradation (IFLD) was developed, where a degrader containing a c(RGDyK) peptide was linked to a small-

molecule binder of PD-L1. The PD-L1 degraders driven by integrin displayed a significant antitumor effect in mice, however, the tumor-specific degradation of PD-L1 was not conclusively demonstrated in these studies[110]. Tang group further expanded on this strategy by developing integrin-targeting chimeras (ITACs), composed of c(RGDfK) peptides and the antibodies against POIs. ITACs exhibited superior EGFR degradation in cancer cells compared to normal cells, illustrating the potential for selective degradation in tumor tissues[111]. Another promising approach is the use of folate receptor-targeting chimeras (FRTACs), which exploit the overexpression of folate receptors in cancer cells and their limited accessibility in normal tissues. Notably, an FRTAC targeting PD-L1 exhibited superior antitumor effects compared to therapeutic antibodies in three different mouse models and demonstrated both in vitro and in vivo cancer-selective PD-L1 degradation[112]. In addition to transmembrane receptors, glucose transporters (GLUTs) involved in solute carrier (SLC) transport into cancer cells have also been leveraged for the development of GLUT-targeting chimeras (GTACs), created by conjugating multiple glucose ligands to targeting antibodies. The GTAC targeting HER2 exhibited enhanced tumor accumulation and tumorous HER2 degradation compared to unmodified antibody[113]. Furthermore, transferrin receptor-targeting chimeras (TransTACs) have been developed using recombinant bispecific antibodies, a strategy based on protein engineering, which differs from previously reported degraders that are typically generated through chemical modification. A cathepsin-sensitive linker was incorporated in the TransTACs to reduce POI recycling, thus enhancing degradation. TransTACs allowed for the reversible control of human primary chimeric

antigen receptor (CAR) T cells and effectively targeted drug-resistant, EGFR-driven lung cancers with exon 19 deletion/T790M/C797S mutations in a mouse xenograft model[114].

In addition to TransTACs, several other platforms have recently been developed that rely on fully genetically encoded degraders. Wells group developed recombinant bispecific antibodies as cytokine receptor-targeting chimeras (KineTACs) by fusing a cytokine arm to target-binding antibodies. KineTACs bearing CXCL12, CXCL11, or viral macrophage inflammatory protein-II (vMIP-II) demonstrated effective recruitment of the decoy recycling receptor CXCR7 to degrade both extracellular and membrane proteins. Additionally, the interleukin-2 (IL-2) and IL-2 receptor pair has also been employed for targeted degradation[115]. Another approach involves the use of CI-M6PR, also known as insulin-like growth factor 2 receptor (IGF2R), which can bind IGF2 at a domain distinct from the M6P binding site. Several IGF2-based fusion degraders have been recently developed, including bispecific antibodies fused with IGF2 peptide arms, as well as IGF2-fused nanobodies, affibodies, or IgG-binding Z-domains, termed iLYTACs[116,117]. Moreover, the Ting and Bertozzi groups recently reported the development of genetically encoded LYTACs (GELYTACs). In this approach, engineered primary T cells are designed to express and secrete evolved variant IGF2-fused degraders encoded by a single transgene. This strategy highlights the potential for CAR-T cells to deliver GELYTACs directly into the tumor microenvironment, offering a new avenue for targeted degradation in cancer therapy[118]. Several other genetically encoded degraders leverage transmembrane E3 ligases instead of LTRs to target and degrade membrane POIs. Antibody-based PROTACs (AbTACs) are bispecific antibodies recruiting ring finger protein 43 (RNF43) to remove membrane POIs through lysosome degradation

pathway[15,16]. Another bispecific antibody, proteolysis-targeting antibodies (PROTABs), has shown colorectal cancer-selective degradation mediated by zinc and ring finger 3 (ZNRF3) through both proteasomal and lysosomal degradation pathways. Some of other cell-surface E3 ligases, such as RNF128, RNF130, RNF133, RNF149, RNF150 could also be applied for PROTAB-mediated degradation[16]. Additionally, R-spondins chimeras (ROTACs) are fusion proteins containing natural R-spondin-derived high-affinity-binding domains to target ZNRF3/RNF43 ligases[119].

In addition to the previously discussed LTRs, several other LTRs has been utilized to induce the lysosomal degradation of protein degradation, such as scavenger receptors (SRs)[120,121], macrophage galactose-type lectin 1 (MGL1)[122], glucagon like peptide-1 receptor (GLP-1R)[123], glucose transporter Glut1[124]. While these platforms exploit natural ligand-receptor pairs to trigger endocytosis and lysosomal degradation of POIs, another class of degraders has been developed that employs specific tags to achieve the same function. GluTACs are nanobodies conjugated with a cell-penetrating peptide containing nine arginine residues, which facilitate POI internalization, and a lysosomal-sorting sequence (NPGY) to ensure transport to the lysosome[17]. Similarly, signal-mediated lysosome-targeting chimeras (SignalTACs) are engineered by genetically fusing the signaling motif from the CI-M6PR to an antibody, nanobody, or peptide[125]. Later on, the second generation of SignalTACs containing only a 10-amino acid tyrosine-based endocytic signaling motif derived from CI-M6PR has been designed to mitigate potential toxicity caused by the use of cell-penetrating peptides[126]. Both GluTACs and SignalTACs offer potential solutions for cells that do not express suitable lysosome-targeting receptors (LTRs). To stimulate endocytosis without competing with natural

ligands or by recruiting receptors lacking native ligands, Baker group designed the endocytosis-targeting proteins (EndoTags) for receptors that undergo distinct endocytosis mechanisms, including constitutively cycling receptors, endocytosis via conformational change, and endocytosis via receptor clustering. They produced EndoTags for IGF2R, ASGPR, sortilin and TfR, which cover these diverse endocytosis mechanisms, and since these receptors have distinct tissue distributions, it enables the targeted degradation of proteins in specific tissues. Co-localization-dependent protein switch (Co-LOCKR) system was further generated to selectively degrade EGFR only when HER2 was also present on the surface of cancer cells, allowing for more precise targeting based on the combinations of surface markers. Lastly, EndoTags are also able to significantly amplify the signaling triggered by endocytosis and with endosome[127].

1.5. Summary

TPD is emerging as a promising therapeutic modality, drawing significant attention from both academia and industry. Most efforts have focused on the depletion of cytosolic proteins using PROTACs, which harness the ubiquitin-proteasome degradation pathway. PROTAC technology has shown broad potential in diseases such as cancer, neurodegenerative diseases, and viral infections, with a growing number of PROTAC-based drugs progressing into clinical trials. However, the application of PROTACs is limited to soluble and membrane proteins. Expanding the scope of TPD beyond the proteasome, lysosome-targeting strategies provide a complementary avenue for the degradation of a wider range of intracellular and extracellular materials. Autophagy-targeting platforms enable the degradation of dysfunctional organelles and insoluble protein aggregates through the autophagy-lysosome pathway. While these platforms

hold significant promise, further studies are needed to elucidate their detailed mechanisms of action. Lysosome-targeting degraders offer an alternative approach to deplete extracellular and membrane proteins by directing them into the endosome-lysosome degradation pathway. Several LTRs, some of which are specifically distributed in certain tissues or overexpressed in cancer cells, have been exploited to enable tissue- or cancer-selective degradation, minimizing on-target, off-tissue toxicity. Various degrader modalities—such as small molecules, peptides, antibody conjugates, and recombinant proteins—have been developed through chemical modification and genetic engineering. In addition to platforms that utilize natural ligand-induced receptor endocytosis, there are degraders designed with specific tags to trigger endocytosis without competing with naturally occurring ligands or in cells lacking suitable LTRs or ligands. Further exploration of additional LTRs and endocytosis-inducing tags could broaden the application of lysosome-targeting degraders. The development of homogeneous antibody conjugates, using different chemical labeling methods, allows for more consistent and predictable performance, facilitating a deeper understanding of the degrader's mechanism of action and enabling the fine-tuning of therapeutic efficacy. Mechanistic investigations could enhance the efficacy of these degraders, potentially leading to the development of catalytic degraders. Additionally, expanding the target space to more disease-relevant proteins will help realize the full therapeutic potential of TPD.

1.6. References

1 Xie, X. *et al.* Recent advances in targeting the "undruggable" proteins: from drug discovery to clinical trials. *Signal Transduct Target Ther* **8**, 335 (2023). https://doi.org/10.1038/s41392-023-01589-z

2 Lu, Y. *et al.* Emerging Pharmacotherapeutic Strategies to Overcome Undruggable Proteins in Cancer. *Int J Biol Sci* **19**, 3360-3382 (2023). https://doi.org/10.7150/ijbs.83026

3 Lai, A. C. & Crews, C. M. Induced protein degradation: an emerging drug discovery paradigm. *Nat Rev Drug Discov* **16**, 101-114 (2017). https://doi.org/10.1038/nrd.2016.211

4 Wang, X., Zhang, H. & Chen, X. Drug resistance and combating drug resistance in cancer. *Cancer Drug Resist* **2**, 141-160 (2019). https://doi.org/10.20517/cdr.2019.10

5 Schapira, M., Calabrese, M. F., Bullock, A. N. & Crews, C. M. Targeted protein degradation: expanding the toolbox. *Nat Rev Drug Discov* **18**, 949-963 (2019). https://doi.org/10.1038/s41573-019-0047-y

6 Burslem, G. M. *et al.* The Advantages of Targeted Protein Degradation Over Inhibition: An RTK Case Study. *Cell Chem Biol* **25**, 67-77.e63 (2018). https://doi.org/10.1016/j.chembiol.2017.09.009

7 Burke, M. R., Smith, A. R. & Zheng, G. Overcoming Cancer Drug Resistance Utilizing PROTAC Technology. *Front Cell Dev Biol* **10**, 872729 (2022). https://doi.org/10.3389/fcell.2022.872729

8 Békés, M., Langley, D. R. & Crews, C. M. PROTAC targeted protein degraders: the past is prologue. *Nat Rev Drug Discov* **21**, 181-200 (2022). https://doi.org/10.1038/s41573-021-00371-6

9 Kozicka, Z. *et al.* Design principles for cyclin K molecular glue degraders. *Nat Chem Biol* **20**, 93-102 (2024). https://doi.org/10.1038/s41589-023-01409-z

10 Ma, Z., Ji, Y., Yu, Y. & Liang, D. Specific non-genetic IAP-based protein erasers (SNIPERs) as a potential therapeutic strategy. *Eur J Med Chem* **216**, 113247 (2021). https://doi.org/10.1016/j.ejmech.2021.113247

11 Nabet, B. *et al.* Rapid and direct control of target protein levels with VHL-recruiting dTAG molecules. *Nat Commun* **11**, 4687 (2020). https://doi.org/10.1038/s41467-020-18377-w

12 Takahashi, D. *et al.* AUTACs: Cargo-Specific Degraders Using Selective Autophagy. *Mol Cell* **76**, 797-810.e710 (2019). https://doi.org/10.1016/j.molcel.2019.09.009

13 Li, Z. *et al.* Allele-selective lowering of mutant HTT protein by HTT-LC3 linker compounds. *Nature* **575**, 203-209 (2019). https://doi.org/10.1038/s41586-019-1722-1

14 Banik, S. M. *et al.* Lysosome-targeting chimaeras for degradation of extracellular proteins. *Nature* **584**, 291-297 (2020). https://doi.org/10.1038/s41586-020-2545-9

15 Cotton, A. D., Nguyen, D. P., Gramespacher, J. A., Seiple, I. B. & Wells, J. A. Development of Antibody-Based PROTACs for the Degradation of the Cell-Surface Immune Checkpoint Protein PD-L1. *J Am Chem Soc* **143**, 593-598 (2021). https://doi.org/10.1021/jacs.0c10008

16 Marei, H. *et al.* Antibody targeting of E3 ubiquitin ligases for receptor degradation. *Nature* **610**, 182-189 (2022). https://doi.org/10.1038/s41586-022-05235-6
17 Zhang, H. *et al.* Covalently Engineered Nanobody Chimeras for Targeted Membrane Protein Degradation. *J Am Chem Soc* **143**, 16377-16382 (2021). https://doi.org/10.1021/jacs.1c08521
18 Ciechanover, A. & Schwartz, A. L. The ubiquitin-proteasome pathway: the complexity and myriad functions of proteins death. *Proc Natl Acad Sci U S A* **95**, 2727-2730 (1998). https://doi.org/10.1073/pnas.95.6.2727
19 Amm, I., Sommer, T. & Wolf, D. H. Protein quality control and elimination of protein waste: the role of the ubiquitin-proteasome system. *Biochim Biophys Acta* **1843**, 182-196 (2014). https://doi.org/10.1016/j.bbamcr.2013.06.031
20 Morreale, F. E. & Walden, H. Types of Ubiquitin Ligases. *Cell* **165**, 248-248.e241 (2016). https://doi.org/10.1016/j.cell.2016.03.003
21 Petroski, M. D. & Deshaies, R. J. Function and regulation of cullin-RING ubiquitin ligases. *Nat Rev Mol Cell Biol* **6**, 9-20 (2005). https://doi.org/10.1038/nrm1547
22 Lorenz, S. Structural mechanisms of HECT-type ubiquitin ligases. *Biol Chem* **399**, 127-145 (2018). https://doi.org/10.1515/hsz-2017-0184
23 Middleton, A. J. & Day, C. L. From seeds to trees: how E2 enzymes grow ubiquitin chains. *Biochem Soc Trans* **51**, 353-362 (2023). https://doi.org/10.1042/BST20220880
24 Timms, R. T. *et al.* Defining E3 ligase-substrate relationships through multiplex CRISPR screening. *Nat Cell Biol* **25**, 1535-1545 (2023). https://doi.org/10.1038/s41556-023-01229-2
25 Cowan, A. D. & Ciulli, A. Driving E3 Ligase Substrate Specificity for Targeted Protein Degradation: Lessons from Nature and the Laboratory. *Annu Rev Biochem* **91**, 295-319 (2022). https://doi.org/10.1146/annurev-biochem-032620-104421
26 Iconomou, M. & Saunders, D. N. Systematic approaches to identify E3 ligase substrates. *Biochem J* **473**, 4083-4101 (2016). https://doi.org/10.1042/BCJ20160719
27 Bhat, S. A. *et al.* Ubiquitin proteasome system in immune regulation and therapeutics. *Curr Opin Pharmacol* **67**, 102310 (2022). https://doi.org/10.1016/j.coph.2022.102310
28 Arkinson, C., Dong, K. C., Gee, C. L. & Martin, A. Mechanisms and regulation of substrate degradation by the 26S proteasome. *Nat Rev Mol Cell Biol* (2024). https://doi.org/10.1038/s41580-024-00778-0
29 Sahu, I. & Glickman, M. H. Proteasome in action: substrate degradation by the 26S proteasome. *Biochem Soc Trans* **49**, 629-644 (2021). https://doi.org/10.1042/BST20200382
30 Collins, G. A. & Goldberg, A. L. The Logic of the 26S Proteasome. *Cell* **169**, 792-806 (2017). https://doi.org/10.1016/j.cell.2017.04.023
31 Bard, J. A. M. *et al.* Structure and Function of the 26S Proteasome. *Annu Rev Biochem* **87**, 697-724 (2018). https://doi.org/10.1146/annurev-biochem-062917-011931

32 Futai, M., Sun-Wada, G. H., Wada, Y., Matsumoto, N. & Nakanishi-Matsui, M. Vacuolar-type ATPase: A proton pump to lysosomal trafficking. *Proc Jpn Acad Ser B Phys Biol Sci* **95**, 261-277 (2019). https://doi.org/10.2183/pjab.95.018

33 Perera, R. M. & Zoncu, R. The Lysosome as a Regulatory Hub. *Annu Rev Cell Dev Biol* **32**, 223-253 (2016). https://doi.org/10.1146/annurev-cellbio-111315-125125

34 Bonam, S. R., Wang, F. & Muller, S. Lysosomes as a therapeutic target. **18**, 923-948 (2019).

35 Luzio, J. P., Hackmann, Y., Dieckmann, N. M. & Griffiths, G. M. The biogenesis of lysosomes and lysosome-related organelles. *Cold Spring Harb Perspect Biol* **6**, a016840 (2014). https://doi.org/10.1101/cshperspect.a016840

36 Braulke, T., Carette, J. E. & Palm, W. Lysosomal enzyme trafficking: from molecular mechanisms to human diseases. *Trends Cell Biol* **34**, 198-210 (2024). https://doi.org/10.1016/j.tcb.2023.06.005

37 Yang, C. & Wang, X. Lysosome biogenesis: Regulation and functions. *J Cell Biol* **220** (2021). https://doi.org/10.1083/jcb.202102001

38 Hurley, J. H. & Young, L. N. Mechanisms of Autophagy Initiation. *Annu Rev Biochem* **86**, 225-244 (2017). https://doi.org/10.1146/annurev-biochem-061516-044820

39 Feng, Y., He, D., Yao, Z. & Klionsky, D. J. The machinery of macroautophagy. **24**, 24-41 (2014).

40 Parzych, K. R. & Klionsky, D. J. An overview of autophagy: morphology, mechanism, and regulation. *Antioxid Redox Signal* **20**, 460-473 (2014). https://doi.org/10.1089/ars.2013.5371

41 Marzella, L., Ahlberg, J. & Glaumann, H. Autophagy, heterophagy, microautophagy and crinophagy as the means for intracellular degradation. *Virchows Arch B Cell Pathol Incl Mol Pathol* **36**, 219-234 (1981). https://doi.org/10.1007/bf02912068

42 Chiang, H. L., Terlecky, S. R., Plant, C. P. & Dice, J. F. A role for a 70-kilodalton heat shock protein in lysosomal degradation of intracellular proteins. *Science* **246**, 382-385 (1989). https://doi.org/10.1126/science.2799391

43 Cuervo, A. M. & Dice, J. F. A receptor for the selective uptake and degradation of proteins by lysosomes. *Science* **273**, 501-503 (1996). https://doi.org/10.1126/science.273.5274.501

44 Traub, L. M. & Bonifacino, J. S. Cargo recognition in clathrin-mediated endocytosis. *Cold Spring Harb Perspect Biol* **5**, a016790 (2013). https://doi.org/10.1101/cshperspect.a016790

45 Schmid, E. M. & McMahon, H. T. Integrating molecular and network biology to decode endocytosis. *Nature* **448**, 883-888 (2007). https://doi.org/10.1038/nature06031

46 Kelly, B. T. *et al.* Clathrin adaptors. AP2 controls clathrin polymerization with a membrane-activated switch. *Science* **345**, 459-463 (2014). https://doi.org/10.1126/science.1254836

47 Miller, S. E. *et al.* CALM regulates clathrin-coated vesicle size and maturation by directly sensing and driving membrane curvature. *Dev Cell* **33**, 163-175 (2015). https://doi.org/10.1016/j.devcel.2015.03.002

48 Ma, L. *et al.* Transient Fcho1/2·Eps15/R·AP-2 Nanoclusters Prime the AP-2 Clathrin Adaptor for Cargo Binding. *Dev Cell* **37**, 428-443 (2016). https://doi.org/10.1016/j.devcel.2016.05.003

49 Cocucci, E., Aguet, F., Boulant, S. & Kirchhausen, T. The first five seconds in the life of a clathrin-coated pit. *Cell* **150**, 495-507 (2012). https://doi.org/10.1016/j.cell.2012.05.047

50 Charpentier, J. C. & King, P. D. Mechanisms and functions of endocytosis in T cells. *Cell Commun Signal* **19**, 92 (2021). https://doi.org/10.1186/s12964-021-00766-3

51 Antonny, B. *et al.* Membrane fission by dynamin: what we know and what we need to know. *EMBO J* **35**, 2270-2284 (2016). https://doi.org/10.15252/embj.201694613

52 Kaksonen, M. & Roux, A. Mechanisms of clathrin-mediated endocytosis. *Nat Rev Mol Cell Biol* **19**, 313-326 (2018). https://doi.org/10.1038/nrm.2017.132

53 Pelkmans, L. & Helenius, A. Endocytosis Via Caveolae. *Traffic* **3**, 311-320 (2002).

54 Chadda, R. *et al.* Cholesterol-Sensitive Cdc42 Activation Regulates Actin Polymerization for Endocytosis via the GEEC Pathway. *Traffic* **8**, 702-717 (2007).

55 Kovtun, O., Tillu, V. A., Ariotti, N., Parton, R. G. & Collins, B. M. Cavin family proteins and the assembly of caveolae. *J Cell Sci* **128**, 1269-1278 (2015). https://doi.org/10.1242/jcs.167866

56 Sonnino, S. & Prinetti, A. Sphingolipids and membrane environments for caveolin. *FEBS Lett* **583**, 597-606 (2009). https://doi.org/10.1016/j.febslet.2009.01.007

57 Kiss, A. L. & Botos, E. Endocytosis via caveolae: alternative pathway with distinct cellular compartments to avoid lysosomal degradation? *J Cell Mol Med* **13**, 1228-1237 (2009). https://doi.org/10.1111/j.1582-4934.2009.00754.x

58 Prakash, S., Krishna, A. & Sengupta, D. Caveolin induced membrane curvature and lipid clustering: two sides of the same coin? *Faraday Discuss* **232**, 218-235 (2021). https://doi.org/10.1039/d0fd00062k

59 Mundy, D. I., Machleidt, T., Ying, Y. S., Anderson, R. G. & Bloom, G. S. Dual control of caveolar membrane traffic by microtubules and the actin cytoskeleton. *J Cell Sci* **115**, 4327-4339 (2002). https://doi.org/10.1242/jcs.00117

60 Parton, R. G., Taraska, J. W. & Lundmark, R. Is endocytosis by caveolae dependent on dynamin? *Nat Rev Mol Cell Biol* **25**, 511-512 (2024). https://doi.org/10.1038/s41580-024-00735-x

61 Torrino, S. *et al.* EHD2 is a mechanotransducer connecting caveolae dynamics with gene transcription. **217**, 4092-4105 (2018).

62 Grassart, A., Dujeancourt, A., Lazarow, P. B., Dautry-Varsat, A. & Sauvonnet, N. Clathrin-independent endocytosis used by the IL-2 receptor is regulated by Rac1, Pak1 and Pak2. *EMBO reports* **9**, 356-362-362 (2008).

63 Basquin, C. *et al.* Membrane protrusion powers clathrin-independent endocytosis of interleukin-2 receptor. *The EMBO Journal* **34**, 2147-2161-2161 (2015).

64 Gundu, C. *et al.* Dynamin-Independent Mechanisms of Endocytosis and Receptor Trafficking. *Cells* **11** (2022). https://doi.org/10.3390/cells11162557

65 Gupta, G. D. *et al.* Analysis of endocytic pathways in Drosophila cells reveals a conserved role for GBF1 in internalization via GEECs. *PLoS One* **4**, e6768 (2009). https://doi.org/10.1371/journal.pone.0006768

66 Lundmark, R. *et al.* The GTPase-Activating Protein GRAF1 Regulates the CLIC/GEEC Endocytic Pathway. **18**, 1802-1808 (2008).

67 Rivera-Milla, E., Stuermer, C. A. & Málaga-Trillo, E. Ancient origin of reggie (flotillin), reggie-like, and other lipid-raft proteins: convergent evolution of the SPFH domain. *Cell Mol Life Sci* **63**, 343-357 (2006). https://doi.org/10.1007/s00018-005-5434-3

68 Schweitzer, J. K., Sedgwick, A. E. & D'Souza-Schorey, C. ARF6-mediated endocytic recycling impacts cell movement, cell division and lipid homeostasis. *Semin Cell Dev Biol* **22**, 39-47 (2011). https://doi.org/10.1016/j.semcdb.2010.09.002

69 Uribe-Querol, E. & Rosales, C. Phagocytosis: Our Current Understanding of a Universal Biological Process. *Front Immunol* **11**, 1066 (2020). https://doi.org/10.3389/fimmu.2020.01066

70 Lin, X. P., Mintern, J. D. & Gleeson, P. A. Macropinocytosis in Different Cell Types: Similarities and Differences. *Membranes (Basel)* **10** (2020). https://doi.org/10.3390/membranes10080177

71 Zeigerer, A. *et al.* Rab5 is necessary for the biogenesis of the endolysosomal system in vivo. *Nature* **485**, 465-470 (2012). https://doi.org/10.1038/nature11133

72 Mohrmann, K., Gerez, L., Oorschot, V., Klumperman, J. & van der Sluijs, P. Rab4 function in membrane recycling from early endosomes depends on a membrane to cytoplasm cycle. *J Biol Chem* **277**, 32029-32035 (2002). https://doi.org/10.1074/jbc.M203064200

73 Sönnichsen, B., De Renzis, S., Nielsen, E., Rietdorf, J. & Zerial, M. Distinct membrane domains on endosomes in the recycling pathway visualized by multicolor imaging of Rab4, Rab5, and Rab11. *J Cell Biol* **149**, 901-914 (2000). https://doi.org/10.1083/jcb.149.4.901

74 Vagnozzi, A. N. & Praticò, D. Endosomal sorting and trafficking, the retromer complex and neurodegeneration. **24**, 857-868 (2019).

75 Frankel, E. B. & Audhya, A. ESCRT-dependent cargo sorting at multivesicular endosomes. *Semin Cell Dev Biol* **74**, 4-10 (2018). https://doi.org/10.1016/j.semcdb.2017.08.020

76 Gruenberg, J. Life in the lumen: The multivesicular endosome. *Traffic* **21**, 76-93 (2020). https://doi.org/10.1111/tra.12715

77 Poteryaev, D., Datta, S., Ackema, K., Zerial, M. & Spang, A. Identification of the switch in early-to-late endosome transition. *Cell* **141**, 497-508 (2010). https://doi.org/10.1016/j.cell.2010.03.011

78 Maxson, M. E. & Grinstein, S. The vacuolar-type H^+-ATPase at a glance - more than a proton pump. *J Cell Sci* **127**, 4987-4993 (2014). https://doi.org/10.1242/jcs.158550

79 Hessvik, N. P. & Llorente, A. Current knowledge on exosome biogenesis and release. *Cell Mol Life Sci* **75**, 193-208 (2018). https://doi.org/10.1007/s00018-017-2595-9

80 Sakamoto, K. M. *et al.* Protacs: chimeric molecules that target proteins to the Skp1-Cullin-F box complex for ubiquitination and degradation. *Proc Natl Acad Sci U S A* **98**, 8554-8559 (2001). https://doi.org/10.1073/pnas.141230798

81 Sakamoto, K. M. *et al.* Development of Protacs to target cancer-promoting proteins for ubiquitination and degradation. *Mol Cell Proteomics* **2**, 1350-1358 (2003). https://doi.org/10.1074/mcp.T300009-MCP200

82 Schneekloth, A. R., Pucheault, M., Tae, H. S. & Crews, C. M. Targeted intracellular protein degradation induced by a small molecule: En route to chemical proteomics. *Bioorg Med Chem Lett* **18**, 5904-5908 (2008). https://doi.org/10.1016/j.bmcl.2008.07.114

83 Ishida, T. & Ciulli, A. E3 Ligase Ligands for PROTACs: How They Were Found and How to Discover New Ones. *SLAS Discov* **26**, 484-502 (2021). https://doi.org/10.1177/2472555220965528

84 Tseng, Y.-L. *et al.* Degradation of neurodegenerative disease-associated TDP-43 aggregates and oligomers via a proteolysis-targeting chimera. **30**, 27 (2023).

85 Kargbo, R. B. PROTAC Molecules for the Treatment of Autoimmune Disorders. *ACS Med Chem Lett* **10**, 276-277 (2019). https://doi.org/10.1021/acsmedchemlett.9b00042

86 Galla, M. S., Sharma, N., Mishra, P. & Shankaraiah, N. Recent insights of PROTAC developments in inflammation-mediated and autoimmune targets: a critical review. *RSC Medicinal Chemistry* **15**, 2585-2600 (2024).

87 Li, X. *et al.* Proteolysis-targeting chimeras (PROTACs) in cancer therapy. **21**, 99 (2022).

88 Ge, J. *et al.* PROTAC-DB 3.0: an updated database of PROTACs with extended pharmacokinetic parameters. gkae768 (2024).

89 Wang, X. *et al.* Annual review of PROTAC degraders as anticancer agents in 2022. *Eur J Med Chem* **267**, 116166 (2024). https://doi.org/10.1016/j.ejmech.2024.116166

90 Xue, G., Wang, K., Zhou, D., Zhong, H. & Pan, Z. Light-Induced Protein Degradation with Photocaged PROTACs. *J Am Chem Soc* **141**, 18370-18374 (2019). https://doi.org/10.1021/jacs.9b06422

91 Naro, Y., Darrah, K. & Deiters, A. Optical Control of Small Molecule-Induced Protein Degradation. *J Am Chem Soc* **142**, 2193-2197 (2020). https://doi.org/10.1021/jacs.9b12718

92 Pfaff, P., Samarasinghe, K. T. G., Crews, C. M. & Carreira, E. M. Reversible Spatiotemporal Control of Induced Protein Degradation by Bistable PhotoPROTACs. *ACS Cent Sci* **5**, 1682-1690 (2019). https://doi.org/10.1021/acscentsci.9b00713

93 Zhang, L. *et al.* Development of a novel PROTAC using the nucleic acid aptamer as a targeting ligand for tumor selective degradation of nucleolin. *Molecular Therapy Nucleic Acids* **30**, 66-79 (2022).

94 Liu, J. *et al.* Cancer Selective Target Degradation by Folate-Caged PROTACs. *J Am Chem Soc* **143**, 7380-7387 (2021). https://doi.org/10.1021/jacs.1c00451

95 Dong, G., Ding, Y., He, S. & Sheng, C. Molecular Glues for Targeted Protein Degradation: From Serendipity to Rational Discovery. *Journal of Medicinal Chemistry* **64**, 10606-10620 (2021).

96 Asatsuma-Okumura, T., Ito, T. & Handa, H. Molecular mechanisms of cereblon-based drugs. *Pharmacol Ther* **202**, 132-139 (2019). https://doi.org/10.1016/j.pharmthera.2019.06.004

97 Fu, Y. *et al.* Degradation of lipid droplets by chimeric autophagy-tethering compounds. *Cell Res* **31**, 965-979 (2021). https://doi.org/10.1038/s41422-021-00532-7

98 Pei, J. *et al.* Developing potent LC3-targeting AUTAC tools for protein degradation with selective autophagy. *Chem Commun (Camb)* **57**, 13194-13197 (2021). https://doi.org/10.1039/d1cc04661f

99 Ji, C. H. *et al.* Targeted protein degradation via the autophagy-lysosome system: AUTOTAC (AUTOphagy-TArgeting Chimera). *Autophagy* **18**, 2259-2262 (2022). https://doi.org/10.1080/15548627.2022.2091338

100 Ahn, G. *et al.* LYTACs that engage the asialoglycoprotein receptor for targeted protein degradation. *Nat Chem Biol* **17**, 937-946 (2021). https://doi.org/10.1038/s41589-021-00770-1

101 Caianiello, D. F. *et al.* Bifunctional small molecules that mediate the degradation of extracellular proteins. *Nat Chem Biol* **17**, 947-953 (2021). https://doi.org/10.1038/s41589-021-00851-1

102 Zhou, Y., Teng, P., Montgomery, N. T., Li, X. & Tang, W. Development of Triantennary N-Acetylgalactosamine Conjugates as Degraders for Extracellular Proteins. *ACS Cent Sci* **7**, 499-506 (2021). https://doi.org/10.1021/acscentsci.1c00146

103 Stevens, C. M. *et al.* Development of Oligomeric Mannose-6-phosphonate Conjugates for Targeted Protein Degradation. *ACS Med Chem Lett* **14**, 719-726 (2023). https://doi.org/10.1021/acsmedchemlett.2c00479

104 Donahue, T. C. *et al.* Synthetic Site-Specific Antibody-Ligand Conjugates Promote Asialoglycoprotein Receptor-Mediated Degradation of Extracellular Human PCSK9. *ACS Chem Biol* **18**, 1611-1623 (2023). https://doi.org/10.1021/acschembio.3c00229

105 Zhang, X. *et al.* Site-Specific Chemoenzymatic Conjugation of High-Affinity M6P Glycan Ligands to Antibodies for Targeted Protein Degradation. *ACS Chem Biol* **17**, 3013-3023 (2022). https://doi.org/10.1021/acschembio.1c00751

106 Miao, Y. *et al.* Bispecific Aptamer Chimeras Enable Targeted Protein Degradation on Cell Membranes. *Angew Chem Int Ed Engl* **60**, 11267-11271 (2021). https://doi.org/10.1002/anie.202102170

107 Wu, Y. *et al.* Aptamer-LYTACs for Targeted Degradation of Extracellular and Membrane Proteins. *Angew Chem Int Ed Engl* **62**, e202218106 (2023). https://doi.org/10.1002/anie.202218106

108 Wang, K. *et al.* Nano-LYTACs for Degradation of Membrane Proteins and Inhibition of CD24/Siglec-10 Signaling Pathway. *Adv Sci (Weinh)* **10**, e2305364 (2023). https://doi.org/10.1002/advs.202305364

109 Bagdanoff, J. T. *et al.* Clearance of plasma PCSK9 via the asialoglycoprotein receptor mediated by heterobifunctional ligands. *Cell Chem Biol* **30**, 97-109.e109 (2023). https://doi.org/10.1016/j.chembiol.2022.12.003

110 Zheng, J. *et al.* Bifunctional Compounds as Molecular Degraders for Integrin-Facilitated Targeted Protein Degradation. *J Am Chem Soc* **144**, 21831-21836 (2022). https://doi.org/10.1021/jacs.2c08367

111 Zhou, Y., Liao, Y., Zhao, Y. & Tang, W. Development of Integrin Targeting Chimeras (ITACs) for the Lysosomal Degradation of Extracellular Proteins. *ChemMedChem*, e202300643 (2024). https://doi.org/10.1002/cmdc.202300643

112 Zhou, Y. *et al.* Development of folate receptor targeting chimeras for cancer selective degradation of extracellular proteins. *Nat Commun* **15**, 8695 (2024). https://doi.org/10.1038/s41467-024-52685-9

113 Yun, C. *et al.* Glucose Transporter-Targeting Chimeras Enabling Tumor-Selective Degradation of Secreted and Membrane Proteins. *ACS Chem Biol* **19**, 2254-2263 (2024). https://doi.org/10.1021/acschembio.4c00584

114 Zhang, D. *et al.* Transferrin receptor targeting chimeras for membrane protein degradation. *Nature* (2024). https://doi.org/10.1038/s41586-024-07947-3

115 Pance, K. *et al.* Modular cytokine receptor-targeting chimeras for targeted degradation of cell surface and extracellular proteins. *Nat Biotechnol* (2022). https://doi.org/10.1038/s41587-022-01456-2

116 Zhang, B. *et al.* Insulin-like Growth Factor 2 (IGF2)-Fused Lysosomal Targeting Chimeras for Degradation of Extracellular and Membrane Proteins. *J Am Chem Soc* **145**, 24272-24283 (2023). https://doi.org/10.1021/jacs.3c08886

117 Mikitiuk, M. *et al.* IGF2 Peptide-Based LYTACs for Targeted Degradation of Extracellular and Transmembrane Proteins. *Molecules* **28** (2023). https://doi.org/10.3390/molecules28227519

118 Yang, J. L. *et al.* Directed evolution of genetically encoded LYTACs for cell-mediated delivery. *Proc Natl Acad Sci U S A* **121**, e2320053121 (2024). https://doi.org/10.1073/pnas.2320053121

119 Sun, R., Meng, Z., Lee, H., Offringa, R. & Niehrs, C. ROTACs leverage signaling-incompetent R-spondin for targeted protein degradation. *Cell Chem Biol* **30**, 739-752.e738 (2023). https://doi.org/10.1016/j.chembiol.2023.05.010

120 Wang, Q. *et al.* A co-assembly platform engaging macrophage scavenger receptor A for lysosome-targeting protein degradation. *Nat Commun* **15**, 1663 (2024). https://doi.org/10.1038/s41467-024-46130-0

121 Zhu, C., Wang, W., Wang, Y., Zhang, Y. & Li, J. Dendronized DNA Chimeras Harness Scavenger Receptors To Degrade Cell Membrane Proteins. *Angew Chem Int Ed Engl* **62**, e202300694 (2023). https://doi.org/10.1002/anie.202300694

122 Liu, Z. *et al.* Enantioselective Degrader for Elimination of Extracellular Aggregation-Prone Proteins hIAPP Associated with Type 2 Diabetes. *ACS Nano* **17**, 8141-8152 (2023). https://doi.org/10.1021/acsnano.2c11476

123 Zhu, L. *et al.* Conjugation with glucagon like peptide-1 enables targeted protein degradation. *Bioorg Chem* **141**, 106908 (2023). https://doi.org/10.1016/j.bioorg.2023.106908

124 Luo, J. *et al.* Lysosome Targeting Chimaeras for Glut1-Facilitated Targeted Protein Degradation. *J Am Chem Soc* **146**, 17728-17737 (2024). https://doi.org/10.1021/jacs.4c02463

125 Yu, J. *et al.* Harnessing the Lysosomal Sorting Signals of the Cation-Independent Mannose-6-Phosphate Receptor for Targeted Degradation of Membrane Proteins. *J Am Chem Soc* **145**, 19107-19119 (2023). https://doi.org/10.1021/jacs.3c07687

126 Fang, T. *et al.* Lysosome-targeting chimeras containing an endocytic signaling motif trigger endocytosis and lysosomal degradation of cell-surface proteins. *Chem Sci* (2024). https://doi.org/10.1039/d4sc05093b

127 Huang, B. *et al.* Designed endocytosis-inducing proteins degrade targets and amplify signals. *Nature* (2024). https://doi.org/10.1038/s41586-024-07948-2

Chapter 2

A platform for the rapid synthesis of proteolysis targeting chimeras (Rapid-TAC) under miniaturized conditions

This chapter is adapted from a manuscript published in *European Journal of Medicinal Chemistry*.

Guo, L.[#], **Zhou, Y.[#]**, Nie, X.[#], Zhang, Z., Zhang, Z., Li, C., Wang, T., and Tang, W.* A Platform for the Rapid Synthesis of Proteolysis Targeting Chimeras (Rapid-TAC) under Miniaturized Conditions" *Eur. J. Med. Chem.* **2022**, *236*, 114317.

[#]These authors contributed equally to this work

*To whom correspondence should be addressed

2.1. Abstract

Proteolysis targeting chimera (PROTAC) is one of the most frequently used technologies for targeted protein degradation. PROTACs are composed of target protein ligand, E3 ligase ligand and a linker between them. Traditional methods for the development of PROTACs involve step-by-step synthesis and are time consuming. Herein, we report a platform for the rapid synthesis of PROTACs (Rapid-TAC) via a traceless coupling reaction between ortho-phthalaldehyde (OPA) motif on the ligand of targeting protein and an amine functional group on the commercially available partial PROTAC library that is composed of different E3 ligase ligands and various types and lengths of linkers. Under our optimized miniaturized conditions, the full PROTACs can be synthesized in a high throughput manner and the products can be directly used for screening without any further manipulations including purification. We demonstrated the utility of this platform by quickly identifying active degraders for androgen receptor (AR) and Bromodomain-containing protein 4 (BRD4) with DC_{50} of 41.9 nM and 8.9 nM, respectively. It is expected that this Rapid-TAC platform can be easily extended to many other targets, thus lowering the barrier to access this novel modality for small molecule drug discovery and facilitate structure activity relationship studies.

2.2. Introduction

Proteolysis targeting chimera (PROTAC), initially introduced twenty years ago[1], represents a revolutionary technology for small molecule drug discovery. PROTACs are composed of a ligand for the protein of interest (POI), a ligand for E3 ubiquitin ligase, and a linker between the two ligands. Upon forming the E3-PROTAC-POI ternary complex, the POI is polyubiquitinated and undergoes subsequent proteasomal

degradation[2-7]. Traditional small molecule drugs need to bind to the protein target and change its function. In contrast, PROTAC only needs a binder, which can be non-functional by itself. This opens up the opportunity to target a large number of undrugged proteins that lack functional binding sites for small molecules[8]. In addition, PROTACs can act catalytically to degrade the entire POI via an event-driven mode, which offers great opportunities for achieving the desired pharmacological outcomes. Since its discovery, numerous protein targets in various families have been successfully degraded using the PROTAC strategy. A number of PROTACs are currently under investigated clinically for the treatment of various human diseases[9].

For the development of PROTACs, synthesis and screening of a library of compounds is still the most viable approach to integrate the three components including the ligand of POI, the ligand of E3 ligase and the linker between them for the generation of active degraders. The length, type, and position of the linker can often significantly affect the activity of the degraders. Various chemical methods have been used to accelerate the development of PROTACs and facilitate the SAR studies, such as coupling one ligand bearing the linker with the other ligand using activated esters[10,11], click chemistry[12,13], solid-phase synthesis[14], alkylation reaction[15], Staudinger ligation[16], and multicomponent synthesis[17]. However, the PROTACs need to be synthesized one by one and the final product needs to be purified for further biological evaluations using these methods. It is thus difficult to prepare the library in a high throughput manner. Our group previously reported a strategy for the rapid synthesis of PROTACs (Rapid-TAC) by reacting hydrazide A1 in the POI ligand with aldehyde A2 containing a E3 ligase ligand and various linkers (Fig. 2.1)[18]. The reaction can be carried out under

miniaturized conditions for the high throughput synthesis of PROTACs in DMSO solution, which can be directly used for biological testing without further manipulation including purification, because the conversion is generally higher than 80% and the only byproduct is water. Most functional groups in both ligands are also compatible with the conditions.

However, the acylhydrazone motif in product A3 is hydrolytically labile, which can be a significant issue for assays that require long treatment time and long-term storage after multiple rounds of free-thaw cycles. To solve this problem, we used a two-stage strategy for the development of active and stable PROTACs. In the first stage, we identified active degraders with an appropriate E3 ligase ligand and an optimal linker (e.g., type and length) from a library of compounds A3 using assays that require a relatively short period of time. In the second stage, we replaced the acylhydrazone motif in the linker region by a more stable isostere such as an amide while keeping the rest of the active molecule largely intact. The two-strategy led to the successful development of stable and potent PROTACs for estrogen receptor quickly[18]. However, the change of the acylhydrazone motif to its isosteres can often significantly alter the activity of the degraders and further time-consuming optimization may be required in some cases. In addition, the aldehyde-containing partial PROTAC library A2 is not commercially available and needs to be prepared by step-by-step synthesis.

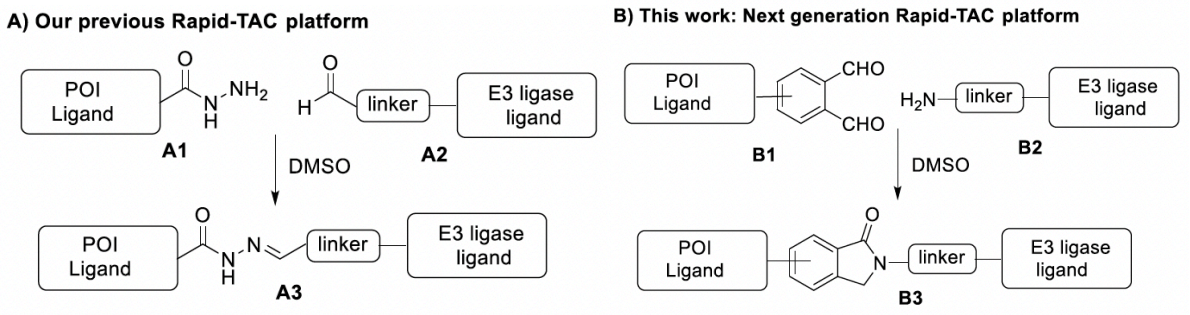

Figure 2.1. Platforms for the rapid synthesis of PROTACs (Rapid-TAC) under miniaturized conditions for direct screening without further manipulations. A) Our previous Rapid-TAC Platform based on hydrazide-aldehyde coupling chemistry. **B)** Our new Rapid-TAC platform based on OPA-amine coupling chemistry.

We recently reported our next generation Rapid-TAC platform that can overcome many of the limitations in our previous strategy while keeping most of the advantages for the development of PROTACs. The key to our new platform is the formation of phthalimidine B3 from ortho-phthalaldehyde (OPA) B1 and amine B2, a reaction that has been known for a long time[19]. The phthalimidine motif can be part of the POI ligand or part of the linker. The addition of amine RNH2 to ortho-phthalaldehyde first produces the isoindolinediol intermediate, which can tautomerize to phthalimidine after the elimination of water[20,21]. The reaction has been recently optimized for the modification of peptides and protein labeling and profiling under biocompatible conditions[22-25]. Dr. Le Guo prepared two PROTACs libraries, one for androgen receptor (AR) and the other for bromodomain-containing protein 4 (BRD4), using this highly efficient OPA-amine coupling chemistry from two building blocks B1 and a library of commercially available amine-containing E3 ligase ligands with various linkers. With an appropriate building block B1 in hand, the library can be completed under miniaturized conditions in parallel in a reaction block, which does not require any further manipulation before

the cell-based screening because the only byproduct is water and the conversion is generally very high, a nearly ideal reaction[26].

2.3. Design of Rapid-TAC platform

Chemistry postdoc Dr. Le Guo first set out to optimize the reaction conditions to fit the Rapid-TAC platform for a model reaction in Fig. 2. The choice of solvent is limited to either water or DMSO to avoid any further manipulation after the synthesis. Although the desired product C3 could be detected under previously reported conditions in PBS (pH 7.4) buffer, a complex mixture was obtained (Fig. 2.2, entry 1). He observed much better results after switching the solvent from PBS buffer to DMSO and the purity of the crude product could reach 84%. He then found that the addition of HOAc additive could significantly improve the conversion and the purity of the product C3 could reach 99%! Because the products will be diluted by buffer before adding to the cells, the HOAc additive is generally inconsequential for the screening.

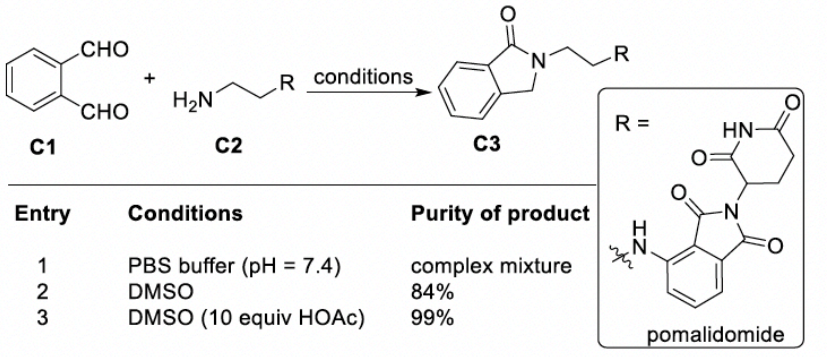

Entry	Conditions	Purity of product
1	PBS buffer (pH = 7.4)	complex mixture
2	DMSO	84%
3	DMSO (10 equiv HOAc)	99%

Figure 2.2. Optimization of the OPA-amine coupling reaction for the Rapid-TAC platform. Reaction was conducted with C1 (20 mL of 50 mM DMSO solution), C2 (20 mL of 50 mM DMSO solution), additive, and solvent at 80 °C for 48 h. The purity of C3 directly from the reaction mixture was determined by HPLC. Note: These experiments were completed by Dr. Le Guo.

To this end, he prepared AR ligand 3 bearing a OPA motif by linking part of AR ligand 1 with the carboxylic acid-containing OPA precursor 2 (Fig. 2.3). The benzene ring of the phthalimidine motif is actually part of the AR ligand in this case[27,28]. For the E3 ligase ligand portion, he used two commercially available partial PROTAC libraries. One of them has 9 members that are composed of a pomalidomide cereblon E3 ligase ligand and various alkyl or polyethylene glycol units (PEG) linkers. The other one has 11 members that are composed of a Von-Hippel-Lindau (VHL) E3 ubiquitin ligase ligand and various alkyl or PEG linkers. These two commercially available partial PROTAC library all contain the NH2 group on the other end of the linker. Each of these building blocks was dissolved in DMSO as a 50 mM stock solution. OPA derivative 3 was also dissolved in DMSO with the same concentration. Dr. Le Guo next mixed 20 mL of solution 3 with the stock solution of each member of the amine-linker-E3 ligase ligand partial PROTAC library in a 1:1 ratio. The solution was then heated at 80 °C for 24 h. After cooling it to room temperature, to the solution was added another 60 mL of DMSO. The resulting solution was heated at 80°C for another 24 h. The solution was then cooled down to room temperature and the purity of the product was analyzed by HPLC. Out of the 21 potential AR PROTACs LG-AR-1 to LG-AR-21, we found that the purity ranged from 88% to 98% (Fig. 2.3). The “linker-less” PROTAC LG- AR-21 bearing a lenalidomide motif was prepared by reacting 3 with 3-aminopiperidine-2,6-dione directly. Without any further manipulation including purification, this PROTAC library can be directly evaluated for their biological activity. The reaction worked smoothly for all members of the partial PROTAC library bearing a cereblon ligand. For all members of partial PROTAC library that contain a VHL ligand, however, we observed significant

amount of byproducts derived from the cleavage of amide bond between the proline residue and the a-tBu glycine residue. Dr. Le Guo then found that the addition of 2 equivalent of KOAc could suppress this cleavage. Because all of the partial PROTAC library were purchased as their hydrochloride salt, it is likely that the HCl in the system caused the issue and needs to be quenched by KOAc.

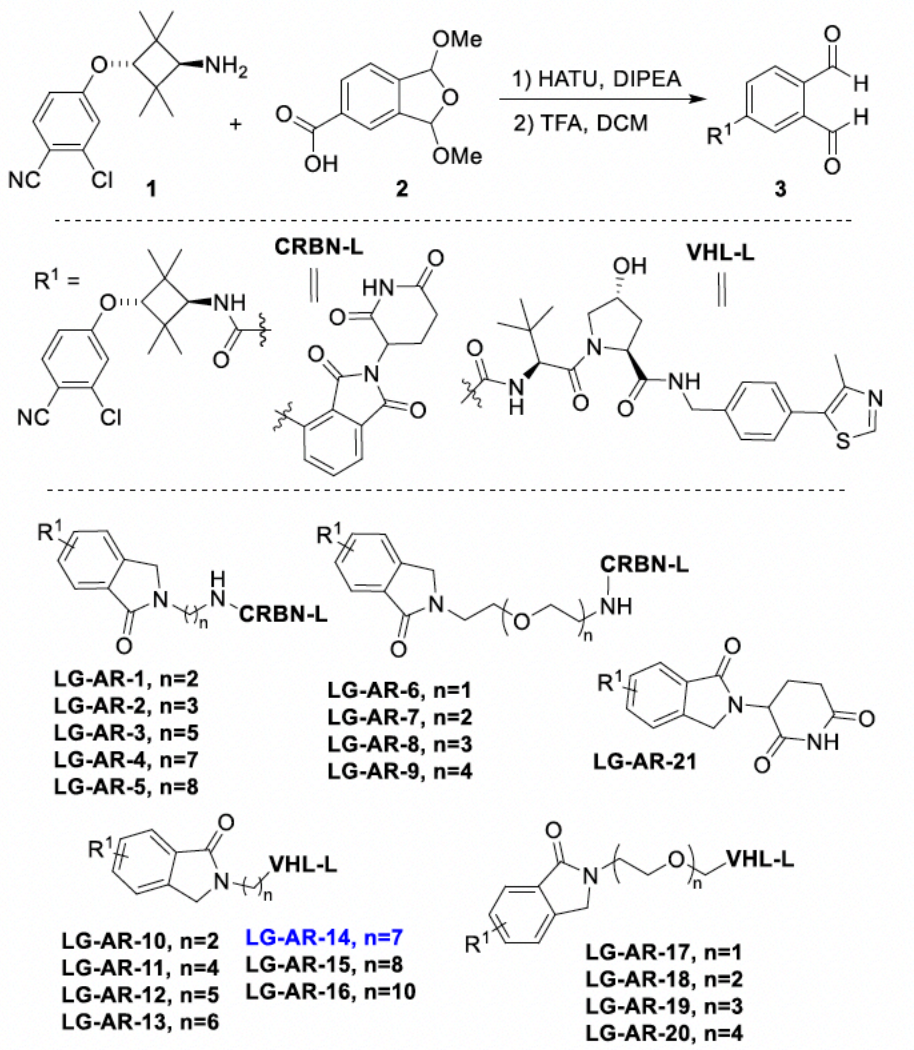

Figure 2.3. Synthesis of 21 AR PROTACs using the Rapid-TAC platform. Note: All compounds are prepared by Dr. Le Guo.

2.4. Result and discussion

2.4.1. The degradation of AR by Rapid-TAC platform in LNCap cells

Next, I tested the activity of the 21 potential AR PROTACs LG- AR-1 to LG-AR-21 at 1 and 10 μM concentrations in LNCap prostate cancer cells. For the cereblon-recruiting AR PROTACs, no significant degradation was observed (Fig. 2.4). For VHL-recruiting AR PROTACs, many of them showed certain degree of degradation. Not surprisingly, the type and length of linkers played a significant role. Based on the screening result, LG-AR-14 (n = 7) containing a linker with seven methylene groups, is the most effective degrader for AR (Figs. 2.4). Interestingly, LG-AR-14 reduced AR protein by 40% at 10 μM and by 73% at 1 μM, a classical “hook” effect that has been observed for many PROTACs[29].

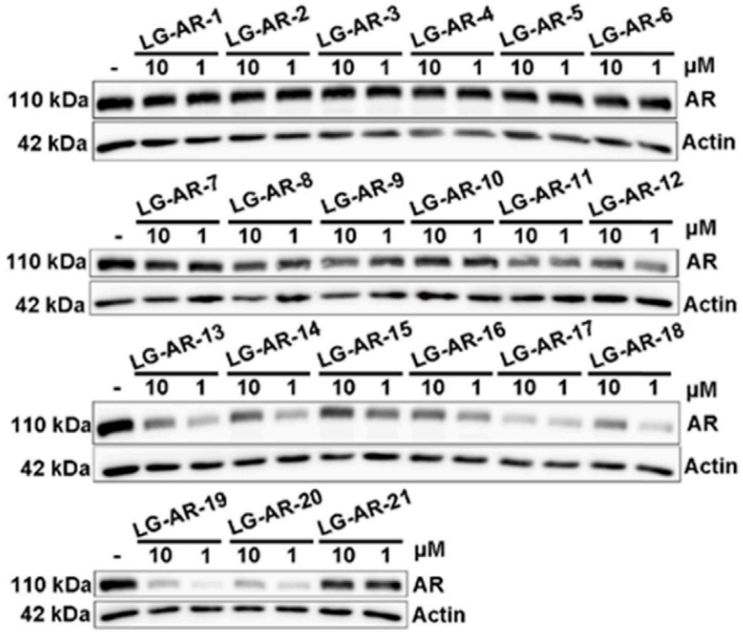

Figure 2.4. A library of 21-members of AR PROTACs was tested by Western blot assay in LNCap cell line for 16 h at 1 μM and 10 μM concentrations.

2.4.2. Comparison of cyclic amide AR degrader with two isomers of LG-AR-14

The coupling of substituted OPA with amine will always lead to two isomers that are differ from each other on the position of the carbonyl oxygen in phthalimidine product. The difference between the two isomers is so small that we do not expect this difference impacts the activity. In addition, the cyclic amide is generally exposed to the solvent and should not impact the binding to the POI. Nevertheless, we still decided to synthesize the two isomers, LG-AR-14-A and LG-AR-14-B, separately using the standard chemistry and purification procedures to compare their activity (Fig. 2.5A). In addition, we also synthesized and purified compound LG-AR-14-C with a secondary amide, which is closely related LG-AR-14A/B. These three AR PROTACs were evaluated by Western blot assay for their degradation activity for AR. Not surprisingly, the degradation activity of LG-AR-14A and LG-AR-14B is almost identical to LG-AR-14, the mixture generated from our Rapid-TAC platform without any purification (Fig. 2.5B). Interestingly, PROTAC LG-AR-14-C showed slightly lower degradation activity of AR protein than LG-AR-14A and LG-AR-14B, indicating that the cyclic tertiary amide is better than the acyclic secondary amide as part of the linker in this case. Based on these results, it is reasonable to expect that the PROTACs derived from OPA-amine coupling Rapid-TAC platform without purification will have similar activity comparing to the step-by-step synthesized PROTACs with purifications after each step.

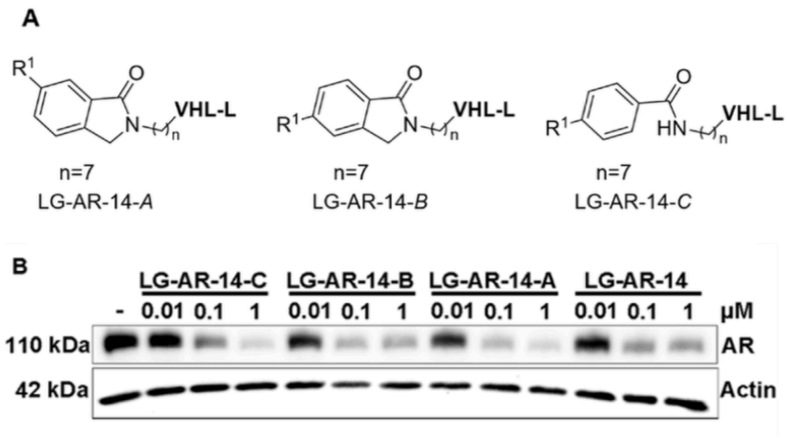

Figure 2.5. Optimization of LG-AR-14. A) The structures of three AR PROTACs based on LG-AR-14. They are synthesized and purified using standard protocols by Dr. Le Guo. **B)** AR PROTACs were tested by Western blot in LNCap cell line for 16 h at 0.1 μM, 1 μM and 10 μM concentrations.

2.4.3. The characterization of candidate AR PROTACs

I then examined the time course of LG-AR-14-A for the induction of AR degradation in LNCap cell line. The data showed that LG-AR-14-A effectively reduced the AR protein level within 6 h and it was sufficient to reach the max degradation at 16 h (Fig. 2.6A). I next tested the dose response of LG-AR-14-A in LNCap cell line. The results showed that LG-AR-14-A induced degradation of AR protein in a dose-dependent manner (Fig. 2.6B). The concentration at which half-maximal degradation occurs (DC_{50}) for LG-AR-14-A was 41.9 nM in the LNCap cell line. I next investigated the mechanism of action of LG-AR-14-A in the LNCaP cell line. The results showed that AR degradation induced by LG-AR-14-A can be effectively abolished by the pretreatment with NEDD8-activating enzyme inhibitor MLN4924, VHL ligand, AR ligand or proteasome inhibitor MG132 (Figs. 2.6C). These results clearly demonstrated that LG-AR-14-A followed the conventional PROTAC mechanism that requires the participation of E3 ligase, AR, neddylation, and proteasome.

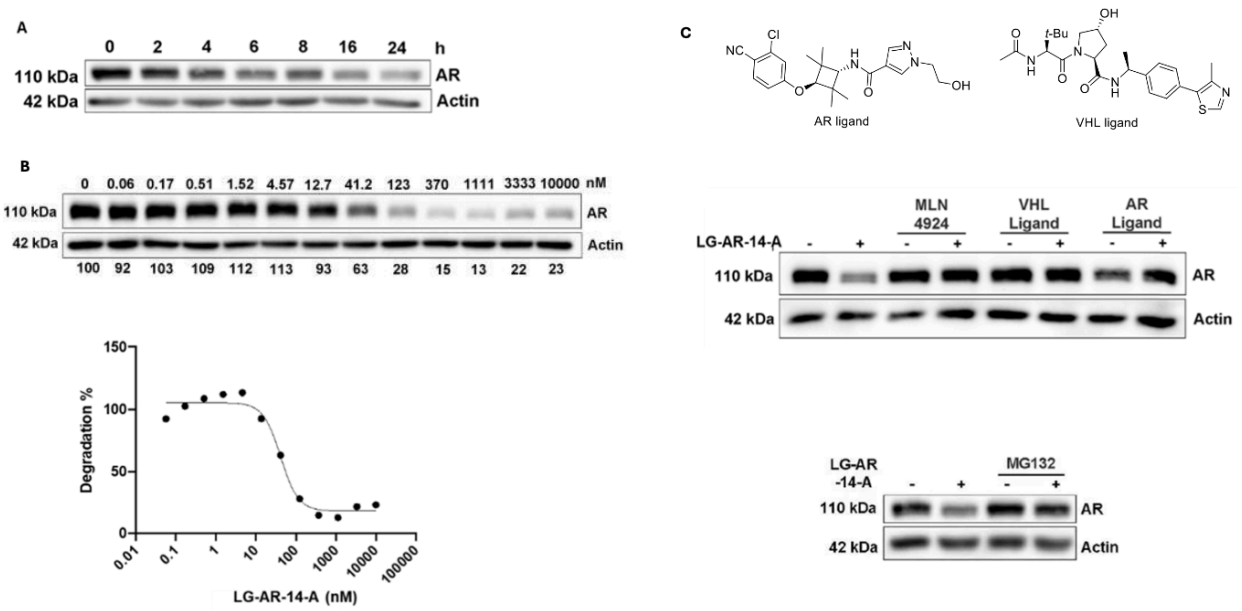

Figure 2.6. Characterization of LG-AR-14-A. A) Time course of LG-AR-14-A. LNCap cells were treated with LG-AR-14-A at 100 nM for different time and the results were analyzed by Western blot. **B)** Dose response of LG-AR-14-A. LNCap cells were treated with LG-AR-14-A for 16 h at different concentrations and the results were analyzed by Western blot. **C)** Mechanistic studies of AR degradation induced by LG-AR-14-A in LNCap cells. Cells were co-treated with AR ligand (10 μM), VHL ligand (10 μM), and MLN4924 (0.5 μM) together with LG- AR-14-A (100 nM) for 8 h; Cell were co-treated with MG132 (5 μM) for 2 h and then together with LG-AR-14-A (100 nM) for another 6 h.

2.4.4. The degradation of BRD4 by Rapid-TAC platform in MV-4-11 cells

To further demonstrate the utility of OPA-amine coupling based Rapid-TAC platform, Dr. Le Guo prepared a library of potential PROTACs for the second target, BRD4. He first synthesized BRD4 ligand 6 bearing OPA by linking BRD4 ligand 4 derived from JQ1 with the bromide-containing OPA precursor 5 followed by hydrolysis (Fig. 2.7). Previously, the OPA building block contains a carboxylate handle, which can be coupled with an amine-containing ligand of the target. A complementary approach was used for the preparation of key building block 6, which was derived from the cross-coupling reaction between an aryl bromide and a ligand bearing a carboxylate

derivative. OPA building blocks 2 and 5 can be used for any POI ligands with an amine or carboxylate handle, respectively. Using the OPA-amine Rapid-TAC platform, Dr. Le Guo synthesized 21 potential BRD4 PROTACs (LG-BRD-1 to 21) quickly in DMSO solution following the same protocol described previously (Fig. 2.7). Out of the 21 products, their purity ranged from 78% to 96%. Graduate student Xueqing Nie next tested the activity of the 21 potential BRD4 PROTACs in MV-4-11 cell line (Fig. 2.8). Our results showed that there was no obvious degradation for PROTACs LG-BRD-1 to LG-BRD-10 derived by pomalidomide. For PROTACs derived from VHL ligand, LG-BRD-12 with four methylene units in the linker was able to reduce the BRD4 protein significantly at 1 μM as the most potent compound in this series. The classical “hook” effect was observed for some of the PROTACs at 10 μM.

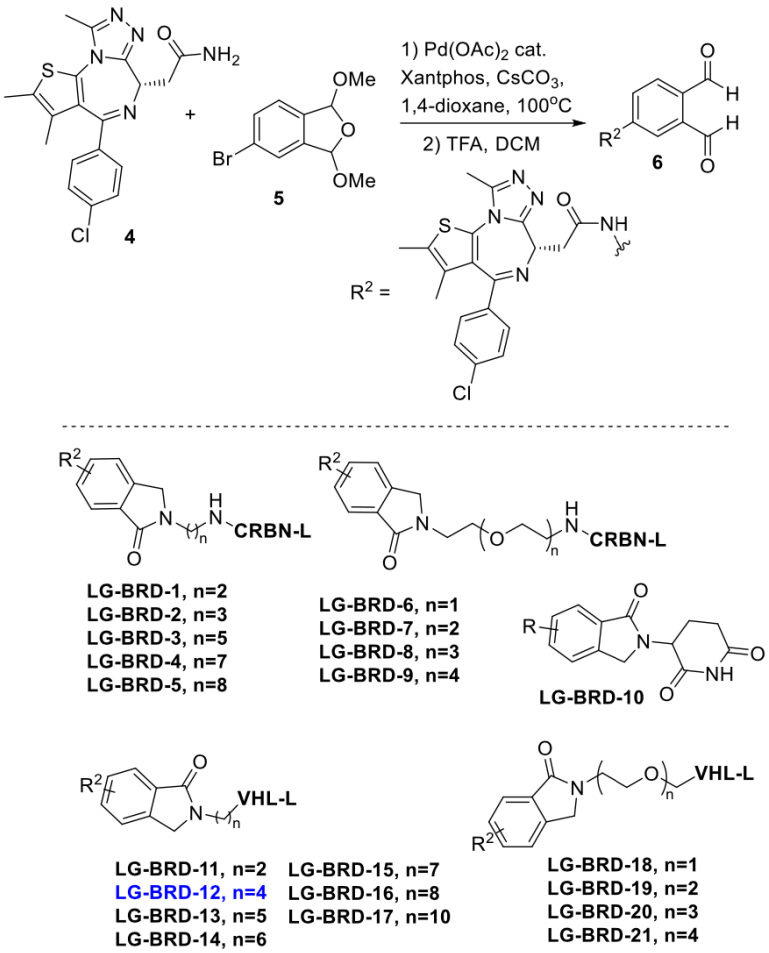

Figure 2.7. Synthesis of 21 BRD4 PROTACs using the Rapid-TAC platform. Note: All compounds were prepared by Le Guo.

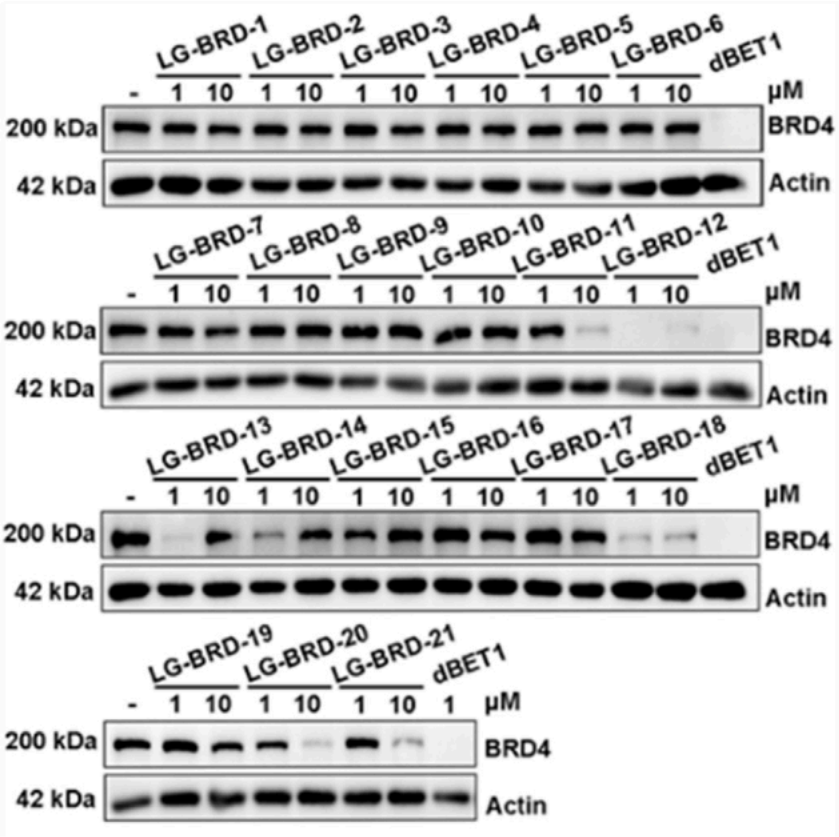

Figure 2.8. A library of 21 members of BRD4 PROTACs was tested by Western blot in MV-4-11 cell line for 24 h at 1 μM and 10 μM concentrations. Note: These experiments were completed by Xueqing Nie.

2.4.5. Comparison of BRD4 degrader LG-BRD-12 with its isomers

Next, Dr. Le Guo synthesized the two isomers of BRD4 degrader, LG-BRD-12A and LG-BRD-12B, separately using the standard chemistry and purification procedures to compare their activity (Fig. 2.9A). These two BRD4 PROTACs were evaluated by Western blot assay for their degradation activity for BRD4 at four different concentrations. Interestingly, LG-BRD-12B showed much higher degradation activity than LG-BRD-12A (Fig. 2.9B). A dose response study was then conducted for compound LG-BRD-12B in MV-4-11 cell line and observed a DC_{50} of 8.9 nM (Fig. 2.9C). We demonstrated that effective BRD4 degraders could be identified quickly using our

OPA-amine coupling reaction based Rapid-TAC platform.

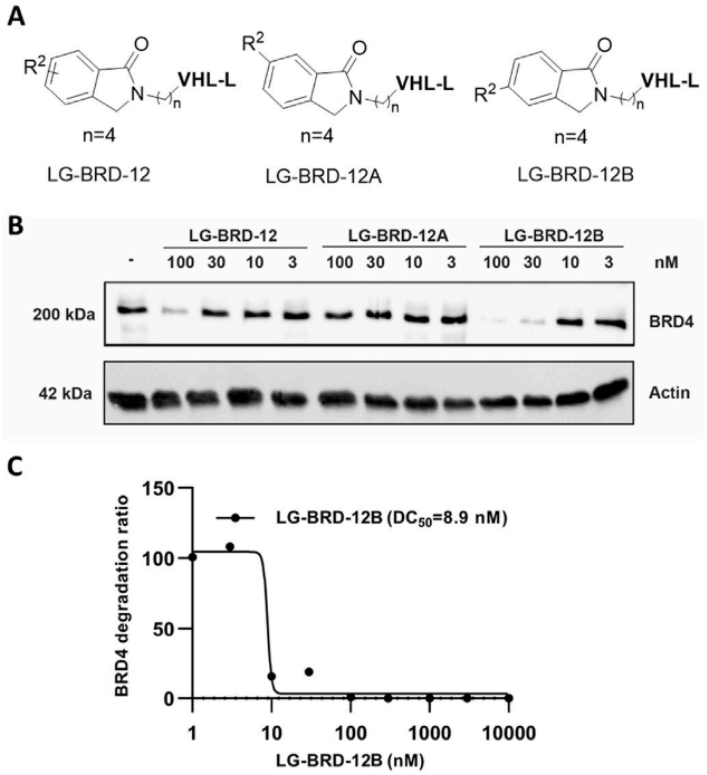

Figure 2.9. Optimization and characterization of LG-BRD-12. A) The structures of two AR PROTACs based on LG-BRD-12. They are synthesized and purified using standard protocols. **B)** BRD4 PROTACs were tested by Western blot in MV-4-11 cell line for 12 h at 100 nM, 30 nM, 10 nM and 3 nM concentrations. **C)** Dose response of LG-BRD-12B. MV-4-11 cells were treated with LG-BRD-12B for 12 h at different concentrations and the results were analyzed by Western blot. **Note:** These experiments were completed by Zhongrui Zhang and Chunrong Li.

2.5. Conclusions

In conclusion, we have developed a novel platform for the rapid synthesis of PROTACs under miniaturized conditions using highly efficient OPA-amine coupling reaction, which produces water as the only byproduct. Using commercially available E3 ligase ligand-linker-NH2 building blocks, this new generation of Rapid-TAC platform can quickly yield a library of stable PROTACs with various linker lengths/types and E3

ligase ligands. The products have sufficient purity and can be directly used for cell-based screening without any further manipulation. The OPA-amine coupling chemistry is compatible with most of the common functional groups. The platform is validated by the quick development of active PROTACs for AR and BRD4. We expect that this new Rapid-TAC platform can be a powerful tool for the development of PROTACs against many other targets. It has the potential to significantly lower the barrier to access PROTACs, a revolutionary technology for small molecule drug discovery, and facilitate the structure activity relationship studies of PROTACs against various targets.

2.6 Experimental procedures

2.6.1. Cell lines and materials

LNCap cells were maintained in RPMI supplemented with 10% fetal bovine serum, 1% HEPES, 1% sodium pyruvate and 1% penicillin/streptomycin under 5% CO_2 at 37 °C. MV-4-11 cells were cultured in Iscove's Modified Dulbecco's Media (IMDM) supplemented with 10% FBS and 1% penicillin/streptomycin under 5% CO_2 at 37 °C. Androgen receptor (#5153) antibody was obtained from Cell Signaling Technologies. b-Actin (C4) HRP (sc-47778) antibody was obtained from Santa Cruz Biotechnologies. Anti-Brd4 antibody (ab128874) was obtained from Abcam.

2.6.2. Western Blotting

Cells were lysed in 1X RIPA lysis buffer containing 25 mM Tris, pH 7-8, 150 mM NaCl, 0.1% (w/v) sodium dodecyl sulfate (SDS), 0.5% sodium deoxycholate, 1% (v/v) Triton X-100, Roche protease inhibitor cocktail and 1 mM phenylmethylsulfonyl fluoride. Protein samples were adjusted to the equal amount after determining the concentrations by

BCA assay and then loaded onto 7.5% SDS polyacrylamide gel electrophoresis. After transferring, the membrane was first blocked in 5% (w/v) nonfat milk in the TBS-T washing buffer (137 mM NaCl, 20 mM Tris, 0.1% (v/v) Tween) and then incubated with primary antibodies at 4 °C overnight. Next day, the membrane was incubated with secondary HRP-linked antibodies for 1 h followed by acquisition of the immunoblot using ChemiDoc MP Imaging Systems.

2.6.3. Cell viability assay

LNCap cells were seeded at the density of 2000 cell per well in a 96-well plate. Next day, cells were treated with LG-AR-14-A at indicated concentrations and incubated in regular media for 6 days. Cell viability was measured using AlamarBlue assay by adding 10x AlamarBlue (0.5 mg/mL) to the well and incubated at 37 °C for 2 h. Fluorescent intensity was then determined at 650 nm excitation/680 nm emission and the percentage of cell viability was generated by normalizing to DMSO treated cells.

2.7. References

1 Sakamoto, K. M. *et al.* Protacs: chimeric molecules that target proteins to the Skp1-Cullin-F box complex for ubiquitination and degradation. *Proc Natl Acad Sci U S A* **98**, 8554-8559 (2001). https://doi.org/10.1073/pnas.141230798

2 Buckley, D. L. & Crews, C. M. Small-molecule control of intracellular protein levels through modulation of the ubiquitin proteasome system. *Angew Chem Int Ed Engl* **53**, 2312-2330 (2014). https://doi.org/10.1002/anie.201307761

3 Luh, L. M. *et al.* Prey for the Proteasome: Targeted Protein Degradation-A Medicinal Chemist's Perspective. *Angew Chem Int Ed Engl* **59**, 15448-15466 (2020). https://doi.org/10.1002/anie.202004310

4 Nalawansha, D. A. & Crews, C. M. PROTACs: An Emerging Therapeutic Modality in Precision Medicine. *Cell Chem Biol* **27**, 998-1014 (2020). https://doi.org/10.1016/j.chembiol.2020.07.020

5 Samarasinghe, K. T. G. & Crews, C. M. Targeted protein degradation: A promise for undruggable proteins. *Cell Chem Biol* **28**, 934-951 (2021). https://doi.org/10.1016/j.chembiol.2021.04.011

6 Tomoshige, S. & Ishikawa, M. PROTACs and Other Chemical Protein Degradation Technologies for the Treatment of Neurodegenerative Disorders.

Angew Chem Int Ed Engl **60**, 3346-3354 (2021). https://doi.org/10.1002/anie.202004746

7 Toure, M. & Crews, C. M. Small-Molecule PROTACS: New Approaches to Protein Degradation. *Angew Chem Int Ed Engl* **55**, 1966-1973 (2016). https://doi.org/10.1002/anie.201507978

8 Dang, C. V., Reddy, E. P., Shokat, K. M. & Soucek, L. Drugging the 'undruggable' cancer targets. *Nat Rev Cancer* **17**, 502-508 (2017). https://doi.org/10.1038/nrc.2017.36

9 Mullard, A. Targeted protein degraders crowd into the clinic. *Nat Rev Drug Discov* **20**, 247-250 (2021). https://doi.org/10.1038/d41573-021-00052-4

10 Papatzimas, J. *et al.* A General Strategy for the Preparation of Thalidomide-Conjugate Linkers. **28** (2017).

11 Brownsey, D. K., Rowley, B. C., Gorobets, E., Gelfand, B. S. & Derksen, D. J. Rapid synthesis of pomalidomide-conjugates for the development of protein degrader libraries. *Chem Sci* **12**, 4519-4525 (2021). https://doi.org/10.1039/d0sc05442a

12 Wurz, R. P. *et al.* A "Click Chemistry Platform" for the Rapid Synthesis of Bispecific Molecules for Inducing Protein Degradation. *J Med Chem* **61**, 453-461 (2018). https://doi.org/10.1021/acs.jmedchem.6b01781

13 Liu, H. *et al.* Construction of an IMiD-based azide library as a kit for PROTAC research. *Org Biomol Chem* **19**, 166-170 (2021). https://doi.org/10.1039/d0ob02120b

14 Krajcovicova, S., Jorda, R., Hendrychova, D., Krystof, V. & Soural, M. Solid-phase synthesis for thalidomide-based proteolysis-targeting chimeras (PROTAC). *Chem Commun (Camb)* **55**, 929-932 (2019). https://doi.org/10.1039/c8cc08716d

15 Qiu, X. *et al.* Chemoselective Synthesis of Lenalidomide-Based PROTAC Library Using Alkylation Reaction. *Org Lett* **21**, 3838-3841 (2019). https://doi.org/10.1021/acs.orglett.9b01326

16 Bemis, T. A., La Clair, J. J. & Burkart, M. D. Traceless Staudinger ligation enabled parallel synthesis of proteolysis targeting chimera linker variants. *Chem Commun (Camb)* **57**, 1026-1029 (2021). https://doi.org/10.1039/d0cc05395c

17 Bhela, I. P. *et al.* A Versatile and Sustainable Multicomponent Platform for the Synthesis of Protein Degraders: Proof-of-Concept Application to BRD4-Degrading PROTACs. *J Med Chem* **65**, 15282-15299 (2022). https://doi.org/10.1021/acs.jmedchem.2c01218

18 Roberts, B. L. *et al.* Two-Stage Strategy for Development of Proteolysis Targeting Chimeras and its Application for Estrogen Receptor Degraders. *ACS Chem Biol* **15**, 1487-1496 (2020). https://doi.org/10.1021/acschembio.0c00140

19 Thiele, J. & Schneider, J. Ueber Condensationsproducte des o-Phtalaldehyds. *Justus Liebigs Annalen der Chemie* **369**, 287-299 (1909).

20 Kulla, E. & Zuman, P. Reactions of orthophthalaldehyde with ammonia and 2-aminoethanol. *Org Biomol Chem* **6**, 3771-3780 (2008). https://doi.org/10.1039/b807714m

21 D'Hollander, A. C. A. & Westwood, N. J. Assessment of the regioselectivity in the condensation reaction of unsymmetrical o-phthaldialdehydes with alanine. **74**, 224-239 (2018).

22 Tung, C. L., Wong, C. T., Fung, E. Y. & Li, X. Traceless and Chemoselective Amine Bioconjugation via Phthalimidine Formation in Native Protein Modification. *Org Lett* **18**, 2600-2603 (2016). https://doi.org/10.1021/acs.orglett.6b00983

23 Zhang, Y., Zhang, Q., Wong, C. T. T. & Li, X. Chemoselective Peptide Cyclization and Bicyclization Directly on Unprotected Peptides. *J Am Chem Soc* **141**, 12274-12279 (2019). https://doi.org/10.1021/jacs.9b03623

24 Zhang, Q. *et al.* OPA-Based Bifunctional Linker for Protein Labeling and Profiling. *Biochemistry* **59**, 175-178 (2020). https://doi.org/10.1021/acs.biochem.9b00787

25 Zhang, Q., Zhang, Y., Li, X. & Chenoweth, D. M. in *Chemical Tools for Imaging, Manipulating, and Tracking Biological Systems: Diverse Methods for Optical Imaging and Conjugation* Vol. 639 237-261 (Academic Press, 2020).

26 Kim, Y. & Li, C.-J. Perspectives on green synthesis and catalysis. **1**, 1-11 (2020).

27 Guo, C. *et al.* Discovery of aryloxy tetramethylcyclobutanes as novel androgen receptor antagonists. *J Med Chem* **54**, 7693-7704 (2011). https://doi.org/10.1021/jm201059s

28 Han, X. *et al.* Strategies toward Discovery of Potent and Orally Bioavailable Proteolysis Targeting Chimera Degraders of Androgen Receptor for the Treatment of Prostate Cancer. *J Med Chem* **64**, 12831-12854 (2021). https://doi.org/10.1021/acs.jmedchem.1c00882

29 Pettersson, M. & Crews, C. M. PROteolysis TArgeting Chimeras (PROTACs) - Past, present and future. *Drug Discov Today Technol* **31**, 15-27 (2019). https://doi.org/10.1016/j.ddtec.2019.01.002

Chapter 3

Development of Oligomeric Mannose-6-phosphonate Conjugates for Targeted Protein Degradation

This chapter is adapted from a manuscript published in *ACS Medicinal Chemistry Letters.*

Stevens C.M[#], **Zhou Y**[#], Teng P[#], Rault L. N, Liao Y, Tang W.* Development of Oligomeric Mannose-6-phosphonate Conjugates for Targeted Protein Degradation. *ACS Med. Chem. Lett.* **2023**, *14*, 719.

[#]These authors contributed equally to this work

*To whom correspondence should be addressed

3.1. Abstract

Lysosome targeting chimera (LYTAC) represents an emerging novel protein degradation strategy. LYTACs utilize the native cell internalization process in the body to target and degrade therapeutically relevant extracellular proteins including both secreted and membrane proteins via the lysosomal pathway. The first lysosomal internalization receptor used for LYTACs is the cation-independent mannose-6-phosphate receptor (CI-M6PR). Because CI-M6PR is expressed across most cell types, it can be used for the internalization and degradation of numerous extracellular proteins in various tissues. We recently reported the development of a series of structurally well-defined glycopeptides with multiple units of mannose-6-phosphonate (M6Pn), which are capable of linking to a variety of protein of interest ligands for successful internalization and degradation of those proteins through CI-M6PR. This may greatly facilitate the development of M6Pn-based LYTACs for therapeutic applications.

3.2. Introduction

The tagging of specific protein targets for degradation is a key area of drug discovery. There are several routes available for targeted protein degradation, such as monovalent molecular glue degraders and heterobifunctional Proteolysis Targeting Chimeras (PROTACs)[1]. These small molecule degraders are gaining more and more attention due to their ability to degrade a wide range of targets, and their ability to degrade targets without requiring a functional binder. The primary utilization of this technique has so far been through PROTACs, wherein a ligand for E3 ligase is linked to a ligand for the POI. PROTAC can first form a ternary complex with the POI and E3 ligase, which tags the POI for ubiquitination followed by degradation via the ubiquitin-proteasome

system. PROTACs have been widely used for the degradation of a large number of protein targets. However, PROTACs can only degrade cytoplasmic proteins or proteins with a binding domain inside the cell. About 40% of proteins in the proteome are outside the cells and many of them are associated with various diseases[2]. It then becomes important to develop methods to efficaciously degrade those proteins that are beyond the reach of PROTACs and related degraders.

Lysosome Targeting Chimera (LYTAC) represents a general strategy for the degradation of extracellular proteins including secreted and cell membrane associated proteins[3]. LYTACs are heterobifunctional molecules containing a ligand for a POI and a ligand for a lysosome targeting receptor such as CI-M6PR. LYTAC can complement existing strategies developed for degrading intracellular proteins. However, the interaction between CI-M6PR and its ligand, mannose-6-phosphate (M6P), is not as well understood. It has led to many different approaches in designing various M6P-containing conjugates for drug delivery with varying degrees of success[4-7]. While it is known that multivalency is important for the interaction between M6P and CI-M6PR, the nature of the multivalency is not specified, especially for LYTAC design. Further probing the M6P/M6PR interaction in a controlled manner is necessary to fully utilize it for targeted protein degradation.

Recently, Bertozzi's group reported the development of LYTACs by utilizing M6P/CI-M6PR, where a polymeric glycopolypeptide incorporating 20-90 mannose-6-phosphonates (M6Pns) was synthesized and then attached to an antibody of a POI[3]. While this serves as an elegant example for the first application of M6P/CI-M6PR in LYTAC development, the reported polymeric glycopeptides employed large

multivalences in M6Pn without well-defined structures, which are challenging for quality control in the drug development process. We recently reported an improved CI-M6PR-recruiting LYTAC design using structurally well-defined CI-M6PR ligands. Our strategy may simplify the development and production process. Our new LYTAC platform contains a short peptide backbone decorated with several M6Pn units separated by various linkers for efficient uptake via CI-M6PR (Fig. 3.1). The modular nature of the peptide backbone and the coupling chemistry used for conjugating the M6Pn to the peptide backbone allows for systematic investigation of the distance between M6Pn units, as well as the multivalency of M6Pn. The synthetic route streamlines those previously explored for CI-M6PR based lysosome targeting degraders, and provides a more controlled and specific targeting of the CI-M6PR that retains efficient uptake and degradation. During our studies, Wang's group reported an elegant alternative for structurally well-defined CI-M6PR ligands by employing a site-specific chemoenzymatic method to attach high affinity M6P glycan ligands to antibodies for targeted protein degradation[8].

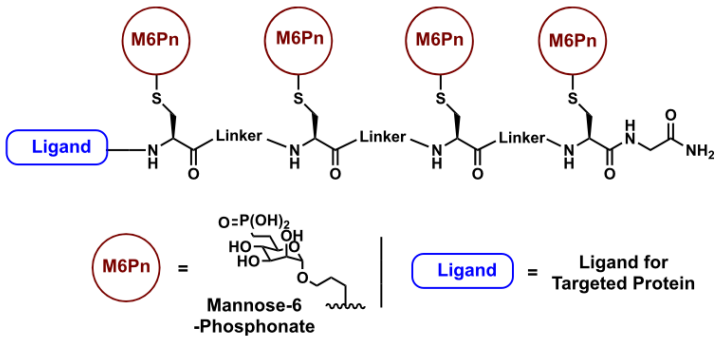

Figure 3.1. Overview of M6Pn Based Structurally Defined LYTACs. The degrader is composed of several M6Pn units conjugated to a peptide backbone and separated by different linkers. This backbone can be linked to a variety of ligands of target proteins.

In order to prepare multivalent ligands that are capable of both effectively targeting the CI-M6PR and conjugating to the peptide backbone of the LYTAC, several considerations must be made. First, the natural 6-phosphoester of M6P has been shown to undergo hydrolysis in human serum[9], which would destroy the M6PR targeting ability of the conjugates in vivo, and potentially lead to unwanted binding to the mannose receptor on macrophages[10]. This would require implementing some other connections to the phosphate, such as M6Pn with a stable carbon linker on the 6-position[11]. Second, to avoid the tedious process of creating a protected M6Pn-conjugated amino acid building block that would be compatible with the Fmoc solid phase peptide synthesis used to create the peptide backbone, the M6Pn would need to be modified in some way to allow easy conjugation to the peptide backbone.

3.3. Results and Discussion

To address the first consideration, Dr. Peng Teng and Christopher Stevens in our group elected to follow the previous LYTAC from Bertozzi's group and install a phosphonate moiety in place of the native phosphate. The attachment of carbohydrates to the peptide scaffold is not an easy task due to the diverse functional groups in carbohydrates and peptides. This is the bottleneck in the recent syntheses of oligomeric M6P for drug delivery and M6Pn for LYTACs. After surveying a variety of options, Dr. Peng Teng decided to address the second consideration using a thiol-ene reaction between a terminal alkene on the anomeric position of the M6Pn and a free thiol on the cysteine of the peptide back bone. The thiol-ene reaction can be carried out under mild conditions that are compatible with all functional groups we have. This reaction provides high

yields and high reaction rates[12], with the added benefit of not needing any protection or manipulation of the peptide backbone side chains or the M6Pn.

Dr. Peng Teng and Christopher Stevens prepared M6Pn-peptide M6Pn **6** in 11 steps that only involved five column chromatography purifications from a penta-acetylated mannose starting material (Scheme 1A). Next, conjugation of the M6Pn to the peptide backbone was achieved via the thiol-ene reaction (Scheme 1B). A number of these peptides were synthesized with different structures for testing uptake and degradation. The deprotected peptides were then combined with the M6Pn in a mixed solvent of water and methanol, and reacted with the photo-initiator 2,2-Dimethoxy-2-phenylacetophenone under an ultraviolet lamp set to 365 nm[13]. It was found that this reaction proceeded quickly and in near quantitative yields as long as the reaction is kept under inert atmosphere with a proper mixture of water and methanol. After lyophilization, the biotinylated M6Pn-peptide conjugates were found by LCMS (liquid chromatography mass spectrometry) analysis to have high purities, and could be used directly for cellular uptake of a model protein target. Our strategy provides an efficacious method for creating controlled and specifically designed M6Pn-peptides that are capable of linking to a variety of targeting ligands for different POIs after replacing the biotin with an azide, which can couple with alkyne-labelled antibodies or other types of binders.

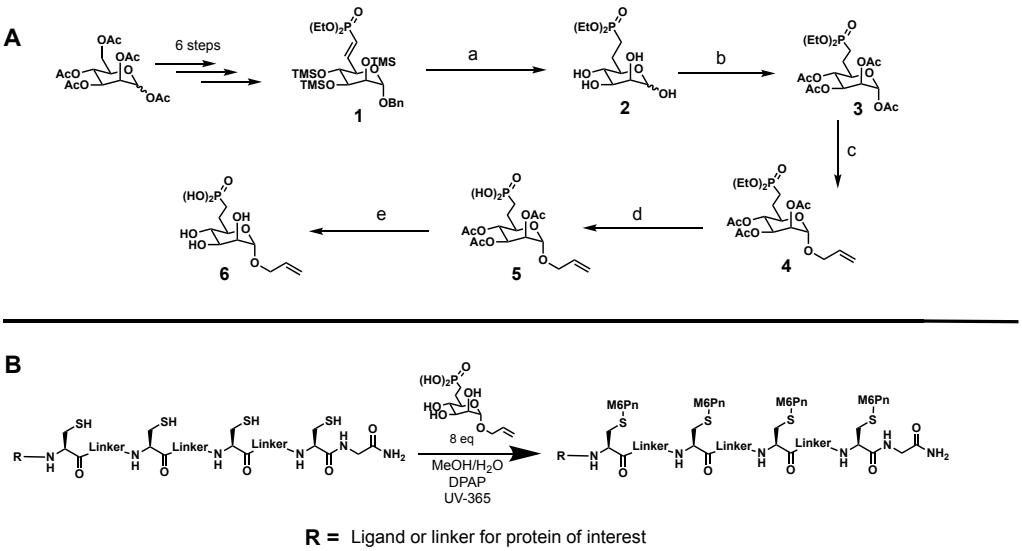

Scheme 1. Synthesis and Incorporation of a Mannose-6-phosphonate (M6Pn) onto a Peptide Backbone. A) Synthesis of M6Pn with anomeric alkene group: a) Pd−C, H2, MeOH/AcOH, 73%; b) Pyr, Ac2O, DMAP, 93%; c) Ally Alcohol, BF3*OEt2, 0°C → 25°C, 54%; d) Pyr, TMSBr, 90%; e) 0.5 M NaOMe in MeOH, Quantitative. **B)** Incorporation of M6Pn to peptide backbone via the thiol−ene reaction. For each cysteine residue on the backbone, 2 equiv of M6Pn were used. DPAP served as the radical initiator, and UV at 365 nm was used to activate. **Note:** These experiments were completed by Dr. Peng Teng and Christopher Stevens.

A series of M6Pn-peptide conjugates were created to test the uptake requirements of the CI-M6PR. Based on the previously reported M6Pn-based ligands for drug delivery through CI-M6PR, adequate binding can be achieved with a multimeric display of around three M6Pn units. In order to test the multivalent requirements in binding M6PR for LYTACs, five initial M6Pn-peptide conjugates were prepared with varying multivalency (Fig. 3.2A). Conjugate **7** consisted of a monomeric M6Pn presenting ligand, conjugate **8** consisted of a dimeric ligand, conjugates **9** and **10** consisted of trimeric ligands, and conjugate **11** consisted of a tetrameric ligand. In order to test for uptake, each of the five conjugates contained a terminal biotin moiety that can bind to a fluorescent neutravidin (NA-650), a model POI.

After receiving the M6Pn-peptide conjugates prepared by Dr. Peng Teng and Christopher Stevens, I tested their biological activity in a cellular uptake assay. To test the uptake of NA-650, a fluorescent model target protein, huh7 (human hepatoma-derived 7) cells were incubated with NA-650 and 10 μM of M6Pn-biotin conjugate for 24 h. The uptake of NA-650 was then measured by examining the fluorescent intensity via plate reader. It was found that the monomeric and dimeric M6Pn-biotin conjugates **7** and **8** were unable to mediate any uptake, and the trimeric conjugates **9** and **10** offered minimal uptake when compared to the tetrameric conjugate **11** (Fig. 3.2B). This supports the idea of specific multivalent requirements for efficient uptake via the M6PR using M6Pn derivatives.

It is interesting to note, however, the large increase in uptake efficacy when going from the trimeric conjugates (**9** and **10**) to the tetrameric conjugate (**11**), when compared to the lesser increase when moving from dimeric to trimeric (Fig. 3.2B). It is possible that this preference of the CI-M6PR for tetrameric M6Pn ligands can be explained using known structure data on the receptor. The CI-M6PR has been found to contain four total binding sites for M6P, two of which are considered high affinity binding sites for M6P that contain essential residues for binding[14-16]. In addition, several reports indicate that CI-M6PR forms receptor dimers as part of the internalization process[5,17-19]. Together, these pieces of information indicated that an effective ligand would consist of a tetrameric M6Pn conjugate composed of two sets of M6Pn dimers separated by a linker, which would be able to bind the two high affinity M6P binding sites on two different M6PR monomers, leading to M6PR dimerization and internalization into the cell. The large increase in uptake efficacy supports this hypothesis and is consistent

with previous reports of M6PR dimerization as a required event for internalization, though more evidence will be necessary to further validate this mechanism. In addition to providing useful structure activity relationship (SAR) data, these results also show that a streamlined and specifically designed M6Pn based LYTAC is capable of recruiting an extracellular protein and bringing it into the cell via CI-M6PR.

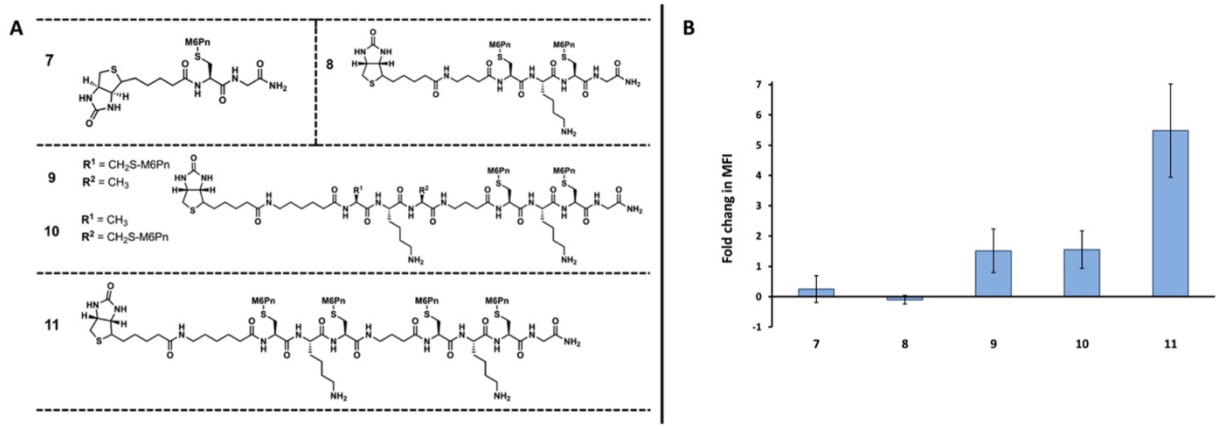

Figure 3.2. Initial M6Pn-conjugate uptake studies using biotin/neutravidin assay. A) Structure of conjugates 7 through 11, ranging from monomeric to tetrameric. All conjugates contain a terminal biotin moiety. **Note:** All compounds are prepared by Christopher M Stevens. **B)** Fold change in mean fluorescent intensity (MFI) data from uptake studies of conjugates 7 through 11. Huh7 cells were incubated with 500 nM of neutravidin-650 (NA-650) and 10 μM of M6Pn-biotin at 37 °C for 24 h. The cells were then washed with PBS, and the uptake was determined by measuring the fluorescent intensity at 650 nm excitation/680 nm emission. Data is shown in relative fluorescent units.

With the results from the NA-650 uptake experiments in hand, conjugate **11** was chosen to test the ability of the designed M6Pn-LYTAC to degrade a target POI by replacing the biotin motif with a binder of POI. Epidermal growth factor receptor (EGFR), which is overexpressed in many tumors[20-23], was chosen as the POI to test the M6Pn-LYTACs. First, the terminal biotin in **11** moiety was replaced with an azido group to create conjugate **12** (Fig. 3.3A). The anti-EGFR antibody Cetuximab (Ctx) was then reacted

with commercially available DBCO-NHS activated ester (dibenzo cyclooctyne-N-hydroxysuccinimidyl ester), which contains a strained alkyne group, to create Ctx-DBCO (Fig. 3.3B). The Ctx-DBCO was then reacted with conjugate **12** through a copper free click reaction to yield the antibody conjugated LYTAC, Ctx-DBCO-**12**. MALDI analysis revealed that each Ctx was labeled with ~2 ligand **12** on average. This full conjugate was then incubated at various concentrations with HeLa cells expressing EGFR for 24 h to establish the dose-dependent degradation by western blot analysis (Fig. 3.3C).

It was found that Ctx-DBCO-**12** was able to induce degradation with as low as 0.1 nM concentration, with the maximum EGFR degradation achieved at 100 nM with ~40% degradation. Following the dose-response, I completed a time-course study to determine the degradation effect over time (Fig. 3.3D). The study was done using 10 nM of Ctx-DBCO-**12**, and showed that significant levels of degradation were achieved as early as 2-4 h, and the effect lasted through the last time point taken at 48 h. This suggests that treatment with the M6Pn based LYTAC may offer a sustained level of protein degradation. Overall, the degradation studies show that our specifically designed M6Pn-LYTAC is capable of targeting and degrading a cell membrane associated protein.

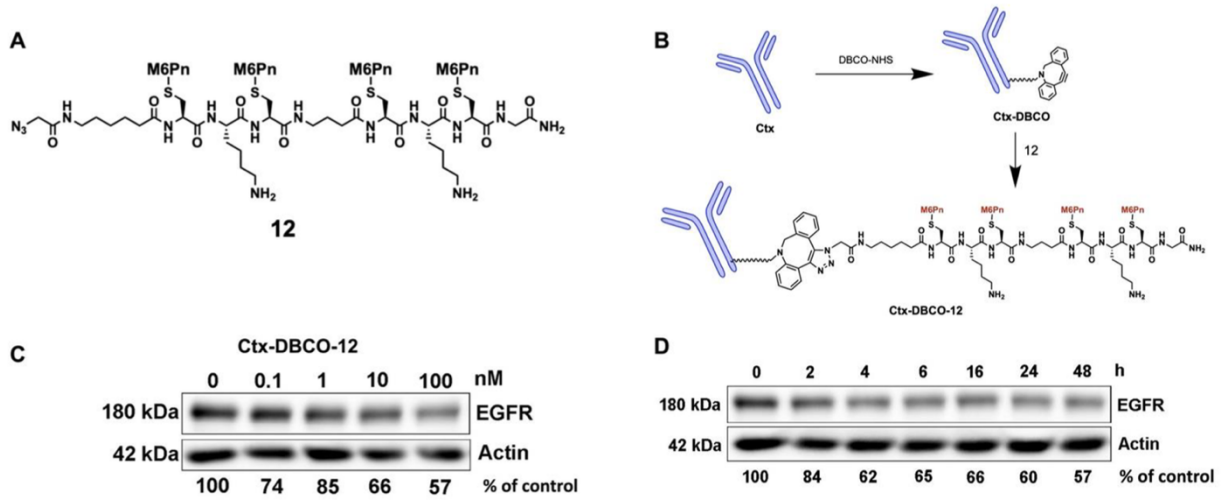

Figure 3.3. Design, synthesis, and degradation study of an antibody conjugated M6Pn LYTAC. A) Structure of conjugate **12**, similar to that of conjugate **11** but with the terminal biotin moiety replaced by an azido group. This modification was made during SPPS of the peptide backbone. **Note:** Conjugate **12** is prepared by Christopher Stevens. **B)** Linkage of conjugate **12** to the EGFR antibody Cetuximab (Ctx). First, Ctx was mixed with DBCO-NHS at a molar ratio of 1:25 and incubated overnight to produce Ctx-DBCO. Next, the Ctx-DBCO was mixed with 25 equiv of conjugate **12** and incubated overnight to yield Ctx-DBCO-**12**, which was characterized by MALDI-TOF-MS. **C)** Dose response study of Ctx-DBCO-**12** on Hela cells with EGFR. Ctx-DBCO-**12** in concentrations of 0, 0.1, 1, 10, and 100 nM were incubated with Hela cells for 24 h. Next, the cells were lysed and EGFR degradation was measured using Western blot analysis. **D)** Time course study of Ctx-DBCO-**12** on Hela cells with EGFR. Hela cells were incubated with 10 nM of Ctx- DBCO-**12**, and samples were collected at various time points and analyzed by Western blot to determine EGFR degradation.

Following the successful degradation of EGFR using Ctx-DBCO-**12**, Christopher Stevens expanded the variety of linkers and multivalency of the conjugates for further improvements. A second series of conjugates were prepared with a terminal biotin moiety for testing uptake using NA-650 as the model target (Fig. 3.4A). These conjugates, **13** through **24**, were designed to expand the scope and variety of conjugate structures. Conjugates **13** through **23** are all tetrameric presenting M6Pn conjugates which follow the outlined design of two sets of M6Pn dimers separated by a linker (linker A). The linker A is composed of an amino acid with increasing degrees of separation,

ranging from one atom separation to seven atom separation, and varying in composition. Each tetrameric conjugate also contains a second linker (linker B) which separates the M6Pn of the dimers. These were varied as well in length and composition. Conjugates **13** through **19** have different linker A in terms of composition and length while keeping linker B as a single lysine residue. Conjugates **20** through **23** have the same C3 linker A used in conjugate **11**, but different linker B. In addition to lysine in each linker B, an additional lysine, glycine, serine, or phenylalanine was incorporated to change the length and composition. Lastly, conjugate **24** expanded the multivalency to a hexameric presenting M6Pn conjugate to further test the effects of multivalency on uptake efficacy. These twelve conjugates were tested for cellular uptake of NA-650, and compared to conjugate **11** (Fig. 3.4B).

While conjugates **13** through **16**, **18**, **22**, and **23** all performed similarly to conjugate **11**, there was more significant difference in the activity of the other conjugates (Fig. 3.4B). Compared to **11**, conjugates **20** and **21** showed obvious less uptake. This is interesting, as the other two conjugates with different linker B, conjugates **22** and **23**, had similar uptake as **11**. It is possible that the composition of the linker as opposed to linker length matters more, as **20** contains two charged lysines, while **22** and **23** contain a lysine and an uncharged residue. Conjugate **21** is a more unique case, as it contains glycine, which would possibly add more flexibility to the conjugate backbone. Conjugate **15** also contained glycine residues, this time for linker A, but showed effective uptake. It is possible that for these M6Pn-LYTACs, flexibility is desirable between the two sets of dimers (in linker A), but less desirable between the M6Pns that target the binding domains on one CI-M6PR (in linker B). In addition to the effect of linker B, conjugates

17 and **19** had increased uptake compared to **11** (Fig. 3.4B). These conjugates contain either a C6 or a C7 linker respectively, and while they are not largely different in terms of linker length compared to the other conjugates (e.g. **18**), their composition of only carbon may offer advantages that lead to more efficacious uptake.

Of particular note is **24**, the hexameric M6Pn conjugate. This conjugate showed the most efficacious uptake of all compounds tested; however, it did not offer the same increase in uptake over the best performing tetrameric conjugate, **19**, compared to the increase in uptake from the trimeric conjugate to the tetrameric. Conjugate **19**, the most efficacious tetrameric conjugate, offered a 3.5-fold increase in uptake over the trimeric conjugate **10**, while the hexameric conjugate **24** only offered a 1.5-fold increase in uptake compared to **19**. While the hexameric conjugate did show the highest uptake, it takes more steps to prepare the peptide backbone and more M6Pn units for the thiol-ene coupling. This suggests that tetrameric conjugates offer the greatest balance of preparation and uptake efficacy in the performed study.

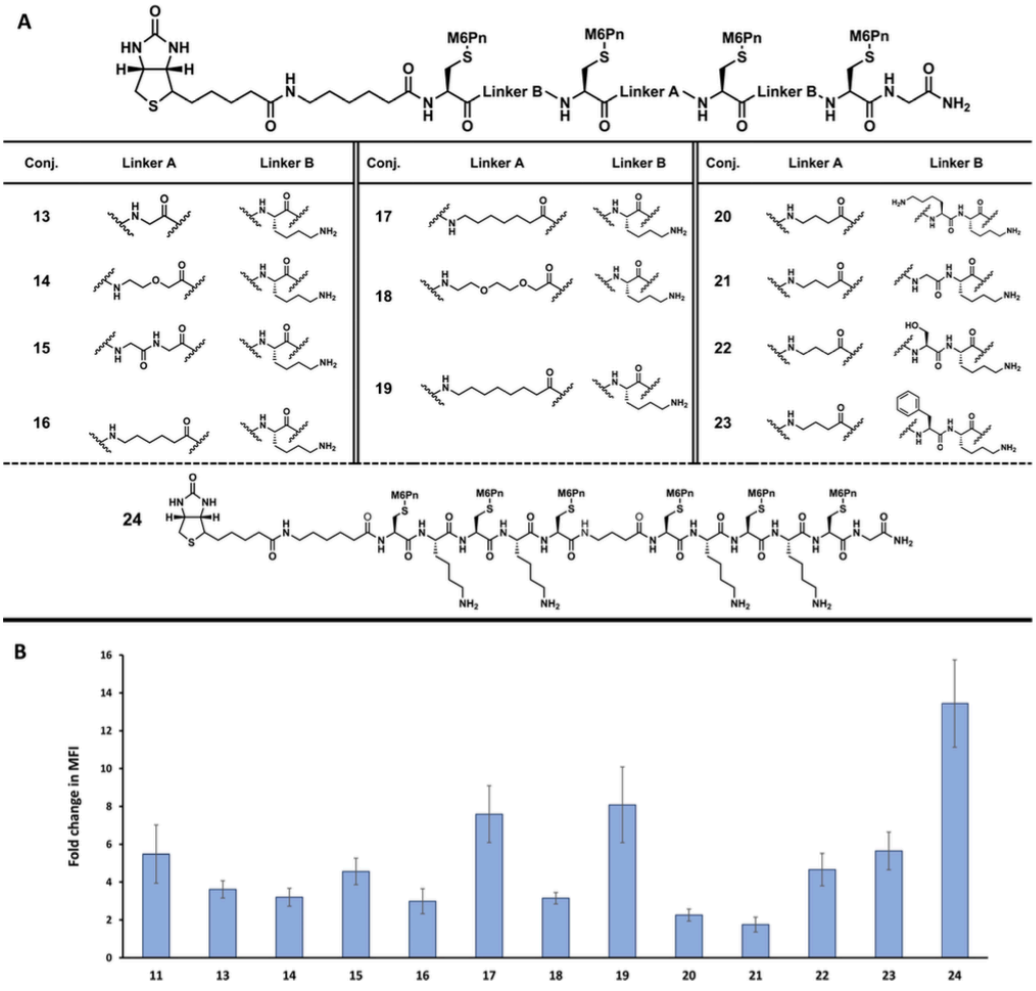

Figure 3.4. Additional M6Pn-conjugate uptake studies using the biotin/neutravidin system. A) Structure of conjugates **13** through **24**. Conjugates **13** through **23** use the general tetrameric structure shown above the table, modifying both linker A and linker B for structure and composition. Conjugate **24** changes the multivalency to a hexameric structure. All conjugates contain a terminal biotin moiety. **Note:** All compounds are prepared by Christopher Stevens. **B)** Fold change in MFI data from uptake studies of conjugates **17** through **24**. Huh7 cells were incubated with 500 nM of neutravidin-650 (NA-650) and 10 μM of M6Pn-biotin at 37 °C for 24 h. The cells were then washed with PBS, and the uptake was determined by measuring the fluorescent intensity at 650 nm excitation/ 680 nm emission. Data is shown in relative fluorescent units.

As previously mentioned, all of the conjugates tested (**7** through **24**) were not purified following the thiol-ene reaction to conjugate the M6Pn to the peptide backbone. While this reaction is highly efficient, it does involve an excess of the M6Pn **6**. To test the

effect this excess reagent had on the uptake data shown in Figure 2B and 4B, the most representative conjugates **7**, **8**, **9**, **19**, and **24** were purified via HPLC and tested for uptake of the NA-650 in comparison to the corresponding non-purified conjugates (Fig. 3.5). This represents the best performing monomeric, dimeric, trimeric, tetrameric, and hexameric conjugates. For all conjugates except **24**, the pure and non-pure had very similar uptake efficiency. For conjugate **24**, the pure compound had noticeable higher uptake than the crude. We can conclude that the impact of the excess M6Pn presented in the system after the thiol-ene reaction on the uptake in the NA-650 assay is minimal and the overall SAR trend remains the same following purification.

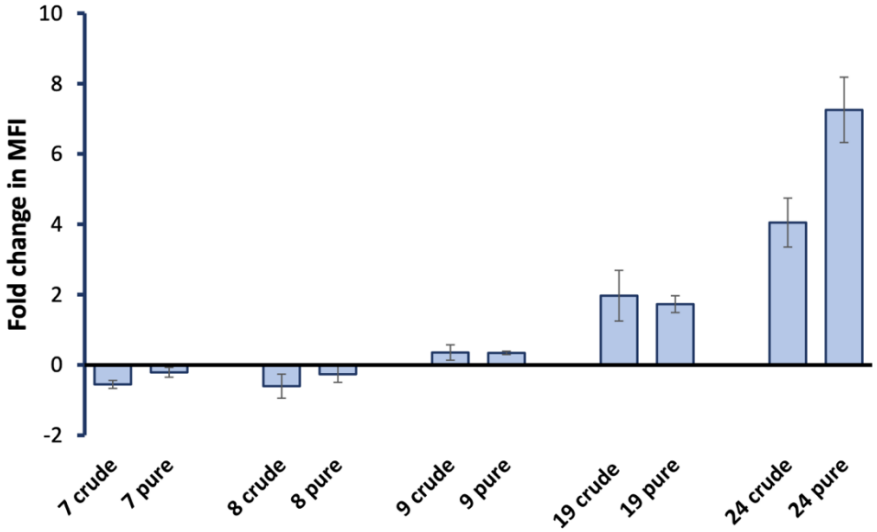

Figure 3.5. Fold change in MFI for crude and pure conjugates. Each conjugate **7**, **8**, **9**, **19**, and **24** was purified and both the crude and pure versions were tested for uptake using the NA-650 assay. All conjugates except **24** showed similar uptake between crude and pure, with pure **24** showing observable higher uptake compared to crude **24**.

In summary, we have shown that specifically designed M6Pn-LYTACs can be prepared and they show successful uptake and degradation. This LYTAC builds on those previously reported, with a simplified synthetic pathway due to the efficient thiol-ene

coupling chemistry and a well-defined modular structure. These M6Pn-peptide conjugates allow for the incorporation of a variety of ligands or linkers for targeted POIs. Showcased here, the conjugates were able to be linked to a small molecule ligand, biotin, for binding a fluorescent neutravidin protein for studying uptake efficacy. In addition, the conjugates could be designed to contain an azido moiety for click-chemistry linkage to an antibody ligand, cetuximab, for EGFR. The resulting cetuximab-M6Pn conjugate was able to successfully internalize and degrade EGFR. While both neutravidin and EGFR served as test systems for the LYTACs, they could readily be adapted for linking to any variety of small molecule, peptide, or antibody ligands in relevant therapeutic applications. While this degrader (Ctx-DBCO-12) had decreased degradation efficacy compared to the first generation M6Pn based LYTACs,[8] the advances in being able to use well defined ligands with the flexibility for further improvement should increase its utility for the community.

In addition to showing the degradation capabilities of the designed M6Pn-LYTACs, the uptake studies enabled the further investigation of the M6PR recruiting requirements. In total, seventeen different M6Pn-peptide conjugates were synthesized by Dr. Peng Teng and Christopher Steven. I then studied their uptake efficacy. Our results revealed the multivalency requirements for recruiting CI-M6PR, as well as the effect of size and composition of the peptide backbone on uptake efficacy. We found that tetrameric M6Pn-conjugates offered the greatest balance of synthetic simplicity and uptake efficacy. We also found that while conjugate length did not seem to be a significant factor in uptake, composition may have an impact. Further studies will continue to expand the variety of conjugate structures to further elucidate the CI-M6PR recruiting

requirements for an effective M6Pn-LYTAC, as well as utilize the existing conjugate designs to target and degrade therapeutically relevant proteins with different ligand types.

3.4. Material and General Methods Safety Statement

No unexpected or unusually high safety hazards were encountered.

3.4.1. Cell culture

Huh7 cells were cultured in T75 flasks and maintained in low-glucose DMEM supplemented with 10% fetal bovine serum, 1% non-essential amino acids, 1% sodium pyruvate, 1% L-glutamine and 1% penicillin/streptomycin under 5 % CO_2 at 37 °C.

3.4.2. NeutrAvidin uptake experiments for M6P-biotin

Cells were seeded at 35,000 cells per well in 100 µL complete culture media in 96-well cell culture plates. The next day, the medium was replaced followed by the sequential addition of 500 nM NA-650 and 10 µM M6P-biotin. The cells were incubated at 37 °C for 24 h and then washed twice with PBS to removed extracellular NA-650. The uptake in 96-well plate was determined by measuring the fluorescent intensity at 650 nm excitation/680 nm emission using the Synergy H1 microplate reader. Data was acquired using Gen5 software.

3.4.3. Antibody labeling and preparation of Ctx-DBCO-12

To label the antibody with M6P, 100µL of the Cetuximab (Ctx) in PBS was mixed with DBCO-NHS at 1:25 molar ratio and incubated overnight at room temperature on a rotator, followed by filtration with 500µL of PBS for 5 times using 10kDa Amicon Centrifugal Filter. After determining the concentration by BCA assay, the DBCO-

tethered Ctx was mixed with 25 equivalence M6P- azido and incubated overnight at room temperature on a rotator, followed by filtration with 500μL of PBS for 5 times using 10kDa Amicon Centrifugal Filter.

3.4.4. MALDI-MS

α-Cyano-4-hydroxycinnamic acid (CHCA) was dissolved in 50% Acetonitrile/H2O to give a 10 mg/mL solution as the matrix solution. The sample was absorbed on Omix C4 pipette tips, washed by 0.1% TFA for three times and then eluted with 20 μL 75% Acetonitrile/H2O. 1 μL sample solution and 1 μL CHCA solution were spotted on the MALDI target plate and mixed thoroughly before the spot was allowed to dry under room temperature. MALDI-MS spectra were acquired on Bruker UltraFlex MALDI-TOF/TOF mass spectrometer operated in linear positive ion mode. Masses were calculated from windowed raw data in Sigmaplot 13.0 by fitting to gaussian curves, with constant baseline as an additional free parameter. Parameter starting values were the default values of the program, and were automatically iterated 200 times to obtain fits. Plots were made in Origin 2020, where high-frequency noise was removed using 100 points windowed FFT filter.

3.4.5. EGFR degradation analysis

Hela were seeded at 1x10^5 cells per well in a 24-well plate. Various concentrations of M6P-bearing Cetuximab as indicated in the figures were added into the well containing 500 μL complete media. Samples were collected at different time points for western blot analysis.

3.4.6. Western blotting

Cells were lysed with 1X RIPA lysis buffer containing 25 mM Tris, pH 7−8, 150 mM NaCl, 0.1% (w/ v) sodium dodecyl sulfate (SDS), 0.5% sodium deoxycholate, 1% (v/ v) Triton X-100, protease inhibitor cocktail (Roche, one tablet per 10 mL) and 1 mM phenylmethylsulfonyl fluoride] on ice for 10 min. The lysates were then centrifuged at 14,000G at 4 °C for 15 min and the supernatant was collected followed by measuring the protein concentration using BCA assay. Lysates were adjusted to the equal amount before mixed with the 4x Laemmli Loading Dye and heated at 95−100 °C for 5 min. A□er cooling down, samples were loaded onto 7.5% SDS−polyacrylamide gel electrophoresis and transferred to PVDF membrane. The membrane was first blocked in 5% (w/v) nonfat milk in the TBS-T washing buffer (137 mM NaCl, 20 mM Tris, 0.1% (v/v) Tween) and then incubated with primary antibodies at 4 °C overnight. After 3 washes with TBST, the membrane was incubated with secondary HRP-linked antibodies for 1 h, and then washed 3 times with TBST. Then the membrane was incubated in the Clarity ECL substrate for 3- 5 min before acquiring the immunoblot by ChemiDoc MP Imaging Systems.

3.5. References

1 Valeur, E., Narjes, F., Ottmann, C. & Plowright, A. T. Emerging modes-of-action in drug discovery. *Medchemcomm* **10**, 1550-1568 (2019). https://doi.org/10.1039/c9md00263d

2 Uhlén, M. *et al.* Proteomics. Tissue-based map of the human proteome. *Science* **347**, 1260419 (2015). https://doi.org/10.1126/science.1260419

3 Banik, S. M. *et al.* Lysosome-targeting chimaeras for degradation of extracellular proteins. *Nature* **584**, 291-297 (2020). https://doi.org/10.1038/s41586-020-2545-9

4 Hoogendoorn, S., van Puijvelde, G. H., Kuiper, J., van der Marel, G. A. & Overkleeft, H. S. A multivalent ligand for the mannose-6-phosphate receptor for endolysosomal targeting of an activity-based probe. *Angew Chem Int Ed Engl* **53**, 10975-10978 (2014). https://doi.org/10.1002/anie.201406842

5 Ali, L. M. A. *et al.* Topological Requirements for CI-M6PR-Mediated Cell Uptake. *Bioconjug Chem* **30**, 2533-2538 (2019). https://doi.org/10.1021/acs.bioconjchem.9b00590

6 Hyun, J. Y., Kim, S., Lee, H. S. & Shin, I. A Glycoengineered Enzyme with Multiple Mannose-6-Phosphates Is Internalized into Diseased Cells to Restore Its Activity in Lysosomes. *Cell Chem Biol* **25**, 1255-1267.e1258 (2018). https://doi.org/10.1016/j.chembiol.2018.07.011

7 Reintjens, N. R. M. *et al.* Multivalent, Stabilized Mannose-6-Phosphates for the Targeted Delivery of Toll-Like Receptor Ligands and Peptide Antigens. *Chembiochem* **22**, 434-440 (2021). https://doi.org/10.1002/cbic.202000538

8 Zhang, X. *et al.* Site-Specific Chemoenzymatic Conjugation of High-Affinity M6P Glycan Ligands to Antibodies for Targeted Protein Degradation. *ACS Chem Biol* **17**, 3013-3023 (2022). https://doi.org/10.1021/acschembio.1c00751

9 Jeanjean, A., Garcia, M., Leydet, A., Montero, J. L. & Morère, A. Synthesis and receptor binding affinity of carboxylate analogues of the mannose 6-phosphate recognition marker. *Bioorg Med Chem* **14**, 3575-3582 (2006). https://doi.org/10.1016/j.bmc.2006.01.024

10 Sly, W. S. *et al.* Enzyme therapy in mannose receptor-null mucopolysaccharidosis VII mice defines roles for the mannose 6-phosphate and mannose receptors. *Proc Natl Acad Sci U S A* **103**, 15172-15177 (2006). https://doi.org/10.1073/pnas.0607053103

11 Gary-Bobo, M., Nirdé, P., Jeanjean, A., Morère, A. & Garcia, M. Mannose 6-phosphate receptor targeting and its applications in human diseases. *Curr Med Chem* **14**, 2945-2953 (2007). https://doi.org/10.2174/092986707782794005

12 Lowe, A. B. Thiol-ene “click” reactions and recent applications in polymer and materials synthesis. *Polymer Chemistry* **1**, 17-36 (2010).

13 Floyd, N., Vijayakrishnan, B., Koeppe, J. R. & Davis, B. G. Thiyl glycosylation of olefinic proteins: S-linked glycoconjugate synthesis. *Angew Chem Int Ed Engl* **48**, 7798-7802 (2009). https://doi.org/10.1002/anie.200903135

14 Olson, L. J. *et al.* Identification of a fourth mannose 6-phosphate binding site in the cation-independent mannose 6-phosphate receptor. *Glycobiology* **25**, 591-606 (2015). https://doi.org/10.1093/glycob/cwv001

15 Olson, L. J. *et al.* Allosteric regulation of lysosomal enzyme recognition by the cation-independent mannose 6-phosphate receptor. *Commun Biol* **3**, 498 (2020). https://doi.org/10.1038/s42003-020-01211-w

16 Tong, P. Y. & Kornfeld, S. Ligand interactions of the cation-dependent mannose 6-phosphate receptor. Comparison with the cation-independent mannose 6-phosphate receptor. *J Biol Chem* **264**, 7970-7975 (1989).

17 Byrd, J. C., Park, J. H., Schaffer, B. S., Garmroudi, F. & MacDonald, R. G. Dimerization of the insulin-like growth factor II/mannose 6-phosphate receptor. *J Biol Chem* **275**, 18647-18656 (2000). https://doi.org/10.1074/jbc.M001273200

18 Kreiling, J. L., Byrd, J. C. & MacDonald, R. G. Domain interactions of the mannose 6-phosphate/insulin-like growth factor II receptor. *J Biol Chem* **280**, 21067-21077 (2005). https://doi.org/10.1074/jbc.M412971200

19 York, S. J., Arneson, L. S., Gregory, W. T., Dahms, N. M. & Kornfeld, S. The rate of internalization of the mannose 6-phosphate/insulin-like growth factor II

receptor is enhanced by multivalent ligand binding. *J Biol Chem* **274**, 1164-1171 (1999). https://doi.org/10.1074/jbc.274.2.1164

20 Pabla, B., Bissonnette, M. & Konda, V. J. Colon cancer and the epidermal growth factor receptor: Current treatment paradigms, the importance of diet, and the role of chemoprevention. *World J Clin Oncol* **6**, 133-141 (2015). https://doi.org/10.5306/wjco.v6.i5.133

21 Zimmermann, M., Zouhair, A., Azria, D. & Ozsahin, M. The epidermal growth factor receptor (EGFR) in head and neck cancer: its role and treatment implications. *Radiat Oncol* **1**, 11 (2006). https://doi.org/10.1186/1748-717X-1-11

22 Rosell, R., Felip, E., Garcia-Campelo, R. & Balaña, C. The biology of non-small-cell lung cancer: identifying new targets for rational therapy. *Lung Cancer* **46**, 135-148 (2004). https://doi.org/10.1016/j.lungcan.2004.04.031

23 Hashmi, A. A. *et al.* Epidermal growth factor receptor (EGFR) overexpression in triple-negative breast cancer: association with clinicopathologic features and prognostic parameters. **2**, 6 (2019).

Chapter 4

Development of Triantennary N-Acetylgalactosamine Conjugates as Degraders for Extracellular Proteins

This chapter is adapted from a manuscript published in *ACS Central Science.*

Zhou Y, Teng P, Montgomery N. Li X, and Tang W*. Development of triantennary N-Acetylgalactosamine conjugates as degraders for extracellular proteins. *ACS Cent. Sci.* **2021**, *7*, 499.

*To whom correspondence should be addressed

4.1. Abstract

Targeted protein degradation (TPD) technology has drawn significant attention from researchers in both academia and industry. It rapidly evolved as a new therapeutic modality and also a useful chemical tool in selectively depleting various protein targets. As most efforts focus on cytosolic proteins using PROteolysis TArgeting Chimera (PROTAC), LYsosome TArgeting Chimera (LYTAC) recently emerged as a promising technology to deliver extracellular protein targets to lysosome for degradation through cation-independent mannose-6-phosphate receptor (CI-M6PR). In this study, we exploited the potential of asialoglycoprotein receptor (ASGPR), a lysosomal targeting receptor specifically expressed on liver cells, for the degradation of extracellular proteins including membrane proteins. The ligand of ASGPR, triantennary *N*-acetylgalactosamine (tri-GalNAc), was conjugated to biotin, antibodies, or fragments of antibodies to generate a new class of degraders. We demonstrated that the extracellular protein targets could be successfully internalized and delivered into lysosome for degradation in liver cell lines specifically by these degraders. This work will add a new dimension to the TPD with cell type specificity.

4.2. Introduction

Protein degradation is essential for maintaining cellular protein homeostasis. Most proteins in eukaryotic cells are degraded through ubiquitin-proteasome system, where the E3 ubiquitin ligase recognizes a specific protein substrate and tags multiple ubiquitin motifs to it, leading to the subsequent proteolysis by the proteasome[1,2]. Lysosome is another major destination for protein degradation. Through autophagy and endocytosis, both intracellular and extracellular proteins enclosed in vesicles can be delivered into

lysosomes for degradation[3,4]. Based on these mechanisms, targeted protein degradation by chimeric molecules emerged as a novel therapeutic modality. These chimeras are heterobifunctional molecules with one end binding to the protein of interest (POI) and the other end directing the ternary complex towards a certain degradation pathway. PROteolysis TArgeting Chimera (PROTAC) has received the most attention to date. PROTACs contain an E3 ligase ligand to route the targeted protein to the proteasome for degradation[5,6]. More recently, AUtophagy-TArgeting Chimera (AUTAC) was developed to degrade not only proteins but also organelles by using S-guanylation as the tag for autophagy[7]. However, these two types of chimeras are only capable of depleting cytoplasmic proteins or membrane proteins with a cytosolic binding domain. To broaden the scope of targets to include proteins without cytosolic binding domains, Bertozzi's group first developed LYsosome TArgeting Chimeras (LYTACs) by conjugating the ligand of the ubiquitously expressed cation-independent mannose-6-phosphate receptor (CI-M6PR) on the cell surface with a molecule that binds to the extracellular protein target[8]. The receptor-ligand interaction triggers the internalization of the extracellular proteins through receptor-mediated endocytosis, further inducing the degradation of the targets in the lysosome. CI-M6PR has been used to deliver therapeutic drugs conjugated with mannose-6-phosphate (M6P) derivatives for lysosomal enzyme replacement therapy and cancer treatment[9,10]. Various molecules, such as peptides, proteins or liposome, were covalently linked to the modified M6P with enhanced affinity and stability to achieve targeted drug delivery[11-14]. To extend the usage of M6PR/M6P system to targeted protein degradation, LYTAC was constructed by conjugating a mixture of polyglycopeptides containing multiple M6P analogues per

polymer to the antibody of POI. Different from drug delivery process, which involves the internalization of a covalent linked M6P-protein target, LYTAC allows the trafficking of a complex formed by the non-covalent interaction between the protein target and LYTAC. It has been shown that LYTAC could successfully degrade both secreted and membrane proteins in the lysosome through CI-M6PR.[8]

Asialoglycoprotein receptor (ASGPR) is another well-defined lysosomal targeting receptor, responsible for clearing glycoproteins via clathrin-mediated endocytosis and lysosomal degradation. Unlike CI-M6PR, ASGPR is primarily and highly expressed in hepatocytes with 500,000 copies per cell[15]. The unique expression pattern together with rapid recycling rate (~15 min)[16] make ASGPR a promising candidate for liver-specific targeted protein degradation. It has been reported that ASGPR binds to galactose (Gal) and N-acetylgalactosamine (GalNAc), with a higher affinity to the latter than the former, in the presence of Ca^{2+} ions[17,18]. Studies using both cluster galactosides and synthetic oligosaccharides indicated that trivalent GalNAc ligand with a 15-20 Å spacing between each sugar exhibited the highest binding affinity and efficiency for endocytosis compared to mono- and bivalent GalNAc ligands[19,20]. Further research on triantennary ligand revealed that cargo size below 70 nm is also required for the proper receptor recognition and efficient endocytosis[21]. The comprehensive understanding of receptor-ligand interaction paved the way for the application of ASGRP/triantennary GalNAc (tri-GalNAc) system in targeted drug delivery, especially for oligonucleotide therapy. Many tri-GalNAc-modified therapeutic nucleic acid agents, including siRNAs, anti-miRNAs and antisense oligonucleotides (ASOs), are now in preclinical or clinical studies[22,23]. It has been shown that the conjugation of tri-GalNAc facilitates the uptake of the

oligonucleotides and thus much lower dose is required compared to the free version[24,25]. Besides direct labeling of the therapeutic drugs, tri-GalNAc was also tagged to some drug carriers, such as lipid nanoparticle or poly-(amidoamine) (PAMAM) dendrimer to achieve targeted delivery[26,27]. It was reported that modifying poly-γ-glutamic acids (PGA) with tri-GalNAc resulted in the exclusive distribution in mice liver, while the non-modified PGA were excreted into urine[28]. However, despite the extensive use in drug delivery, the possibility of ASGPR-mediated targeted protein degradation hasn't been exploited prior to our study. Inspired by Bertozzi's pioneering work on LYTACs based on CI-M6PR and due to our interest in both targeted protein degradation[29-32] and carbohydrate chemistry[33,34], we initiated the investigation of ASGPR-mediated targeted protein degradation using chimeric molecules bearing a trivalent GalNAc ligand as liver cell-specific degraders for extracellular proteins including membrane proteins (Fig. 4.1). Since liver is the major place for protein catabolism, selectively delivering undesired proteins to liver for degradation can be potentially advantageous over ubiquitously delivery of the protein targets to various types of cells unselectively for many therapeutic applications. Right before the submission of our manuscript, research groups of Spiegel and Bertozzi independently reported their development of chimeric molecules with tri-GalNAc for targeted protein degradation in liver cells[35,36]. While the former focused on small molecule-based lysosome targeting degraders[35], the latter investigated antibody-based degraders for extracellular protein targets[36].

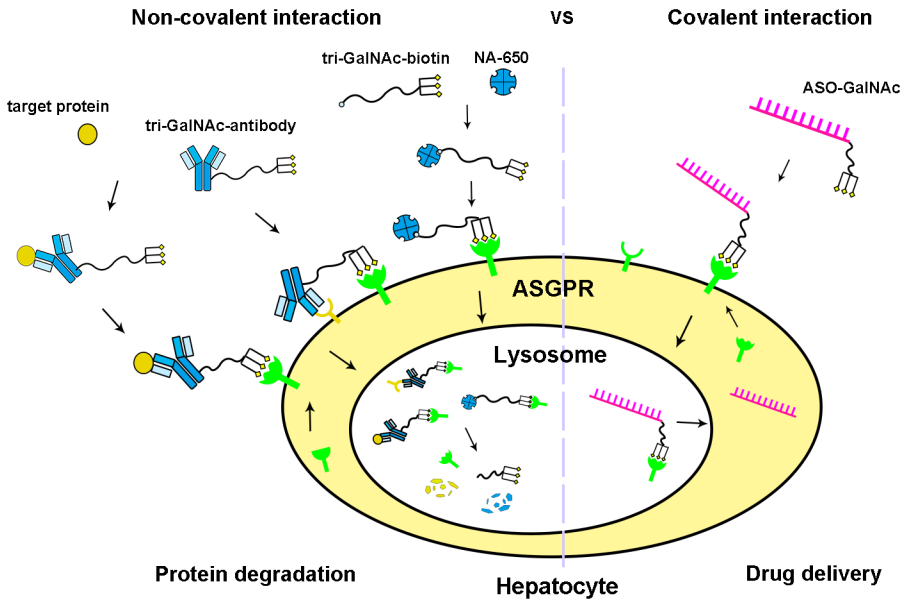

Figure 4.1. Comparison of the application of tri-GalNAc in targeted protein degradation and drug delivery. Small molecule- and antibody-based tri-GalNAc degraders non-covalently capture the protein targets and transport the targets to lysosome for degradation via the interaction with ASGPR. Oligonucleotides covalently linked to tri-GalNAc enable their internalization into the cell through ASGPR. After trafficking to lysosome, small amount of the oligonucleotides can escape from the endosome or lysosome to block or induce degradation of RNA.

4.3. Results and Discussion

4.3.1. Tri-GalNAc-biotin conjugate 1, a small molecule lysosome targeting degrader, can facilitate the uptake of NeutrAvidin through ASGPR in liver cells.

As our initial study, I employed NeutrAvidin (NA) as the targeted protein. Commercially available tri-GalNAc-biotin conjugate **1** was used as the ligand of ASGPR to examine the uptake of NA (Fig. 4.2A). HepG2 cells were treated with 2 μM of **1** and 500 nM of fluorescently labeled NA-650 concurrently for 4 h, and the fluorescence intensity inside the cells was measured by the plate reader to indicate the uptake of the NA-650. The data showed that NA-650 was internalized into the cell in a time-dependent manner in

the presence of **1**. No increase of the fluorescent signal was observed when the cells were treated with NA-650 alone or in the presence of negative control, tri-GalNAc-COOH **2** (Fig. 4.2B). The treatment of increasing concentration of **1** showed reduced uptake of NA-650 at high doses, suggesting that the formation of binary complexes between **1** and receptor or **1** and NA-650 becomes dominant over the formation of ternary complex NA-650/**1**/receptor with excess degrader **1** (Fig. 4.2C), which is often termed as hook effect[37]. I next extended the incubation time for **1** and NA-650 in HepG2 cells to 24 h. A continuous increase of the fluorescent signal was detected in the early phase while the signal gradually reached the plateau after 16-20 h (Fig. 4.2D).

To verify that the internalization of NA-650 was mediated through ASGPR, various concentrations of **2** were added to compete for the receptor with the **1**/NA-650 complex. The results showed that the uptake of NA-650 negatively correlated with the amount of **2**, suggesting that the internalization of NA-650 required the interaction between **1**/NA-650 complex and ASGPR (Fig. 4.2E). I then compared the uptake of NA-650 into HepG2, Huh7 or A549 cells with various ASGPR expression levels (Fig. 4.2F) and found that the amount of NA-650 accumulated in the cells significantly reduced with the decrease of ASGPR level. Similar to Fig. 4.2B, compound **2** without the biotin moiety failed to deliver NA-650 to all of these cell lines (Fig. 4.2G, H). Moreover, the knockdown of ASGPR by siRNA dramatically impeded the internalization of NA-650 into HepG2 cells (Fig. 4.2I, J). All these data confirmed the involvement of ASGPR in the transportation of NA-650 and indicated that the biotinylated ligand containing tri-GalNAc specifically delivered the targeted protein into liver cells.

4.3.2. Tri-GalNAc-biotin conjugate 1 delivers NeutrAvidin to lysosome for degradation

Next, I investigated whether NA-650 was delivered into lysosomes and degraded after being endocytosed into the cell. Confocal images showed the distribution of NA-650 in the cytoplasm and co-localization with the lysosome indicated by Lysotracker. This confirmed the ASGPR-mediated uptake and trafficking of the protein target to the lysosome (Fig. 4.2K). To evaluate the degradation of NA-650, HepG2 cells were incubated with NA-650 and **1** for 1 h, followed by the replacement of fresh media to allow further degradation. Compared to the amount of NA-650 enriched in the cell within 1 h incubation, decreasing amounts of NA-650 were detected at 3 h, 6 h, 24 h post media change. The addition of known lysosome inhibitor leupeptin moderately reduced the degradation of NA-650 at each time point (Fig. 4.2L). These data indicated that the degradation of NA-650 occurred after it was transported into the lysosome.

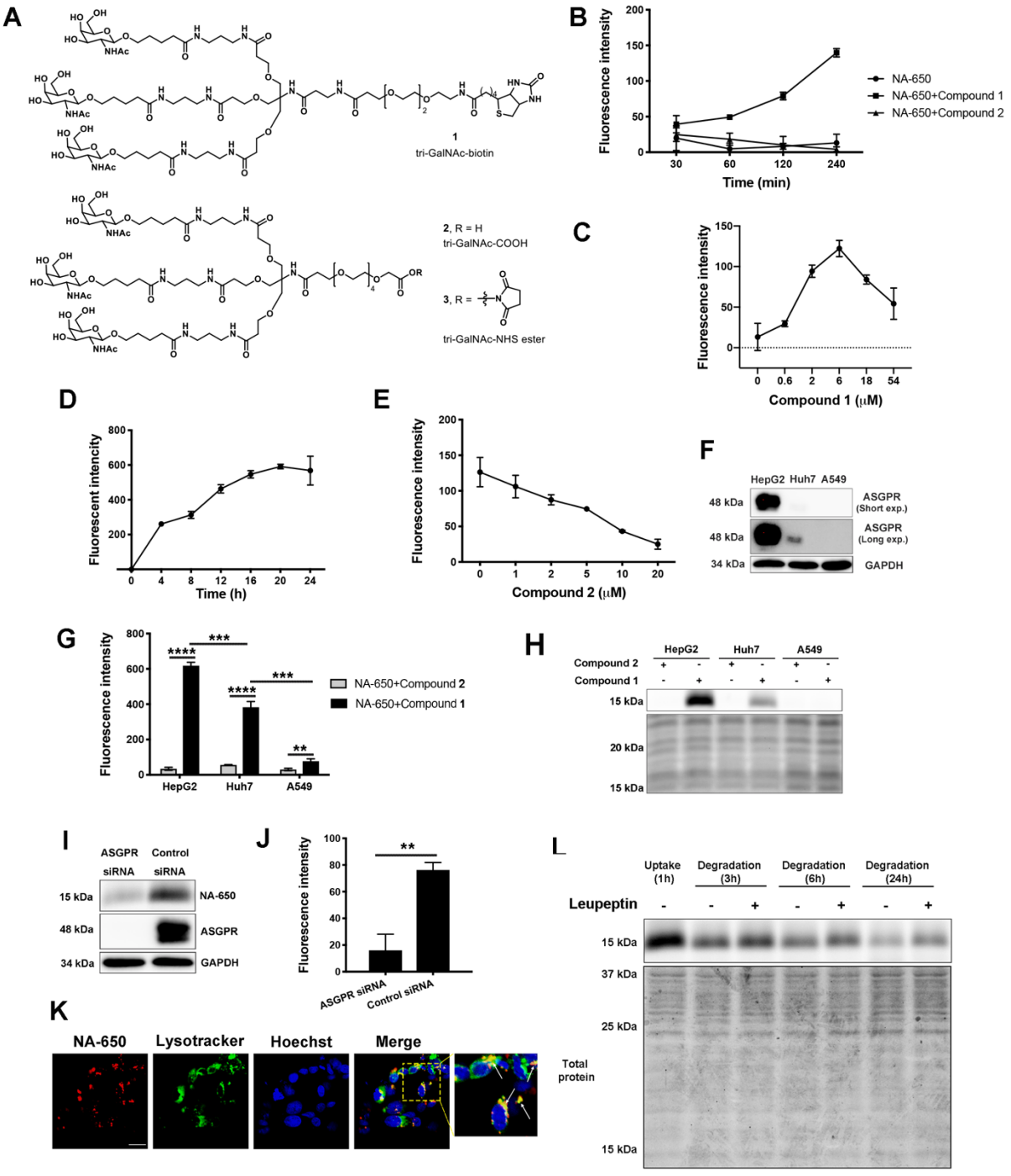

Figure 4.2. Tri-GalNAc-biotin mediates ASGPR-dependent cellular uptake of NA-650 specifically in liver cells and transports NA-650 to lysosome for degradation.

A. Chemical structures of tri-GalNAc-biotin (compound **1**), tri-GalNAc-COOH (compound **2**), and tri-GalNAc-NHS ester (compound **3**). **Note:** Compound 3 is prepared by Dr. Peng Teng. **B.** Cellular uptake of NA-650 in HepG2 cells treated with NA-650 alone (500 nM) or NA-650 (500 nM) and compound **1** (2 μM) or **2** (2 μM). **C.** NA-650 uptake in HepG2 cells treated with NA-650 (500 nM) and increasing

concentrations of compound **1** for 4 h. **D.** Cellular uptake of NA-650 (500 nM) in HepG2 cells in the presence of compound **1** (2 μM) within 24 h. **E.** Inhibition of the internalization of NA-650 (500 nM) mediated by **1** (2 μM) in HepG2 cells by compound **2**. **F.** ASGPR expression levels in HepG2, Huh7 and A549 cell lines. **G, H.** Comparison of the internalization of NA-650 (500 nM) mediated by **1** (2 μM) among HepG2, Huh7, and A549 cells incubated with NA-650 and Compound **1** or **2** for 16 h (G) or 6 h (H). Data presented as Mean±SD, n=3. **p<0.01, ***p<0.001, ****p<0.0001. **I, J.** Uptake of NA-650 (500 nM) in the presence of **1** (2 μM) within 4 h in HepG2 cells treated with control or ASGPR siRNA. **K.** Confocal microscopy images of HepG2 cells treated with NA-650 (500 nM) and compound **1** (2 μM) for 18 h. Red: internalized NA-650; Green: lysosome stained by Lysotracker; Blue: nuclei stained by Hoechst 33342; Yellow: merged area. White arrows indicate the co-localization of NA-650 and the lysosome. Scale bar: 20 μm. **L.** In gel fluorescence analysis of NA-650 (500 nM) internalization and degradation in HepG2 cells by compound **1** (2 μM) in the presence or absence of leupeptin (0.1 mg/mL).

4.3.3. A tri-GalNAc labelled full length antibody (goat anti-mouse IgG) facilitates the uptake of its protein target (mouse anti-biotin IgG-647).

Given the successful internalization and degradation of NA by **1** in the model system, we hypothesized that an antibody conjugated with tri-GalNAc can function similarly as **1** tested above - capturing the extracellular targeted protein and delivering it into the lysosome for degradation. To validate the feasibility of our hypothesis, I first functionalized an antibody with tri-GalNAc to generate an antibody-based degrader (tri-GalNAc-antibody). Tri-GalNAc-COOH **2** was converted to its active *N*-hydroxysuccinimide (NHS)-ester **3** under standard conditions, prepare by Dr. Peng Teng. The antibody was then conjugated with NHS ester **3** by reacting with the lysine residues on the antibody. After testing different molar ratios for the antibody conjugation, we found that the best labeling efficiency was achieved by using 25 equivalent of NHS ester **3** (Fig. 4.3A). Moreover, comparing the internalization of antibodies coupled with various equivalents of tri-GalNAc revealed that higher degree of tri-GalNAc labeling on the antibody resulted in a greater internalization capacity (Fig. 4.3B).

I then examined the uptake of the targeted protein by co-treating HepG2 cells with tri-GalNAc-modified goat anti-mouse IgG (Ab-GN) and fluorescent protein target mouse anti-biotin IgG-647 for 6 h. The addition of Ab-GN increased the uptake of mouse anti-biotin IgG-647 compared to the cells treated with mouse anti-biotin IgG-647 alone, but the efficiency was relatively low (Fig. 4.3C). To identify the factors that gave rise to the low uptake efficiency, fluorescent goat anti-mouse IgG-647 was directly labeled with NHS ester **3** (Ab-647-GN). Greater fluorescent intensity was observed in the cells treated with Ab-647-GN alone than the cells co-treated with Ab-GN and mouse IgG-647 (Fig. 4.3D), suggesting the low uptake of the targeted protein was not restrained by the internalization efficiency of tri-GalNAc-Ab itself. I then pre-incubated mouse anti-biotin IgG-647 and Ab-GN to allow the complex formed prior to the treatment. The pre-mixing did not enhance the amount of internalized mouse IgG-647 (Fig. 4.3D), suggesting that the complex formation is not the rate-limiting step for the tri-GalNAc-Ab mediated uptake.

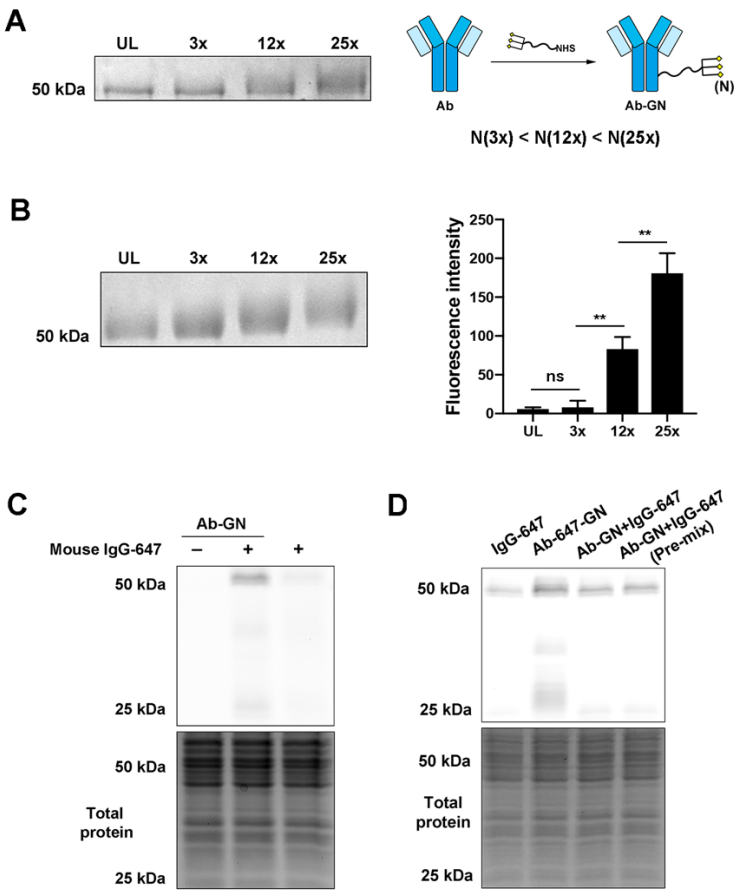

Figure 4.3. A tri-GalNAc labelled full length antibody goat anti-mouse IgG (Ab-GN) delivers target protein mouse anti-biotin IgG-647 into the cells. A. Goat anti-mouse full length antibody labeling with various amounts of tri-GalNAc. UL: unlabeled; 3x: 3 molar equivalent; 12x: 12 molar equivalent; 25x: 25 molar equivalent. N: the number of tri-GalNAc labeled on the antibody. **B.** Goat anti-mouse-647 antibody labeled with various amounts of tri-GalNAc and cellular uptake of Ab-647-GN (25 nM) with different degrees of labeling in 16 h. UL: unlabeled; 3x: 3 molar equivalent; 12x: 12 molar equivalent; 25x: 25 molar equivalent. Data presented as Mean±SD, n=3. Ns: not significant, **p<0.01. **C.** Uptake of mouse anti-biotin IgG-647 (50 nM) in the HepG2 cells treated with or without Ab-GN (25 nM) for 6 h. **D.** Mouse anti-biotin IgG-647 (50 nM) uptake mediated by Ab-GN (25 nM) with or without 1 h pre-mix before treatment for 6 h. The uptake of anti-biotin IgG-647 (50 nM) and Ab-647-GN (25 nM) were measured for comparison.

4.3.4. Comparison of the uptake efficiency of the protein targets (mouse anti-biotin IgG-647 and mouse anti-rabbit IgG-647) mediated by Fab fragment and full length antibodies labelled with different numbers of tri-GalNAc.

It has been reported that the size of the complex plays a critical role in the recognition and processing by the ASGPR. Efficient uptake of liposome could only be achieved when their sizes are less than 70 nm[21]. To compare the internalization efficiency of the protein target by degraders with different sizes, I labelled goat anti-mouse IgG Fab monomer (MW = 50 kDa) with NHS ester **3** to yield a smaller degrader, Fab-GN (Fig. 4.4A), in addition to the full-size goat anti-mouse IgG (MW = 150 kDa). Apart from size, the number of ligands labelled on each antibody may influence the accessibility of the degrader to the receptor and contribute to the difference in the target protein uptake efficiency. By adjusting the initial antibody concentration, I was able to produce two types of full-length antibody degraders with high (Ab-GN1) or low (Ab-GN2) tri-GalNAc labeling numbers. MALDI-MS indicated that Ab-GN1 was labelled with 5.7 tri-GalNAc residues in average per antibody, while Ab-GN2 had a lower average labeling number around 4.7 (Fig. 4.4A). All three antibodies (Ab-GN1, Ab-GN2, and Fab-GN) should bind to mouse anti-biotin IgG-647 with similar affinity. We then co-treated HepG2 and Huh7 cells with 50 nM of the protein target (mouse anti-rabbit IgG-647) together with 25 nM of goat anti-mouse IgG (Ab) and goat anti-mouse IgG Fab (Fab) with or without tri-GalNAc (GN) labeling. The amount of fluorescent mouse anti-rabbit IgG-647 inside the cells was monitored 6 h post-treatment. In gel fluorescence analysis showed that all three types of tri-GalNAc-antibodies were able to enhance the internalization of mouse anti-rabbit IgG-647 compared to the cells treated with non-modified antibodies. Among them, Ab-GN1, with only one more labelled tri-GalNAc residues than Ab-GN2 in average, exhibited higher uptake efficiency, suggesting that even slightly higher number of ligands on the degrader could facilitate the target protein internalization (Fig. 4.4B). Interestingly, Fab-

GN significantly boosted the uptake of the mouse IgG-647 compared to both of Ab-GNs, despite that fewer tri-GalNAc residues (~3.2) were modified on the antibody. Fab-GN, the tri-GalNAc conjugate with the lowest molecular weight and size, can promote the most efficient uptake of the protein target among the three antibody-based degraders, suggesting that the size of the tri-GalNAc-Ab may affect the endocytosis process mediated by ASGPR.

To further verify the potential role of molecule size in ASGPR mediated cellular uptake, I next compared the uptake efficiency of proteins in different sizes using the same small molecule-based degrader, **1**. Incubating mouse anti-biotin IgG-647 with goat anti-mouse IgG or anti-mouse IgG Fab fragment could enable the formation of protein complexes with increased molecular weight and sizes. HepG2 cells were treated with mouse anti-biotin IgG-647 (P1), pre-mixed mouse anti-biotin IgG-647/goat anti-mouse IgG Fab (P2) and pre-mixed mouse anti-biotin IgG-647/goat anti-mouse IgG (P3) in the presence of **2** or **1** for 6 h. The results showed that the uptake efficiency of protein targets decreased as the size of the complex increased when cells co-treated with the same amount of **1** (Fig. 4.4C). Acid **2** didn't induce the internalization of protein targets at all. Consistent with the results of tri-GalNAc-antibodies, **1** also displayed a higher uptake efficiency for the smaller degrader-target complex. The affinity of **1** to mouse anti-biotin IgG-647 (P1), pre-mixed mouse anti-biotin IgG-647/goat anti-mouse IgG Fab (P2), and pre-mixed mouse anti-biotin IgG-647/goat anti-mouse IgG (P3) should be very similar. The decreased uptake efficiency from P1 to P2 and from P2 to P3 appears to correlate with the increased size of the target complexes. These data indicate that the internalization

driven by a small molecule tri-GalNAc-conjugate through ASGPR is also more efficient for smaller degrader-protein target complexes.

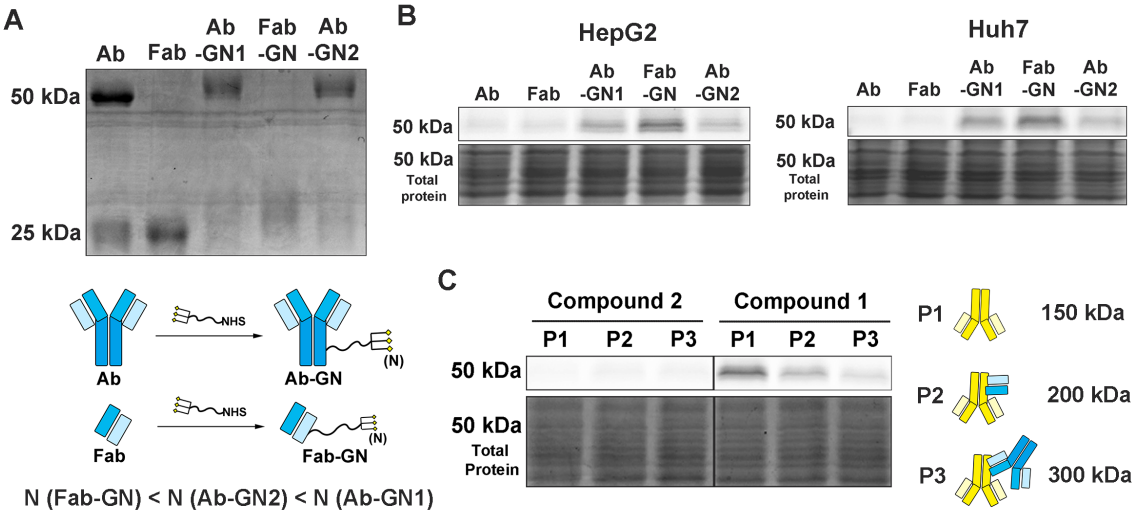

Figure 4.4. Uptake of mouse IgG-647 mediated by tri-GalNAc-labeled antibodies and compound 1. A. Antibody labeled with tri-GalNAc (25 molar equivalent). **B.** Comparison of the 6 h uptake of mouse anti-rabbit IgG-647 (50 nM) mediated by 25 nM of the goat anti-mouse IgG and goat anti-mouse IgG Fab with or without tri-GalNAc (GN) labeling. **C.** Cellular uptake of mouse anti-biotin IgG-647 (P1, 50 nM), pre-mixed mouse anti-biotin IgG-647 (50 nM) / goat anti-mouse IgG Fab (200 nM) complex (P2) and pre-mixed mouse anti-biotin IgG-647 (50 nM) / goat anti-mouse IgG (200 nM) complex (P3) in the presence of compound **1** (200 nM) or **2** (200 nM) for 6 h.

4.3.5. Tri-GalNAc-antibody mediates the uptake and degradation of both exogenous and endogenous protein targets through ASGPR in liver cells.

Different uptake efficiencies were observed for two different protein targets (mouse anti-biotin IgG-647 and mouse anti-rabbit IgG-647) using three different antibody-based degraders: full size antibody with high or low tri-GalNAc labeling, as well as tri-GalNAc-labelled Fab fragment. Owing to the highest uptake efficiency mediated by Fab-GN, I next compared the uptake of mouse anti-biotin IgG-647 in HepG2, Huh7 and A549 cell lines in the presence of Fab-GN. Similar to the small molecule-based degrader, the

amount of target protein internalized into cells was highly dependent on the ASGPR expression in different cell lines, meaning that the highest uptake was observed in HepG2 cells followed by Huh7 cells. No detection of the mouse IgG-647 in A549 cells indicated that the protein target can only be efficiently transported into ASGPR-expressing cell with the assistance of tri-GalNAc-modified antibody (Fig. 4.5A). The degradation of internalized mouse IgG-647 was detected after the removal of Fab-GN and mouse IgG-647 from the media for 3 h. The addition of leupeptin moderately inhibited the degradation (Fig. 4.5B). Moreover, we found that continuous treatment of known lysosome inhibitors chloroquine or leupeptin for 6 h increased the accumulation of mouse IgG-647 in both HepG2 and Huh7 cells (Fig. 4.5C). These results indicated that the protein was depleted through lysosome degradation pathway.

We next explored the application of the lysosome targeting degraders for endogenous proteins. I generated an antibody-based degrader targeting the cellular membrane protein, epidermal growth factor receptor (EGFR), which is commonly overexpressed and mutated in human tumors[38-41]. Cetuximab (Ctx), a monoclonal antibody against EGFR approved by the Food and Drug Administration (FDA), was conjugated with tri-GalNAc following the same procedure as secondary antibody used previously to generate the degrader Ctx-GN (Fig. 4.5D). MALDI analysis revealed that each Ctx was labelled with 6.0 tri-GalNAc motifs in average. To explore Ctx-GN-mediated EGFR degradation, HepG2 and Huh7 cells were treated with 30 nM Ctx-GN for 48 h, and a nearly 40% downregulation of EGFR was observed in Ctx-GN-treated cells compared to the cells incubated with non-modified Ctx or without treatment (Fig 4.5E). This result demonstrated the feasibility of our degraders on degrading endogenous proteins.

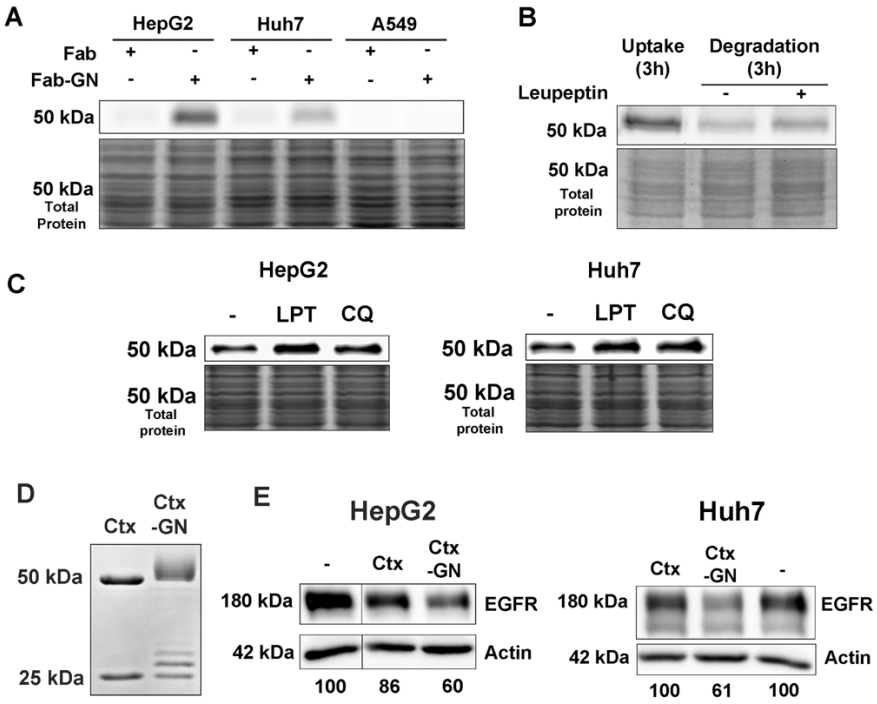

Figure 4.5. Tri-GalNAc-antibody mediates the uptake and degradation of mouse anti-biotin IgG-647 and EGFR in liver cells. A. Internalization of mouse anti-biotin IgG-647 in cells incubated with mouse anti-biotin IgG-647 (50 nM) and 25 nM of goat anti-mouse IgG Fab with or without tri-GalNAc (GN) labeling for 6 h. **B.** Mouse anti-biotin IgG-647 (50 nM) endocytosis and degradation in HepG2 cells in the presence or absence of leupeptin (0.1 mg/mL) for 6 h. **C.** Increased amount of internalized mouse anti-biotin IgG-647 in HepG2 and Huh7 cells in the presence of 10 μM chloroquine or 0.1 mg/mL leupeptin for 6 h. **D.** Ctx labeling with tri-GalNAc (25 molar equivalent). **E.** EGFR degradation in the presence of 30 nM Ctx-GN in HepG2 and Huh7 cells after 48 h treatment.

4.4. Conclusion

The emergence of chimeric molecules that are capable of depleting pathogenic proteins through native degradation pathways have the potential to overcome a major limitation of traditional therapeutic strategies, which generally need to bind to the protein target and alter its function. Targeted protein degradation using chimeric molecules only needs a binder to the protein target. Depletion of the entire pathogenic protein also offers unique advantages over functional inhibition in many cases. However, the most

developed targeted protein degradation strategy, namely PROTAC, is restricted to degrading intracellular targets. The M6P analogue-based LYTAC opened up a new direction of research area for targeted protein degradation by expanding the scope of targets to extracellular proteins. Similar to proteasome targeting degraders, where only handful of E3 ubiquitin ligase ligands are available, more lysosome targeting ligands need to be explored for expanded utilities of lysosome targeting degraders. We described our initial proof-of-concept studies using a tri-GalNAc-biotin small molecule and tri-GalNAc labelled antibodies to deliver the extracellular protein targets into the lysosome for degradation. We have shown that the internalization and lysosomal degradation of the protein targets through ASGPR are possible by both small molecule-based and antibody-based lysosome targeting degraders. We also observed that smaller complexes[42] exhibited higher uptake efficiency in several cases. In addition to the well-known factors, such as the length of linker, the type of linker, polyvalency, binding affinities to the receptor and protein target, expression levels of receptor and protein target, the size of the complex may be an additional parameter for the optimization of triantennary GalNAc conjugate-mediated lysosomal degradation of extracellular proteins. Overall, our studies demonstrated the feasibility of ASGPR-mediated liver cell-specific targeted protein degradation strategy and uncovered a potential new therapeutic application of triantennary GalNAc in addition to its well-known utilities in liver-specific delivery of oligonucleotides.

4.5. Materials and Methods

4.5.1. Safety Statement

No unexpected or unusually high safety hazards were encountered.

4.5.2. General chemistry methods

Tri-GalNAc-biotin 1 and tri-GalNAc-COOH 2 were purchased from Sussex Research Laboratories Inc. Other reagents and solvents were purchased from Fisher Scientific and used as received. TriGalNAc-NHS ester 3 was prepared from tri-GalNAc-COOH 2 in the presence of Nhydroxysuccinimide and N, N′-dicyclohexylcarbodiimide in dimethylformamide (DMF) as used without further purification. The reaction was monitored by Agilent single quadrupole (SQ) LC/MS.

4.5.3. Cell culture

HepG2 and Huh7 cells were cultured in T75 flasks and maintained in low-glucose DMEM supplemented with 10% fetal bovine serum, 1% non-essential amino acids, 1% sodium pyruvate, 1% L-glutamine and 1% penicillin/streptomycin under 5 % CO_2 at 37 °C. A549 cells were cultured in T75 flasks and maintained in RPMI supplemented with 10% fetal bovine serum, 1% sodium pyruvate, 1% HEPES and 1% penicillin/streptomycin under 5 % CO_2 at 37 °C.

4.5.4. NeutraAvidin uptake experiments

Cells were seeded at 45,000 cells per well in 100 µL complete culture media in 96-well cell culture plates or plated at 250,000 cells per well in a 24-well plate. The next day, the medium was replaced followed by the sequential addition of NA-650 and tri-GalNAc-biotin 1 or tri-GalNAc-COOH 2 with various concentrations. The cells were incubated at 37 °C for different time periods and then washed twice with PBS to removed extracellular NA-650. The uptake in 96-well plate was determined by measuring the fluorescent intensity at 650 nm excitation/680 nm emission using the Synergy H1

microplate reader. Data was acquired using Gen5 software. The cells in 24-well plate were lysed for in gel fluorescence analysis.

4.5.5. Competition assay

HepG2 cells were plated and treated with 500 nM of NA-650 and 2 μM of tri-GalNAc-biotin 1 in the same manner as mentioned above. Extra tri-GalNAc-COOH 2 (1, 2, 5, 10, 20 μM) was added at the same time before incubation. After 4 h, cells were washed twice with PBS, and the uptake of NA-650 was read by the plate reader as mentioned above.

4.5.6. Knockdown of ASGPR by siRNA

HepG2 cells were seeded at 75,000 cells per well in a 24-well plate one day before transfection. Cells were then transfected with 20 pmol of ASGPR-specific or scramble siRNA and 1.5 μL transfection reagent RNAiMax for 48 h prior to the detection of ASGPR expression level or NA650 uptake.

4.5.7. Confocal microscopy

HepG2 cells were seeded onto 8-well chamber slides at the density of 20,000 cells/well in 200 μL of complete culture medium. After adhesion, cells were treated with 500 nM of NA-650 and 2 μM of tri-GalNAc-biotin 1 for 18 h at 37 °C, followed by the 30-min incubation with LysoTracker Green DND26 (100 nM) at 37 °C. Hoechst 33342 (5 ug/ml) was added 10 min before the end of incubation. After three washes with PBS, the live cells were imaged using FluoView confocal microscope at 20x magnification with a 10x eyepiece. All images were acquired by FV10-ASW and analyzed by ImageJ.

4.5.8. NeutrAvidin degradation analysis

HepG2 cells were seed at 250,000 cells per well in a 24-well plate. Next day, cells were incubated with 500 nM of NA-650 and 2 μM of tri-GalNAc-biotin 1 for 1 h followed by three washes with PBS. Cells were maintained subsequently in fresh media with or without 0.1 mg/mL leupeptin for another 3 h, 6 h, and 24 h before harvested for in gel fluorescence analysis.

4.5.9. Antibody labeling

The antibody solution was first loaded onto a 10 kDa Amicon Centrifugal Filter to remove the preservative and concentrate the antibody before labeling. To label the antibody with tri-GalNAc, 50 μL of the antibody (concentration above 1 mg/mL) in PBS was mixed with tri-GalNAc-NHS ester 3 at 1:3, 1:12 or 1:25 molar ratio. The reaction was incubated overnight at room S4 temperature on a rotator, followed by filtration with 500 μL of PBS for 5 times using 10 kDa Amicon Centrifugal Filter.

4.5.10. Tri-GalNAc-antibody uptake experiment

HepG2 cells were plated at 45,000 cells per well in 100 μL complete culture media in a 96-well cell culture plate 8 h prior to the treatment. Cells were then incubated with 25 nM Ab-647-GN with different modification levels for 16 h before measuring the fluorescence intensity in the cells.

4.5.11. Mouse IgG uptake experiment

HepG2, Huh7 and A549 cells were plated at 250,000 cells per well in a 24-well plate. Complete growth media supplemented with 50 nM of mouse anti-biotin-IgG-647 (protein target in Fig. S4) or mouse anti-rabbit-IgG-647 (protein target in Fig. 4B) and 25 nM of tri-GalNAc labelled goat anti-mouse IgG or goat anti-mouse IgG Fab was sequentially

added. The cells were incubated at 37 °C for 6 h and then lysed for in gel fluorescence analysis.

4.5.12. Mouse IgG degradation analysis

HepG2 cells were seed at 250,000 cells per well in a 24-well plate. Next day, cells were incubated with 50 nM of mouse anti-biotin IgG-647 and 25 nM of tri-GalNAc goat-anti-mouse IgG Fab for 3 h followed by three washes with PBS. Cells were maintained subsequently in fresh media with or without 0.1 mg/mL leupeptin for another 3 h before harvested for in gel fluorescence analysis. For the co-treatment assay, HepG2 or Huh7 cells were seed at 250,000 cells per well in a 24-well plate. Next day, cells were incubated with 50 nM of mouse anti-biotin IgG-647, 25 nM of triGalNAc goat-anti-mouse IgG Fab, together with 10 μM chloroquine or 0.1 mg/mL leupeptin for 6 h followed by the collection of samples for in gel fluorescence analysis.

4.5.13. NeutrAvidin and IgG complex uptake experiment

HepG2 cells were plated at 250,000 cells per well in a 24-well plate. Next day, 50 nM mouse antibiotin IgG-647 was mixed with 200 nM goat anti-mouse IgG or goat anti-mouse IgG Fab on a rotator at room temperature for 1 h before treatment. Cells were then respectively incubated with mouse anti-biotin IgG-647, anti-biotin IgG-647/goat anti-mouse IgG Fab and anti-biotin IgG- S5 647/goat anti-mouse IgG complex together with 200 nM tri-GalNAc-COOH 2 or tri-GalNAcbiotin 1 for 6 h. The cells were then harvested and lysed for in gel fluorescence analysis.

4.5.14. MALDI-MS

α-Cyano-4-hydroxycinnamic acid (CHCA) was dissolved in 50% Acetonitrile/H2O to give a 10 mg/mL solution as the matrix solution. The sample was absorbed on Omix C4 pipette tips, washed by 0.1% TFA for three times and then eluted with 20 μL 75% Acetonitrile/H2O. 1 μL sample solution and 1 μL CHCA solution were spotted on the MALDI target plate and mixed thoroughly before the spot was allowed to dry under room temperature. MALDI-MS spectra were acquired on Bruker UltraFlex MALDI-TOF/TOF mass spectrometer operated in linear positive ion mode. Masses were calculated from windowed raw data in Sigmaplot 13.0 by fitting to gaussian curves, with constant baseline as an additional free parameter. Parameter starting values were the default values of the program, and were automatically iterated 200 times to obtain fits. Plots were made in Origin 2020, where high-frequency noise was removed using 100 points windowed FFT filter.

4.5.15. EGFR degradation analysis

HepG2 cells were seeded at 100,000 cells per well and Huh7 cells were seeded at 75,000 cells per well in a 24-well plate. Next day, cells were treated with 30 nM Ctx or Ctx-GN for 48 h before collection for western blot analysis.

4.5.16. Western blotting

Cells were lysed with 1X RIPA lysis buffer containing 25 mM Tris, pH 7−8, 150 mM NaCl, 0.1% (w/ v) sodium dodecyl sulfate (SDS), 0.5% sodium deoxycholate, 1% (v/ v) Triton X-100, protease inhibitor cocktail (Roche, one tablet per 10 mL) and 1 mM phenylmethylsulfonyl fluoride on ice for 10 min. The lysates were then centrifuged at 14 000g at 4 °C for 15 min and the supernatant was collected followed by measuring the protein concentration using BCA assay. Lysates were adjusted to the equal amount

before mixed with the 4x Laemmli Loading Dye and heated at 95−100 °C for 5 min. After cooling down, samples were loaded onto 7.5% SDS−polyacrylamide gel electrophoresis and transferred to PVDF membrane. The membrane was first blocked in 5% (w/v) non-fat milk in the TBS-T washing buffer (137 mM NaCl, 20 mM Tris, 0.1% (v/v) Tween) S6 and then incubated with primary antibodies at 4 °C overnight. After 3 washes with TBST, the membrane was incubated with secondary HRP-linked antibodies for 1 h, and then washed 3 times with TBST. Then the membrane was incubated in the Clarity ECL substrate for 3- 5 min before acquiring the immunoblot by ChemiDoc MP Imaging Systems.

4.6. References

1 Rock, K. L. *et al.* Inhibitors of the proteasome block the degradation of most cell proteins and the generation of peptides presented on MHC class I molecules. *Cell* **78**, 761-771 (1994). https://doi.org/10.1016/s0092-8674(94)90462-6

2 Ciechanover, A. & Schwartz, A. L. The ubiquitin-proteasome pathway: the complexity and myriad functions of proteins death. *Proc Natl Acad Sci U S A* **95**, 2727-2730 (1998). https://doi.org/10.1073/pnas.95.6.2727

3 Yim, W. W. & Mizushima, N. Lysosome biology in autophagy. *Cell Discov* **6**, 6 (2020). https://doi.org/10.1038/s41421-020-0141-7

4 Lamb, C. A., Dooley, H. C. & Tooze, S. A. Endocytosis and autophagy: Shared machinery for degradation. *Bioessays* **35**, 34-45 (2013). https://doi.org/10.1002/bies.201200130

5 Sakamoto, K. M. *et al.* Protacs: chimeric molecules that target proteins to the Skp1-Cullin-F box complex for ubiquitination and degradation. *Proc Natl Acad Sci U S A* **98**, 8554-8559 (2001). https://doi.org/10.1073/pnas.141230798

6 Schapira, M., Calabrese, M. F., Bullock, A. N. & Crews, C. M. Targeted protein degradation: expanding the toolbox. *Nat Rev Drug Discov* **18**, 949-963 (2019). https://doi.org/10.1038/s41573-019-0047-y

7 Takahashi, D. *et al.* AUTACs: Cargo-Specific Degraders Using Selective Autophagy. *Mol Cell* **76**, 797-810.e710 (2019). https://doi.org/10.1016/j.molcel.2019.09.009

8 Banik, S. M. *et al.* Lysosome-targeting chimaeras for degradation of extracellular proteins. *Nature* **584**, 291-297 (2020). https://doi.org/10.1038/s41586-020-2545-9

9 Basile, I. *et al.* Efficient therapy for refractory Pompe disease by mannose 6-phosphate analogue grafting on acid α-glucosidase. *J Control Release* **269**, 15-23 (2018). https://doi.org/10.1016/j.jconrel.2017.10.043

10 Bouffard, E. *et al.* Efficient Photodynamic Therapy of Prostate Cancer Cells through an Improved Targeting of the Cation-Independent Mannose 6-Phosphate Receptor. *Int J Mol Sci* **20**, 2809 (2019). https://doi.org/10.3390/ijms20112809

11 Hyun, J. Y., Kim, S., Lee, H. S. & Shin, I. A Glycoengineered Enzyme with Multiple Mannose-6-Phosphates Is Internalized into Diseased Cells to Restore Its Activity in Lysosomes. *Cell Chem Biol* **25**, 1255-1267.e1258 (2018). https://doi.org/10.1016/j.chembiol.2018.07.011

12 Das, S., Parekh, N., Mondal, B. & Gupta, S. Controlled Synthesis of End-Functionalized Mannose-6-phosphate Glycopolypeptides for Lysosome Targeting. *ACS Macro Lett.* **5**, 809-813 (2016).

13 Crucianelli, E. *et al.* Liposomes containing mannose-6-phosphate-cholesteryl conjugates for lysosome-specific delivery. *RSC Advances* **4**, 58204-58207 (2014). https://doi.org/10.1039/C4RA08681C

14 Agarwal, V. *et al.* Enhancing the efficacy of cation-independent mannose 6-phosphate receptor inhibitors by intracellular delivery. *Chem Commun (Camb)* **52**, 327-330 (2016). https://doi.org/10.1039/c5cc06826f

15 Spiess, M. The asialoglycoprotein receptor: a model for endocytic transport receptors. *Biochemistry* **29**, 10009-10018 (1990). https://doi.org/10.1021/bi00495a001

16 Schwartz, A. L., Fridovich, S. E. & Lodish, H. F. Kinetics of internalization and recycling of the asialoglycoprotein receptor in a hepatoma cell line. *J Biol Chem* **257**, 4230-4237 (1982).

17 Baenziger, J. U. & Fiete, D. Galactose and N-acetylgalactosamine-specific endocytosis of glycopeptides by isolated rat hepatocytes. *Cell* **22**, 611-620 (1980). https://doi.org/10.1016/0092-8674(80)90371-2

18 Drickamer, K. Ca2+-dependent carbohydrate-recognition domains in animal proteins. *Curr Opin Struct Biol.* **3**, 393-400 (1993).

19 Lee, Y. C. *et al.* Binding of synthetic oligosaccharides to the hepatic Gal/GalNAc lectin. Dependence on fine structural features. *J Biol Chem* **258**, 199-202 (1983).

20 Biessen, E. A. *et al.* Synthesis of cluster galactosides with high affinity for the hepatic asialoglycoprotein receptor. *J Med Chem* **38**, 1538-1546 (1995). https://doi.org/10.1021/jm00009a014

21 Rensen, P. C. *et al.* Determination of the upper size limit for uptake and processing of ligands by the asialoglycoprotein receptor on hepatocytes in vitro and in vivo. *J Biol Chem* **276**, 37577-37584 (2001). https://doi.org/10.1074/jbc.M101786200

22 Glazier, D. A. *et al.* Chemical Synthesis and Biological Application of Modified Oligonucleotides. *Bioconjug Chem* **31**, 1213-1233 (2020). https://doi.org/10.1021/acs.bioconjchem.0c00060

23 Huang, Y. Preclinical and Clinical Advances of GalNAc-Decorated Nucleic Acid Therapeutics. *Mol Ther Nucleic Acids* **6**, 116-132 (2017). https://doi.org/10.1016/j.omtn.2016.12.003

24 Prakash, T. P. *et al.* Targeted delivery of antisense oligonucleotides to hepatocytes using triantennary N-acetyl galactosamine improves potency 10-fold in mice. *Nucleic Acids Res* **42**, 8796-8807 (2014). https://doi.org/10.1093/nar/gku531

25 Schmidt, K. *et al.* Characterizing the effect of GalNAc and phosphorothioate backbone on binding of antisense oligonucleotides to the asialoglycoprotein receptor. *Nucleic Acids Res* **45**, 2294-2306 (2017). https://doi.org/10.1093/nar/gkx060

26 Medina, S. H. *et al.* N-acetylgalactosamine-functionalized dendrimers as hepatic cancer cell-targeted carriers. *Biomaterials* **32**, 4118-4129 (2011). https://doi.org/10.1016/j.biomaterials.2010.11.068

27 Chen, S. *et al.* Development of lipid nanoparticle formulations of siRNA for hepatocyte gene silencing following subcutaneous administration. *J Control Release* **196**, 106-112 (2014). https://doi.org/10.1016/j.jconrel.2014.09.025

28 Tomiya, N. *et al.* Liver-targeting of primaquine-(poly-γ-glutamic acid) and its degradation in rat hepatocytes. *Bioorg Med Chem* **21**, 5275-5281 (2013). https://doi.org/10.1016/j.bmc.2013.06.028

29 Yang, K. *et al.* Development of the first small molecule histone deacetylase 6 (HDAC6) degraders. *Bioorg Med Chem Lett* **28**, 2493-2497 (2018). https://doi.org/10.1016/j.bmcl.2018.05.057

30 Wang, B. *et al.* Development of selective small molecule MDM2 degraders based on nutlin. *Eur J Med Chem* **176**, 476-491 (2019). https://doi.org/10.1016/j.ejmech.2019.05.046

31 Roberts, B. L. *et al.* Two-Stage Strategy for Development of Proteolysis Targeting Chimeras and its Application for Estrogen Receptor Degraders. *ACS Chem Biol* **15**, 1487-1496 (2020). https://doi.org/10.1021/acschembio.0c00140

32 Yang, K. *et al.* A Cell-Based Target Engagement Assay for the Identification of Cereblon E3 Ubiquitin Ligase Ligands and Their Application in HDAC6 Degraders. *Cell Chem Biol* **27**, 866-876.e868 (2020). https://doi.org/10.1016/j.chembiol.2020.04.008

33 Wang, H. Y., Blaszczyk, S. A., Xiao, G. & Tang, W. Chiral reagents in glycosylation and modification of carbohydrates. *Chem Soc Rev* **47**, 681-701 (2018). https://doi.org/10.1039/c7cs00432j

34 Blaszczyk, S. A., Homan, T. C. & Tang, W. Recent advances in site-selective functionalization of carbohydrates mediated by organocatalysts. *Carbohydr Res* **471**, 64-77 (2019). https://doi.org/10.1016/j.carres.2018.11.012

35 David, C. *et al.* Bifunctional Small Molecules That Mediate the Degradation of Extracellular Proteins. *ChemRxiv* (2020, July 29). https://doi.org/10.26434/chemrxiv.12732689.v2

36 Green, A. *et al.* Lysosome Targeting Chimeras (LYTACs) That Engage a Liver-Specific Asialoglycoprotein Receptor for Targeted Protein Degradation. *ChemRxiv* (2020, July 30). https://doi.org/10.26434/chemrxiv.12736778.v1

37 Douglass, E. F., Miller, C. J., Sparer, G., Shapiro, H. & Spiegel, D. A. A comprehensive mathematical model for three-body binding equilibria. *J Am Chem Soc* **135**, 6092-6099 (2013). https://doi.org/10.1021/ja311795d

38 Hashmi, A. A. *et al.* Epidermal growth factor receptor (EGFR) overexpression in triple-negative breast cancer: association with clinicopathologic features and prognostic parameters. **2**, 6 (2019).

39 Rosell, R., Felip, E., Garcia-Campelo, R. & Balaña, C. The biology of non-small-cell lung cancer: identifying new targets for rational therapy. *Lung Cancer* **46**, 135-148 (2004). https://doi.org/10.1016/j.lungcan.2004.04.031

40 Zimmermann, M., Zouhair, A., Azria, D. & Ozsahin, M. The epidermal growth factor receptor (EGFR) in head and neck cancer: its role and treatment implications. *Radiat Oncol* **1**, 11 (2006). https://doi.org/10.1186/1748-717X-1-11

41 Pabla, B., Bissonnette, M. & Konda, V. J. Colon cancer and the epidermal growth factor receptor: Current treatment paradigms, the importance of diet, and the role of chemoprevention. *World J Clin Oncol* **6**, 133-141 (2015). https://doi.org/10.5306/wjco.v6.i5.133

Chapter 5

Development of Integrin Targeting Chimeras (ITACs) for the Lysosomal Degradation of Extracellular Proteins

This chapter is adapted from a manuscript published in *ChemMedChem.*

Zhou Y, Liao Y, Zhao Y, Tang W.* Development of Integrin Targeting Chimeras (ITACs) for the Lysosomal Degradation of Extracellular Proteins. *ChemMedChem* **2024,** e202300643.

*To whom correspondence should be addressed

5.1. Abstract

The emerging lysosomal targeting chimera (LYTAC) expands the field of targeted protein degradation (TPD) to include the extracellular proteins for precise depletion. However, most of the reported LYTACs either induce ubiquitous degradation of the protein of interest (POI) in a broad range of tissues or specifically target liver cells. More tissue-selective degraders are highly desirable. In this chapter, we describe the development of cyclic RGD (cRGD) peptide-antibody conjugates as a novel class of integrin targeting chimeras (ITACs) with potential cancer selectivity. Our results indicate that the ITACs are able to recruit integrin to induce the degradation of both soluble and membrane targets in the lysosome. We observed higher efficiency of ITACs on degrading membrane protein in cancer cells, providing a promising platform for cancer-selective TPD strategy.

5.2. Introduction

Recently, lysosomal targeting chimera (LYTAC) emerged as a novel and promising therapeutic paradigm for drug discovery[1]. LYTAC, composed of a ligand of lysosomal targeting receptor (LTR) and a binder of the extracellular protein of interest (POI), recruits LTR to trigger the internalization of POI through receptor-mediated endocytosis and further deliver POI in the lysosome for degradation utilizing intrinsic cellular degradation pathway. Different forms, such as small molecule conjugates, antibody conjugates, or recombinant proteins, have been generated as LYTACs to trigger the degradation of various POIs. LYTAC expands the scope of targeted protein degradation (TPD) strategy to include therapeutically relevant extracellular POIs. It thus complements proteolysis targeting chimera (PROTAC), which mainly depletes intracellular POIs via ubiquitin-proteasome degradation pathway[2-4]. However, compared

to PROTAC, the most successful strategy for TPD, only limited progresses have been made for LYTAC development. Most of the reported LYTACs targeting oncogenic POIs leverage the LTRs ubiquitously expressed on a broad range of tissues, including cation-independent mannose-6-phosphate receptor (CI-M6PR) and cytokine receptor CXCR7, which in turn raise potential issues due to on-target, off-tissue side effects[5-7]. Several groups including ours endowed LYTACs with tissue selectivity by utilizing asialoglycoprotein receptor (ASGPR) to specifically degrade POIs in liver cells[8-10]. However, it is highly desirable to selectively degrade membrane-bound cancer-related POIs outside of liver[11]. For example, LYTACs that can selectively degrade tumorigenic POIs on cancer cells can reduce the exposure of healthy tissues to the degraders and improve therapeutic efficacy and index of LYTACs.

Integrins are transmembrane cell adhesion receptors composed of noncovalently connected α-and β-subunits, totally 24 different heterodimers[12]. Some subtypes of integrin, such as αvβ3, αvβ5 and α5β1, are overexpressed and associated with different stages of tumor progression on various cancer types[13-16]. The elevated expression level on cancer cells makes integrin a heavily sought receptor to direct the therapeutic or diagnosis reagents to the cancer cells. Arginine-glycine-aspartic acid (RGD) sequence identified from fibronectin and other extracellular matrix (ECM) proteins is the basic recognition motif for integrin in the application of antagonist development and targeted drug delivery[17,18]. One of the widely used derivatives of RGD ligand is c(RGDfK) (abbreviated as cRGD thereafter). Cyclization and introduction of the D-phenylalanine renders RGD ligand with enhanced stability, binding affinity (nanomolar range) and higher specificity towards αvβ3 integrin compared to the linear RGD peptide[19,20]. The

attachment of cRGD to the drug carriers, such as liposome and nanoparticle, allows the drug to accumulate in the cancer cells via the interaction between cRGD and integrin followed by the internalization and transportation of the drug to the endosome or lysosome[21-23]. Given the successful application of cRGD/integrin system in the targeted drug delivery, we hypothesize that cRGD conjugated with a binder of POI can form a cancer-selective degrader for the POI. While we were preparing our manuscript, a similar work of integrin-facilitated lysosomal degradation (IFLD) using the degrader containing a c(RGDyK) peptide linked by a small molecule binder of PD-L1 was reported[24]. However, selective degradation of PD-L1 in cancer cells or tumor tissues was not experimentally demonstrated. In this chapter, we attached cRGD to the antibodies against model target anti-biotin-647 and epidermal growth factor receptor (EGFR). We demonstrated the antibody-peptide conjugate could recruit integrin and mediate the lysosomal degradation of POIs as a novel class of integrin targeting chimeras (ITACs). Moreover, the ITAC degrades EGFR more effectively on various cancer cells than normal cells.

5.3. Results and Discussion

We first explored whether cRGD-biotin can mediate the uptake of fluorescent neutravidin-650 (NA-650), a model target protein, into the cells. Graduate student Yuan Zhao treated Huh7 and MCF7 cells with 2 μM cRGD-biotin and 500 nM NA-650 for 6 h. In-gel fluorescence analysis showed a significant increase of internalized NA-650 in the presence of cRGD-biotin (Fig. 5.1A, B). To investigate the intracellular location of NA-650 after internalization, I stained the lysosome with lysoTracker and found that NA-650 was co-localized with lysosome when co-incubated with cRGD-biotin for 4 or 24h (Fig.

5.1C). These results indicated that cRGD-biotin could deliver the target protein into lysosome for degradation.

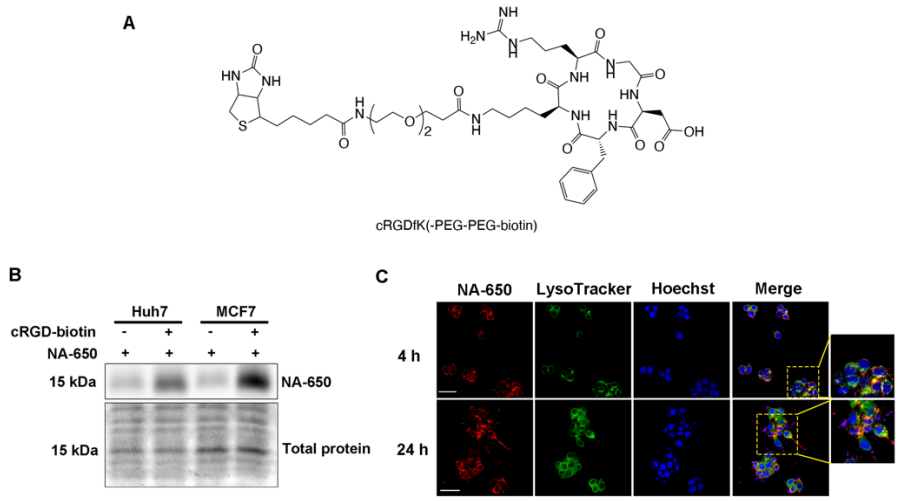

Figure 5.1. cRGD-biotin mediates the uptake and lysosomal degradation of NA-650. A. Structure of cRGD-biotin. **B.** Uptake of 500 nM NA-650 in Huh7 and MCF7 cells induced by 2 μM cRGD-biotin for 6 h. **Note:** This experiment was done by Yuan Zhao. **C.** Colocalization of internalized NA-650 with lysosome. Scale bar: 75 μm.

Next, I tested the feasibility of target protein internalization mediated by an antibody-based degrader (Ab-cRGD). Anti-mouse IgG antibody was first tethered with DBCO-PEG3-NHS or DBCO-PEG12-NHS followed by reacting with cRGD-azide through click chemistry to generate degraders with different linker lengths (Fig. 5.2A). The results showed that Ab-cRGD was able to induce the uptake of model target anti-biotin-647 into the cells and the linker length between cRGD and antibody had minimal effect on the uptake efficiency (Fig. 5.2B). Pre-incubation with 6 μM of cRGD-azide for 1 h at 4 °C could interrupt the interaction between Ab-cRGD and integrin and abolish the internalization of anti-biotin-647 mediated by Ab-cRGD. This observation demonstrated the role of integrin in the endocytosis process (Fig. 5.2C). To verify the degradation occurred in lysosome, I first treated MCF7 cells with Ab-cRGD and anti-biotin-647 for 24

h to allow the internalization of target protein. The media containing the degrader and target protein was then removed and replaced with fresh media with or without 50 nM lysosomal degradation inhibitor Bafilomycin A1 (BAF1) to incubate for another 3 h. We found that anti-biotin-647 was accumulated in the cells within the first 24 h and then diminished in the following 3 h after replacing the media. BAF1 partially rescued the intracellular anti-biotin-647 level, suggesting the target protein was transported into lysosome for degradation after internalization (Fig. 5.2D).

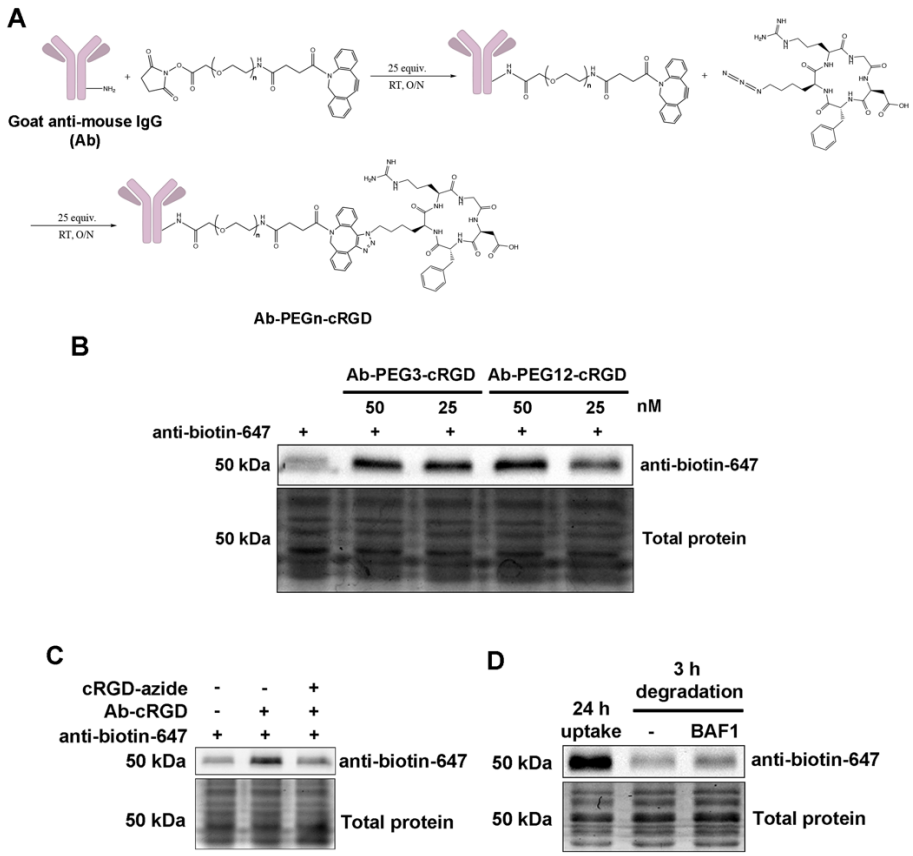

Figure 5.2. Ab-cRGD mediates the uptake and lysosomal degradation of anti-biotin-647 through the interaction with integrin. A. Synthesis of Ab-cRGD. **B.** Competition of Ab-cRGD-induced anti-biotin-647 uptake by 6 μM of cRGD-azide. **C.** Comparison of 50 nM of anti-biotin-647 uptake mediated by 50 or 25 nM of Ab-PEG3-cRGD or Ab-PEG12-cRGD for 3 h in HepG2 cells. **D.** inhibition of lysosomal degradation of anti-biotin-647 by 50 nM of Bafilomycin A1 (BAF1).

Next, we determined if the cRGD-tethered degrader can also be applied on membrane proteins. Cetuximab (Ctx), the therapeutic antibody against EGFR, was tagged with cRGD via two-step labeling method as mentioned above (Fig. 5.3A). Degraders with PEG3 or PEG12 linker were synthesized and compared for their degradation efficiency in MCF7 cells. The results showed that Ctx-PEG12-cRGD, which was equipped with a longer linker, induced more significant EGFR degradation compared to the degrader with a shorter linker, Ctx-PEG3-cRGD. Unlike soluble target proteins, our results indicate that the distance between cRGD and antibody can impact the degradation efficiency of membrane proteins (Fig. 5.3B). Given higher target protein degradation efficacy was obtained by the degrader with a longer linker, Yaxian Liao and I then characterized the dose response and time course of EGFR degradation induced by Ctx-PEG12-cRGD. Increasing the amount of Ctx-PEG12-cRGD could lead to lower EGFR levels in MCF7 cells after 24 h of treatment, with the maximal degradation (~50%) detected at 1 nM (Fig 5.3C). The time-course study revealed that 10 nM of cRGD-antibody conjugate induced EGFR degradation in a time-dependent manner. Significant degradation of EGFR was observed at 8 h, reached maximum at 16 h, and lasted till 48 h (Fig 5.3D). The degradation of EGFR induced by the degrader was then verified by me via immune-fluorescent staining. I observed dramatic reduction of EGFR level on the cellular membrane on cells treated with Ctx-PEG12-cRGD compared to the untreated and Ctx-treated cells (Fig. 5.3E). To demonstrate that the target protein degradation requires the interaction with integrin, cells were pre-treated with excess cRGD-azide at 4 °C for 1 h before incubating with Ctx-PEG12-cRGD for 8 h. I found that cRGD-azide could block EGFR degradation in a dose-dependent manner, indicating the

involvement of integrin in the degradation process (Fig. 5.3F). To further elucidate the mechanism, I tracked the intracellular location of EGFR after degrader treatment by co-staining EGFR and lysosome-associated membrane protein 1 (LAMP1) with corresponding antibodies (Fig. 5.3G). The co-localization of internalized EGFR with lysosome indicated that the degradation occurred in lysosome. I further verified the lysosomal degradation of EGFR by treating cells with lysosomal degradation inhibitor Bafilomycin A1 (BAF1) and Chloroquine (CQ) in the presence of Ctx-PEG12-cRGD, which impeded the EGFR degradation induced by the degrader (Fig. 5.3H).

Finally, I investigated the selectivity of cRGD-attached degraders or ITACs towards cancer cells by comparing the potency of the degrader in another two cancer cell lines, Hela and HepG2 cells, with the normal keratinocyte, HACAT cell. Similar to what we observed in MCF7 cells, which showed around 50% of EGFR depletion, 10 nM of cRGD-PEG12-Ctx significantly reduced the level of EGFR to 40% in Hela cells and 60% in HepG2 cells after 24 h, while minimal EGFR was reduced (~20%) in HACAT cells, indicating the potential cancer selectivity of ITACs (Fig 5.4).

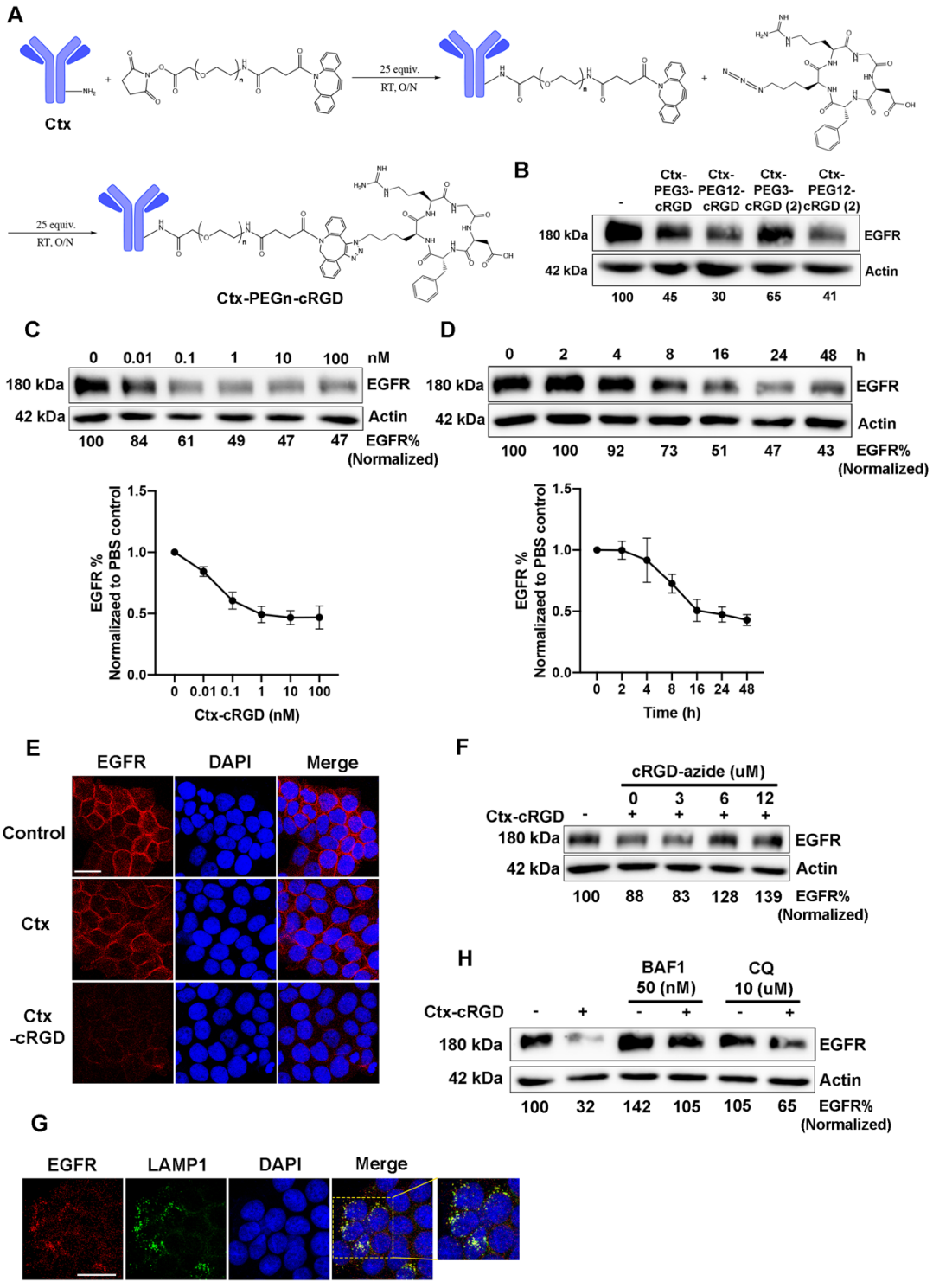

Figure 5.3. Ctx-cRGD mediates lysosomal degradation of EGFR via interacting with integrin. A. Synthesis of Ctx-cRGD. **B.** Comparison of EGFR degradation induced by 10 nM of Ctx-PEG3-cRGD or Ctx-PEG12-cRGD for 24 h in MCF7 cells. **C.** Dose response of Ctx-cRGD-induced EGFR degradation for 24 h. Data presented as mean ±

SD, n = 3. D. Time course of 10 nM Ctx-cRGD- induced EGFR degradation. **E.** Immunofluorescent staining of EGFR degradation. Scale bar: 25 μm. **F.** Inhibition of EGFR degradation by increasing concentrations of cRGD-azide. **G.** Colocalization of internalized EGFR with lysosome in the presence of 10 nM Ctx-cRGD. Scale bar: 25 μm. **H.** Inhibition of EGFR degradation by lysosomal degradation inhibitors Bafilomycin A1 (BAF1, 50 nM) and Chloroquine (CQ, 10 uM).

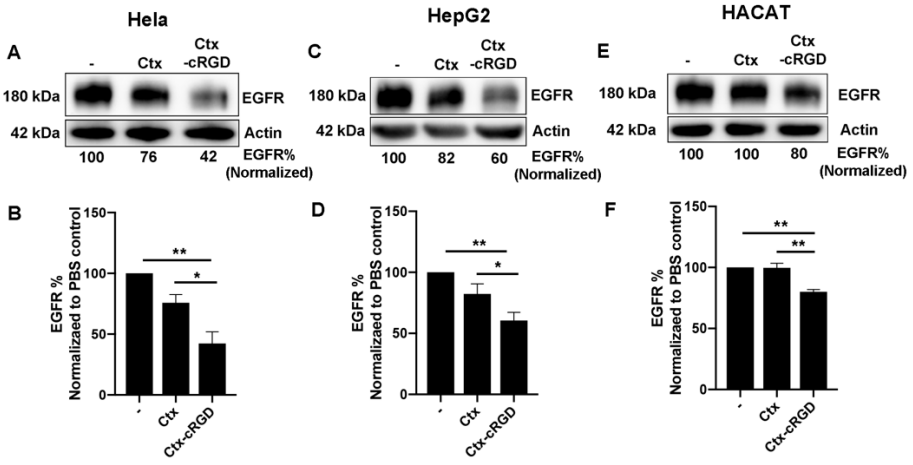

Figure 5.4. Ctx-cRGD has higher degradation efficacy on cancer cells. A, C, E. EGFR degradation induced by 10 nM Ctx-cRGD in Hela, HepG2, and HACAT cells. **B, D, F.** Quantification of **A, C, E.** Data presented as mean ± SD, n = 3. The statistical significance was assessed using paired t test, *P < 0.05, **P < 0.01.

5.4. Conclusion

In summary, we developed integrin targeting chimeras or ITACs by conjugating the cyclic peptide binder of integrin, cRGD, to the antibody against soluble and membrane targets. We demonstrated that the ITACs could deplete both soluble and membrane POIs in the lysosome after integrin-mediated endocytosis. Degraders with a longer linker between cRGD and antibody induced significantly more EGFR degradation, but had minimal advantage on uptake efficiency of soluble protein compared to the one with a shorter linker. Higher EGFR degradation efficiency of the degrader was observed on

several cancer cells compared to the normal cell line HACAT, suggesting ITACs have the potential to selectively degrade POIs on cancer cells. Our work paves the path for precise degradation of cancer-associated POIs in malignant cells. This approach could potentially offer a significant reduction in toxicity compared to most current degraders, which often induce widespread degradation of target proteins, affecting a broad spectrum of tissues including healthy ones.

5.5. Experimental Procedures

5.5.1. Cell culture

HepG2 and Huh7 cells were cultured in low-glucose DMEM supplemented with 10% fetal bovine serum, 1% non-essential amino acids, 1% sodium pyruvate, 1% L-glutamine and 1% penicillin/streptomycin under 5 % CO_2 at 37 °C. MCF7, Hela, and HACAT cells were maintained in high-glucose DMEM supplemented with 10% fetal bovine serum, and 1% penicillin/streptomycin under 5 % CO_2 at 37 °C.

5.5.2. Cellular uptake of NeutrAvidin (NA)-650 and anti-biotin-647

Cells were seeded in a 48-well plate at 70% confluence in 200 μL complete culture media one day before treatment. Cells were then treated sequentially with 25 μL medium containing 500 nM NA-650 or 50 nM anti-biotin-647 and 25 μL medium containing 2 μM cRGD-biotin or 25 nM Ab-cRGD and incubated at 37 °C for indicated time periods, followed by washed twice with PBS before harvested for in gel fluorescence analysis.

5.5.3. Anti-biotin-647 degradation analysis

MCF7 cells were seeded in a 48-well plate at 70% confluence and maintained in 200 μL complete culture media. Next day, cells were incubated with 25 nM of Ab-cRGD and 50 nM of anti-biotin-647 for 3 h followed by three washes with PBS. Cells were then maintained in fresh media with or without 50 nM Bafilomycin A1 (BAF1) or 10 μM Chloroquine (CQ) for another 3 h before harvested for in gel fluorescence analysis.

5.5.4. Antibody labeling with DBCO-PEGn-NHS and cRGD-N_3 (n=3 or 12)

Antibody with the concentration of 1.8 mg/ml in 200 μL PBS was reacted with DBCO-PEG3-NHS or DBCO-PEG12-NHS ester at 1:25 molar ratio overnight at room temperature on a rotator. The mixture was then purified with 500 μL of PBS for 5 times using 10 kDa Amicon Centrifugal Filter, followed by measuring the concentration of DBCO-labeled antibody by BCA assay and reacting with 25 equivalent cRGD-N_3 overnight at room temperature on a rotator. The resulting antibody conjugate was then purified with 500 μL of PBS for 5 times using 10 kDa Amicon Centrifugal Filter.

5.5.5. MALDI-MS

The sample was first absorbed on Omix C4 pipette tips, and then washed by 0.1% TFA for three times followed by elution with 20 μL 75% Acetonitrile/H_2O. 1 μL sample solution and 1 μL CHCA solution (10 mg/ml α-Cyano-4-hydroxycinnamic acid (CHCA) in 50% Acetonitrile/H_2O) were spotted on the MALDI target plate and mixed thoroughly before the spot was dried under room temperature. MALDI-MS spectra were acquired on Bruker UltraFlex MALDI-TOF/TOF mass spectrometer operated in linear positive ion mode and the plots were generated by Bruker flexAnalysis.

5.5.6. Targeted protein degradation

Cells were seeded at 70% confluence in a 24-well plate and incubated in 350 μL complete culture media overnight. Then, cells were treated with Ctx-cRGD in 50 μL culture media at various concentrations for indicated time periods before collection for western blot analysis.

5.5.7. Western blotting and in-gel fluorescence analysis

Cells were first washed with cold PBS for three times and then lysed with 1X RIPA lysis buffer including 25 mM Tris, pH 7−8, 150 mM NaCl, 0.1% (w/ v) sodium dodecyl sulfate (SDS), 0.5% sodium deoxycholate, 1% (v/ v) Triton X-100, protease inhibitor cocktail (Roche, one tablet per 10 mL) and 1 mM phenylmethylsulfonyl fluoride on ice for 10 min. The lysates were then collected and centrifuged at 16 000g at 4 °C for 15 min. The supernatant was collected and the protein concentration was determined using BCA assay. Samples were adjusted to the equal amount and mixed with the 4x Laemmli Loading Dye. After heating at 99 °C for 5 min and cooling down on ice, samples were loaded onto 7.5% or 12% SDS−polyacrylamide gel electrophoresis. For in-gel fluorescence analysis, the fluorescence images of the gel were directly taken by ChemiDoc MP Imaging Systems, followed by Coomassie blue staining of the gel. For western blot, the samples on the gel were transferred to PVDF membrane, followed by blocking with 5% (w/v) nonfat milk in the TBS-T washing buffer (137 mM NaCl, 20 mM Tris, 0.1% (v/v) Tween). The membrane was then incubated with primary antibodies at 4 °C overnight and incubated with secondary HRP-linked antibodies for 1 h. The membrane was washed 3 times with TBST after each antibody incubation. Lastly, the membrane was incubated in the Clarity ECL substrate for 3-5 min before acquiring the immunoblot by ChemiDoc MP Imaging Systems.

5.5.8. Confocal microscopy

MCF7 cells at the density of 20,000 cells/well was distributed onto 8-well chamber slides in 200 µL of complete culture medium. To detect the co-localization of internalized soluble target with lysosome, cells were treated with 500 nM NA-650 and 2 µM cRGD-biotin for 4 or 24 h at 37 °C. Cells were then incubated with LysoTracker Green DND26 (100 nM) or Hoechst 33342 (5 ug/ml) for 30 min or 10 min before the end of incubation. After three washes with PBS, the live cells were imaged using Leica SP8 3x STED super-resolution microscope at 20x magnification with a 10x eyepiece and analyzed by ImageJ. For EGFR degradation, cells were treated with 10 nM Ctx-cRGD for 24 h at 37 °C, followed by 3 washes with PBS. Cells were then fixed with 4% paraformaldehyde for 15 min followed by permeabilization with 0.5% Triton-100 for 5 min and blocking with 5% BSA for 1 h at RT. Cells were then incubated with anti-EGFR antibody alone or co-incubated with anti-LAMP1 antibody in 1% BSA overnight at 4 °C. The next day, cells were incubated with anti-rabbit-488 or anti-mouse-488 and anti-rabbit-594 secondary antibody for 1 h at RT. Cells was washed 3 times with PBS after each antibody incubation. Then the cells were mounted with slowfade-antifade mounting medium containing DAPI. Images were acquired by Leica SP8 3x STED super-resolution microscope at 60x magnification with a 10x eyepiece and analyzed by ImageJ.

5.6. References

1 Zhao, L., Zhao, J., Zhong, K., Tong, A. & Jia, D. Targeted protein degradation: mechanisms, strategies and application. *Signal Transduct Target Ther* **7**, 113 (2022). https://doi.org/10.1038/s41392-022-00966-4

2 Békés, M., Langley, D. R. & Crews, C. M. PROTAC targeted protein degraders: the past is prologue. *Nat Rev Drug Discov* **21**, 181-200 (2022). https://doi.org/10.1038/s41573-021-00371-6

3 Gopalsamy, A. Selectivity through Targeted Protein Degradation (TPD). *J Med Chem* **65**, 8113-8126 (2022). https://doi.org/10.1021/acs.jmedchem.2c00397

4 Chen, S., Cui, J., Chen, H., Yu, B. & Long, S. Recent progress in degradation of membrane proteins by PROTACs and alternative targeted protein degradation techniques. *Eur J Med Chem* **262**, 115911 (2023). https://doi.org/10.1016/j.ejmech.2023.115911

5 Banik, S. M. *et al.* Lysosome-targeting chimaeras for degradation of extracellular proteins. *Nature* **584**, 291-297 (2020). https://doi.org/10.1038/s41586-020-2545-9

6 Pance, K. *et al.* Modular cytokine receptor-targeting chimeras for targeted degradation of cell surface and extracellular proteins. *Nat Biotechnol* (2022). https://doi.org/10.1038/s41587-022-01456-2

7 Stevens, C. M. *et al.* Development of Oligomeric Mannose-6-phosphonate Conjugates for Targeted Protein Degradation. *ACS Med Chem Lett* **14**, 719-726 (2023). https://doi.org/10.1021/acsmedchemlett.2c00479

8 Ahn, G. *et al.* LYTACs that engage the asialoglycoprotein receptor for targeted protein degradation. *Nat Chem Biol* **17**, 937-946 (2021). https://doi.org/10.1038/s41589-021-00770-1

9 Zhou, Y., Teng, P., Montgomery, N. T., Li, X. & Tang, W. Development of Triantennary N-Acetylgalactosamine Conjugates as Degraders for Extracellular Proteins. *ACS Cent Sci* **7**, 499-506 (2021). https://doi.org/10.1021/acscentsci.1c00146

10 Caianiello, D. F. *et al.* Bifunctional small molecules that mediate the degradation of extracellular proteins. *Nat Chem Biol* **17**, 947-953 (2021). https://doi.org/10.1038/s41589-021-00851-1

11 Chen, X., Zhou, Y., Zhao, Y. & Tang, W. Targeted degradation of extracellular secreted and membrane proteins. *Trends Pharmacol Sci* **44**, 762-775 (2023). https://doi.org/10.1016/j.tips.2023.08.013

12 Barczyk, M., Carracedo, S. & Gullberg, D. Integrins. *Cell Tissue Res* **339**, 269-280 (2010). https://doi.org/10.1007/s00441-009-0834-6

13 Roca-Cusachs, P., Gauthier, N. C., Del Rio, A. & Sheetz, M. P. Clustering of alpha(5)beta(1) integrins determines adhesion strength whereas alpha(v)beta(3) and talin enable mechanotransduction. *Proc Natl Acad Sci U S A* **106**, 16245-16250 (2009). https://doi.org/10.1073/pnas.0902818106

14 Takayama, S. *et al.* The relationship between bone metastasis from human breast cancer and integrin alpha(v)beta3 expression. *Anticancer Res* **25**, 79-83 (2005).

15 Hamidi, H. & Ivaska, J. Every step of the way: integrins in cancer progression and metastasis. *Nat Rev Cancer* **18**, 533-548 (2018). https://doi.org/10.1038/s41568-018-0038-z

16 Desgrosellier, J. S. & Cheresh, D. A. Integrins in cancer: biological implications and therapeutic opportunities. *Nat Rev Cancer* **10**, 9-22 (2010). https://doi.org/10.1038/nrc2748

17 Pierschbacher, M. D. & Ruoslahti, E. Cell attachment activity of fibronectin can be duplicated by small synthetic fragments of the molecule. *Nature* **309**, 30-33 (1984). https://doi.org/10.1038/309030a0

18 Danhier, F., Le Breton, A. & Préat, V. RGD-based strategies to target alpha(v) beta(3) integrin in cancer therapy and diagnosis. *Mol Pharm* **9**, 2961-2973 (2012). https://doi.org/10.1021/mp3002733

19 Goodman, S. L., Hölzemann, G., Sulyok, G. A. & Kessler, H. Nanomolar small molecule inhibitors for alphav(beta)6, alphav(beta)5, and alphav(beta)3 integrins. *J Med Chem* **45**, 1045-1051 (2002). https://doi.org/10.1021/jm0102598

20 Li, N., Qiu, S., Fang, Y., Wu, J. & Li, Q. Comparison of Linear vs. Cyclic RGD Pentapeptide Interactions with Integrin α. *Biology (Basel)* **10** (2021). https://doi.org/10.3390/biology10070688

21 Zhou, R. *et al.* Functional cRGD-Conjugated Polymer Prodrug for Targeted Drug Delivery to Liver Cancer Cells. *ACS Omega* **7**, 21325-21336 (2022). https://doi.org/10.1021/acsomega.2c02683

22 Gajbhiye, K. R., Gajbhiye, V., Siddiqui, I. A. & Gajbhiye, J. M. cRGD functionalised nanocarriers for targeted delivery of bioactives. *J Drug Target* **27**, 111-124 (2019). https://doi.org/10.1080/1061186X.2018.1473409

23 Song, Z. *et al.* Cyclic RGD peptide-modified liposomal drug delivery system for targeted oral apatinib administration: enhanced cellular uptake and improved therapeutic effects. *Int J Nanomedicine* **12**, 1941-1958 (2017). https://doi.org/10.2147/IJN.S125573

24 Zheng, J. *et al.* Bifunctional Compounds as Molecular Degraders for Integrin-Facilitated Targeted Protein Degradation. *J Am Chem Soc* **144**, 21831-21836 (2022). https://doi.org/10.1021/jacs.2c08367

Chapter 6

Development of Folate Receptor Targeting Chimeras (FRTACs) for Cancer Selective Degradation of Extracellular Proteins

This chapter is adapted from a manuscript published in *Nature Communications*.

Zhou Y, Li C, Chen X, Zhao Y, Liao Y, Huang P, Wu W, Nieto N, Li L, Tang W.* Development of Folate Receptor Targeting Chimeras (FRTACs) for Cancer Selective Degradation of Extracellular Proteins. *Nat. Commun.* **2024**, *15*, 8695.

*To whom correspondence should be addressed

6.1. Abstract

Targeted protein degradation has emerged as a novel therapeutic modality to treat human diseases by utilizing the cell's own disposal systems to remove protein target. Significant clinical benefits have been observed for degrading many intracellular proteins. Recently, the degradation of extracellular proteins in the lysosome has been reported. However, there have been limited successes in selectively degrading protein targets in disease-relevant cells or tissues, which would greatly enhance the development of precision medicine. Additionally, most degraders are not readily available due to their complexity. In this chapter, we describe a novel class of easily accessible Folate Receptor TArgeting Chimeras (FRTACs) to recruit the folate receptor, primarily expressed on malignant cells, to degrade extracellular soluble and membrane cancer-related proteins *in vitro* and *in vivo*. Our results indicate that FRTAC is a general platform for developing more precise and effective chemical probes and therapeutics for the study and treatment of cancers.

6.2. Introduction

Targeted protein degradation (TPD) exploiting the cells' own degradation machinery to remove the protein of interest (POI) is emerging as a novel therapeutic modality[1,2]. There are numerous advantages of TPD over traditional strategies that block the functional sites, such as more sustained response and potential accessibility to the undruggable targets[3-5]. PROteolysis TArgeting Chimeras (PROTACs) were developed first and received the most attention[6-9]. Over a dozen PROTACs that recruit cereblon or Von Hippel-Lindau E3 ligases have progressed into human clinical trials for the treatment of cancer and other diseases[10]. In addition, about one dozen other E3 ligases

were demonstrated in their utility for the development of PROTACs[11], such as RNF114[12] and DCAF16[13]. Although many E3 ubiquitin ligases have different expression profiles in tissues[14], they have not been exploited for selective degradation of proteins in the disease-relevant cells or tissues due to the lack of cell permeable ligands. In addition to PROTACs, many platforms have been developed to degrade the intracellular POI through other mechanisms[15-17]. In contrast, fewer novel strategies are available for the degradation of extracellular proteins[18], though they are consisted of 40% of the proteome[19].

The initial LYsosome TArgeting Chimeras (LYTACs), composed of a polymeric glycopeptide ligand of cation-independent mannose-6-phosphate receptor (CI-M6PR) and a binder of the extracellular POI, were reported in 2020[20]. LYTACs could induce the degradation of a broad range of soluble and membrane protein targets in many tissues due to the ubiquitous expression profile of CI-M6PR. Later, several groups including ours reported LYTACs with tissue selectivity by recruiting asialoglycoprotein receptor (ASGPR) to restrict the TPD in liver cells only[21-23]. Before we started the work in this chapter, only lectins had been employed as the lysosomal targeting receptor (LTR) for TPD. While we were preparing the manuscript for the work in this chapter, degraders that recruit non-lectin LTRs were reported for the degradation of extracellular proteins[18,24,25]. Integrin and transferrin receptor 1, overexpressed in cancer cells, have been recently leveraged for TPD. Degraders that recruit these receptors hold the possibility of selectively depleting the extracellular proteins in cancer cells. However, the cancer selectivity has not been examined[25,26].

Similar to CI-M6PR and ASGPR, the folate receptor (FR) has also been investigated for drug delivery[27,28]. FR has been recognized as a major biomarker for tumor cells. The overexpression of FR is found in various cancer cells, such as ovarian cancer, non-small-cell lung cancer (NSCLC), and myeloid leukemia, while most normal tissues lack the expression of FR on the cell surface[29-31]. We reasoned that it would be ideal to recruit FR to selectively degrade extracellular proteins associated with cancers in cancer cells to achieve high efficiency and selectivity.

Two isoforms of FR, FR1 and FR2, are glycosylphosphatidylinositol-anchored membrane proteins functioning as high-affinity receptors for folate (FA) to import FA into the cell via receptor-mediated endocytosis[32,33]. The detectable FR expression on normal tissues, predominantly in the kidney, lung, and choroid plexus, is largely restricted to the apical surface of the polarized epithelial cells, preventing the exposure of FR to the folate-drug conjugates in the blood circulation, thus reducing cytotoxic effects on healthy tissues. Upon tumorigenesis, the change in tissue architecture enables FR to be accessible to the circulating folate-drug conjugates[34-36]. These unique expression features make FR a promising receptor for cancer-selective targeting. FA, the ligand of FR, has the advantages of non-immunogenic, low cost, high stability, and maintaining high binding affinity to FR after conjugation[37,38]. It has been reported that the folate-conjugate is engulfed by the cell through FR-mediated endocytosis followed by the transportation into endosome and lysosome. The drop in pH can trigger the release of folate-conjugate into the cell, while the FR is recycled back to the membrane for the transport of more folate-conjugates[39-41]. Currently, various folate-tethered drugs in the forms of folate-nanoparticles, small-molecule drug conjugates, and radio-

immunoconjugates are being investigated for delivering imaging and therapeutic reagents into tumors[42]. While most of these reagents are still undergoing clinical trials, a FA-based fluorescent imaging reagent (Cytalux)[43] and an ADC targeting FR (Elahere)[44] were approved for cancer surgery and treatment, respectively. Recently, the FR-targeting strategy has been explored in the field of TPD. Studies have demonstrated that attaching folate to molecular glues or PROTACs allows for selective degrading cytosolic proteins in cancer cells[45,46]. In this chapter, we report our development of Folate Receptor TArgeting Chimeras (FRTACs) as a general platform for selectively degrading extracellular cancer-relevant proteins in cancer cells (Fig. 6.1a). The FRTACs are composed of a FA ligand that can bind to FR and antibodies that can bind to cancer-relevant targets. We demonstrated that the FRTACs are able to mediate the degradation of protein targets *in vitro* and *in vivo*. The FRTAC showed more significant tumor growth suppression than the corresponding blocking antibody in three different syngeneic mouse cancer models. Most importantly, the FRTACs can be easily obtained from commercially available FA conjugating reagents and antibodies against any extracellular target. Our results support that FRTACs can be a precise and effective technology for the study and treatment of cancers.

6.3. Results

6.3.1. Degradation of soluble proteins mediated by FRTACs *in vitro*

Antibody-based FRTAC was generated through a two-step labeling method by treating the antibody sequentially with two commercially available reagents, cyclic alkyne (DBCO-PEG3-NHS ester) and azido-PEG-linker (MW = 2K)-folate, which could be coupled together through click chemistry (Fig. 6.1b). To test whether the soluble protein

can be taken into cells by FRTACs, I used goat anti-mouse IgG antibody attached with folate (Ab-FA) and folate-PEG (MW = 2K)-FITC (FA-FITC) as antibody- and small molecule-based FRTACs, respectively, to mediate the endocytosis of a model target - mouse anti-FITC-594 (Fig. 6.1c). HepG2 cells were treated with 50 nM anti-FITC-594 and increasing concentrations of each degrader for 3 h. The results showed that Ab-FA induced the cellular uptake of anti-FITC-594 in a dose-dependent manner, while the uptake of anti-FITC-594 mediated by FA-FITC peaked at 200 nM and decreased at 1000 nM, reflecting a typical hook effect of small molecule degraders, where more FA-FITC/anti-FITC-594 or FA-FITC/FR binary complexes are formed than the ternary complex of FR/FA-FITC/anti-FITC-594 (Fig. 6.1d,e). By directly comparing the cellular uptake of anti-FITC-594 mediated by 50 nM Ab-FA and 200 nM FA-FITC, a significantly greater amount of internalized anti-FITC-594 was observed in the cells treated with Ab-FA than FA-FITC, suggesting that antibody-based degrader Ab-FA has higher uptake efficiency over FA-FITC (Fig. 6.1f). In addition to anti-FITC-594, the uptake of mouse anti-biotin (-594 or -647) mediated by Ab-FA further verified that different soluble proteins can be internalized by FA-conjugates. Antibody without folate modification cannot take the anti-biotin-594 into the cells (Fig. 6.1g).

I then monitored the degradation of internalized protein target by a pulse-and-chase assay. HepG2 cells were first treated with Ab-FA and anti-biotin-647 for 3 h to allow the cellular uptake of target, followed by another 3 h incubation in fresh media with or without lysosomal degradation inhibitors Chloroquine (CQ), Bafilomycin A1 (BAF), or the proteasome degradation inhibitor MG132. I found that the level of anti-biotin-647 accumulated in the cells within the first 3 h was significantly decreased after the removal

of the degrader and target from the media, suggesting the degradation of target occurred after internalization. The treatment of CQ and BAF significantly inhibited the degradation of anti-biotin-647, while MG132 did not rescue the reduction of anti-biotin-647, which indicated that the FRTAC routes the protein target into lysosome rather than proteasome for degradation (Fig. 6.1h). To further demonstrate that the internalized soluble protein was delivered into lysosome for degradation, I treated Hela cells with 25 nM Ab, 25 nM Ab plus 125 nM free FA, or 25 nM Ab-FA together with 50 nM anti-Rabbit-647 for 24 h, and found that Ab-FA significantly increased the intracellular level of anti-Rabbit-647 compared to the other two groups. By staining the live cells with LysoTracker, I also observed the colocalization of internalized anti-Rabbit-647 with lysosomes in the presence of Ab-FA (Fig. 6.1i). Rab7 is an essential protein that mediates the late endosome/lysosome trafficking[47]. I then downregulated Rab7 level in Hela cells by siRNA and compared the amount of anti-Rabbit-647 in the cells transfected with scramble or Rab7 siRNA. The results showed that the level of anti-Rabbit-647 was higher in the Rab7 knockdown cells compared to the control when co-treated with Ab-FA, suggesting that anti-Rabbit-647 was accumulated in the cells due to reduced degradation, resulting from the disrupted transport from late endosome to lysosome caused by Rab7 knockdown (Fig. 6.1j). Overall, all data support that FRTAC delivers extracellular soluble proteins into lysosome for degradation.

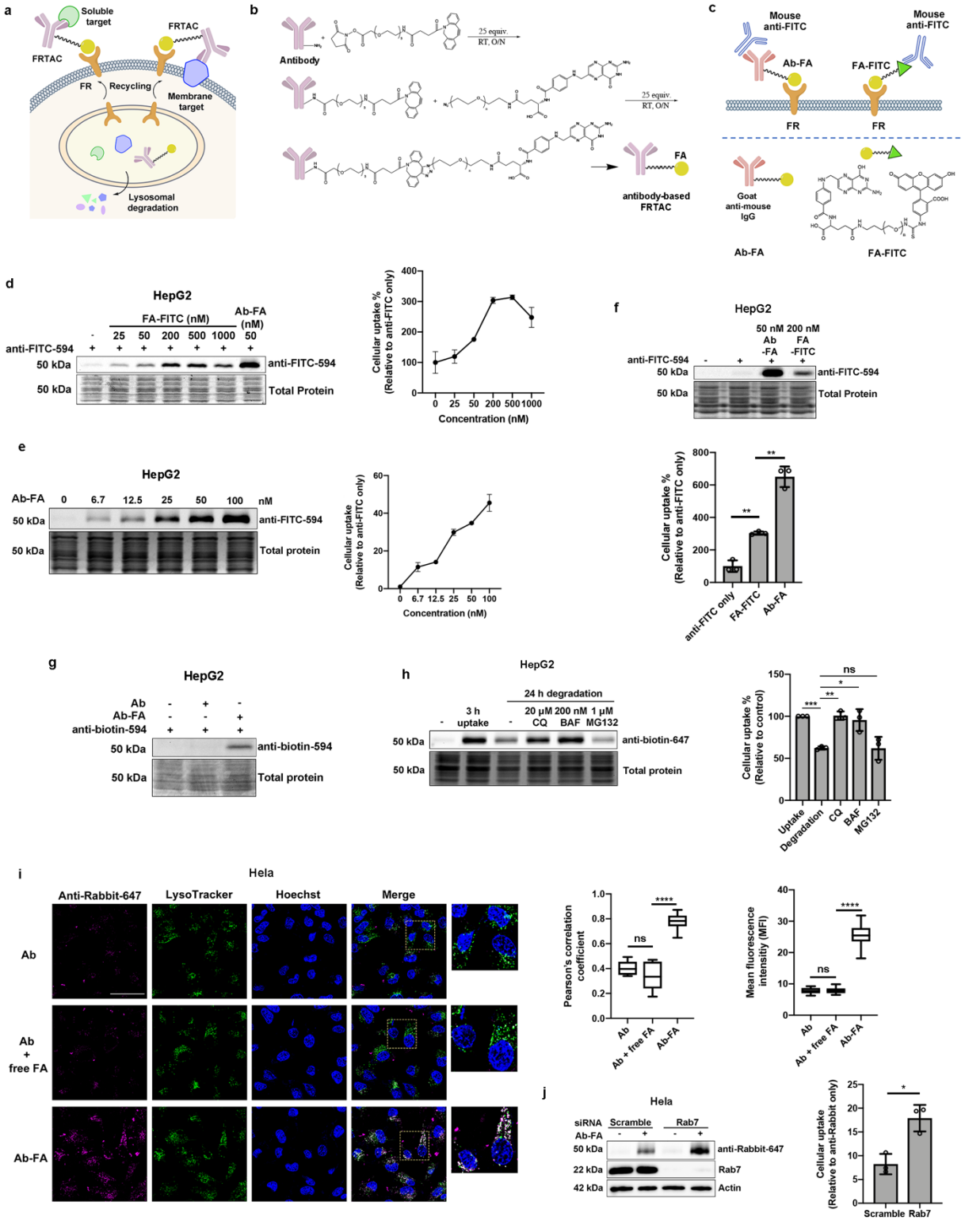
a
Soluble target
FRTAC
FRTAC
FR
Recycling
Membrane target
Lysosomal degradation
b
Antibody
25 equiv.
RT, O/N
25 equiv.
RT, O/N
FA
antibody-based FRTAC
c
Mouse anti-FITC
Mouse anti-FITC
Ab-FA
FA-FITC
FR
FR
Goat anti-mouse IgG
Ab-FA
FA-FITC
d
HepG2
FA-FITC (nM)
Ab-FA (nM)
anti-FITC-594
50 kDa
anti-FITC-594
Total Protein
Cellular uptake % (Relative to anti-FITC only)
Concentration (nM)
e
HepG2
Ab-FA
nM
anti-FITC-594
Total protein
Cellular uptake (Relative to anti-FITC only)
Concentration (nM)
f
HepG2
50 nM Ab -FA
200 nM FA -FITC
anti-FITC-594
anti-FITC-594
Total Protein
Cellular uptake % (Relative to anti-FITC only)
anti-FITC only
FA-FITC
Ab-FA
g
HepG2
Ab
Ab-FA
anti-biotin-594
anti-biotin-594
Total protein
h
HepG2
24 h degradation
3 h uptake
20 μM CQ
200 nM BAF
1 μM MG132
anti-biotin-647
Total protein
Cellular uptake % (Relative to control)
Uptake
Degradation
CQ
BAF
MG132
i
Hela
Anti-Rabbit-647
LysoTracker
Hoechst
Merge
Ab
Ab + free FA
Ab-FA
Pearson's correlation coefficient
Mean fluorescence intensity (MFI)
Ab
Ab + free FA
Ab-FA
j
Hela
siRNA
Scramble
Rab7
Ab-FA
anti-Rabbit-647
Rab7
Actin
Cellular uptake (Relative to anti-Rabbit only)
Scramble
Rab7

Figure 6.1. FRTACs mediate the uptake and lysosomal degradation of soluble proteins. a. Illustration of FRTAC-induced lysosomal targeted protein degradation. **b.** Generation of FRTAC through a two-step labeling method. **c.** Schematic of mouse anti-FITC uptake mediated by Ab-FA and FA-FITC. **d.** Dose response of anti-FITC-594 (50 nM) uptake induced by FA-FITC and comparison with 50 nM Ab-FA in HepG2 cells for 3 h (n = 3). **e.** Dose response of anti-FITC-594 (50 nM) uptake induced by Ab-FA in HepG2 cells for 3 h (n = 3). **f.** Uptake of anti-FITC-594 (50 nM) in HepG2 cells treated with Ab-FA (25 nM) and FA-FITC (200 nM) for 3 h (n = 3). **g.** Uptake of anti-biotin-594 (50 nM) in HepG2 cells treated with Ab-FA (25 nM) for 3 h. **h.** In-gel fluorescence analysis of anti-biotin-647 (50 nM) internalization and degradation in HepG2 cells by Ab-FA (25 nM) in the presence or absence of Chloroquine (CQ, 20 μM), Bafilomycin A1 (BAF, 200 nM), and MG132 (1 μM) for 24 h (n = 3). **i.** Cellular uptake and lysosome colocalization of anti-Rabbit-647 (50 nM) in the presence of Ab (25 nM), Ab (25 nM) + free FA (125 nM), and Ab-FA (25 nM) in Hela cells for 24 h by immunofluorescent staining. Scale bar: 50 μm. The colocalization of internalized anti-Rabbit-647 with lysosomes was analyzed by Pearson's correlation coefficients. The intracellular fluorescence intensity is presented as mean fluorescence intensity (MFI) (n = 15 images from three biologically independent experiments). Box plot: minima (lower whisker), maxima (upper whisker), center (median), bounds of the box (25th and 75th percentiles), whiskers (range from minima to maxima). **j.** Uptake of anti-Rabbit-647 (50 nM) mediated by Ab-FA (25 nM) in Hela cells transfected with scramble siRNA or Rab7 siRNA for 3 h (n = 3). N indicates biologically independent experiments except for figure 2f. Data are presented as mean ± SD. The statistical significance was assessed using an unpaired two-tailed t-test, *P < 0.05, **P < 0.01, ***P < 0.001, ****P < 0.0001, ns: not significant.

Next, I treated cells with the bifunctional degrader (25 nM) and excess free folate (300 μM), which can occupy FR to prevent its interaction with the degrader. The results showed that the uptake of anti-biotin-647 in HepG2 cells was significantly decreased in the presence of excess free folate, which indicates the involvement of FR in the process of protein target internalization (Fig. 6.2a). To further validate the role of FR in transporting FRTAC/target protein into the cells, I downregulated the expression of FR1, the dominant isotype of FR, in Hela cells by siRNA. After incubating with Ab-FA for 6 h, a significantly lower amount of internalized anti-Rabbit-647 was detected in the FR1 knockdown cells than the cells transfected with scrambled siRNA (Fig. 6.2b). Additionally, I treated Hela cells that transiently overexpressing FR1-FLAG with Ab-FA

and anti-Rabbit-647 for 6 h, and the results showed that compared to the non-transfected cells and cells transfected with empty vector, the elevation of FR1 expression level significantly boosted the uptake of anti-Rabbit-647 mediated by Ab-FA (Fig. 6.2c). Interestingly, I observed that Hela cells overexpressing FR2 also exhibited enhanced anti-Rabbit-647 internalized when co-treated with Ab-FA, suggesting that FRTAC can interact with both isotypes of FR to mediate the target protein delivery (Fig. 6.2d). To elucidate the endocytosis pathway utilized by FRTAC to transport soluble proteins into the cells, I pre-treated cells with methyl-β-cyclodextrin (MβCD, inhibitor of caveolae/lipid-raft-mediated endocytosis), chlorpromazine (CHP, inhibitor of clathrin-mediated endocytosis) or cytochalasin D (cyto-D, inhibitor of macropinocytosis) for 1 h and then incubated with 25 nM Ab-FA and 50 nM anti-FITC-594 for 3 h. The results showed that the treatment of MβCD significantly blocked the cellular uptake of anti-FITC-594 induced by Ab-FA, while CHP and cyto-D failed to reduce the level of internalized anti-FITC-594, which indicated that Ab-FA mediated the soluble protein internalization primarily through caveolae/lipid-raft-mediated endocytosis, which is consistent with the endocytosis pathway reported for FR (Fig. 6.2e)[47-49]. Last, I compared the uptake of anti-biotin-594 mediated by Ab-FA across different cancer cell lines (Fig. 6.2f). The expression levels of FRs on these cell lines were quantified with FA-FITC by flow cytometry (Fig. 6.2g). The results showed that the uptake efficiency of soluble proteins varied among different cancer cell lines and well correlated with corresponding folate receptor level (Fig. 6.2h). All of the above data support the involvement of FR in the endocytosis process.

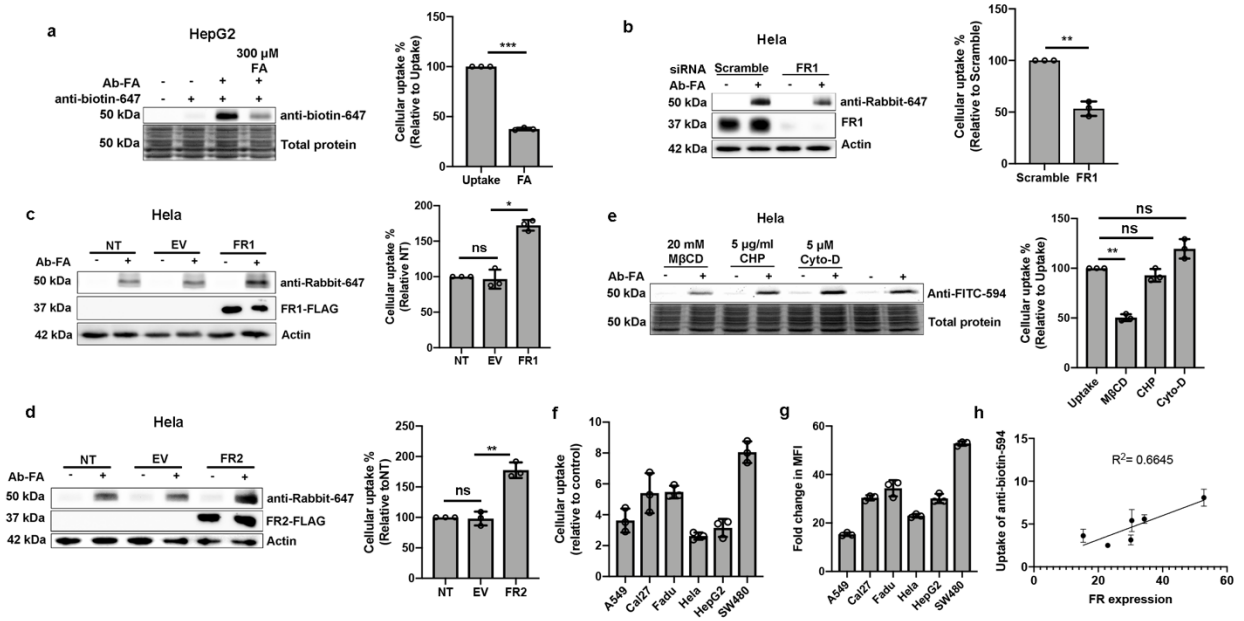

Figure 6.2. FRTACs recruit FR to induce lysosomal degradation of soluble proteins. a. Inhibition of anti-biotin-647 (50 nM) internalization in the presence of Ab-FA (25 nM) by free FA (300 μM) in HepG2 cells for 3 h (n = 3). **b.** Uptake of anti-rabbit-647 (50 nM) mediated by Ab-FA (50 nM) in Hela cells transfected with scramble or FR1 siRNA for 6 h (n = 3). **c.** Uptake of anti-rabbit-647 (50 nM) mediated by Ab-FA (50 nM) in Hela cells transfected with plasmid expressing FLAG-FR1 for 6 h. Non-transfected (NT) cells and cells transfected with empty vector (EV) were used as negative controls (n = 3). **d.** Uptake of anti-Rabbit-647 (50 nM) in FR2 overexpression cells. Non-transfected (NT) cells and cells transfected with empty vector (EV) were used as negative controls (n = 3). **e.** Inhibition of anti-FITC-594 (50 nM) internalization in the presence of Ab-FA (25 nM) by methyl-β-cyclodextrin (MβCD, 20 mM), chlorpromazine (CHP, 5 μg/ml) or cytochalasin D (cyto-D, 5 μM) in Hela cells for 3 h (n = 3). **f.** Uptake of anti-biotin-594 (50 nM) in different cancer cell lines (n = 3). **g.** Quantification of FR expression levels on different cancer cell lines by flow cytometry (n = 3). **h.** Correlation of uptake efficiency with FR expression levels on different cancer cell lines (n = 3). N indicates biologically independent experiments. Data are presented as mean ± SD. The statistical significance was assessed using an unpaired two-tailed t-test, *P < 0.05, **P < 0.01, ***P < 0.001, ns: not significant.

6.3.2. Degradation of endogenous membrane proteins mediated by FRTACs *in vitro*

After demonstrating that FRTACs can induce the uptake and degradation of model soluble proteins via their interaction with FR, I next evaluated the possibility of selectively degrading membrane proteins in cancer cells. I previously attached tri-GalNAc-NHS ester to Cetuximab (Ctx), the therapeutic antibody against epidermal growth factor receptor (EGFR), by reacting with lysine residues on the antibody[22]. These tri-GalNAc conjugates can recruit ASGPR and mediate the degradation of EGFR selectively in liver cells. Using the same method, Ctx was reacted with 3, 12, or 25 equivalent of commercially available folate-NHS ester to generate degraders with increasing numbers of ligands on each antibody (Fig. 6.3a). The data indicated that a higher degree of folate labeling led to greater EGFR degradation at both 10 nM and 200 nM concentrations (Fig. 6.3b). To further improve the degradation efficiency of FRTAC on membrane targets, Xuankun Chen, a first-year graduate student in our group, and I compared this direct labeling method using folate-NHS ester with the two-step labeling method as mentioned above. We tried two different PEG-linkers and controlled the degree of FA labeling on each antibody by adjusting the equivalence of DBCO-PEG3-NHS ester in the reaction. Our results showed that consistent with earlier findings, degraders produced by both methods exhibited higher EGFR degradation efficiency when labeled with more folate. Degraders bearing either a 1k-PEG-linker or a 2k-PEG-linker reduced EGFR level to the similar extent when the degraders are generated via the same labeling method. While most degraders with the same linker length and degree of labeling showed no significant difference in EGFR degradation efficiency

between the one-step and two-step labeling methods, the degrader with a 2k-PEG-linker from the two-step labeling method (N3, 2k, 25x) showed higher degradation efficiency than the degrader with either 1k or 2k PEG-linker from one-step labeling method (Fig. 6.3c).

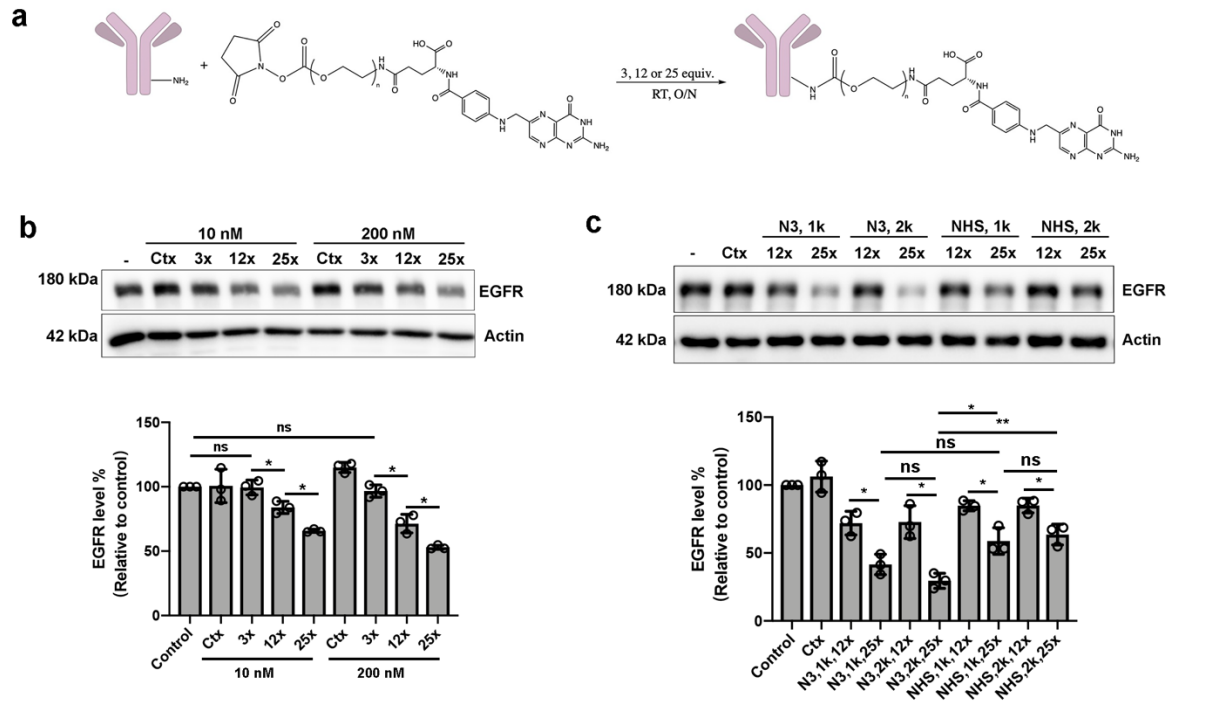

Figure 6.3. FRTACs generated by two-step labeling method with more FA labeling and longer linker length have higher protein degradation efficiency. a. Generation of FRTAC by one-step labeling method. **b.** EGFR degradation mediated by FRTACs prepared by one-step labeling method using different amounts of folate-NHS ester (3x, 12x, and 25x) (n = 3). **c.** Comparison of EGFR degradation induced by FRTACs prepared by one- or two-step labeling method with various amounts of reagents (n = 3). **Note:** Blot was provided by Xuankun Chen. 3x: 3 molar equivalents, 12x: 12 molar equivalents, 25x: 25 molar equivalents, 1k: PEG1k linker, 2k: PEG2k linker. N3: two-step labeling (12x and 25x indicate the equivalence of the DBCO-NHS ester in the first step; 25 equivalents of folate-azide was used in the second step). NHS: one-step labelling. N indicates biologically independent experiments. Data are presented as mean ± SD. The statistical significance was assessed using an unpaired two-tailed t-test, *P < 0.05, **P < 0.01, ns: not significant.

The FRTAC (Ctx-FA) with a 2k-PEG-linker introduced by click chemistry was selected for the following studies due to more efficient EGFR degradation detected (Fig. 6.4a). First, Yaxian Liao, a graduate student in our group, and I verified the dose- and time-dependency of the EGFR degradation mediated by Ctx-FA in Fadu and Hela cells. Ctx-FA displayed a DC_{50} of 0.41 nM and a D_{max} of 75% in Fadu cells, while it induced the EGFR degradation with a DC_{50} of 0.24 nM and a D_{max} of 80% in Hela cells (Fig. 6.4b). The EGFR degradation became significant around 4-6 h post-treatment and the maximal degradation lasted at least till 72 h (Fig. 6.4c). No EGFR degradation was detected in Fadu cells treated with Ctx, free FA, the combination of Ctx and free FA, or FA attached human IgG isotype (Fig. 6.4d,e). The degradation induced by Ctx-FA was confirmed by confocal imaging in Fadu cells, which revealed not only a significant decrease of EGFR in the cells treated with the degrader compared to control groups, but also a clear translocation of EGFR from the cell surface into the cytoplasm after 24 h of Ctx-FA treatment (Fig. 6.4d). To track the EGFR after internalization, I co-stained EGFR and lysosome marker LAMP1 after incubating with the degrader and found that EGFR was primarily co-localized with lysosomes (Fig. 6.4d). The results also showed that the degradation of EGFR was partially abolished when the cells were treated with the lysosomal degradation inhibitor, Bafilomycin A1, while the proteasome inhibitor MG132 was not able to rescue EGFR degradation in the presence of Ctx-FA, demonstrating that Ctx-FA triggered EGFR degradation involves lysosome but not proteasome (Fig. 6.4f,g). Moreover, I found that decreasing the level of Rab7 partially prohibited the depletion of EGFR mediated by Ctx-FA, further confirming that FRTAC could transport membrane protein into lysosome for degradation (Fig. 6.4h).

To investigate the involvement of FR in degrader-induced EGFR degradation, Fadu cells were incubated with excess free folate (3 mM) and the results showed that less EGFR was degraded in the presence of excess free folate, suggesting the engagement of FR in inducing EGFR degradation (Fig. 6.4f). However, it is somewhat surprising that a large excess of free folate (3 mM of folate for 10 nM of degrader) is needed to abolish the degradation effect, which is consistent with results from the uptake of soluble proteins (Fig. 6.2a). No significant difference in the FR1 and FR2 levels was detected after the degrader treatment, indicating that FRTAC only routes the protein target for degradation without affecting the recycling of the FRs (Fig. 6.4i). I also determined EGFR degradation in various cancer cell lines and analyzed their correlation with FR expression levels on each cell line. The results suggested that unlike the uptake of soluble protein, the EGFR degradation efficiency of the degrader was related not only to the expression level of FR but also to the expression level of EGFR in different cell lines. The degradation efficiency of Ctx-FA correlated more strongly with the ratio of FR to EGFR expression levels than with FR expression level alone, due to the involvement of both proteins in the ternary complex. A higher FR to EGFR expression ratio resulted in increased EGFR degradation efficiency (Fig. 6.4j-m). Overall, these data demonstrate that the lysosomal degradation of EGFR induced by the degrader is mediated through the interaction between folate and FR.

Lastly, I investigated how Ctx-FA regulates the EGFR downstream signaling pathway by monitoring the phosphorylation of EGFR and MAPK upon activation. I found that the treatment of Ctx-FA downregulated the level of EGFR and abolished the phosphorylation of EGFR compared to the untreated cells after the stimulation with 100

ng/mL EGF for either 10 or 60 min. The level of p-MAPK, though increased after EGF stimulation, was suppressed after Ctx-FA treatment compared to the antibody-treated and untreated cells, while the expression of MAPK was not changed in the presence of Ctx-FA (Fig. 6.4n). The results indicate that the FRTAC can downregulate EGFR level in cancer cells and further modulate the associated downstream signaling pathway.

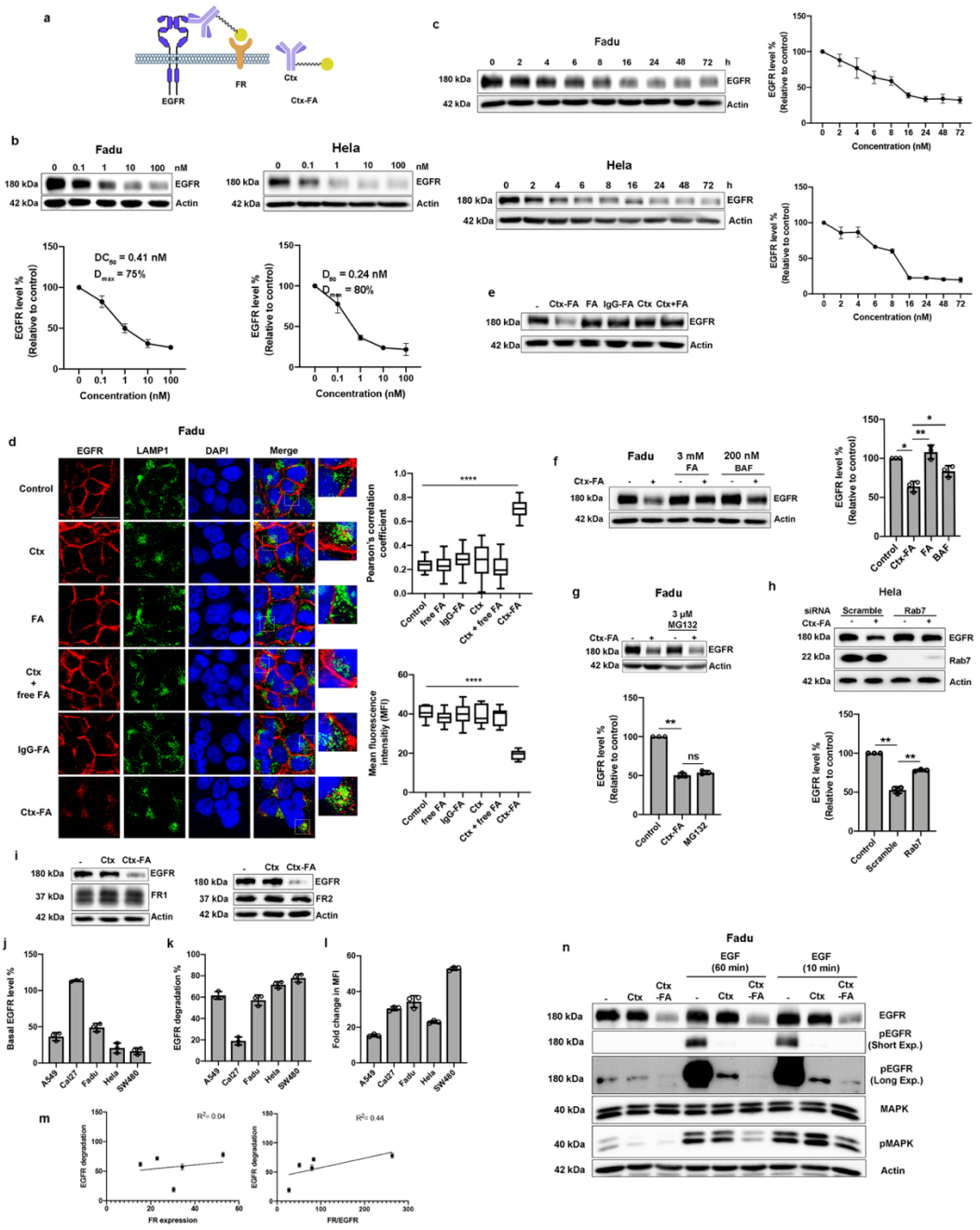

Figure 6.4. FRTACs mediate the lysosomal degradation of EGFR via their interaction with FR. a. Schematic of Ctx-FA targeting EGFR. **b.** Dose response of EGFR degradation (24 h) in Fadu and Hela cells (n = 3). Note: Provided by Yaxian Liao. **c.** Time course of EGFR degradation mediated by Ctx-FA (10 nM) in Fadu and Hela cells (n = 3). **Note:** Blots of Fadu cells were provided by Yaxian Liao. **d.** Immunofluorescent staining of EGFR degradation and lysosome colocalization after treatment of Ctx (10 nM), FA (50 nM), Ctx (10 nM) + free FA (50 nM), IgG-FA (10 nM) and Ctx-FA (10 nM) for 24 h in Fadu cells. Scale bar: 25 μm. The colocalization was analyzed by Pearson's correlation coefficients (n = 15). The intracellular fluorescence intensity is presented as mean fluorescence intensity (MFI) (n = 10). Box plot: minima (lower whisker), maxima (upper whisker), center (median), bounds of the box (25th and 75th percentiles), whiskers (range from minima to maxima). **e.** EGFR degradation mediated by Ctx-FA and negative controls (n = 3). **f.** Inhibition of EGFR degradation in the presence of Ctx-FA (10 nM) by free FA (3 mM) and Bafilomycin A1 (BAF, 200 nM) in Fadu cells for 6 h (n = 3). **g.** Inhibition of EGFR degradation in the presence of Ctx-FA (10 nM) by MG132 (3 μM) in Fadu cells for 6 h (n = 3). **h.** EGFR degradation mediated by Ctx-FA (10 nM) in Hela cells transfected with scramble siRNA or Rab7 siRNA for 6 h (n = 3). **i.** FR1 and FR2 level before and after degrader treatment (n = 2). **j.** Endogenous EGFR expression level in different cancer cell lines (n = 3). **k.** EGFR degradation in different cancer cell lines. **l.** Quantification of FR expression levels on different cancer cell lines by flow cytometry (n = 3). **m.** Correlation of EGFR degradation efficiency with FR expression level alone or the ratio of FR and endogenous EGFR on different cancer cell lines. N indicates biologically independent experiments. **n.** Downregulation of EGFR and MAPK phosphorylation in Fadu cells. Representative blots from three biologically independent experiments. N indicates images from three biologically independent experiments (d) or biologically independent experiments.Data are presented as mean ± SD. The statistical significance was assessed using an unpaired two-tailed t-test, *P < 0.05, **P < 0.01, ****P < 0.0001, ns: not significant.

In addition to EGFR, I explored whether FRTACs can be used for degrading other therapeutic targets, such as PD-L1 and CD47, which are both highly expressed on cancer cells. Atezolizumab (Atz), the therapeutic antibody against PD-L1, and anti-CD47 monoclonal antibody were reacted with DBCO-NHS ester and folate-azide sequentially to form the degraders against PD-L1 (Atz-FA) and CD47 (Ab2-FA), respectively. The treatment of MDA-MB-231 and A549 cells with 10 nM Atz-FA led to significant degradation of PD-L1 in both cell lines after 24 h (Fig. 6.5a-c). Similarly, the amount of CD47 was significantly reduced in MDA-MB-231 and A549 cells when

incubated with 100 nM of degrader (Fig. 6.5d-f). These data indicate that FRTACs have a broad scope for the degradation of cancer-associated protein targets.

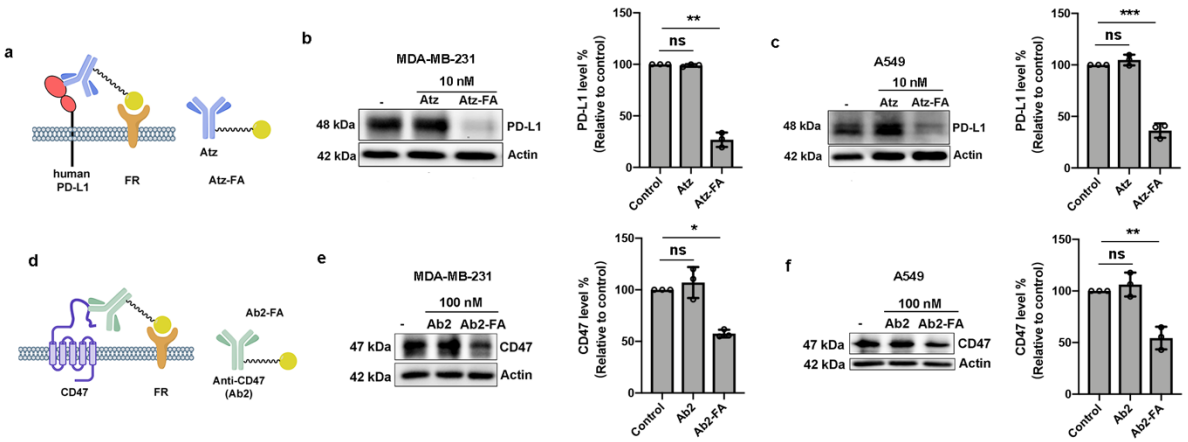

Figure 6.5. FRTACs mediate the lysosomal degradation of membrane proteins PD-L1, and CD47 via their interaction with FR. a. Schematic of Atz-FA targeting PD-L1. **b,c.** Degradation of PD-L1 in MDA-MB-231 and A549 cells treated with Atz-FA (10 nM) for 24 h (n = 3). **d.** Schematic of Ab2-FA targeting CD47. e,f. Degradation of CD47 in MDA-MB-231 and A549 cells treated with Ab2-FA (100 nM) for 24 h (n = 3). N indicates biologically independent experiments. Data are presented as mean ± SD. The statistical significance was assessed using an unpaired two-tailed t-test, *P < 0.05, **P < 0.01, ***P < 0.001, ns: not significant.

6.3.3. Anti-tumor effect of FRTACs targeting PD-L1 *in vivo*

Encouraged by the *in vitro* degradation of several membrane protein targets in multiple cancer cell lines, we then investigated the effect of the FRTACs *in vivo*. PD-L1 is an immune checkpoint interacting with its receptor PD-1 on the immune cells to induce T cell immunosuppression. Its role in assisting the evasion of cancer cells from host immune surveillance makes PD-L1 a validated target for cancer immunotherapy[50,51]. However, current therapeutics targeting PD-L1 has low patient response rate and significant side effects due to undesired inhibition of PD-L1 on normal tissues[52-54]. We

hypothesize that degraders specifically targeting PD-L1 in cancer cells may have the potential to be a more selective therapeutic with higher efficacy and better safety profiles. To test this hypothesis, we first generated the FRTAC targeting mouse PD-L1 (Ab3-FA) using rat anti-mouse PD-L1 antibody (Ab3) through the two-step labeling method (Fig. 6.6a). The binding affinity of Ab3-FA with mouse PD-L1 was determined as 24.6 ± 4.67 nM using Micro-Scale Thermophoresis (MST) assay, which is comparable to the affinity between unmodified antibody and mouse PD-L1 (Kd= 9.05 ± 0.78 nM), indicating the attachment of FA on the antibody does not significantly interfere the interaction between the FRTAC and target protein (Fig. 6.6b). Graduate student Xuankun Chen and I then tested the degradation of mouse PD-L1 in murine colon cell line CT26 and melanoma cell line B16F10. Both cell lines were treated with 100 ng/mL IFNγ for 24 h to induce the PD-L1 expression before the treatment of anti-mouse PD-L1 antibody or degrader. We found that antibody slightly reduced mouse PD-L1 level in both CT26 and B16F10 cells, while FRTAC could result in more significant downregulation of PD-L1 in both cell lines compared to control and antibody-treated groups (CT26: DC_{50} = 0.29 nM, D_{max} = 51%; B16F10: DC_{50} = 0.52 nM, D_{max} = 64%; Fig. 6.6c,d). Degradation occurred after 8 h post-treatment and lasted at least till 48 h (Fig. 6.6e,f). Similar to EGFR, the degrader transported mouse PD-L1 into the lysosomal degradation pathway after interacting with FR on both cell lines (Fig. 6.6g,h). Similar to results observed for the degradation of EGFR in Fadu cells (Fig. 6.4f), large excess of free folate (3 mM of free folate for CT26 and 1 mM of free folate for B16F10) is needed to abolish the degradation effect induced by the FRTAC (10 nM). In addition, we also

demonstrated the degradation of PD-L1 in mouse head & neck cancer cell line MOC1 (Fig. 6.6i).

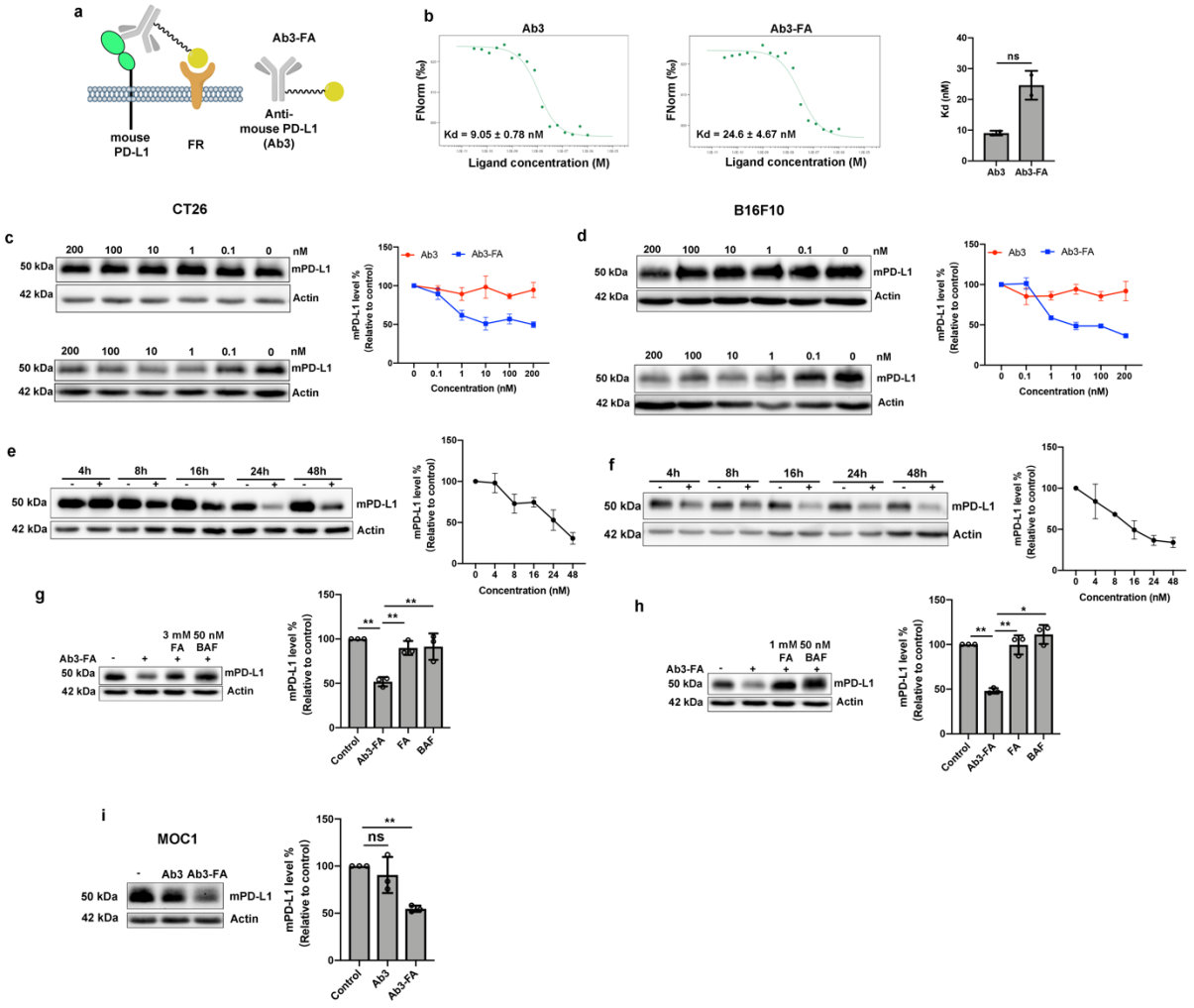

Figure 6.6. FRTACs mediate the lysosomal degradation of mPD-L1 via their interaction with FR in three mouse cell lines (CT26: c, e, g; B16F10: d, f, h; MOC1: i). a. Schematic of Ab3-FA targeting mouse PD-L1 (mPD-L1). **b.** Representative plot of the binding affinity of Ab3 and Ab3-FA to mPD-L1 characterized by MicroScale Thermophoresis (MST) (n = 2). **c, d.** Dose response of mPD-L1 degradation (24 h) mediated by Ab3 and Ab3-FA (n = 3). **e, f.** Time course of mPD-L1 degradation mediated by Ab3-FA (10 nM) (n = 3). **Note:** Blots were provided by Xuankun Chen. **g, h.** Inhibition of Ab3-FA (10 nM) mediated mPD-L1 degradation by free FA (3 mM for CT26, 1 mM for B16F10) and Bafilomycin A1 (BAF, 50 nM) for 24 h (n = 3). **i.** Cellular mPD-L1 degradation in MOC1 cells mediated by Ab3-FA (10 nM, 24 h) (n = 3). N indicates biologically independent experiments. Data are presented as mean ± SD. The statistical significance was assessed using an unpaired two-tailed t-test, *P < 0.05, **P < 0.01, ns: not significant.

Dr. Chunrong Li and I then evaluated the pharmacokinetics (PK) of the mouse PD-L1 degraders *in vivo*. To study whether the number of folate labelled on each antibody could affect the clearance rate of the degrader, degraders with 2-3 FA per antibody (Ab3-FA-12x) or 4-5 FA per antibody (Ab3-FA-25x) were generated by adjusting the equivalence of folate-azide in the second step of labeling. The PK of unmodified PD-L1 antibody and two PD-L1 degraders were determined by intraperitoneal (IP) injection at a dose of 2.5 mg/kg into C57BL/6 mice and blotting the Rat IgG level in the plasma at different time points. The analysis of PK in mice indicated that the $T_{1/2}$s for Ab3, Ab3-FA-12x, and Ab3-FA-25x were around 24 h, 18 h, and 15 h, respectively (Fig. 6.7a). The amount of FA ligands on the antibody has some effect on the PK, but the difference between Ab3-FA-12x and Ab3-FA-25x is relatively small. Because the latter has higher degradation efficiency in the cell-based assay, it was chosen for the following studies. Before testing the anti-tumor efficacy of the degrader *in vivo,* we evaluated the plasma concentration of Ab3-FA-25x in B16F10 tumor-bearing C57BL/6 mice by administering at a dose of 2.5 mg/kg via IP injection. The concentration peaked around 10 μg/ml at 3 h post-treatment, followed by a gradual decline to 5 μg/ml at 8 h and approached 0 μg/mL by 48 h (Fig. 6.7b).

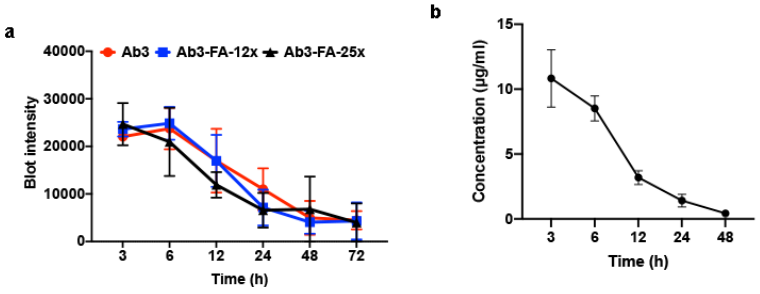

Figure 6.7. Evaluation of the pharmacokinetics (PK) for PD-L1 degraders *in vivo*. **a.** Blot intensity of rat IgG in the plasma of C57BL/6 mice treated with Ab3, Ab3-FA-12x, Ab3-FA-25x at different time points (2.5 mg/kg via IP injection). Data are presented as

mean ± SD, n = 4. **b.** Concentration of Ab3-FA-25x in C57BL/6 mice bearing B16F10 tumor at different time points (2.5 mg/kg via IP injection) Data are presented as mean ± SD, n = 3. (12x and 25x: 12 or 25 molar equivalents of DBCO-NHS ester in the first step; 25 equivalents of folate-azide were used in the second step). N indicates mice. **Note:** Dr. Chunrong Li injected mice and collected blood from mice.

Next, Dr. Chunrong Li and I investigated whether our PD-L1 degrader can impede tumor growth *in vivo.* To assess the efficacy of the PD-L1 degrader across different types of cancer, we tested the anti-tumor effect in three different syngeneic mouse models. B16F10 tumor-bearing C57BL/6 mice, CT26 tumor-bearing BALB/c mice and MOC1 tumor-bearing C57BL/6 mice were randomized into three groups respectively. Mice in each group were treated with PBS, PD-L1 antibody (Ab3) or PD-L1 degrader (Ab3-FA) via IP injection, and continuously treated every other day for a total of 5 doses. 7.5 mg/kg/dose of Ab3 and Ab3-FA was administered into CT26 mouse model, while 2.5mg/kg/dose was administered into B16F10 and MOC1 mouse (Fig. 6.8a-c). By monitoring the tumor size *in-situ,* we found that Ab3-FA could suppress tumor burden in all three mouse models. The most dramatic inhibitory effect was observed for MOC1 tumors, while CT26 and B16F10 tumor models showed less reduction on the tumor growth. Even though the mice exhibited varying responses to the treatment, our PD-L1 degrader Ab3-FA consistently induced a more significant tumor growth delay compared to the Ab3-treated group in all three tumor models (Fig. 6.8d-f). No obvious adverse effect was observed throughout our studies. The body weight was similar among all three groups in all mouse models (Fig. 6.8g-i). We then isolated and analyzed the CT26 and MOC1 tumors at the end of the experiment. Our results showed that mice injected with the degrader had significant smaller tumor sizes and lower tumor weights than the antibody-treated mice (Fig. 6.8j,k). In addition, we treated 4 groups of CT26 tumor-

bearing mice with PBS, IgG-FA (7.5 mg/kg), Ab3 (7.5 mg/kg) and the combination of Ab3 (7.5 mg/kg) and free FA (0.11 mg/kg) respectively via IP injection every other day for a total of 5 doses. We found that the non-targeting FA-conjugated IgG did not reduce the tumor growth compared to PBS-treated group. Mice treated with Ab3 or Ab3 + free FA exhibited similar trends in tumor growth, indicating that the addition of free FA had no effect on tumor progression (Fig. 6.9). These data suggest that our PD-L1 degrader could effectively slow the tumor progression in multiple tumor models, and exhibit more potent anti-tumor efficacy than the blocking antibody.

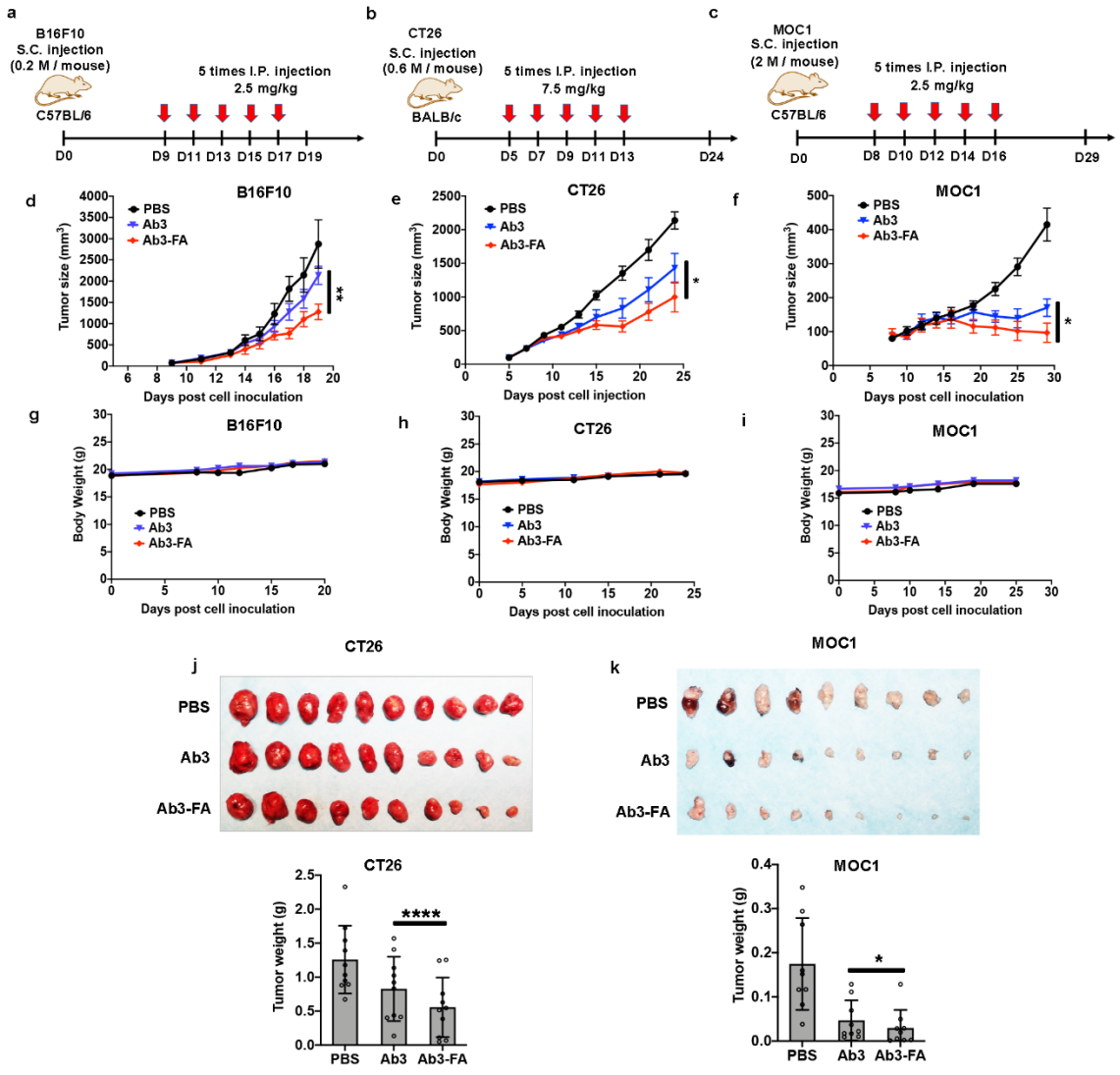

Figure 6.8. FRTAC targeting PD-L1 inhibits tumor growth in B16F10, CT26 and MOC1 syngeneic mouse models. a. Schematic illustration of FRTAC treatment in B16F10 mouse model. **b.** Schematic illustration of FRTAC treatment in CT26 mouse model. **c.** Schematic illustration of FRTAC treatment in MOC1 mouse model. **d.** Tumor growth curves after different treatments as indicated by **a** (n = 8). **e.** Tumor growth curves after different treatments as indicated by **b** (n = 10). **f.** Tumor growth curves after different treatments as indicated by **c** (n = 9). **g.** Body weight curves after different treatments as indicated by **a** (n = 8). **h.** Body weight curves after different treatments as indicated by **b** (n = 10). **i.** Body weight curves after different treatments as indicated by **c** (n = 9). **j.** Images and weight of excised tumors on day 24 after different treatments as indicated by **b** (n = 10). Data are presented as mean ± SD, n = 10. **k.** Images and weight of excised tumors on day 29 after different treatments as indicated by **c** (n = 9). N indicates mice. Data are presented as mean ± SD. The statistical significance was assessed using a paired one-tailed t-test for **d-f** and a paired two-tailed t-test for **j,k,** *P < 0.05, **P < 0.01, ****P < 0.0001. **Note:** These experiments were done by Dr. Chunrong Li.

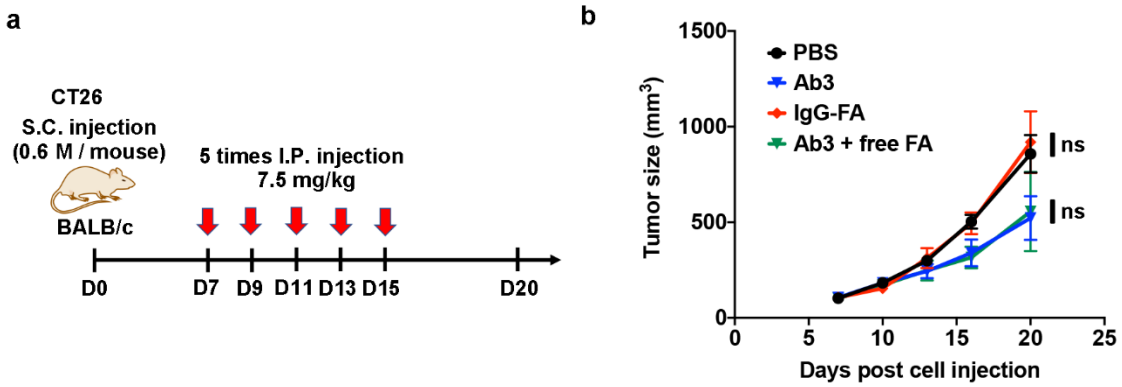

Figure 6.9. Non-targeting FA conjugates and free FA have no effects on tumor growth in CT26 syngeneic mouse model. a. Schematic illustration of control treatment in CT26 mouse model. **b.** Tumor growth curves after different treatments as indicated by **a**. Data are presented as mean ± SD, n = 6 mice. The statistical significance was assessed using a paired t-test, ns: not significant. **Note:** These experiments were done by Dr. Chunrong Li and Xuankun Chen.

We then tried to elucidate the potential mechanism underlying the anti-tumor effect of Ab3-FA in CT26 mouse model. Mice bearing 100-200 mm^3 CT26 tumors were randomly divided into five groups (n=3), and received PBS, 7.5 mg/kg IgG-FA, the combination of 7.5 mg/kg Ab3 plus 0.11 mg/kg free FA, 7.5 mg/kg Ab3, or 7.5 mg/kg Ab3-FA

respectively via IP injection continuously for 3 days. Tumors were collected on day 4 and analyzed for protein levels of PD-L1 and CD8 (a marker for cytotoxic T cell population) by western blot and immunohistochemistry (IHC) staining. We found that Ab3-FA induced a remarkable decrease in tumorous PD-L1 and an increase in CD8 in the tumor tissues compared to the control groups. The FA conjugated isotype and the addition of free FA did not reduce PD-L1 level nor enhance CD8 compared to the mice treated with PBS or Ab3, respectively, indicating FA alone cannot influence the target protein level and $CD8^+$ T cell infiltration (Fig. 6.10). Our results supported the feasibility of FRTACs on depleting protein target *in vivo*, which is consistent with our *in vitro* results. The elevation of $CD8^+$ T cell infiltration in tumor tissues from mice treated with the degrader than those with antibody suggested that the FRTAC could promote the penetration of more cytotoxic T lymphocytes into the tumor to induce the tumor killing effect, therefore suppressing tumor growth more significantly than the antibody. Overall, our results indicate that the FRTAC targeting PD-L1 is more effective immunotherapy than the PD-L1 blocker in all three models.

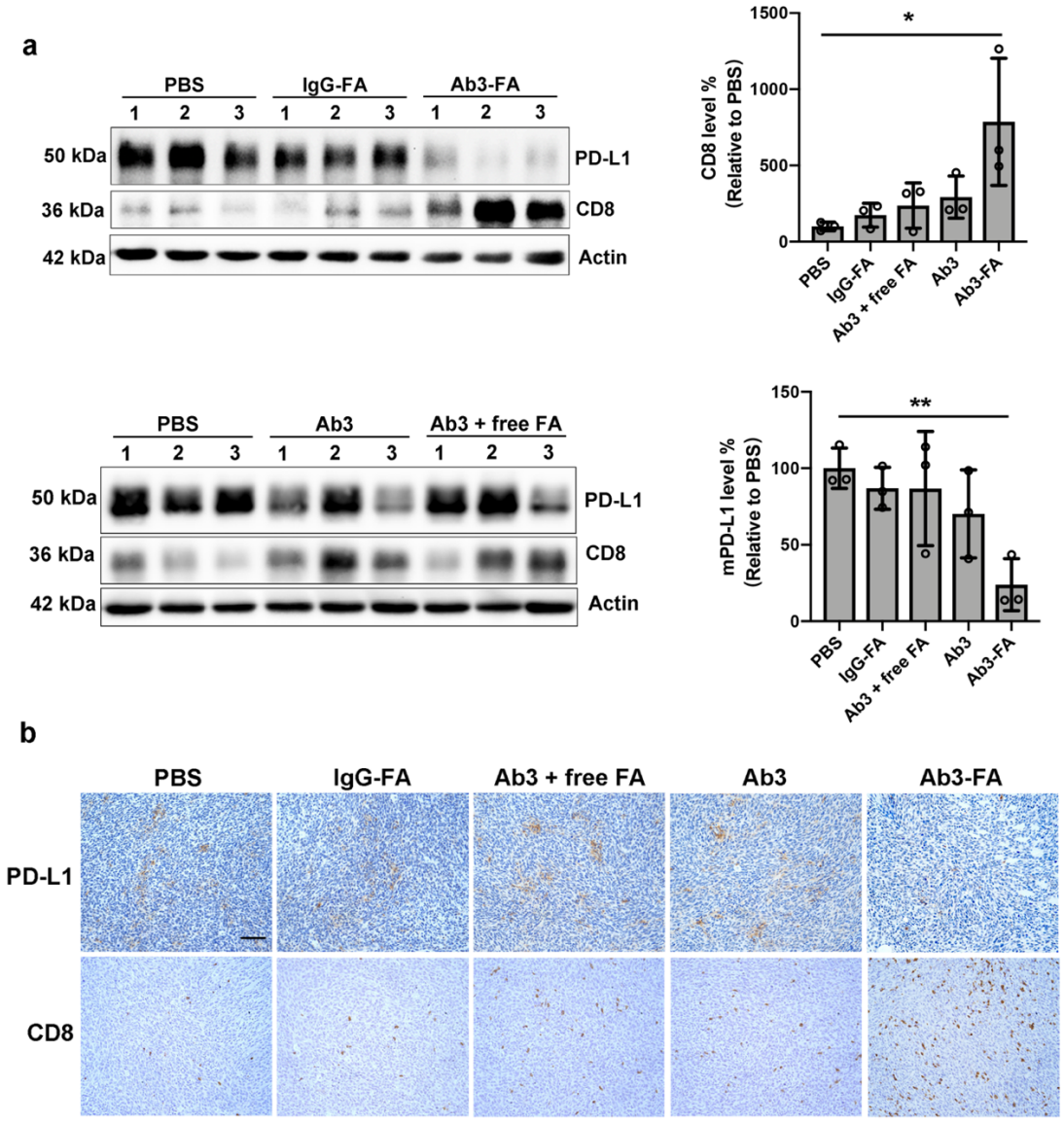

Figure 6.10. FRTAC reveals anti-tumor effect by degrading PD-L1 and recruiting cytotoxic T cell into the tumor. a. Western blot analysis of PD-L1 and CD8a level in tumor tissues isolated from CT26 tumor-bearing mice (7.5 mg/kg daily for 3 days, 3 mice/cohort). **b.** Detection of PD-L1 and CD8 in CT26 tumors by IHC staining (7.5 mg/kg daily for 3 days, 3 mice/cohort). **Note:** Mice treatment and IHC imaging were done by Dr. Chunrong Li. Scale bar: 100 μm. Representative figures from three mice. Data are presented as mean ± SD, n=3 mice. The statistical significance was assessed using an unpaired two-tailed t-test, *P < 0.05, **P < 0.01.

6.3.4. Cancer selectivity of FRTACs targeting EGFR and PD-L1

Lastly, to demonstrate that FRTAC can selectively degrade the protein targets in cancer cells, thereby reducing the on-target/off-tumor effect in normal cells, I compared the degradation efficiency of two FRTACs, Ctx-FA and Atz-FA, in a non-cancerous cell (human keratinocyte line HACAT) with selected cancer cells expressing similar basal EGFR or PD-L1 expression level as the HACAT cells, respectively. The results showed that no significant degradation of EGFR was observed in HACAT cells, while the level of EGFR was dramatically reduced in Huh7 cells. Similarly, Atz-FA induced significant degradation of PD-L1 in Huh7 and TU138 cells, whereas minimal degradation of PD-L1 was detected in HACAT cells. (Fig. 6.11a,b). Western blot showed significantly lower expression level of FR in HACAT cells compared to the cancer cell lines, which may contribute to the much lower degradation efficiency of both FRTACs on normal cell lines (Fig. 6.11c). Next, Dr. Chunrong Li and I assessed the cancer selectivity *in vivo* by characterizing the morphology and detecting PD-L1 level on normal tissues in the CT26 syngeneic mouse model under the conditions indicated in Fig. 6.12a. H&E staining showed that no obvious morphological changes in spleen and lung were observed in the degrader-treated mice. Moreover, the treatment of Ab3-FA resulted in no PD-L1 degradation in spleen and lung, as evidenced by both western blot and IHC staining results, which contrasted with the significant reduction of PD-L1 detected in tumor tissues (Fig. 6.12b-d). Overall, these data indicate the potential of FRTACs for selective degradation of the protein targets in cancer cell lines.

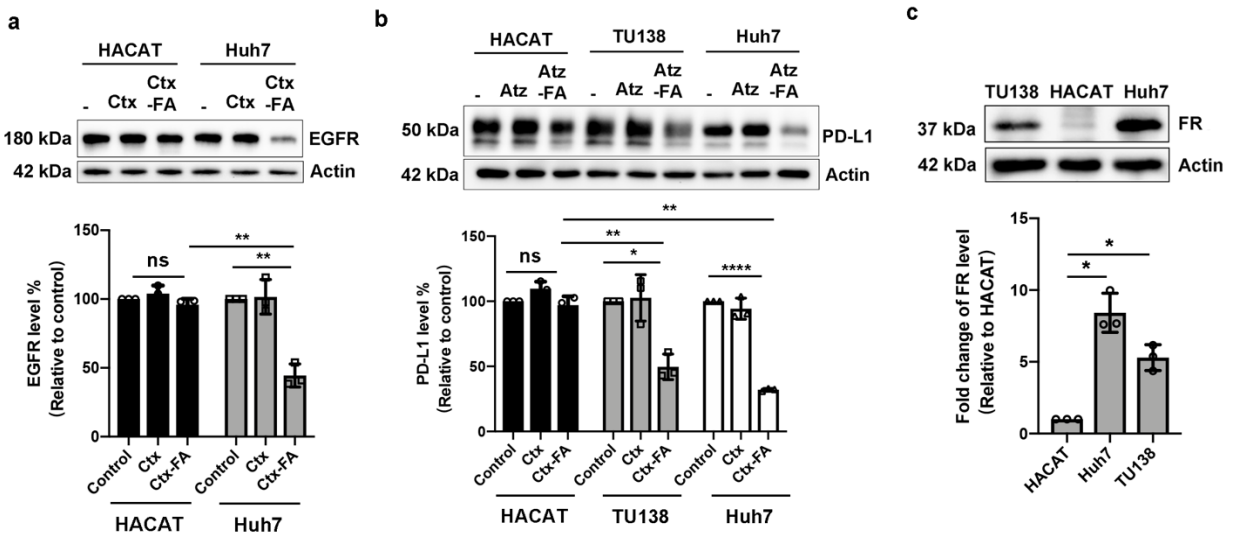

Figure 6.11. FRTACs show cancer selectivity for the degradation of EGFR and PD-L1 *in vitro*. a. Comparison of EGFR degradation efficiency mediated by Ctx-FA (10 nM) in normal cell line HACAT, and cancer cell line Huh7 (n = 3). **b.** Comparison of PD-L1 degradation efficiency of Atz-FA in normal cell line, HACAT, and cancer cell line Huh7 and TU138 (n = 3). **c.** Quantification of FR expression levels on HACAT, Huh7, and TU138 by western blot (n = 3). N indicates biologically independent experiments. Data are presented as mean ± SD. The statistical significance was assessed using an unpaired two-tailed t-test, *P < 0.05, **P < 0.01, ****P < 0.0001, ns: not significant.

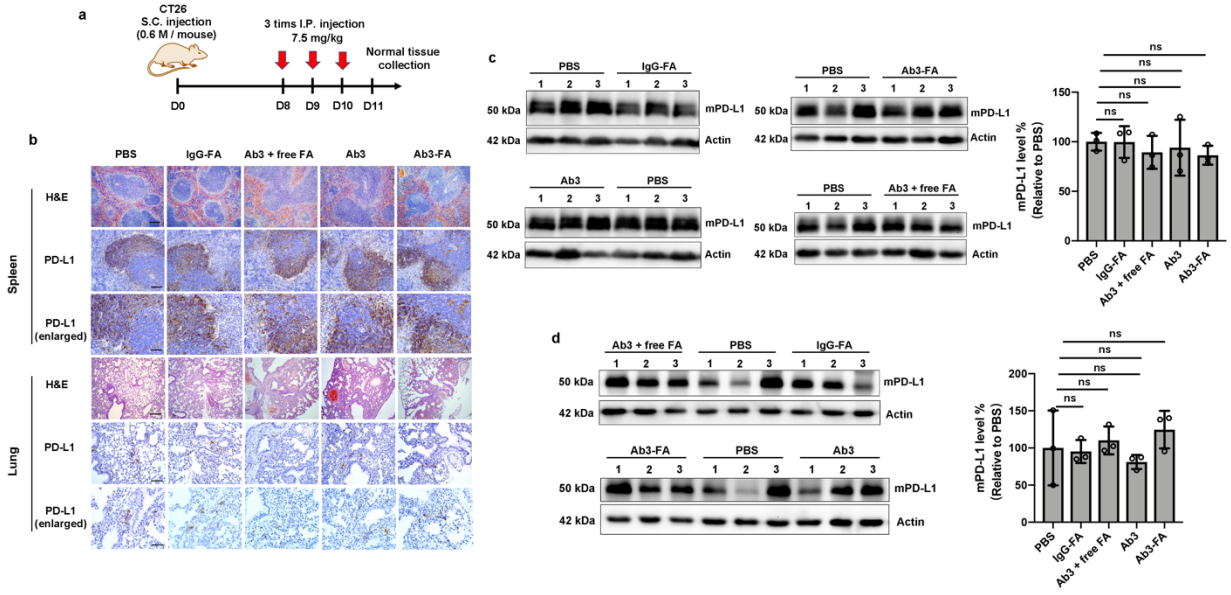

Figure 6.12. FRTACs show cancer selectivity for the degradation of EGFR and PD-L1 *in vivo*. a. Schematic illustration of FRTAC treatment in CT 26 mouse model. **b.** Characterization of spleen and lung morphology by H&E staining and detection of PD-L1 level in spleen and lung after FRTAC treatment by IHC staining. **Note:** Mice treatment and H&E staining were done by Dr. Chunrong Li. Scale bar for H&E staining and PD-L1: 500 μm, Scale bar for PD-L1 enlarged: 100 μm. Scale bar for PD-L1 enlarged: 50 μm. Representative figures from three mice. **c.** Mouse PD-L1 level in spleen, n = 3 mice. **d.** Mouse PD-L1 level in lung, n = 3 mice. N indicates biologically independent experiments. Data are presented as mean ± SD. The statistical significance was assessed using an unpaired two-tailed t-test, ns: not significant.

6.4. Discussion

In summary, we demonstrated for the first time that FR could serve as a LTR for the efficient degradation of both soluble and membrane protein targets by novel chimeric FRTACs. FRTACs were shown to leverage both isoforms of FR to transport the protein targets into the lysosome for depletion without impeding the recycling of the receptors. In addition to factors such as the degree of FA labeling and linker length, we found that the degradation efficiency also highly depends on the cellular FR expression level for extracellular soluble proteins. Other parameters, such as the expression of the endogenous protein target and potential interactions between the FR and protein target induced by FRTACs, may also play roles in the degradation efficiency. Degraders exhibit lower degradation efficiency for membrane proteins on cells expressing abundant amounts of the target protein but low levels of FR. This is likely due to insufficient FR-mediated targeting, leading to suboptimal engagement of the degraders with the target protein. The ratio between FR and endogenous target expression levels is a better determinant of membrane protein degradation compared to FR expression alone. A series of FRTACs was generated and validated for their capability of depleting corresponding targets with different structures and functions, including mouse IgG,

EGFR, PD-L1 and CD47, in a variety of human and mouse cancer cell lines. We demonstrated that FRTAC targeting PD-L1 exhibited similar clearance rate but superior *in vivo* anti-tumor effects than the therapeutic antibody in B16F10, CT26, and MOC1 tumor models. This tumor killing effect of FRTAC could be attributed to the reduction of tumorous PD-L1 and the increased cytotoxic T cells in the tumor. Finally, a much more significant degradation of EGFR and PD-L1 observed in cancer cells over normal cells, as well as no degradation of PD-L1 in normal tissues after FRTAC treatment in mice indicate the potential for lower toxicity and high cancer selectivity of FRTACs.

To date, only a limited number of LTRs have been explored for the development of degraders of extracellular proteins. Most of these LTRs are ubiquitously expressed in many types of cells and tissues with the exception of ASGPR, which is primarily expressed in the liver. Degraders that can recruit LTRs primarily expressed in relevant pathogenic tissues would significantly reduce potential toxicity issues caused by on-target/off-tissue effect. Although integrin and transferrin receptor have been employed as LTRs[25,26], no cancer selectivity was demonstrated. Other recycling receptors with selective expression pattern may contribute to the tissue specific degraders, such as follicle-stimulating hormone receptor and prostate-specific membrane antigen[55,56].

The development of FRTAC expands the landscape of LTR that can be used for degraders of extracellular secreted and membrane proteins. The readily available FR ligand represents a significant advantage over existing lectin type of LTRs that require complex polymeric or oligomeric carbohydrate ligands. More importantly, in addition to the overexpression of FR in various cancers, the inaccessibility of FR in normal tissues to the circulating FA conjugates, a characteristic not shared by other cancer-

overexpressing receptors, enables selective degradation of cancer-relevant protein targets in cancer cells. Indeed, higher degradation efficiency for targets in malignant cells/tissues than normal cells/tissues suggests that on-target/off-tumor effect can be minimized using FRTACs. Furthermore, the successful degradation of multiple therapeutically relevant protein targets in a number of different cancer cell lines indicates that the scope of FRTAC on depleting various cancer-associated protein targets is broad. Beyond the targets examined in this paper, FRTAC can also be applied to various other cancer-relevant targets to reduce the on-target/off-cancer toxicity associated with current therapeutic inhibitors. These include enzymes found in the tumor extracellular matrix, such as matrix metalloproteinases (MMPs) and heparanase, which play critical roles in tumor invasion and metastasis[57,58]. Additionally, FRTAC can target the pH regulator carbonic anhydrase IX (CAIX) to disrupt tumor metabolism and microenvironment[59]. It can also target cytokines such as vascular endothelial growth factor (VEGF) and Interleukin-6 (IL-6), as well as membrane targets on cancer cells, including integrin, mucin 1 (MUC1), and human epidermal growth factor receptor 2 (HER2)[60-65]. In addition to the antibody-based FRTACs, the possibility of transporting the soluble protein targets into the cells by small molecule FRTAC has also been demonstrated. Higher uptake efficiency of antibody-based FRTAC over small molecule FRTAC was observed, which is likely due to the multivalency of the antibody-based degrader. One of the reasons for relatively low degradation efficacy of many lysosome targeting degraders is the competitive binding of the LTRs by endogenous LTR ligands. We found that the competitive binding of free folate is not an issue because the uptake or degradation induced by several different FRTACs is abolished only by high

concentrations of free folate (0.3 to 3 mM of free folate for 10-25 nM of degraders, Fig. 6.2a, 6.4f, and 6.6g,h).

Immune checkpoint blockade (ICB) therapy against PD-L1 is hindered by the low patient response rate and toxicity issues due to non-selective recognition of PD-L1 in normal tissues. As indicated in three mouse models with distinct response efficacy to PD-L1 inhibition and degradation, our FRTAC led to more prominent delayed tumor progression and elicited a stronger immune response than the therapeutic antibody. The modification of FA on the antibody only slightly altered the circulating time *in vivo*. Taken together, FRTACs have the potential to become a more effective cancer immunotherapy than the blocking antibody by increasing the response rate and reduce the on-target/off-tumor side effect.

Collectively, our study demonstrated the feasibility of a new FR-mediated cancer-selective TPD platform and uncovered a potential new therapeutic alternative for ICB therapy with improved precision and efficiency. This work will add a new dimension to TPD with cancer cell selectivity and FRTAC could be a general, effective, and easily accessible technology to degrade cancer-associated protein targets.

6.5. Methods

6.5.1. Cell culture

HepG2 and Huh7 cells were cultured in low-glucose DMEM supplemented with 10% fetal bovine serum, 1% non-essential amino acids, 1% sodium pyruvate, 1% L-glutamine and 1% penicillin/streptomycin under 5 % CO_2 at 37 °C. Hela, Fadu, SW480, Cal27, TU138, HACAT, and MDA-MB-231 cells were maintained in high-glucose DMEM supplemented with 10% fetal bovine serum, and 1% penicillin/streptomycin under 5 %

CO_2 at 37 °C. CT26, B16F10, MOC1 and A549 cells were cultured in RPMI supplemented with 10% fetal bovine serum, 1% sodium pyruvate, 1% HEPES and 1% penicillin/streptomycin under 5 % CO_2 at 37 °C. B16F10, HepG2, Huh7, Hela, MDA-MB-231 and A549 were obtained from the American Tissue Culture Collection (ATCC). Fadu, SW480, Cal27, HACAT, CT26, MOC1, TU138 were obtained from UW-Madison Head Neck Cancer SPORE Pathology Core.

6.5.2. Cellular uptake of anti-FITC and anti-biotin

Cells were seeded at 70% confluence and maintained in 200 μL complete culture media in a 48-well plate. The next day, cells were treated sequentially with 25 μL medium containing anti-FITC or anti-biotin and 25 μL medium containing PBS, antibody, or degrader at different concentrations. The cells were incubated at 37 °C for different time periods and then washed twice with PBS before being harvested for in-gel fluorescence analysis.

6.5.3. Anti-biotin degradation analysis

Cells were seeded at 70% confluence and maintained in 200 μL complete culture media in a 48-well plate. The next day, cells were incubated with 25 nM of Ab-FA and 50 nM of anti-biotin-647 for 3 h, followed by three washes with PBS. Cells were maintained subsequently in fresh media with or without 20 μM chloroquine (CQ), 200 nM Bafilomycin A1 (BAF), and 1 μM MG132 for another 24 h before being harvested for in-gel fluorescence analysis.

6.5.4. FR1 knockdown

Hela cells were seeded at 200,000 cells per well in a 6-well plate one day before transfection. Cells were transfected with 60 pmol of scramble or FR1 siRNA and 7.5 µL RNAiMAX for 24 h and then re-seeded in a 48-well plate at a density of 70,000 cells per well. Cells were then incubated with 25 nM Ab-FA and 50 nM anti-Rabbit-647 for another 6 h before harvested to analyze FR1 levels by western blot and the uptake of anti- Rabbit-647 by in-gel fluorescence.

6.5.5. FR1 and FR2 overexpression

Hela cells were seeded at 70,000 cells per well in a 24-well plate one day before transfection. Cells were transfected with 140 ng plasmid expressing FLAG-FR1 or FLAG-FR2 and Fugene transfection reagent at 1:3.5 w/v ratio for 48 h. Cells transfected with the same amount of empty vectors were used as a negative control. After replacing the media containing the transfection reagent and plasmid with fresh media, cells were incubated with 50 nM Ab-FA and 50 nM anti-Rabbit-647 for another 6 h. Then cells were harvested to analyze FLAG-FR1 and FLAG-FR2 expression levels by western blot and the uptake of anti-rabbit-647 by in-gel fluorescence.

6.5.6. Quantification of cell surface FR level

The expression of cell surface FR was analyzed by flow cytometry. Briefly, flow buffer was prepared as 2% FBS in PBS. $4x10^5$ cells were harvested, washed with PBS, and then re-suspended in 400 µL ice-cold flow buffer containing 10 µM folate-FITC to incubate for 1 h at 37 °C. Cells were then washed twice with 1 mL ice-cold flow buffer and resuspended in 500 µL flow buffer with 1 µg/mL DAPI before flow analysis. Flow cytometry data were acquired using ThermoFisher Attune NxT cytometric software (v 6). FlowJo (v 10.8.1) was used for flow cytometry data analysis.

6.5.7. Antibody labeling with FA-PEGn-NHS (1k- or 2k-PEG-linker)

To label the antibody with folate, 100 µL of the antibody (concentration at 1.8 mg/mL) in PBS was mixed with folate-PEGn-NHS ester at 1:3, 1:12, or 1:25 molar ratio. The reaction was incubated overnight at room temperature on a rotator, followed by filtration with 500 µL of PBS 5 times using a 10 kDa Amicon Centrifugal Filter. The mass of unmodified antibody and FA-labelled antibody was analyzed by MALDI-MS, and the average number of FA per antibody was calculated as below:

$$\boldsymbol{Ave.NO\ of\ FA\ per\ Ab} = \frac{\boldsymbol{Mass\ of\ (FA-antibody) - Mass\ of\ antibody}}{\boldsymbol{Molecular\ weight\ of\ (FA-PEGn-NHS)}}$$

6.5.8. Antibody labeling with DBCO-PEG3-NHS and Folic acid-PEG_n-N_3 (1k- or 2k-PEG-linker)

To label the antibody with DBCO, 200 µL of the antibody (concentration at 1.8 mg/mL) in PBS was mixed with DBCO-PEG3-NHS ester at a 1:25 molar ratio. The reaction was incubated overnight at room temperature on a rotator, followed by filtration with 500 µL of PBS 5 times using a 10 kDa Amicon Centrifugal Filter. Then, the concentration of DBCO-labeled antibody was determined by BCA assay and mixed with Folic acid-PEG1k-N_3 or Folic acid-PEG2K-N_3 at a 1:25 molar ratio. The reaction was incubated overnight at room temperature on a rotator, followed by filtration with 500 µL of PBS 5 times using a 10 kDa Amicon Centrifugal Filter. The mass of unmodified antibody, antibody-DBCO, and FA-labelled antibody was analyzed by MALDI-MS, and the average number of FA per antibody was calculated as below:

$$\boldsymbol{Ave.NO\ of\ FA\ per\ Ab} = \frac{\boldsymbol{Mass\ of\ (FA-antibody) - Mass\ of\ \ (DBCO-antibody)}}{\boldsymbol{Molecular\ weight\ of\ (FA-PEGn-N_3)}}$$

6.5.9. MALDI-MS

Part of the samples were characterized by the following method: Matrix solution was made by dissolving α-Cyano-4-hydroxycinnamic acid (CHCA) in 50% Acetonitrile/H_2O at a final concentration of 10 mg/mL. The sample was absorbed on Omix C4 pipette tips, followed by washing with 0.1% TFA three times and then eluted with 20 µL 75% Acetonitrile/H_2O. 1 µL sample solution and 1 µL CHCA solution were spotted on the MALDI target plate and mixed thoroughly before the spot was allowed to dry at room temperature. MALDI-MS spectra were acquired on the Bruker UltraFlex MALDI-TOF/TOF mass spectrometer operated in linear positive ion mode and plots were generated by Bruker flexAnalysis 4.2. The rest of the samples were characterized by the following method: Matrix solution was made by dissolving sinapic acid (SA) in 70% Acetonitrile/H_2O with 0.1% TFA at a final concentration of 20 mg/mL. The sample was absorbed on Omix C4 pipette tips, followed by washing with 0.1% TFA five times and then eluted with 15 µL 75% Acetonitrile/H_2O. After desalting the sample with Omix C4 pipette tips, 1 µL sample solution and 1 µL SA solution were spotted on the MALDI target plate and mixed thoroughly before the spot was allowed to dry under room temperature. MALDI-MS spectra were acquired on Bruker RapifleX MALDI TOF mass spectrometer (Bruker Scientific, LLC, Bremen, Germany) operated in linear positive ion mode. The smartbeam laser was set to 100% with few thousand shots (labeled on each of the spectrum) per spot at a repetitive rate of 1000 Hz, and detector gain was set at

600 V for the experiments after method optimization. Spectra were processed in Bruker flexAnalysis 4.2.

6.5.10. Targeted protein degradation

Cells were seeded at 70% confluence in a 24-well plate one day before treatment. Then, cells were treated with FRTACs targeting EGFR, PD-L1, or CD47 at various concentrations for indicated time periods before collection for western blot analysis. For mouse PD-L1, B16F10, CT26 and MOC1 cells were pre-incubated with 100 ng/mL mouse IFNγ for 24 h to induce PD-L1 expression before degrader treatment. For human PD-L1, Huh7, HACAT, and TU138 cells were pre-incubated with 100 ng/mL human IFNγ for 16 h to induce PD-L1 expression before degrader treatment.

6.5.11. Rab7 knockdown

Hela cells were seeded at 200,000 cells per well in a 6-well plate one day before transfection. Cells were transfected with 100 pmol of scramble or Rab7 siRNA and 7.5 µL RNAiMAX for 48 h and then re-seeded in a 48-well plate at a density of 70,000 cells per well. To test the uptake of soluble protein, cells were then incubated with 50 nM Ab-FA and 50 nM anti-Rabbit-647 for another 3 h before being harvested to analyze Rab7 levels by western blot and the uptake of anti-rabbit-647 by in-gel fluorescence. To test EGFR degradation, cells were treated with 10 nM Ctx-FA for 6 h before being harvested for western blot analysis.

6.5.12. Western blotting and in-gel fluorescence analysis

Cells were lysed in 1x RIPA lysis buffer (25 mM Tris, pH 7−8, 150 mM NaCl, 0.1% (w/v) sodium dodecyl sulfate (SDS), 0.5% sodium deoxycholate, 1% (v/v) Triton X-100,

protease inhibitor cocktail (Roche, one tablet per 10 mL)) on ice for 10 min, followed by centrifugation at 16 000 g at 4 °C for 15 min. The supernatant was collected and adjusted to the equal amounts after determining the protein concentration using the BCA assay. Lysates were then mixed with the 4x Laemmli Loading Dye and heated at 99 °C for 5 min before being loaded onto 7.5% or 12% SDS−polyacrylamide gel electrophoresis. For western blotting, the gel was transferred to a PVDF membrane, blocked in 5% (w/v) nonfat milk in the TBST washing buffer (137 mM NaCl, 20 mM Tris, 0.1% (v/v) Tween) and then incubated with primary antibodies at 4 °C overnight. After 3 washes with TBST, the membrane was incubated with secondary HRP-linked antibodies for 1 h, and then washed 3 times with TBST. Then the membrane was incubated in the Clarity ECL substrate for 3-5 min before acquiring the immunoblot by ChemiDoc MP Imaging Systems. For in-gel fluorescence analysis, the fluorescence images of the gel were directly acquired by ChemiDoc MP Imaging Systems and the total protein was detected using Coomassie blue staining. Western blot and in-gel fluorescence images were acquired by Image Lab Touch Software (v 2.0.1.35). Western blot bands intensity was analyzed using ImageJ (v 1.53a).

6.5.13. Confocal microscopy

Hela cells were seeded onto 8-well chamber slides at density of 30,000 cells per well in 200 µL of complete culture medium. After adhesion, cells were treated with 50 nM Ab-FA and 50 nM anti-Rabbit-647 for 24 h at 37 °C, followed by the 30-min incubation with LysoTracker Green DND26 (100 nM) at 37 °C. Hoechst 33342 (5 µg/ml) was added 10 min before the end of incubation. After three washes with PBS, the live cells were imaged using Leica SP8 3X STED super-resolution microscope at 20x magnification

with a 10x eyepiece and analyzed by ImageJ. The Pearson's correlation coefficients and mean fluorescence intensity (MFI) were analyzed by Leica LAS-X software (v 2.6).

Fadu cells were seeded onto 8-well chamber slides at a density of 20,000 cells per well in 200 µL of complete culture medium. After adhesion, cells were treated with 10 nM of Ctx-FA for 24 h at 37 °C. Cells were then washed with PBS for 3 times and fixed with 4% paraformaldehyde for 15 min followed by permeabilization with 0.5% Triton X-100 for 5 min. After blocking with 5% BSA for 1 h at room temperature, the cells were co-incubated with anti-LAMP1 antibody in 1% BSA overnight at 4 °C. The next day, cells were washed with PBS and then incubated with anti-mouse-488 and anti-rabbit-594 secondary antibodies for 1 h at room temperature. Then the cells were mounted with slowfade-antifade mounting medium containing DAPI after three washes. Images were acquired by Leica SP8 3X STED super-resolution microscope at 60x magnification with a 10x eyepiece and analyzed by ImageJ. The Pearson's correlation coefficients and mean fluorescence intensity (MFI) were analyzed by Leica LAS-X software (v 2.6).

6.5.14. Animal studies

All animal work were approved by the University of Wisconsin-Madison Institutional Animal Care and Use Committee (IACUC) and conducted in accordance with the NIH Guide for the care and use of laboratory animals (animal protocol number M006396). Mice that were 6 to 8 weeks of age were purchased from the Jackson Laboratory. Mice were group-housed, with no more than five mice per cage. Environmental conditions were maintained at a temperature of 22-25°C and a humidity level of 40-60%. The mice were kept on a 12-hour light/dark cycle with ad libitum access to food and water.

6.5.15. Pharmacokinetics (PK) analysis

The pharmacokinetics of antibody and degrader were determined by intraperitoneally injecting 2.5 mg/kg of antibody and FRTAC into C57BL/6 mice or C57BL/6 mice bearing B16F10 tumor. A small amount of blood was collected from mouse tail vein at different time points and the corresponding levels of antibody and FRTAC were measured by blotting the Rat IgG level in the plasma. Ab3-FA-25x at different concentrations were used as standards.

6.5.16. Tumor growth experiments

B16F10 ($2x10^5$ cells/mouse to C57BL/6), CT26 cells ($6.0x10^5$ cells/mouse to BALB/c) and MOC1 cells ($2x10^6$ cells/mouse to C57BL/6) were inoculated in mice subcutaneously. When tumor volumes reached 50-150 mm^3, C57BL/6 mice (n=8/cohort) bearing B16F10 tumor were treated with PBS, Ab3 or Ab3-FA at a dose of 2.5 mg/kg via IP injection, and continuously treated every other day for a total of 5 doses. When tumor volumes reached 50-150 mm^3, BALB/C mice (n=10/cohort) bearing CT26 tumor were treated with PBS, Ab3 or Ab3-FA at a dose of 7.5 mg/kg via IP injection, and continuously treated every other day for a total of 5 doses. For control groups, BALB/C mice (n=6/cohort) bearing CT26 tumor were treated with PBS, IgG-FA, Ab3 or Ab3 + free FA at a dose of 7.5 mg/kg via IP injection, and continuously treated every other day for a total of 5 doses. When tumor volumes reached 20-100 mm^3, C57BL/6 mice (n=9/cohort) bearing MOC1 tumor were treated with PBS, Ab3 or Ab3-FA at a dose of 2.5 mg/kg via IP injection, and continuously treated every other day for a total of 5 doses. The mouse body weight was monitored, and tumor volume size was measured every 2 days with a caliper and calculated with the formula 0.5 x length x $(width)^2$.

6.5.17. Evaluation of PD-L1 and CD8a level *in vivo*

CT26 cells ($6.0x10^5$ cells/mouse to BALB/C) were inoculated in mice subcutaneously. When the tumor volume reached to 100-200 mm^3, the mice were treated with PBS, IgG-FA, the combination of Ab3 plus free FA (0.11 mg/kg), Ab3, or Ab3-FA (7.5 mg/kg daily for 3 days, 3 mice/cohort). Half of tumors, spleen, and lung from CT26 syngeneic mouse model were frozen and lysed in RIPA buffer for western blot analysis. The remaining tumors, spleen, and lung were fixed in formalin, and embedded in paraffin. Paraffin-embedded tumor and normal tissue specimens were cut into 5-μm sections for immunohistochemistry (IHC) staining.

6.5.18. Immunohistochemistry (IHC) staining

In brief, tumor sections were deparaffinized and rehydrated, followed by antigen retrieval in citrate buffer (10 mmol/L, pH 6.0) for 15 minutes at 98°C. After quenching with 3% hydrogen peroxide and blocking with 2.5% goat serum, slides were incubated at 4°C overnight with primary antibodies against PD-L1 or CD8 followed by a 30-minute incubation with HRP-conjugated secondary antibody. Slides were then visualized using the Dakocytomation Liquid DAB+Substrate Chromogen System. After counterstaining with hematoxylin, the tumor sections were dehydrated and mounted with coverslips.

6.6. References

1 Salami, J. & Crews, C. M. Waste disposal-An attractive strategy for cancer therapy. *Science* **355**, 1163-1167 (2017). https://doi.org/10.1126/science.aam7340

2 Békés, M., Langley, D. R. & Crews, C. M. PROTAC targeted protein degraders: the past is prologue. *Nat Rev Drug Discov* **21**, 181-200 (2022). https://doi.org/10.1038/s41573-021-00371-6

3 Samarasinghe, K. T. G. & Crews, C. M. Targeted protein degradation: A promise for undruggable proteins. *Cell Chem Biol* **28**, 934-951 (2021). https://doi.org/10.1016/j.chembiol.2021.04.011

4 Poso, A. The Future of Medicinal Chemistry, PROTAC, and Undruggable Drug Targets. *J Med Chem* **64**, 10680-10681 (2021). https://doi.org/10.1021/acs.jmedchem.1c01126

5 Schneider, M. *et al.* The PROTACtable genome. *Nat Rev Drug Discov* **20**, 789-797 (2021). https://doi.org/10.1038/s41573-021-00245-x

6 Sakamoto, K. M. *et al.* Protacs: chimeric molecules that target proteins to the Skp1-Cullin-F box complex for ubiquitination and degradation. *Proc Natl Acad Sci U S A* **98**, 8554-8559 (2001). https://doi.org/10.1073/pnas.141230798

7 Bondeson, D. P. *et al.* Catalytic in vivo protein knockdown by small-molecule PROTACs. *Nat Chem Biol* **11**, 611-617 (2015). https://doi.org/10.1038/nchembio.1858

8 Winter, G. E. *et al.* DRUG DEVELOPMENT. Phthalimide conjugation as a strategy for in vivo target protein degradation. *Science* **348**, 1376-1381 (2015). https://doi.org/10.1126/science.aab1433

9 Zengerle, M., Chan, K. H. & Ciulli, A. Selective Small Molecule Induced Degradation of the BET Bromodomain Protein BRD4. *ACS Chem Biol* **10**, 1770-1777 (2015). https://doi.org/10.1021/acschembio.5b00216

10 Mullard, A. Targeted protein degraders crowd into the clinic. *Nat Rev Drug Discov* **20**, 247-250 (2021). https://doi.org/10.1038/d41573-021-00052-4

11 Guenette, R. G., Yang, S. W., Min, J., Pei, B. & Potts, P. R. Target and tissue selectivity of PROTAC degraders. *Chem Soc Rev* **51**, 5740-5756 (2022). https://doi.org/10.1039/d2cs00200k

12 Spradlin, J. N. *et al.* Harnessing the anti-cancer natural product nimbolide for targeted protein degradation. *Nat Chem Biol* **15**, 747-755 (2019). https://doi.org/10.1038/s41589-019-0304-8

13 Zhang, X., Crowley, V. M., Wucherpfennig, T. G., Dix, M. M. & Cravatt, B. F. Electrophilic PROTACs that degrade nuclear proteins by engaging DCAF16. *Nat Chem Biol* **15**, 737-746 (2019). https://doi.org/10.1038/s41589-019-0279-5

14 Schapira, M., Calabrese, M. F., Bullock, A. N. & Crews, C. M. Targeted protein degradation: expanding the toolbox. *Nat Rev Drug Discov* **18**, 949-963 (2019). https://doi.org/10.1038/s41573-019-0047-y

15 Gerry, C. J. & Schreiber, S. L. Unifying principles of bifunctional, proximity-inducing small molecules. *Nat Chem Biol* **16**, 369-378 (2020). https://doi.org/10.1038/s41589-020-0469-1

16 Paudel, R. R., Lu, D., Roy Chowdhury, S., Monroy, E. Y. & Wang, J. Targeted Protein Degradation via Lysosomes. *Biochemistry* **62**, 564-579 (2023). https://doi.org/10.1021/acs.biochem.2c00310

17 Hua, L. *et al.* Beyond Proteolysis-Targeting Chimeric Molecules: Designing Heterobifunctional Molecules Based on Functional Effectors. *J Med Chem* **65**, 8091-8112 (2022). https://doi.org/10.1021/acs.jmedchem.2c00316

18 Chen, X., Zhou, Y., Zhao, Y. & Tang, W. Targeted degradation of extracellular secreted and membrane proteins. *Trends Pharmacol Sci* **44**, 762-775 (2023). https://doi.org/10.1016/j.tips.2023.08.013

19 Uhlén, M. *et al.* Proteomics. Tissue-based map of the human proteome. *Science* **347**, 1260419 (2015). https://doi.org/10.1126/science.1260419

20 Banik, S. M. *et al.* Lysosome-targeting chimaeras for degradation of extracellular proteins. *Nature* **584**, 291-297 (2020). https://doi.org/10.1038/s41586-020-2545-9

21 Ahn, G. *et al.* LYTACs that engage the asialoglycoprotein receptor for targeted protein degradation. *Nat Chem Biol* **17**, 937-946 (2021). https://doi.org/10.1038/s41589-021-00770-1

22 Zhou, Y., Teng, P., Montgomery, N. T., Li, X. & Tang, W. Development of Triantennary N-Acetylgalactosamine Conjugates as Degraders for Extracellular Proteins. *ACS Cent Sci* **7**, 499-506 (2021). https://doi.org/10.1021/acscentsci.1c00146

23 Caianiello, D. F. *et al.* Bifunctional small molecules that mediate the degradation of extracellular proteins. *Nat Chem Biol* **17**, 947-953 (2021). https://doi.org/10.1038/s41589-021-00851-1

24 Pance, K. *et al.* Modular cytokine receptor-targeting chimeras for targeted degradation of cell surface and extracellular proteins. *Nat Biotechnol* (2022). https://doi.org/10.1038/s41587-022-01456-2

25 Zheng, J. *et al.* Bifunctional Compounds as Molecular Degraders for Integrin-Facilitated Targeted Protein Degradation. *J Am Chem Soc* **144**, 21831-21836 (2022). https://doi.org/10.1021/jacs.2c08367

26 Zhang, D. *et al.* Transferrin Receptor Targeting Chimeras (TransTACs) for Membrane Protein Degradation. *bioRxiv*, 2023.2008.2010.552782 (2023).

27 Low, P. S., Henne, W. A. & Doorneweerd, D. D. Discovery and development of folic-acid-based receptor targeting for imaging and therapy of cancer and inflammatory diseases. *Acc Chem Res* **41**, 120-129 (2008). https://doi.org/10.1021/ar7000815

28 Srinivasarao, M. & Low, P. S. Ligand-Targeted Drug Delivery. *Chem Rev* **117**, 12133-12164 (2017). https://doi.org/10.1021/acs.chemrev.7b00013

29 Ross, J. F. *et al.* Folate receptor type beta is a neutrophilic lineage marker and is differentially expressed in myeloid leukemia. *Cancer* **85**, 348-357 (1999). https://doi.org/10.1002/(sici)1097-0142(19990115)85:2<348::aid-cncr12>3.0.co;2-4

30 Kalli, K. R. *et al.* Folate receptor alpha as a tumor target in epithelial ovarian cancer. *Gynecol Oncol* **108**, 619-626 (2008). https://doi.org/10.1016/j.ygyno.2007.11.020

31 Nunez, M. I. *et al.* High expression of folate receptor alpha in lung cancer correlates with adenocarcinoma histology and EGFR [corrected] mutation. *J Thorac Oncol* **7**, 833-840 (2012). https://doi.org/10.1097/JTO.0b013e31824de09c

32 Chen, C. *et al.* Structural basis for molecular recognition of folic acid by folate receptors. *Nature* **500**, 486-489 (2013). https://doi.org/10.1038/nature12327

33 Sabharanjak, S. & Mayor, S. Folate receptor endocytosis and trafficking. *Adv Drug Deliv Rev* **56**, 1099-1109 (2004). https://doi.org/10.1016/j.addr.2004.01.010

34 Lu, Y. & Low, P. S. Immunotherapy of folate receptor-expressing tumors: review of recent advances and future prospects. *J Control Release* **91**, 17-29 (2003). https://doi.org/10.1016/s0168-3659(03)00215-3

35 Marchetti, C. *et al.* Targeted drug delivery via folate receptors in recurrent ovarian cancer: a review. *Onco Targets Ther* **7**, 1223-1236 (2014). https://doi.org/10.2147/OTT.S40947

36 Kelemen, L. E. The role of folate receptor alpha in cancer development, progression and treatment: cause, consequence or innocent bystander? *Int J Cancer* **119**, 243-250 (2006). https://doi.org/10.1002/ijc.21712

37 Sudimack, J. & Lee, R. J. Targeted drug delivery via the folate receptor. *Adv Drug Deliv Rev* **41**, 147-162 (2000). https://doi.org/10.1016/s0169-409x(99)00062-9

38 Müller, C. & Schibli, R. Folic acid conjugates for nuclear imaging of folate receptor-positive cancer. *J Nucl Med* **52**, 1-4 (2011). https://doi.org/10.2967/jnumed.110.076018

39 Srinivasarao, M., Galliford, C. V. & Low, P. S. Principles in the design of ligand-targeted cancer therapeutics and imaging agents. *Nat Rev Drug Discov* **14**, 203-219 (2015). https://doi.org/10.1038/nrd4519

40 Reddy, J. A. & Low, P. S. Folate-mediated targeting of therapeutic and imaging agents to cancers. *Crit Rev Ther Drug Carrier Syst* **15**, 587-627 (1998).

41 Lu, Y. & Low, P. S. Folate-mediated delivery of macromolecular anticancer therapeutic agents. *Adv Drug Deliv Rev* **54**, 675-693 (2002). https://doi.org/10.1016/s0169-409x(02)00042-x

42 Scaranti, M., Cojocaru, E., Banerjee, S. & Banerji, U. Exploiting the folate receptor α in oncology. *Nat Rev Clin Oncol* **17**, 349-359 (2020). https://doi.org/10.1038/s41571-020-0339-5

43 Van Keulen, S., Hom, M., White, H., Rosenthal, E. L. & Baik, F. M. The Evolution of Fluorescence-Guided Surgery. *Mol Imaging Biol* **25**, 36-45 (2023). https://doi.org/10.1007/s11307-022-01772-8

44 https://www.fda.gov/drugs/resources-information-approved-drugs/fda-grants-accelerated-approval-mirvetuximab-soravtansine-gynx-fra-positive-platinum-resistant. *FDA grants accelerated approval to mirvetuximab soravtansine-gynx for FRα positive, platinum-resistant epithelial ovarian, fallopian tube, or peritoneal cancer*, 2022).

45 Liu, J. *et al.* Cancer Selective Target Degradation by Folate-Caged PROTACs. *J Am Chem Soc* **143**, 7380-7387 (2021). https://doi.org/10.1021/jacs.1c00451

46 Chen, H., Liu, J., Kaniskan, H., Wei, W. & Jin, J. Folate-Guided Protein Degradation by Immunomodulatory Imide Drug-Based Molecular Glues and Proteolysis Targeting Chimeras. *J Med Chem* **64**, 12273-12285 (2021). https://doi.org/10.1021/acs.jmedchem.1c00901

47 Vanlandingham, P. A. & Ceresa, B. P. Rab7 regulates late endocytic trafficking downstream of multivesicular body biogenesis and cargo sequestration. *J Biol Chem* **284**, 12110-12124 (2009). https://doi.org/10.1074/jbc.M809277200

48 Dong, S., Cho, H. J., Lee, Y. W. & Roman, M. Synthesis and cellular uptake of folic acid-conjugated cellulose nanocrystals for cancer targeting. *Biomacromolecules* **15**, 1560-1567 (2014). https://doi.org/10.1021/bm401593n

49 Langston Suen, W. L. & Chau, Y. Size-dependent internalisation of folate-decorated nanoparticles via the pathways of clathrin and caveolae-mediated endocytosis in ARPE-19 cells. *J Pharm Pharmacol* **66**, 564-573 (2014). https://doi.org/10.1111/jphp.12134

50 Zou, W., Wolchok, J. D. & Chen, L. PD-L1 (B7-H1) and PD-1 pathway blockade for cancer therapy: Mechanisms, response biomarkers, and combinations. *Sci Transl Med* **8**, 328rv324 (2016). https://doi.org/10.1126/scitranslmed.aad7118

51 Sharma, P. & Allison, J. P. The future of immune checkpoint therapy. *Science* **348**, 56-61 (2015). https://doi.org/10.1126/science.aaa8172

52 Sun, J. Y. *et al.* Resistance to PD-1/PD-L1 blockade cancer immunotherapy: mechanisms, predictive factors, and future perspectives. *Biomark Res* **8**, 35 (2020). https://doi.org/10.1186/s40364-020-00212-5

53 Chen, S. *et al.* Response Efficacy of PD-1 and PD-L1 Inhibitors in Clinical Trials: A Systematic Review and Meta-Analysis. *Front Oncol* **11**, 562315 (2021). https://doi.org/10.3389/fonc.2021.562315

54 Naidoo, J. *et al.* Toxicities of the anti-PD-1 and anti-PD-L1 immune checkpoint antibodies. *Ann Oncol* **26**, 2375-2391 (2015). https://doi.org/10.1093/annonc/mdv383

55 Banerjee, A. A., Joseph, S. & Mahale, S. D. From cell surface to signalling and back: the life of the mammalian FSH receptor. *FEBS J* **288**, 2673-2696 (2021). https://doi.org/10.1111/febs.15649

56 Zhang, J. *et al.* A prostate-specific membrane antigen activated molecular rotor for real-time fluorescence imaging. *Nat Commun* **12**, 5460 (2021). https://doi.org/10.1038/s41467-021-25746-6

57 Jayatilleke, K. M. & Hulett, M. D. Heparanase and the hallmarks of cancer. *J Transl Med* **18**, 453 (2020). https://doi.org/10.1186/s12967-020-02624-1

58 Niland, S., Riscanevo, A. X. & Eble, J. A. Matrix Metalloproteinases Shape the Tumor Microenvironment in Cancer Progression. *Int J Mol Sci* **23** (2021). https://doi.org/10.3390/ijms23010146

59 Pastorekova, S. & Gillies, R. J. The role of carbonic anhydrase IX in cancer development: links to hypoxia, acidosis, and beyond. *Cancer Metastasis Rev* **38**, 65-77 (2019). https://doi.org/10.1007/s10555-019-09799-0

60 Mei, Z. *et al.* MUC1 as a target for CAR-T therapy in head and neck squamous cell carinoma. *Cancer Med* **9**, 640-652 (2020). https://doi.org/10.1002/cam4.2733

61 Ahmed, N. *et al.* HER2-Specific Chimeric Antigen Receptor-Modified Virus-Specific T Cells for Progressive Glioblastoma: A Phase 1 Dose-Escalation Trial. *JAMA Oncol* **3**, 1094-1101 (2017). https://doi.org/10.1001/jamaoncol.2017.0184

62 Liu, F., Wu, Q., Dong, Z. & Liu, K. Integrins in cancer: Emerging mechanisms and therapeutic opportunities. *Pharmacol Ther* **247**, 108458 (2023). https://doi.org/10.1016/j.pharmthera.2023.108458

63 Rini, B. I., Campbell, S. C. & Escudier, B. Renal cell carcinoma. *Lancet* **373**, 1119-1132 (2009). https://doi.org/10.1016/S0140-6736(09)60229-4

64 Niu, G. & Chen, X. Vascular endothelial growth factor as an anti-angiogenic target for cancer therapy. *Curr Drug Targets* **11**, 1000-1017 (2010). https://doi.org/10.2174/138945010791591395

65 Rašková, M. *et al.* The Role of IL-6 in Cancer Cell Invasiveness and Metastasis-Overview and Therapeutic Opportunities. *Cells* **11** (2022). https://doi.org/10.3390/cells11223698

Chapter 7

Development of transferrin receptor-recruiting cancer-selective catalytic lysosomal targeting degraders

7.1. Introduction

Targeted protein degradation (TPD) is an innovative therapeutic approach that leverages bifunctional molecules to selectively capture and eliminate a protein of interest (POI) by harnessing endogenous degradation pathways[1]. This strategy has led to the development of multiple platforms, such as PROteolysis TArgeting Chimeras (PROTACs) and AUtophagy-TArgeting Chimeras (AUTACs), which primarily target cytosolic proteins through either ubiquitin-proteasome or autophagy pathways[2,3]. Recently, the scope of TPD has been expanded to extracellular proteins, comprising approximately 40% of the proteome, with the advent of Lysosome Targeting Chimeras (LYTACs). LYTACs are composed of a ligand for a lysosomal targeting receptor (LTR) and a binder specific to the extracellular POI. Upon binding to both LTR and POI, the receptor-ligand interaction initiates receptor-mediated endocytosis, leading to the degradation of the targeted extracellular proteins within lysosomes[4].

The first LYTAC system employed the cation-independent mannose-6-phosphate receptor (CI-M6PR), which is expressed in a broad range of tissues[4]. The degradation of extracellular proteins in various tissues raises concerns regarding potential on-target and off-tissue toxicity. Later, LYTACs targeting the asialoglycoprotein receptor (ASGPR) were developed by us and others to induce selective degradation of POIs in liver cells, addressing tissue specificity to some extent[5-7]. Recently, several cancer-targeting strategies have been reported leveraging lysosome targeting receptors overexpressed on tumor tissues, including integrin, folate receptor and transferrin receptor[8-11], after the initiation of the work presented in this chapter. Unlike PROTACs, which act catalytically

and can be recycled, existing LYTACs are degraded along with their targets in the lysosome, limiting their reusability.

Transferrin receptor 1 (TfR1), also known as CD71, is a type II transmembrane glycoprotein existing as a homodimer on the cell surface to constitutively transport iron-loaded transferrin into cell to maintain iron homeostasis and regulate cell proliferation[12]. The pH and iron-dependent binding affinity between TfR1 and transferrin allows the recycle of transferrin efficiently. Transferrin carrying up to two ferric ions in the blood stream to form “holo-transferrin”, which then binds to TfR1 with a high binding affinity (K_d = 4 nM) at neutral pH. This binding event triggers the internalization of the ligand/receptor complex through clathrin-mediated endocytosis pathway. After being transported into early endosome, the acid environment induces the conformational change of both transferrin and TfR1, resulting in the release of the ferric ion from transferrin, while the transferrin without ferric ions, termed as “apo-transferrin”, is recycled back to the cell surface together with TfR1 and dissociated from the receptor at the neutral pH due to reduced binding affinity (K_d = 30 nM)[13,14]. The recycling property of transferrin opens the possibility of generating catalytic LYTAC using transferrin conjugates. Because of the critical role of iron in cell proliferation, highly dividing cells, such as cancer cells, demands more iron compared to normal cells, leading to elevated expression level of TfR1 on cancer cells. In fact, the overexpression of TfR1 is regulated by numerous tumorigenic factors and has been recognized as a biomarker for tumor progression, which makes it a promising candidate for cancer-selective targeting. TfR1 has been used as an attractive target for cancer cell-selective drug delivery[15]. The natural ligand of TfR1, Transferrin, and anti-TfR antibody, antibody fragment or peptide

binder of TfR1 have been directly conjugated with chemotherapeutic drugs, nucleotide, toxic proteins or decorated on nanoparticle or liposome loaded with cytotoxic drugs to selectively direct therapeutic reagents to malignant cells[16]. In this study, we propose utilizing transferrin as the ligand and TfR1 as the lysosome-targeting receptor to develop catalytic LYTACs, which leverage the unique recycling properties of transferrin. Two degrader modalities were generated: one via chemical conjugation and the other through genetic expression. We hypothesized that the plasmid-encoded degrader could be expressed and secreted by the cell, and the degraders in both modalities could catalytically promote lysosomal degradation of the target protein (Fig.7.1).

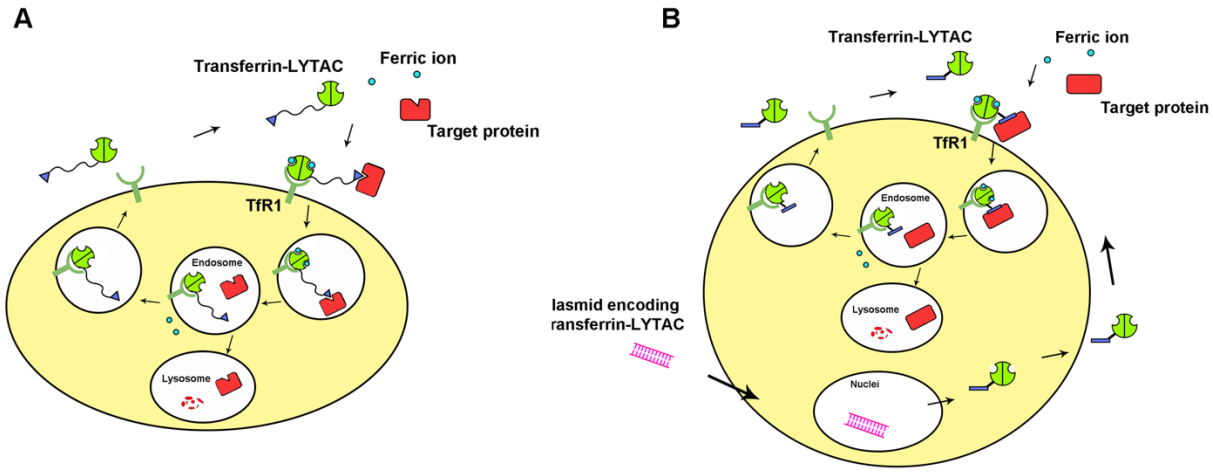

Figure 7.1. Illustration of transferrin-induced lysosomal targeted protein degradation. A. Catalytic degradation of POIs mediated by transferrin conjugates. **B.** Catalytic degradation of POIs mediated by genetically encoded transferrin-based degrader.

7.2. Results

Unlike previous degraders that utilize small-molecule binders for lysosomal targeting receptors, our transferrin-based degrader relies on the protein-protein interaction

between transferrin and the transferrin receptor (TfR1). To assess feasibility, I employed mouse anti-biotin IgG-647 as the model target and biotinylated transferrin as the degrader. I initially tested the uptake of anti-biotin IgG-647 mediated by biotinylated transferrin across various cell lines with differing TfR1 expression levels. The results demonstrated that uptake efficiency varied across cell lines and showed a strong correlation with TfR1 expression levels. The treatment of the degrader did not change TfR1 expression level in these cell lines (Fig. 7.2A). I then characterized the uptake of anti-biotin IgG-647 mediated by transferrin-biotin in MCF7 cells cultured in both serum-containing and serum-free media. Our data demonstrated that the target protein internalization mediated by transferrin-biotin was dose- and time-dependent with the maximum uptake of 50 nM mouse anti-biotin IgG-647 achieved at 2 h using 25 nM of the degrader. Similar to PROTAC, a typical hook effect was observed when cells were treated with higher amount of transferrin-biotin. Importantly, these uptake dynamics were consistent regardless of the absence or presence of serum in the media (Fig. 7.2B). Next, I investigated whether anti-biotin IgG-647 was delivered into lysosomes for degradation. The results showed that the treatment of lysosome inhibitor, Bafilomycin A1 and chloroquine, increased the intracellular target amount by inhibiting the lysosomal degradation of the internalized target protein (Fig. 7.2C). Moreover, confocal images demonstrated the distribution of internalized anti-biotin IgG-647 in the cytoplasm and partial co-localization with the lysosome indicated by Lysotracker (Fig. 7.2D). These data indicated that the model target (mouse anti-biotin IgG-647) was delivered into the lysosome for degradation. Next, to investigate the role of TfR1 in the process, free holo-transferrin was added to compete with the degrader for the binding to TfR1. I found that

less anti-biotin IgG-647 was internalized in the presence of free transferrin, suggesting the involvement of TfR1 in mediating cellular uptake of the target protein (Fig. 7.2E). In addition, downregulation of TfR1 by siRNA also reduced the amount of target protein internalized into the cell in MCF7 cells (Fig. 7.2F). Overall, we demonstrated that the transferrin-based degrader can transport target protein into lysosome for degradation via the interaction with TfR1.

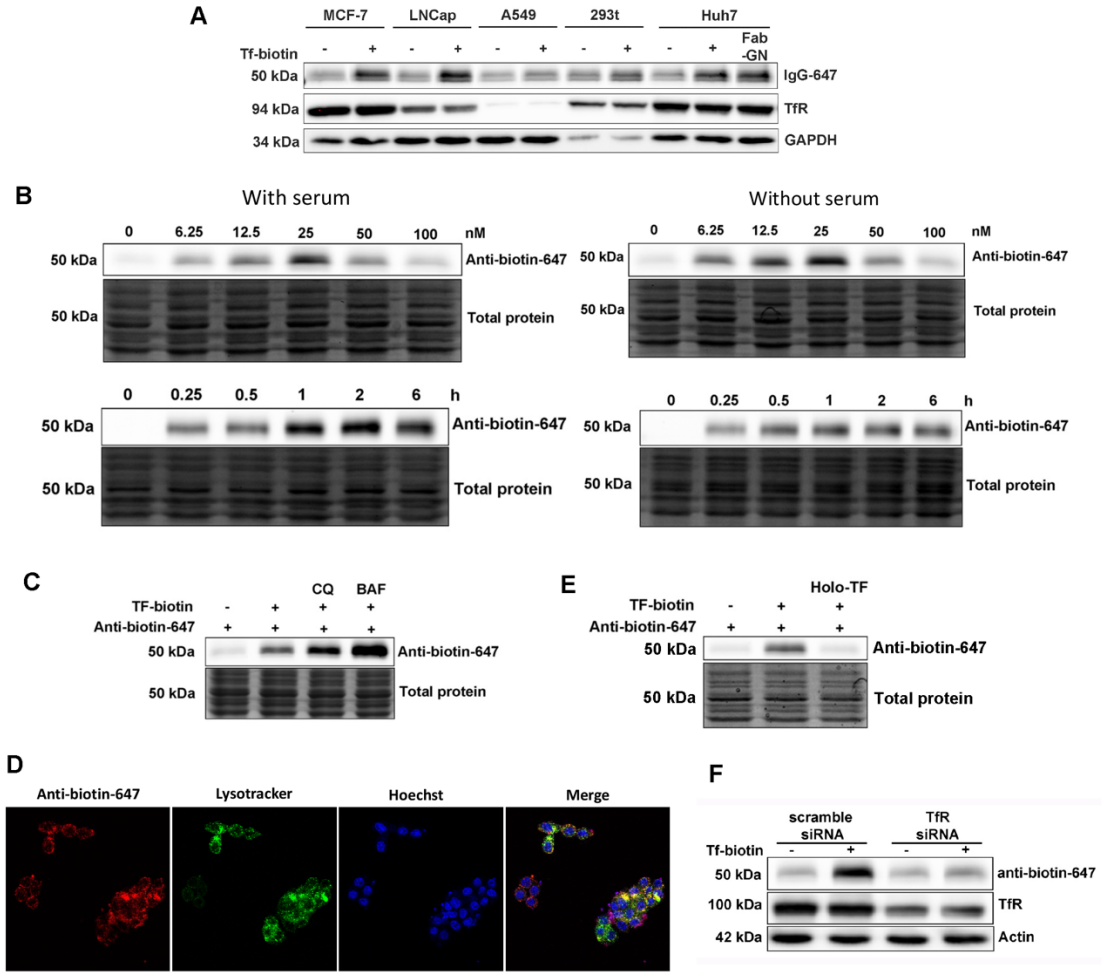

Figure 7.2. Transferrin-based degrader mediates soluble protein degradation in the lysosome via the interaction with TfR1. A. Uptake of 50 nM anti-biotin-647 mediated by 25 nM transferrin-biotin in different cancer cell lines. **B.** Dose-response and time course of transferrin-biotin mediated uptake of anti-biotin-647 in MCF7 cells cultured with or without serum. **C.** Inhibition of internalized anti-biotin-647 degradation

by lysosomal degradation inhibitors. **D.** Colocalization of internalized anti-biotin-647 with lysosome. **E.** Inhibition of anti-biotin-647 uptake by free transferrin. **F.** Uptake of anti-biotin-647 in TfR1 knockdown cells.

I next performed a transferrin-biotin recycling assay to assess whether the transferrin-based degrader could function catalytically. I first used anti-biotin-647 as an indicator to monitor the recycling of the degrader. Cells were treated with anti-biotin IgG-647 and transferrin-biotin for 1 hour, after which the media containing the degrader and target protein was removed. Fresh media containing Holo-TF and the iron chelator deferoxamine mesylate were then added for an additional 2 hours. The levels of anti-biotin IgG-647 in both the cell lysate and media were analyzed by in-gel fluorescence. Our results showed that anti-biotin-647 was internalized and accumulated in the cell after 1 h incubation with anti-biotin-647 and transferrin-biotin. Upon media replacement, intracellular anti-biotin IgG-647 levels decreased, while levels in the media increased, indicating that the internalized anti-biotin IgG-647 was subsequently secreted back into the media. Moreover, cells incubated without Holo-TF and deferoxamine mesylate retained higher levels of intracellular anti-biotin IgG-647, suggesting that free transferrin inhibits re-entry of the secreted target into cells. In comparison, Fab-tri-GalNAc and tri-GalNAc biotin also induced the internalization of anti-biotin-647, but did not result in secretion into the media (Fig. 7.3A). I then elongated the incubation time with Fab-tri-GalNAc and tri-GalNAc-biotin to allowed for equal levels of anti-biotin IgG-647 internalization as observed with transferrin-biotin. Similar to what was observed before, only transferrin-biotin but not Fab-tri-GalNAc or tri-GalNAc-biotin could facilitate re-export of the protein from cells (Fig. 7.3B). These findings suggest that the transferrin-based degrader can act catalytically by cycling between intracellular and extracellular

environments. I also tried to detect the depletion of the target protein in the media, but as the amount internalized into the cells was minimal compared to the total protein presented in the media, no significant reduction was detected (Fig. 7.3C).

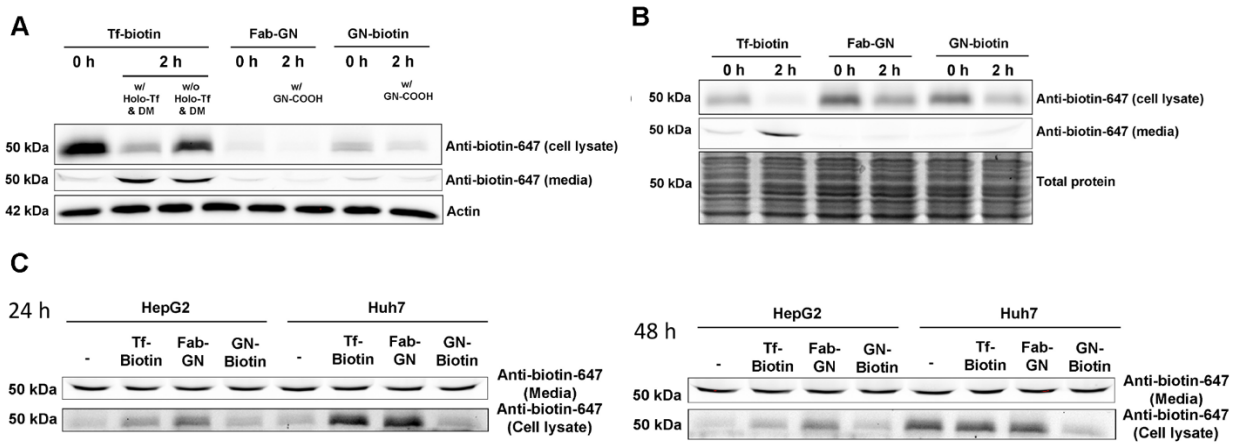

Figure 7.3. Recycling of transferrin-based degrader. A, B. Uptake and recycling of anti-biotin-647 mediated by transferrin-and tri-GalNAc-based degrader. **C, D.** Depletion of anti-biotin-647 in the media.

To directly study the recycling of the degrader, I generated fluorescently labeled transferrin-biotin conjugates by attaching NHS-biotin and NHS-594-BP to transferrin through NHS-lysine reactions. Different biotin labeling conditions were first tested. Transferrin was incubated with 3, 12, or 25 equiv. biotin-HNS on ice for 2 h, or 25 equiv. biotin-NHS on ice for 4 h or at room temperature (RT) for 1h. Uptake assays in MCF7 cells indicated that the condition of 25x biotin-NHS at RT for 1 hour resulted in the highest uptake efficiency (Fig. 7.4A). Next, I optimized the condition for NHS-594 labeling by testing four labeling conditions: 1. 20x BP-594-NHS, RT, 2 h; 20x biotin-NHS, RT, 2 h; 2: 20x BP-594-NHS, RT, 2 h; 20 x biotin-NHS, RT, 4 h; 3: 20x biotin-NHS, RT, 1 h; 20 x BP-594-NHS, RT, 2 h; 4: 20x biotin-NHS, RT, 1 h; 20 x BP-594-NHS, RT, 4

h. Cells treated with degraders generated from all four conditions demonstrated internalization. MALDI-MASS analysis showed that degraders were labeled with ~ 2 BP-594-NHS molecules across all methods. Methods 3 and 4 yielded higher numbers of biotin labeling compared to methods 1 and 2. Given that method 3 required less reaction time and effectively mediated anti-biotin-647 internalization, I selected this method to produce biotin- and BP-594-labeled degraders for subsequent studies (Fig. 7.4B).

I then conducted a transferrin-biotin recycling assay in MCF7 and HepG2 cells to monitor the recycling of transferrin-biotin-594. In addition to anti-biotin-647, I used NA-650 as an additional target protein. After the initial 2-hour uptake, both transferrin-biotin-594 and the target proteins (anti-biotin-647 or NA-650) accumulated in the cells. Following incubation in fresh media for an additional 2 hours, intracellular levels of both the degrader and the target proteins decreased significantly, while their levels in the media increased, indicating their release from the cells. These findings suggest that the degrader can facilitate the uptake of soluble proteins into cells and subsequently recycle them back into the media, demonstrating its catalytic capability (Fig. 7.4C).

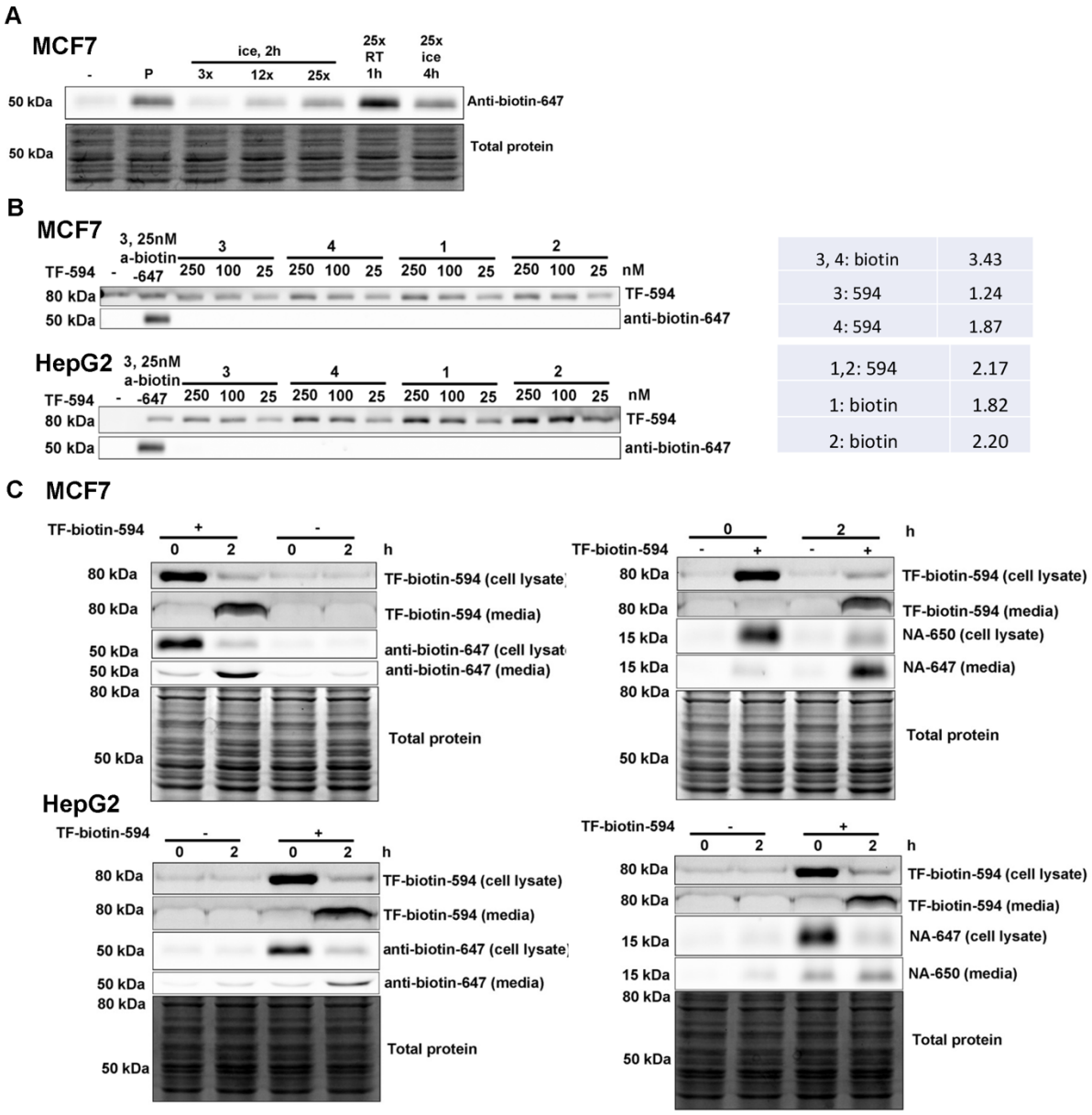

Figure 7.4. Direct detection of recycling of transferrin-based degrader. A. Optimization of biotin labeling. **B.** Uptake of transferrin-biotin-594 prepared via different conjugation conditions. **C.** Uptake and recycling of transferrin-biotin-647 and anti-biotin-647 or NA650 in MCF7 and HepG2 cells.

In addition to using transferrin-biotin conjugate as the degrader, fusion protein-based degraders can also be actively expressed in the cells and secreted into the media to

facilitate target protein uptake for degradation. To test this concept, I transfected Huh7 cells with plasmid encoding transferrin with the FLAG tag at either N or C terminus. The results showed that C-terminally tagged transferrin had a higher expression efficiency, with detectable levels of secreted transferrin-FLAG in the media (Fig. 7.5A). I then treated transfected cells with anti-flag-647 as the target protein 24 h post-transfection. I detected transferrin-flag in both the cells and media, suggesting that the degrader was successfully expressed and secreted by the cell. Additionally, anti-FLAG-647 was detected inside the cells, demonstrating that the secreted transferrin-FLAG could capture and internalize the soluble target protein (Fig. 7.5B). Collectively, these data support the feasibility of this platform for targeted protein degradation and the potential for developing catalytic lysosome targeting degraders.

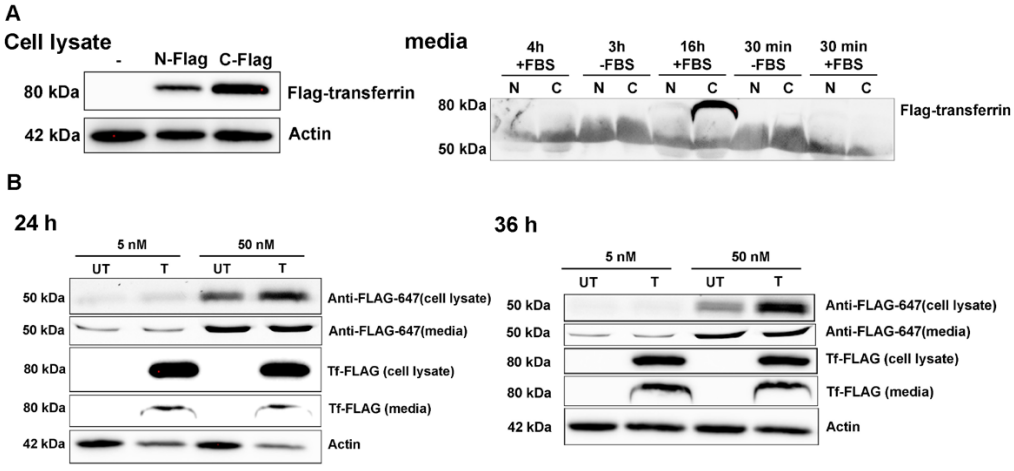

Figure 7.5. Uptake of target protein mediated by plasmid encoding transferrin degrader. A. Expression of transferrin-Flag in the cell and secretion to the media. **B.** Uptake of anti-Flag-647 mediated by expressed transferrin-flag.

In addition to the transferrin-based degrader, I explored the use of a TfR-binding peptide as a ligand for TfR to create peptide-antibody conjugates capable of mediating protein

degradation. Three TfR-binding peptides were selected from the literature: P9 (GHKAKGPRK), P7 (HAIYPRH), and P12 (THRPPMWSPVWP). To test whether the peptide-antibody conjugates could facilitate the uptake of soluble proteins, I generated the degraders by attaching each peptide to a goat anti-mouse IgG antibody. This was achieved through a two-step labeling process in which the antibody was first modified with a strained cyclic alkyne, followed by coupling with an azido-peptide via click chemistry. MCF7 cells were then treated with 50 nM anti-biotin-647 and 100, 50, or 25 nM of ab-TF-P7, ab-TF-P9, or ab-TF-P12 for 6 hours. In-gel fluorescence analysis demonstrated that all three degraders mediated target protein uptake into MCF7 cells in a dose-dependent manner, with ab-TF-P9 showing the highest uptake efficiency (Fig. 7.6A). I further developed degraders targeting EGFR, incorporating either PEG3 or PEG12 linkers between the peptide and the antibody Cetuximab. A549 and Huh7 cells treated with PEG3-linked degraders at 10 nM for 24 hours showed minimal EGFR degradation (Fig. 7.6B). In contrast, PEG12-linked degraders induced moderate EGFR degradation in HepG2, HeLa, and MCF7 cells under the same conditions (10 nM for 24 hours; Fig. 7.6C). These preliminary data suggest that degraders with a longer linker length, such as PEG12, enhance EGFR degradation efficiency.

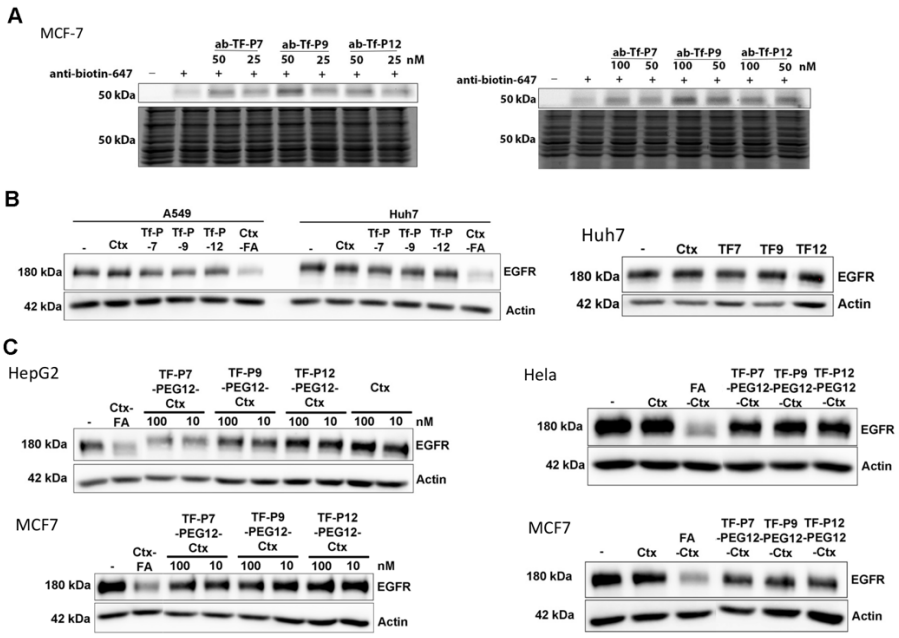

Figure 7.6. EGFR degradation and anti-biotin uptake mediated by TfR binding peptide-based degrader. A. Uptake of anti-biotin-647 mediated by peptide-based degraders. **Note:** This experiment was performed by Yuan Zhao. **B.** EGFR degradation mediated by degraders containing PEG3 linker. C. EGFR degradation mediated by degraders containing PEG12 linker.

7.3. Conclusion

In this study, we demonstrated that TfR1 could serve as a lysosomal targeting receptor (LTR) to enable efficient degradation of both soluble and membrane-bound protein targets. Degraders incorporating the natural TfR ligand, transferrin, can deliver soluble proteins to the lysosome for degradation via TfR1 binding. Importantly, they may also act catalytically by escaping lysosomal degradation, recycling back to the extracellular environment to engage additional target proteins. This catalytic potential of lysosomal-targeted degraders has not been previously reported. However, both the degrader and target protein can potentially be exported from the cell, which may reduce degradation efficiency. To improve selectivity, incorporating a pH-sensitive target binder could enable

target protein release in the early endosome, ensuring that only the target is directed to the lysosome while the degrader is recycled. Additionally, transferrin-based degraders can be produced through chemical conjugation or expressed and secreted by cells to reveal their functional activity. We further showed that TfR-binding peptides could serve as alternative TfR ligands for degrader development, with peptide-antibody conjugates utilizing extended linker lengths showing more effective protein degradation. Overall, we illustrate various degrader modalities that leverage TfR1 for lysosomal targeted protein degradation. This work advances the development of catalytic degraders and targeted degradation of cancer-related proteins in malignant cells, offering a foundation for next-generation degraders with enhanced degradation efficiency and reduced toxicity.

7.4. Experimental Procedures

7.4.1. Cell culture

HepG2 and Huh7 cells were cultured in low-glucose DMEM supplemented with 10% fetal bovine serum, 1% non-essential amino acids, 1% sodium pyruvate, 1% L-glutamine and 1% penicillin/streptomycin under 5 % CO_2 at 37 °C. MCF7, Hela, and 293T cells were maintained in high-glucose DMEM supplemented with 10% fetal bovine serum, and 1% penicillin/streptomycin under 5 % CO_2 at 37 °C. A549 and Lncap cells were cultured in RPMI supplemented with 10% fetal bovine serum, 1% sodium pyruvate, 1% HEPES and 1% penicillin/streptomycin under 5 % CO_2 at 37 °C.

7.4.2. Mouse IgG uptake with Tf-biotin

Cells were plated at 70% confluence in a 24-well plate. Media with or without serum supplemented with 50 nM of mouse anti-biotin-IgG-647 and 25 nM of biotin-labelled

transferrin was sequentially added. The cells were incubated at 37 °C for indicated time points and then lysed for in gel fluorescence analysis.

7.4.3. Transferrin-biotin recycling assay

Cells were plated at 70% confluence in a 12-well plate. Cells were starved by replacing complete growth media with the media without serum 1 h before treatment. Then cells were incubated with 50 nM of mouse anti-biotin-IgG-647 and 25 nM of biotin-labelled transferrin for 30 min, followed by 5-time washes with cold PBS. Cells were incubated with 2.5 μM Holo-TF and 100 μM deferoxamine mesylate for 30 or 90 min to prevent the re-entering of the Tf-biotin/target protein complex into the cells. Cell lysate and media were collected for in gel fluorescence analysis.

7.4.5. Comparison of the recycling of Tf-biotin, Fab-GN, and GN-biotin

Huh7 cells were seeded at 70% confluence in a 12-well plate. Cells were starved by replacing complete growth media with the media without serum 1 h before treatment. Then cells were incubated with 50 nM of mouse anti-biotin-IgG-647 and 25 nM of biotin-labelled transferrin or 25 nM Fab-GN or 200 nM GN-biotin for 2 h, followed by 5-time washes with cold PBS. Cells were incubated with 2.5 μM Holo-TF and 100 μM deferoxamine mesylate or 2 μM GN-COOH for 2 h to prevent the re-entering of the Tf-biotin/target protein complex into the cells. Cell lysate and media were collected for in gel fluorescence analysis.

7.4.6. Confocal microscopy

MCF7 cells were seeded onto 8-well chamber slides at the density of 20,000 cells/well in 200 µL of complete culture medium. After adhesion, cells were treated with 50 nM

anti-biotin-647 and 25 nM transferrin-biotin for 24 h at 37 °C, followed by the 30-min incubation with LysoTracker Green DND26 (100 nM) at 37 °C. Hoechst 33342 (5 ug/ml) was added 10 min before the end of incubation. After three washes with PBS, the live cells were imaged using FluoView confocal microscope at 20x magnification with a 10x eyepiece. All images were acquired by FV10-ASW and analyzed by ImageJ.

7.4.7. TfR1 knockdown

MCF7 cells were seeded at 200,000 cells per well in a 6-well plate one day before transfection. Cells were transfected with 60 pmol of scramble or TfR1 siRNA and 7.5 µL RNAiMAX for 24 h and then re-seeded in a 48-well plate at a density of 70,000 cells per well. Cells were then incubated with 25 nM transferrin-biotin and 50 nM anti-biotin-647 for another 6 h before harvested to analyze TfR1 levels by western blot and the uptake of anti-biotin-647 by in-gel fluorescence.

7.4.8. Mouse IgG uptake with Tf-Flag

293 cells were transfected with plasmid expressing transferrin-Flag for 24 h. After washing and replacing with the media containing no serum, cells were treated with 25 nM anti-flag-647 for 24 or 36 h to allow the uptake of anti-flag-647. Cell lysates and media were collected for in gel fluorescence and western blot analysis.

7.4.9. Western blotting

Cells were lysed in 1X RIPA lysis buffer containing 25 mM Tris, pH 7−8, 150 mM NaCl, 0.1% (w/ v) sodium dodecyl sulfate (SDS), 0.5% sodium deoxycholate, 1% (v/ v) Triton X-100, protease inhibitor cocktail (Roche, one tablet per 10 mL) and 1 mM phenylmethylsulfonyl fluoride on ice for 10 min. The lysates were then centrifuged at 16

000g at 4 °C for 15 min and the supernatant was collected followed by measuring the protein concentration using BCA assay. Lysates were adjusted to the equal amount before mixed with the 4x Laemmli Loading Dye and heated at 99 °C for 5 min. After cooling down, samples were loaded onto 7.5% SDS−polyacrylamide gel electrophoresis and transferred to PVDF membrane. The membrane was first blocked in 5% (w/v) nonfat milk in the TBS-T washing buffer (137 mM NaCl, 20 mM Tris, 0.1% (v/v) Tween) and then incubated with primary antibodies at 4 °C overnight. After 3 washes with TBST, the membrane was incubated with secondary HRP-linked antibodies for 1 h, and then washed 3 times with TBST. Then the membrane was incubated in the Clarity ECL substrate for 3- 5 min before acquiring the immunoblot by ChemiDoc MP Imaging Systems.

7.5. References

1 Schapira, M., Calabrese, M. F., Bullock, A. N. & Crews, C. M. Targeted protein degradation: expanding the toolbox. *Nat Rev Drug Discov* **18**, 949-963 (2019). https://doi.org/10.1038/s41573-019-0047-y

2 Sakamoto, K. M. *et al.* Protacs: chimeric molecules that target proteins to the Skp1-Cullin-F box complex for ubiquitination and degradation. *Proc Natl Acad Sci U S A* **98**, 8554-8559 (2001). https://doi.org/10.1073/pnas.141230798

3 Takahashi, D. *et al.* AUTACs: Cargo-Specific Degraders Using Selective Autophagy. *Mol Cell* **76**, 797-810.e710 (2019). https://doi.org/10.1016/j.molcel.2019.09.009

4 Banik, S. M. *et al.* Lysosome-targeting chimaeras for degradation of extracellular proteins. *Nature* **584**, 291-297 (2020). https://doi.org/10.1038/s41586-020-2545-9

5 Caianiello, D. F. *et al.* Bifunctional small molecules that mediate the degradation of extracellular proteins. *Nat Chem Biol* **17**, 947-953 (2021). https://doi.org/10.1038/s41589-021-00851-1

6 Zhou, Y., Teng, P., Montgomery, N. T., Li, X. & Tang, W. Development of Triantennary N-Acetylgalactosamine Conjugates as Degraders for Extracellular Proteins. *ACS Cent Sci* **7**, 499-506 (2021). https://doi.org/10.1021/acscentsci.1c00146

7 Green, A. *et al.* Lysosome Targeting Chimeras (LYTACs) That Engage a Liver-Specific Asialoglycoprotein Receptor for Targeted Protein Degradation. *ChemRxiv* (2020). https://doi.org/10.26434/chemrxiv.12736778.v1

8 Zheng, J. *et al.* Bifunctional Compounds as Molecular Degraders for Integrin-Facilitated Targeted Protein Degradation. *J Am Chem Soc* **144**, 21831-21836 (2022). https://doi.org/10.1021/jacs.2c08367

9 Zhou, Y., Liao, Y., Zhao, Y. & Tang, W. Development of Integrin Targeting Chimeras (ITACs) for the Lysosomal Degradation of Extracellular Proteins. *ChemMedChem*, e202300643 (2024). https://doi.org/10.1002/cmdc.202300643

10 Zhou, Y. *et al.* Development of folate receptor targeting chimeras for cancer selective degradation of extracellular proteins. *Nat Commun* **15**, 8695 (2024). https://doi.org/10.1038/s41467-024-52685-9

11 Zhang, D. *et al.* Transferrin receptor targeting chimeras for membrane protein degradation. *Nature* (2024). https://doi.org/10.1038/s41586-024-07947-3

12 Kleven, M. D., Jue, S. & Enns, C. A. Transferrin Receptors TfR1 and TfR2 Bind Transferrin through Differing Mechanisms. *Biochemistry* **57**, 1552-1559 (2018). https://doi.org/10.1021/acs.biochem.8b00006

13 Candelaria, P. V., Leoh, L. S., Penichet, M. L. & Daniels-Wells, T. R. Antibodies Targeting the Transferrin Receptor 1 (TfR1) as Direct Anti-cancer Agents. *Front Immunol* **12**, 607692 (2021). https://doi.org/10.3389/fimmu.2021.607692

14 Kawabata, H. Transferrin and transferrin receptors update. *Free Radic Biol Med* **133**, 46-54 (2019). https://doi.org/10.1016/j.freeradbiomed.2018.06.037

15 Daniels, T. R. *et al.* The transferrin receptor and the targeted delivery of therapeutic agents against cancer. *Biochim Biophys Acta* **1820**, 291-317 (2012). https://doi.org/10.1016/j.bbagen.2011.07.016

16 Daniels, T. R., Delgado, T., Helguera, G. & Penichet, M. L. The transferrin receptor part II: targeted delivery of therapeutic agents into cancer cells. *Clin Immunol* **121**, 159-176 (2006). https://doi.org/10.1016/j.clim.2006.06.006

Chapter 8

Summary and Discussion

8.1. Summary of the thesis

Targeted protein degradation (TPD) represents a promising therapeutic strategy that harnesses the cell's own degradation machinery to eliminate pathogenic proteins. Among TPD approaches, Proteolysis Targeting Chimeras (PROTACs) are the most advanced. However, their traditional synthesis involves lengthy, sequential steps[1]. In Chapter 2, we present a novel, rapid synthesis platform for PROTACs, designed under miniaturized conditions and employing the highly efficient OPA-amine coupling reaction, which yields water as the sole byproduct. We demonstrated that this platform enabled the expedited synthesis of bioactive PROTACs targeting androgen receptor (AR) and bromodomain-containing protein 4 (BRD4). This platform holds the potential to extend to additional targets, facilitating structure-activity relationship (SAR) studies across diverse protein targets[2].

The development of Lysosome Targeting Chimeras (LYTACs) expanded TPD to include extracellular secreted proteins and membrane proteins lacking cytosolic binding domains. The first reported LYTACs recruited the cation-independent mannose-6-phosphate receptor (CI-M6PR) using polymeric glycopeptides with high mannose-6-phosphate (M6Pn) multivalency. However, the complex synthesis of large M6Pn-based ligands poses challenges in quality control for drug development. In Chapter 3, we address these limitations by simplifying the synthesis of M6PR ligands, producing structurally well-defined ligands based on a short peptide backbone decorated with several M6Pn units. We demonstrate that these M6Pn-peptide conjugates can effectively mediate the internalization of soluble proteins and degradation of membrane proteins, with tetrameric M6Pn-conjugates showing the

optimal balance of synthetic simplicity and uptake efficiency. Notably, uptake efficiency is primarily influenced by the M6Pn composition rather than linker length. This novel ligand platform has the potential to advance the application of M6PR-based LYTACs in targeted degradation therapies[3].

The initial LYTACs leveraged the CI-M6PR, a ubiquitously expressed lysosomal targeting receptor (LTR), which can potentially lead to unintended toxicity across multiple tissues. In Chapter 4, we introduce the asialoglycoprotein receptor (ASGPR) as an alternative LTR and utilize triantennary GalNAc conjugates to selectively induce lysosomal degradation of soluble and membrane proteins within liver cells. Our findings suggest that the size of the degrader/receptor/target protein complex may serve as a critical parameter for optimizing tri-GalNAc-mediated lysosomal degradation of extracellular proteins. This ASGPR-driven approach provides tissue selectivity, offering a novel strategy to minimize off-target toxicity in lysosomal targeted protein degradation[4].

While liver-targeting degraders restrict membrane protein degradation to liver cells, limiting their applications to cancer-associated targets in other tissues, Chapter 5 addresses this limitation by introducing cyclic RGD (cRGD) peptide-antibody conjugates as a new class of integrin-targeting chimeras (ITACs). These ITACs selectively target and degrade proteins in cancer cells by recruiting integrins, which are overexpressed on cancer cells. Our results demonstrate that ITACs can effectively mediate the lysosomal degradation of both soluble and membrane-bound proteins. Importantly, membrane protein degradation—unlike soluble protein internalization—requires a longer linker within the degrader. Additionally, ITACs demonstrated higher

efficiency in degrading membrane proteins in cancer cells compared to normal cells, establishing this approach as a promising platform for cancer-selective TPD strategies[5].

In Chapter 6, we leveraged another cancer-overexpressing LTR, folate receptor (FR), to develop Folate Receptor Targeting Chimeras (FRTACs) for selective protein degradation in cancer cells. Our studies show that FRTACs can effectively deplete multiple therapeutic targets without disrupting FR recycling. Soluble protein internalization mediated by FRTACs depends on FR expression levels, while membrane protein degradation is influenced by the FR-to-target expression ratio. Notably, FRTACs targeting PD-L1 demonstrated anti-tumor efficacy superior to therapeutic antibodies in three syngeneic mouse models, driven by PD-L1 reduction and enhanced cytotoxic T-cell infiltration. FRTACs also exhibited cancer selectivity, degrading targets like EGFR and PD-L1 more effectively in cancer cells than in normal tissues. This establishes FRTACs as a promising cancer-selective TPD platform with minimal off-target effects[6].

Unlike PROTACs, which function catalytically, most reported lysosomal targeting degraders are co-transported with the target protein into the lysosome, which may limit their degradation efficiency. In Chapter 7, we introduce a novel approach to impact catalytic properties to lysosomal degraders by harnessing the recycling capabilities of transferrin and transferrin receptor 1 (TfR1). Our work demonstrates that transferrin conjugates can deliver soluble targets to the lysosome for degradation and subsequently recycle between the intracellular and extracellular environments. Additionally, transferrin-based degraders can be expressed and secreted by cells,

presenting potential applications in gene and cell therapy. Furthermore, we show that TfR-binding peptides can serve as alternative ligands to induce protein degradation when conjugated to target binders. This innovative system paves the way for developing catalytic lysosomal targeting degraders, expanding the scope and efficiency of targeted protein degradation strategies.

8.2. Future directions

Following the report of the first LYTAC, new platforms have emerged, leveraging diverse lysosomal targeting receptors (LTRs) for selective protein degradation. Some of these LTRs, such as ASGPR, integrin, FR, exhibit tissue-specific or cancer-associated expression, enabling selective degradation with reduced on-target/off-tissue toxicity. Other recycling receptors with exclusive tissue expression pattern, such as the follicle-stimulating hormone receptor (FSHR) for testis or ovary targeting[7] and dendritic cell-specific intercellular adhesion molecule-3-grabbing non-integrin (DC-SIGN) for dendritic cells and macrophages targeting[8], may broaden the scope of tissue-specific degraders. For example, degraders leveraging the prostate-specific membrane antigen (PSMA) could selectively eliminate targets expressed exclusively in prostate cancer cells[9].

Future developments in lysosomal degraders include discovering of novel binding ligands, simplifying ligand synthesis, improving binding affinity, and exploring alternative site-specific conjugation strategies to enhance degrader homogeneity and scalability. Advances in genetic engineering now allow for the development of recombinant degraders with optimized binding epitopes and configurations, further expanding design possibilities[10-12].

Recent mechanistic studies have begun to identify cellular determinants influencing the activity of M6PR-recruiting degraders. Findings indicate that endogenous M6P levels and the recycling of LYTAC-M6PR complexes can reduce degrader efficiency. Additionally, genes involved in the neddylation of cullin 3 (CUL3) play a role in directing LYTAC-M6PR complexes to the lysosome[13]. Detailed mechanistic studies on other types of degraders could similarly uncover factors affecting their activity, paving the way for strategies to enhance degrader efficacy.

Currently, most platforms have been validated primarily on model targets like epidermal growth factor receptor (EGFR) or Programmed death-ligand 1 (PD-L1). Other targets, including CD20, CD47, and proprotein convertase subtilisin/kexin type 9 (PCSK9), have also been successfully depleted using various types of degraders. Additional promising targets include proteins with multiple functional domains that cannot be effectively inhibited by small molecules or blocking antibodies, such as G-protein-coupled receptors (GPCRs). Another key opportunity lies in therapeutic targets that develop treatment-induced mutations, such as receptor tyrosine kinases (RTKs). These mutations often confer resistance to conventional inhibitors, leading to reduced efficacy over time. Furthermore, protein targets with high tissue or cancer-specific abundance, such as human epidermal growth factor receptor 2 (HER2) and vascular endothelial growth factor (VEGF), hold significant therapeutic potential. Selective degraders offer the advantage of minimizing on-target, off-tissue or off-cancer toxicity commonly associated with conventional therapeutic inhibitors. Expanding the range of targets to include more disease-relevant proteins will be crucial for unlocking the full therapeutic potential of TPD.

8.3. References

1 Wang, X. *et al.* Annual review of PROTAC degraders as anticancer agents in 2022. *Eur J Med Chem* **267**, 116166 (2024). https://doi.org/10.1016/j.ejmech.2024.116166

2 Guo, L. *et al.* A platform for the rapid synthesis of proteolysis targeting chimeras (Rapid-TAC) under miniaturized conditions. *Eur J Med Chem* **236**, 114317 (2022). https://doi.org/10.1016/j.ejmech.2022.114317

3 Stevens, C. M. *et al.* Development of Oligomeric Mannose-6-phosphonate Conjugates for Targeted Protein Degradation. *ACS Med Chem Lett* **14**, 719-726 (2023). https://doi.org/10.1021/acsmedchemlett.2c00479

4 Zhou, Y., Teng, P., Montgomery, N. T., Li, X. & Tang, W. Development of Triantennary N-Acetylgalactosamine Conjugates as Degraders for Extracellular Proteins. *ACS Cent Sci* **7**, 499-506 (2021). https://doi.org/10.1021/acscentsci.1c00146

5 Zhou, Y., Liao, Y., Zhao, Y. & Tang, W. Development of Integrin Targeting Chimeras (ITACs) for the Lysosomal Degradation of Extracellular Proteins. *ChemMedChem*, e202300643 (2024). https://doi.org/10.1002/cmdc.202300643

6 Zhou, Y. *et al.* Development of folate receptor targeting chimeras for cancer selective degradation of extracellular proteins. *Nat Commun* **15**, 8695 (2024). https://doi.org/10.1038/s41467-024-52685-9

7 Banerjee, A. A., Joseph, S. & Mahale, S. D. From cell surface to signalling and back: the life of the mammalian FSH receptor. *FEBS J* **288**, 2673-2696 (2021). https://doi.org/10.1111/febs.15649

8 Liu, P. *et al.* Beyond attachment: Roles of DC-SIGN in dengue virus infection. *Traffic* **18**, 218-231 (2017). https://doi.org/10.1111/tra.12469

9 Zhang, J. *et al.* A prostate-specific membrane antigen activated molecular rotor for real-time fluorescence imaging. *Nat Commun* **12**, 5460 (2021). https://doi.org/10.1038/s41467-021-25746-6

10 Cotton, A. D., Nguyen, D. P., Gramespacher, J. A., Seiple, I. B. & Wells, J. A. Development of Antibody-Based PROTACs for the Degradation of the Cell-Surface Immune Checkpoint Protein PD-L1. *J Am Chem Soc* **143**, 593-598 (2021). https://doi.org/10.1021/jacs.0c10008

11 Yang, J. L. *et al.* Directed evolution of genetically encoded LYTACs for cell-mediated delivery. *Proc Natl Acad Sci U S A* **121**, e2320053121 (2024). https://doi.org/10.1073/pnas.2320053121

12 Zhang, D. *et al.* Transferrin receptor targeting chimeras for membrane protein degradation. *Nature* (2024). https://doi.org/10.1038/s41586-024-07947-3

13 Ahn, G. *et al.* Elucidating the cellular determinants of targeted membrane protein degradation by lysosome-targeting chimeras. *Science* **382**, eadf6249 (2023). https://doi.org/10.1126/science.adf6249

Appendix

Appendix 1: Development of glycopeptide ligands for carbohydrate-binding proteins by phage display

1. Introduction

Proteins that can bind to carbohydrate are referred to as carbohydrate-binding proteins (CBPs). Carbohydrate-protein interactions play critical roles in normal cellular processes and are also implicated in many pathological events. Disrupting these interactions using the carbohydrate ligands of CBPs is considered a potential therapeutic strategy. However, the weak affinity between the carbohydrate ligand and CBPs, typically in the millimolar to micromolar range, poses a significant challenge to this application. Incorporating a synergistic motif, such as a peptide, to occupy the position adjacent to the carbohydrate binding site can effectively enhances the affinity of the resulting glycopeptide ligand to the CBPs, improving the therapeutic potential of CBP ligands.

Phage display is a powerful selection technique, which was first introduced by George P. Smith in 1985[1]. By inserting DNA fragments into the filamentous phage genome, fusion coat proteins are expressed, allowing exogenous peptides to be displayed on the surface of the phage. A phage library is composed of millions of genetically modified phages, where the desired peptides can be selected out using a process known as biopanning. In biopanning, the phage library is first incubated with the immobilized target protein. Unbounded phages are washed away, while bounded phages, which contain the specific binders, are eluted out and amplified for the next round of panning.

Usually, the specific binders with high affinity can be enriched within three to five rounds, and the sequences of the peptides can be determined by DNA sequencing.

The M13 phage is one of the most widely used systems for phage display. It consists of a single-strand DNA (6407bp) encapsulated by five types of coat proteins (pVIII, pIII, pVI, pVII, and pIX). M13 phage replicates in *Escherichia coli* (*E. coli*) via chronic infection, during which the virions are continuously released without lysing the host cells. Among the coat proteins, the major coat protein pVIII and the minor coat protein pIII are commonly used as the vectors for displaying foreign peptides. The low copy number of pIII protein (5 copies) enables the discovery of binders with high affinity compared to pVIII protein (~2700 copies)[2,3]. The displayed peptides can be either linear or cyclized to form a constrained loop. The cyclization enhances the selectivity and binding affinity of the peptides, and also makes the peptides more resistant to the proteases, improving their stability and therapeutic potential[4].

Genetic modification of phage genome allows the formation of the large phage library with random peptides for binder selection. Posttranslational chemical modification on the displayed peptides expands the diversity of library by conferring the unnatural properties to the peptides. The peptides modified with carbohydrate, named glycopeptide, bias the phage library toward the carbohydrate-binding pocket, diminishing the non-specific binding of peptides to other sites on the protein. Moreover, the peptides also serve as a synergistic motif, boosting the binding affinity of the carbohydrate to the protein. Concanavalin a (Con A), the model lectin, has been used for demonstrating the successful finding of linear synergistic motif that enhanced the affinity of monosaccharide by panning with mannose-modified phage library[5,6]. In this

study, I constructed a phage library displaying linear or cyclic glycopeptide and performed the panning against two well-studied model proteins, streptavidin and Con A, to verify the feasibility of the phage display protocol for both non-modified and modified phage library.

2. Results and conclusion

2.2. Verification of protocol by panning against streptavidin

Streptavidin has a high affinity with its ligand biotin, with a dissociation constant (K_d) around 10^{-15} mol/L[7]. The peptide binding to streptavidin contains a His-Pro-Gln (HPQ) sequence, which shares the same binding pocket as biotin[8]. It has been reported that the linear peptide that has HPQ sequence binds to streptavidin in a micromolar range while the cyclic peptide showed the binding affinity in a nanomolar range[9]. To validate the feasibility of our protocol, the well-studied streptavidin was first chosen as our target protein. I used an M13 phage library Ph.D-C7C, which has a cyclic heptapeptide fused to the N-terminus of the pIII protein, to incubate with streptavidin. Upon elution with biotin, the peptide containing HPQ sequence was expected to be selected and enriched after three rounds of panning.

Several attempts were made, but no desired results were achieved due to incorrect LB media components (low sodium chloride concentration), improper coating material (petri dish instead of a high binding plate), and a contaminated phage library (T4 phage contamination, leading to lysis of E.coli during amplification). After addressing these issues, the panning was repeated in a 96-well high binding plate. The results showed that the recovered phage number was dramatically increased after each round of panning, indicating the successful enrichment of specific binder (Fig. 1A). Sequencing

the DNA of 8 randomly picked clones revealed that 6 out of them had HPQ sequence, suggesting the success of panning process (Table 1). One clone containing HPQ sequence was used for Phage Elisa. The results showed that the absorbance increased with the increase of phage concentration, further verifying the binding of the selected phage to the streptavidin (Fig. 1B). Our results suggested that the protocol developed was able to successfully select the specific binder of the target protein from the library.

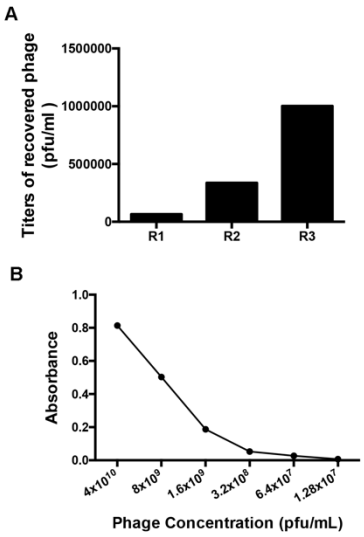

Table 1. Sequences of peptide hits for streptavidin binding

Hit #	Peptide Sequence
1	GTWNHPQ
2	GTWNHPQ
3	GTWNHPQ
4	GTWNHPQ
5	Empty
6	GSWQHPQ
7	GSWQHPQ
8	DGRPDRA

Peptide Sequence	Frequency
GTWNHPQ	4
GSWQHPQ	2

Figure 1. Panning against streptavidin. A. Recovered phage titer after each round of panning. **B.** Binding of HPQ phage to streptavidin. Data shown as binding of HPQ phage to streptavidin substrates the binding of same phage to blank plate.

2.3. Modification of the phage library with mannose

Next I applied the protocol to a model lectin Con A for the proof-of-concept experiment of panning with modified phage library. The heptapeptide displayed on the Ph.D-C7C phage library is flanked by a pair of cysteine residues that are oxidized to form a disulfide bond during phage amplification. Dr. Peng Teng and undergraduate student Mr. Taobo Wang synthesized three biselectrophiles (Fig. 2A) with different linker lengths as

well as two monoelectrophiles (Fig. 2B, C) to attach the mannose to the phage library based on a published protocol[10]. The disulfide bond in the peptide was selectively reduced using immobilized TCEP to prevent reduction within the phage, which could result in phage inactivation. The reduced thiols were then alkylated with either biselectrophile to reform a cyclic peptide or monoelectrophile to become linear peptides with two units of mannose.

The reduction of phage was determined by the pulse-chase assay as described before[11]. The reduced phage was labeled with BIA and captured by the streptavidin beads. Comparing the titer before and after capturing allowed us to quantify the percentage of reduced phage. The alkylation was monitored in a similar way by labeling the reduced but unreacted phage with BIA. The dilution of the modified library before incubating with streptavidin is critical due to the blockage of the binding site on the streptavidin by the excess BIA. The results demonstrated that around 85 % of the phage library was reduced and alkylation with biselectrophile further yielded 50-60 % phages modified with mannose. Empty phage lacking the expression of exogenous heptapeptide was included as negative control and no reduction and alkylation occurred on the empty phage compared to the phage library. In addition, no labeling on the phage library was found in the absence of iTCEP or BIA (Fig. 2D, E). Unlike biselectrophile, I observed significant lower modification rate when adding the same amount of monoelectrophile, especially for TP154 (2.4 %). Raising the amount of mannose to 2 mM rescued the percentage of alkylation by TP163 to a level (42.6 %) that is slightly lower than that of biselectrophile, while the yield of TP154 label-phage still maintained at a relatively low level (7.9 %) (Fig. 2F).

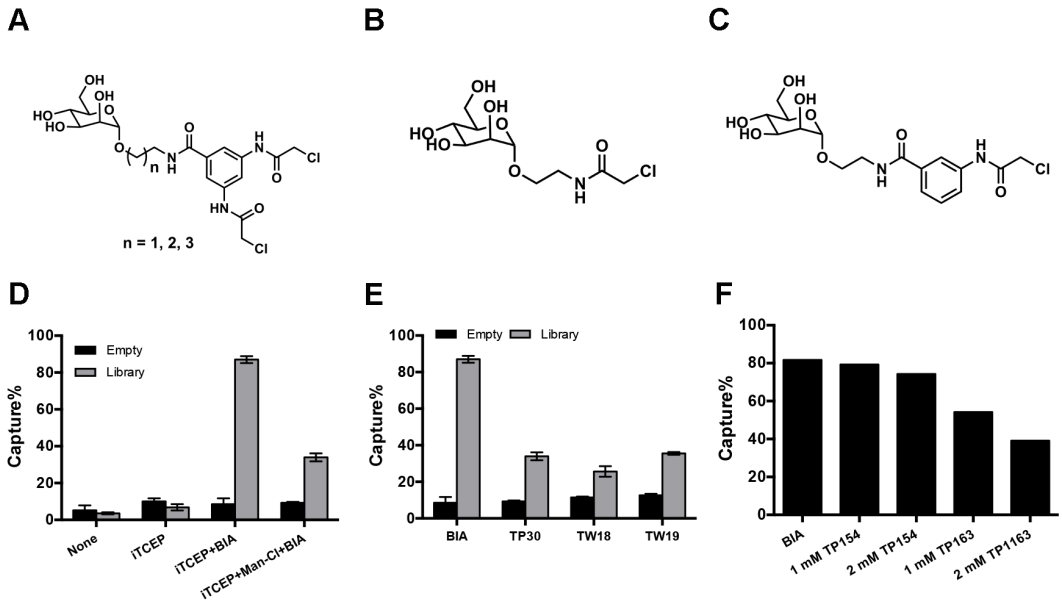

Figure 2. Modification of phage library. A. Structure of biselectrophile. TP30: n=1; TW18: n=2; TW19: n=3. **B.** Structure of monoelectrophile TP154. **C.** Structure of monoelectrophile TP163. **D.** Pulse-chase confirmation of Man-Cl labeling on phage library. **E.** Quantification of modification with biselectrophiles. **F.** Quantification of modification with monoelectrophiles. **Note:** TP30, TW18 and TW19 were synthesized by Dr. Peng Teng and Taobo Wang.

Since the reduction by the immobilized TCEP required a long reaction time, I tried to reduce the phage within 30 min using soluble TCEP to make the reaction more effective. Unexpectedly, the reaction involving soluble TCEP produced less modified phage compared to the yield obtained using iTCEP (Fig. 3A). Further study revealed that soluble TCEP competed with the reduced phage to react with the electrophile, resulting in the decreased yield for the modification of the phage library. Increasing the proportion of electrophile in the reaction enhanced the modification rate (Fig. 3B). Immobilized TCEP reacted much slower with the electrophile compared to the soluble TCEP, which had no obvious effects on the alkylation.

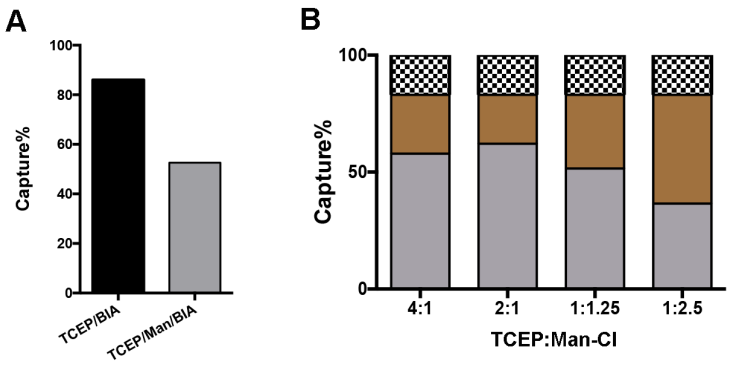

Figure 3. Modification with soluble TCEP. A. Quantification of the modification by soluble TCEP. **B.** Quantification of the modification using different ratio of TCEP:Man-Cl.

2.4. Optimization of the protocol for panning with modified library

To demonstrate the feasibility of the protocol for the modified library, I conducted panning against the model CPB, Con A, following the same procedure, except that a general elute buffer (glycine) was used instead of biotin. The non-modified library was also panned as a background control. However, in the first several attempts for both modified and non-modified library, the output population ranged from 10^4-10^5 pfu/ml with a slight increase for the second round but a drop after the third round, indicating no enrichment of specific binders occurred, which was verified later by sequencing and Elisa (Fig. 4, Table 2).

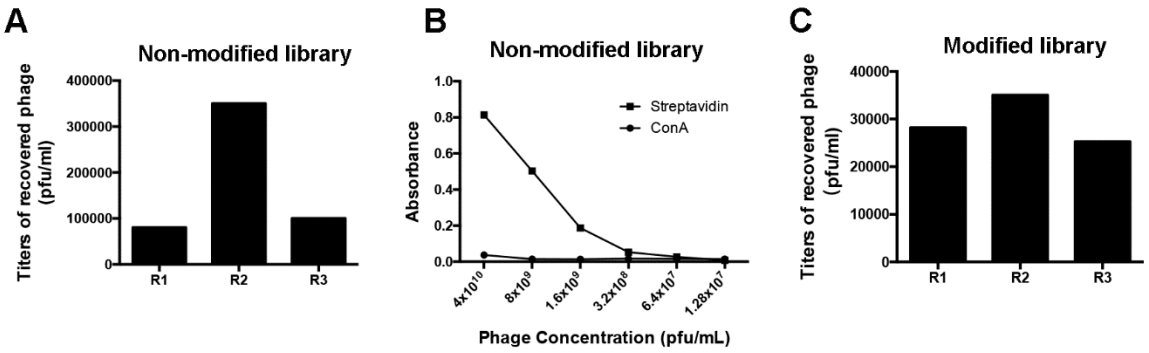

Figure 4. Representative data of attempts on panning against Con A with non-modified and modified library. A. Recovered phage titer after each round of panning with non-modified library. **B.** Binding of selected phage to Con A. Streptavidin-HPQ phage was used as the positive control. Data shown as binding of phage to target proteins substrates the binding of same phage to blank plate. **C.** Recovered phage titer after each round of panning with modified library.

Table 2. Sequences of the peptide hits for Con A from non-modified (A) and modified (B) library.

A

Hit #.	Sequence	Hit #.	Sequence
1	empty	11	empty
2	empty	12	empty
3	DGRPDRA	13	TPRSANY
4	empty	14	empty
5	DGRPDRA	15	empty
6	empty	16	TDKASSS
7	DGRPDRA	17	empty
8	empty	18	NVAAGAL
9	empty	19	empty
10	DGRPDRA	20	empty

B

Hit #	Sequence
1	DGRPDRA
2	Empty
3	SSNTVPA
4	WPPSSQW
5	DGRPDRA
6	DGRPDRA
7	Empty
8	GTNPIKK
9	SSNTVPA
10	DGRPDRA

To troubleshoot, additional information about Con A was researched. Con A has the affinity to mannose in the presence of Ca^{2+} and Mn^{2+}, with the K_d in the micromolar range. The conformation of Con A depends on the pH, in which the low pH renders the dissociation of Con A into a dimer, while the Con A remains as a tetramer at the neutral pH and further aggregates when the pH above 7.0. Considering that ions and pH may affect the activity of Con A, I changed the buffer for panning to the CA buffer which contained required ions with a neutral pH, which has been reported by other groups. Meanwhile, a positive control Man-WYD, which was identified by Derda ’s group, was included in the experiment for the optimization of our protocol.

Man-wyd was first mixed with the library at 1:100 ratio as the input. The proportion of Man-wyd in the output was expected to increase after panning to indicate a successful

enrichment using our protocol. However, no significant changes in the ratio were observed after panning, suggesting the protocol needed to be further optimized. To simplify the experiment, I mixed Man-wyd with WT phage at a 1:1 ratio as the input for panning, testing different types of Con A and varying BSA concentrations in the blocking buffer. However, the man-wyd was still not enriched after panning. To clarify, the recovery rate, defined as the ratio of output/input, was determined separately for Man-wyd and WT phage in wells with and without Con A coating. The results showed that the recovery rates for both Man-wyd and WT phage from the coated wells were significantly higher than the non-coated wells. However, no difference between the two groups in the coated wells was found (Fig. 5A). I verified the method of testing the recovery rate using the pair of streptavidin-HPQ phage, which showed significant higher recovery rate (2 %) than the WT phage. Adjusting other parameters, such as the composition, combinations and the pH of buffer, were not able to enrich the Man-wyd either.

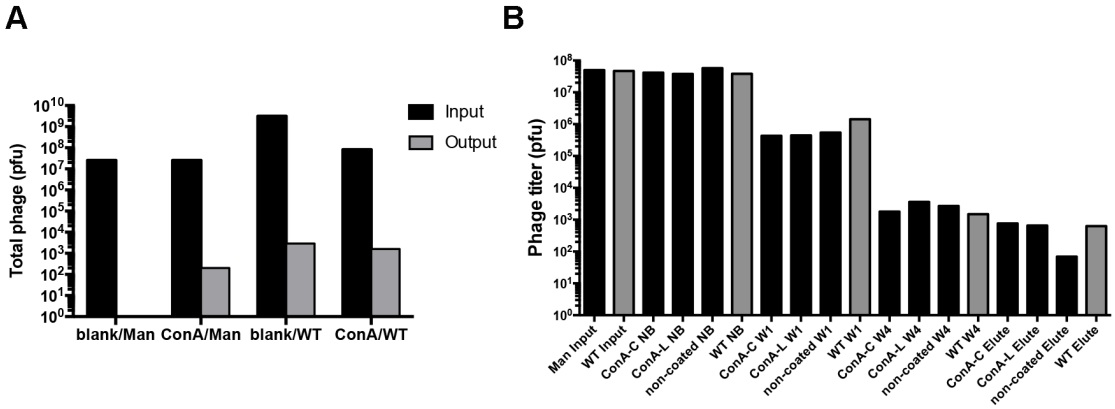

Figure 5. Validation of the protocol with positive control Man-wyd phage. A. Total phage number of the input and output of Man-wyd phage for the one round selection against Con A. The recovery rates were Con A/Man: 0.0007%, blank/WT: 0.00009%, Con A/WT: 0.002% respectively. **B.** Phage number after each step. The recovery rates were: Con A-C Elute: 0.00152%, Con A-L Elute: 0.00131%, non-coated Elute: 0.00014%, WT Elute: 0.00134%. NB: non-binding.

Next, I examined the protocol step by step by monitoring the phage titer after each step. Samples were collected after phage-protein interaction, the first and fourth washes, as well as from the input and eluted phages during panning against two types of Con A, type IV and VI. WT phage was included as negative control. The results for both Man-wyd and WT phage showed that the majority of phage population was lost after incubating with Con A, but not during the washing steps. This suggested that Man-wyd phage, like WT phage, was not able to bind to the protein during the incubation (Fig. 5B).

The results also raised another possibility that the Con A was not coated well on the plate. To test this hypothesis, the biotinylated Con A was coated in PBS or CA buffer with pH at 6.8 or 7.4, and the coating was detected by interacting with streptavidin-HRP. The results showed that the Con A was well coated on the plate and the signal was increased in a dose-dependent manner, which ruled out the possibility of improper coating of Con A (Fig. 6A). Next, I tested the interaction between the Man-wyd and Con A by Elisa. Surprisingly, no binding was detected for both types of Con A in different buffers, PBS and CA buffer, used for the incubation, suggesting Man-wyd I have may not be the real binder for the Con A protein (Fig. 6B, C, D). This was confirmed when another positive control Man3, which was modified on pVIII protein, was tested for its binding to Con A. Elisa revealed that Man3 bound to the Con A in a dose-dependent manner, with significantly higher binding than the WT phage control and the non-coated well (Fig. 6E, F). I further determined the recovery rate for Man3 phage against Con A. The results showed that the recovery rate of Man3 phage was 50-fold higher than WT

phage, and increasing elution time gave rise to more phage released from the plate (Fig. 7A, B). Con A type IV had a higher affinity to Man3 compared to Con A VI (Fig. 7C). Overall, I optimized the protocol for the use of panning against Con A with modified library via changing the buffer component and pH for a better interaction between the protein and phage and elongating the elution time for a higher recovered phage titer.

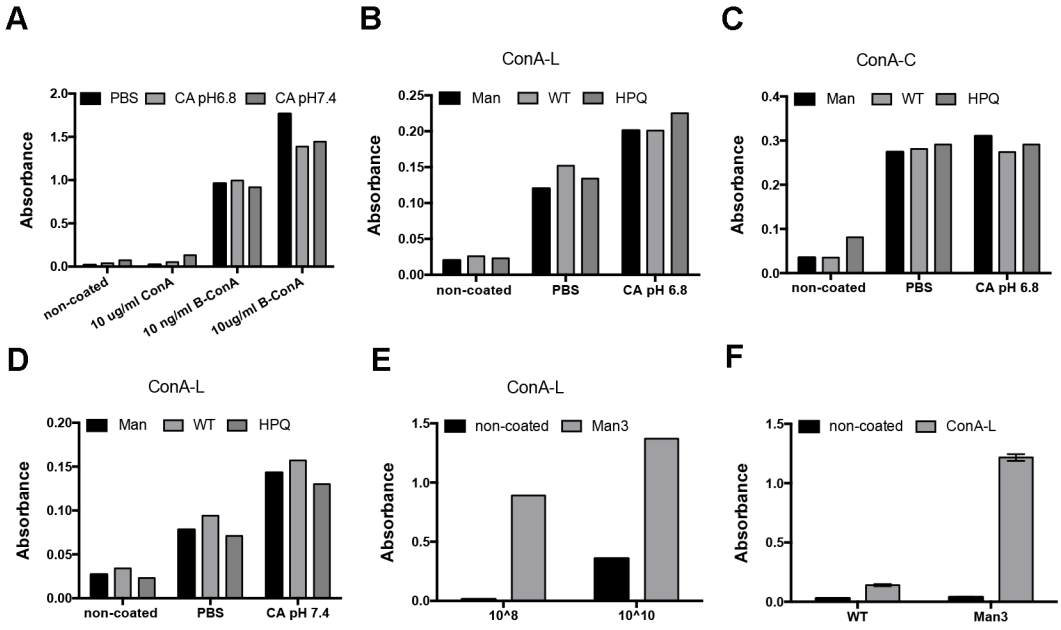

Figure 6. Verification of Con A coating and phage binding. A. Coating of increasing amount of biotinlyated Con A. **B,C,D.** Binding of Man-wyd phage to Con A-L and Con A-C in different binding solution. **E,F.** Binding of Man3 phage to Con A-L.

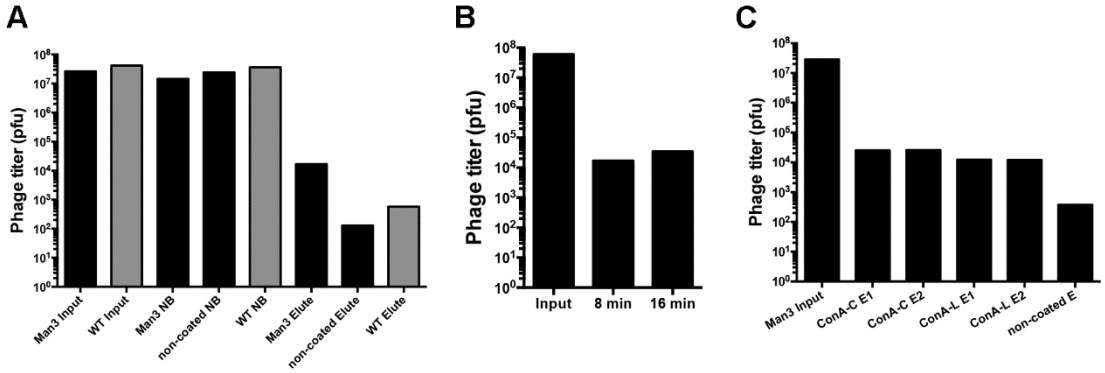

Figure 7. Validation of the protocol with positive control Man3 phage. A. Phage number after each step. The recovery rates were Man3 Elute: 0.0649%, non-coated Elute: 0.0005%, WT Elute: 0.0014%. **B.** Total phage number of the input and output for different elution times. Recovery rate: 8 min: 0.028%, 16 min: 0.057%. **C.** Total phage number of the input and output for the one round selection against Con A-C and Con A-L. Recovery rate: Con A-C E1: 0.0898%, Con A-C E2: 0.0919%, Con A-L E1: 0.0429%, Con A-L E2: 0.0423%， non-coated E: 0.0013%.

2.5. Affinity selection of the mannose-modified library

Next, I panned against Con A using the optimized protocol with the library modified with biselectrophiles (TP30, N=1; TW18, N=2; TW19, N=3) and monoeletrophile (TP163) containing Mannose. The modification of the library was performed and quantified prior to each round of panning. Quantification results revealed a consistent ~80% reduction and ~50 % alkylation of the library for each round of selection. The recovered phage titer of biselectrophiles increased from 10^6 to 10^7 pfu after two rounds of selection and maintained at the same level for the third round. Monoeletrophile modification allowed for a higher output number ranging from 10^7 to 10^8 pfu compared to the biselectrophiles. Regarding the recovered rate, TP30 only showed a slight increase after the third round, while a moderate increase was found for TW18 and TW19 after the second round and a further significant enhance of the recovery rate was only observed for TW19. Although TP163 exhibited a higher recovery rate than the other electrophiles, no enrichment of the binder was found after each round of selection. Panning with non-modified library resulted in a significant lower recovered phage titer and recovery rate than the mannose-modified library (Fig. 8). 20 clones of each modification were randomly picked and amplified for sequencing (Table 3). The affinities of these candidates were then verified by Elisa. Compared to the corresponding non-modified clones, most of the

mannose-modified phage showed higher affinity to Con A in varying degrees (Fig. 9). Top candidates of each group were selected for further analysis based on two criteria: 1) binding of modified phage to Con A has to be higher than plate average (AVE) + standard deviation (STD); 2) fold changes in binding upon modification (column 2) has to be higher than AVE + STD. Totally 9 clones satisfied with these criteria and their binding will be verified by binding assay (Table 3).

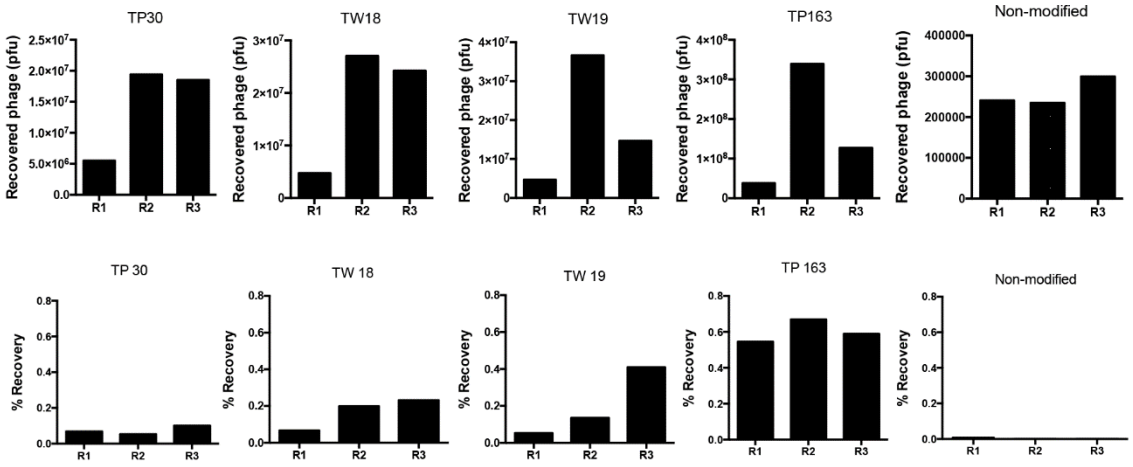

Figure 8. Number of recovered phage and recovery rate of panning with Mannose-modified and non-modified library.

Table 3. Sequences of the peptide hits for Con A from modified library.

No.	TW18	No.	TW19	No.	TP30	No.	TP163
2	FNSWASV	3	STFASPF	1	DSRLLNG	2	AFHWQSA
3	STLHQKL	4	SKVSWYQ	3	MTPNPTT	3	STFASPF
5	HLNNRNF	5	GLRWGNQ	4	NLLVSSQ	4	MKESIRG
6	GKTNVAM	6	FSLTNNT	6	NQVKTKI	5	SSNTVPA
7	PFDGPKV	8	RSEALPK	7	NTTTTLS	8	TDKASSS
8	PRWPNTE	11	KSQGWNW	8	YTTFTRT	9	TIPWNPS
10	SRSMDST	12	KTVDMQV	9	ERLLASK	11	VRSAQAL
11	TNDRNFF	13	SPKSNSV	12	SSSAPRI	13	NNKLPPK
13	YTGHQMM	14	NTWHGSN	14	QLPERGV	16	PLQGRLI
14	GAMQLTS	16	ELNSLQS	15	TMWNTSK	17	NGWPGAS
15	SPHLNTN	17	MTYEYNR	16	PYTTAYA	18	SNQKTMT
16	EGVYFSQ	18	FGTPYTS	17	YIGPSGL	19	LRSFANY
18	DQTYMST	19	REPTYNQ	19	QENLDNF	20	EQANYRI
19	PYEESKL	20	GGASTTA				
20	RVSPSTW						
Selected Top hits							
2	FNSWASV	4	SKVSWYQ	17	YIGPSGL	2	AFHWQSA
8	PRWPNTE	18	FGTPYTS	19	QENLDNF	20	EQANYRI
10	SRSMDST						

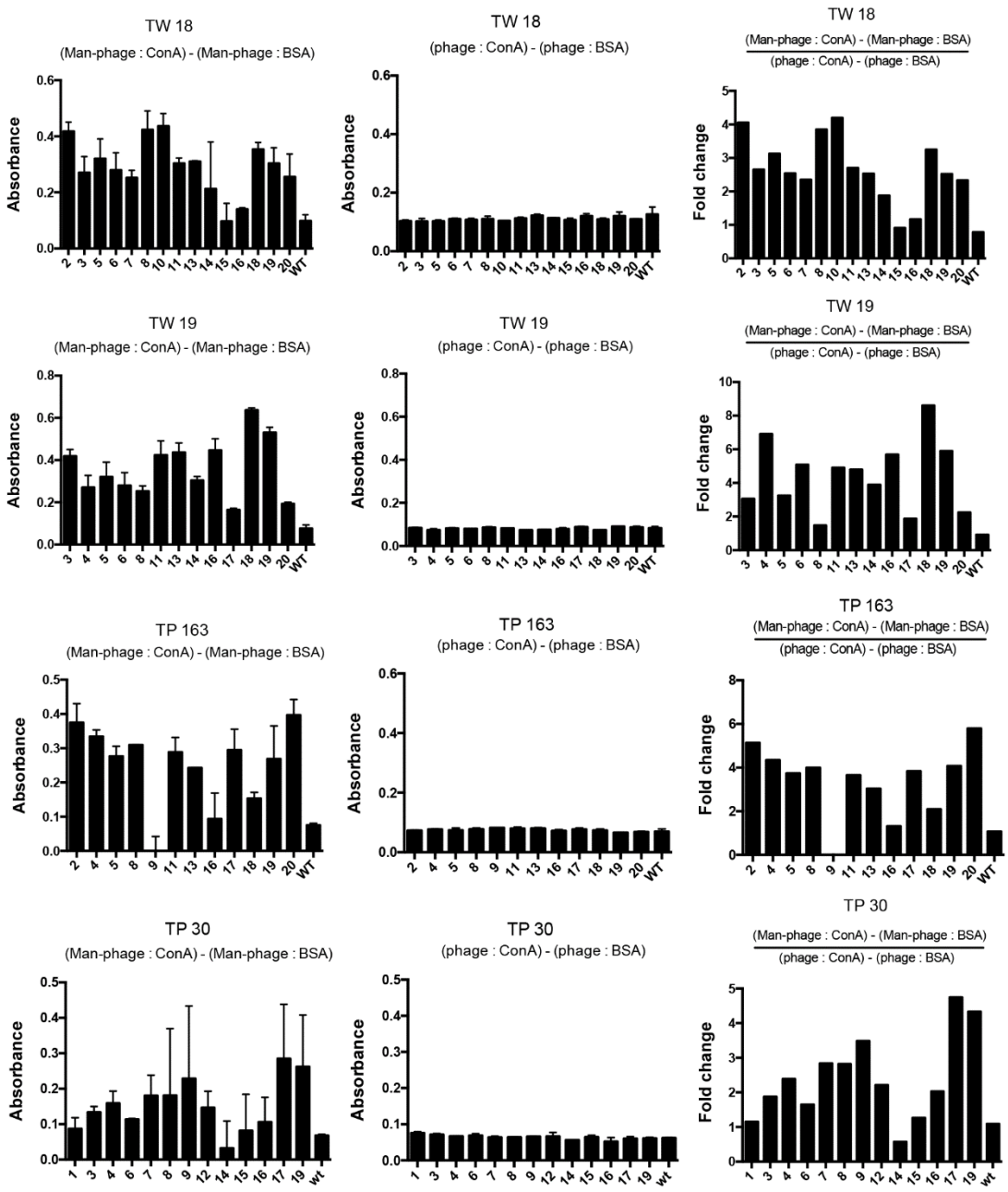

Figure 9. Binding of modified and corresponding non-modified phage to Con A.

Next, competition assay was performed to confirm the binding between the selected peptides and ConA. Various concentrations of mannose (0, 200 nM, 20 uM, 2 mM) were used to co-incubate with phages containing the candidate peptides. Man3 was used as

a positive control. Phage Elisa results indicated that candidate phages but not Man3 were competed out of Con A when the mannose was above 2 μM (Fig. 10A). Significantly reduced binding was observed when the concentration was increased to 5 μM. However, the Man3 was less sensitive to mannose (Fig. 10B). Decreasing bindings of selected phages were detected again when it was co-treated with increasing amount of mannose (Fig.10C). Overall, the results confirmed the binding between Con A and phage peptides selected by phage display. The published positive control Man3 has much higher binding affinity to Con A compared to our peptides. Next, the 9 candidate peptides will be synthesized, and the binding will be confirmed by binding assay.

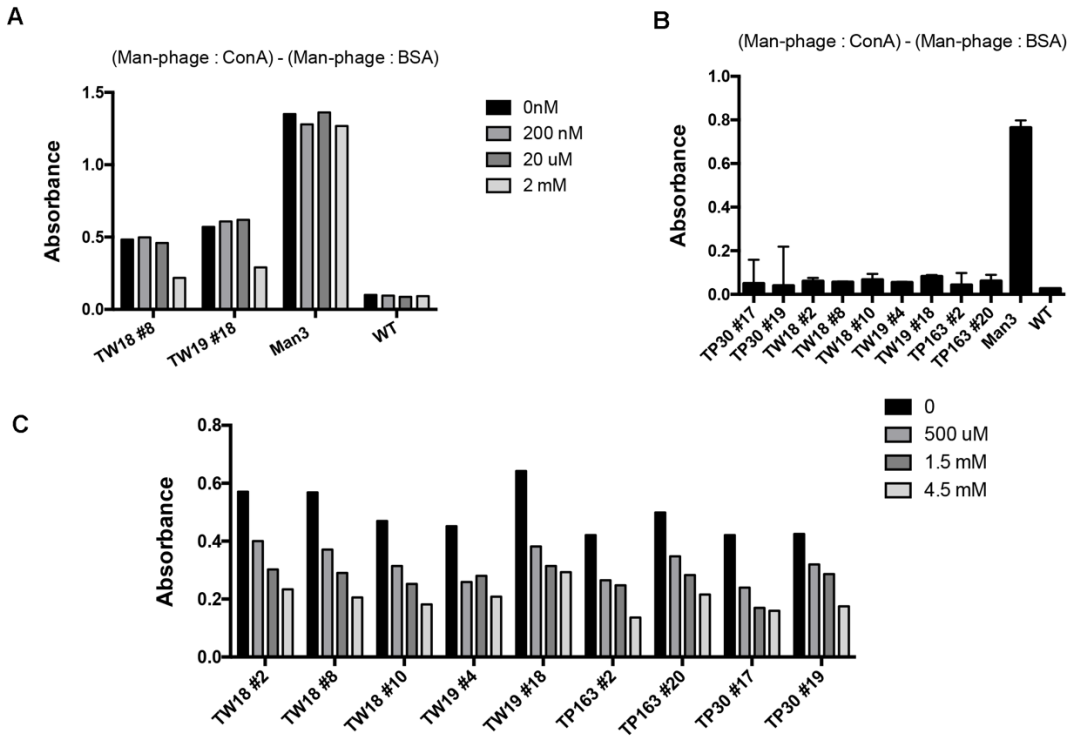

Figure 10. Competition assay of selected phage peptides against Con A. A. Determination of Con A concentration that can compete with the phages. **B.** completely inhibited binding between phages and Con A. **C.** Dose-response of Con A binding.

2.6. Biopanning against siglect-9

I attempted to identify peptides that could bind to siglec-9 by performing biopanning against siglec-9 with non-modified phage library. Two coating and washing methods were used. In method 1, siglec-9 was coated in $NaHCO_3$ solution and 0.1% TBST was used to wash unbound phages in all three rounds of panning. While in method 2, TBS was used to coat siglec-9 and 0.5% TBST was used for the washing step in round 2 and 3. The results showed that the recovery rate, defined as eluted phage number divided by Input phage number, was increased from round 1 to round 2, but then dropped in round 3 for both of the methods, indicating no specific bound phages were identified during biopanning (Fig. 2). In the future, one can try to elute with specific sialic acid solution, and use phage library modified with sialic acid to pan against signec-9.

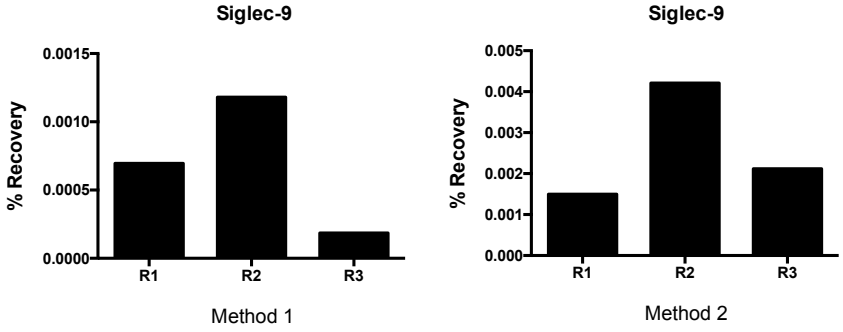

Figure 2. Recovery rate of panning with non-modified library against siglec-9.

3. Methods

3.1. E.coli culture

ER2738 was streaked on the LB agar plate containing 20 μg/ml tetracycline and incubated overnight at 37°C. For titering, one single colony was picked and incubated in 5 ml LB media containing tetracycline with shaking for 4 h at 37°C. For amplification, inoculate 20 ml of LB media with a single colony for 40 min at 37°C before adding the eluted phages. For sequencing and small-scale amplification, a 5 ml culture with a single colony was incubated overnight at 37°C with shaking, and the culture was diluted 100-fold before using.

3.2. Selection of non-modified library against streptavidin

One well of 96 well high-binding plate was coated with streptavidin (100 mg/ml, 100 μL) in $NaHCO_3$ solution overnight at 4°C. Next day, the well was washed once with 200 μL of $NaHCO_3$ solution and then blocked in 200 μL blocking buffer containing 0.5 % BSA and 0.1 μg/ml streptavidin in $NaHCO_3$ solution for 1 h at RT. After washing three times with the washing solution of 0.1 % (v/v) Tween-20 in TBS, 1 μL of Ph.D.-C7C phage library (10^{10} pfu) was mixed with 100 μL of washing buffer and added to the coated well for the 1 h - incubation at RT. Then the well was washed ten times with washing buffer followed by the elution with 0.1 mM biotin in TBS for 1 h at RT. The bounded phages were eluted and amplified as the input for the next round of panning after determination of the phage titer. The percentage of tween-20 was increased to 0.5 % in the washing buffer for the round 2 and 3 panning.

3.3. Amplification of eluted phage

The eluted phages were amplified in 20 ml of ER2738 culture for 4.5 h at 37°C. The culture was centrifuged at 12000 g for 10 min twice at 4°C to remove the E.coli. 80 % of the supernatant was transferred to another tube and incubated with 1/6 volume of NaCl/PEG solution overnight at 4°C to precipitate the phage. The precipitated phages were pelleted down after centrifuging at 12000 g for 15 min at 4°C, and then resuspended in 1 ml TBS. To remove the residual E.coli, the phage solution was centrifuged again at 14000 rpm for 5 min at 4°C, followed by the precipitation with NaCl/PEG solution on ice for 1 h. The precipitated phage was centrifuged down at 14000 rpm for 10 min at 4°C and resuspended in 100 µL TBS.

3.4. Titering

10 µL diluted phage was mixed with 190 µL bacterial culture followed by the addition of 3 ml of melt top agar. The mixture was poured onto the LB/Xgal/IPTG agar plate and incubated overnight at 37°C incubator.

3.5. Chemical modification of phage library

50 µL Immobilized TCEP (iTCEP) Disulfide Reducing Gel was centrifuged down at 1000 g for 1 min to remove the supernatant, followed by washing with 500 µL TBS (pH 8.5). 5 µL of phage library was mixed with 145 µL TBS and then added to the prepared iTCEP beads to allow the incubation for 48 h at 4C in the presence of mini stir bar. After reduction, Mannose (1 µL of 200 mM TP30, TW18, TW19; 2 µL of 200 mM TP163) was directed added into the reaction solution and continue to incubate for 2 h at RT. Then, I separate the beads at 1000 g for 1 min. The supernatant was transferred a new

microtube and the modified phage was precipitated with NaCl/PEG solution for 2 h on ice. The precipitated phage was pelleted at 14000 rpm for 10 min and resuspended in 100 µL CA buffer. To purify the modified phages, the phage solution was loaded into the ultra centrifuge filter and the total volume was filled up to 500 µL with CA buffer followed by centrifugation at 14000 g for 15 min. After 3 repeats, the remaining solution was collect by centrifuging at 7000 g for 2.5 min and additional CAT buffer was added to make the final volume at 100 µL.

3.6. Quantification of chemical modification

The phage library was reduced as described above. To quantify the reduction, 1 µL of 200 mM biotin-PEG2-iodoacetamide (BIA) was added to allow the incubation for 30 min at RT. In a separate reaction tube, mannose was added after reduction followed by the addition of BIA for another 30-min incubation. After precipitation, the modified phage library was diluted 10^5 in PBS to a finally volume of 300 µL, among which 200 µL was incubated with 50 µL streptavidin beads in the rotator. The beads were got rid of the storage buffer and washed with 500 µL PBS before use. The titer of four samples, titer before $_{iTCEP+BIA}$, titer after $_{iTCEP+BIA}$, titer before $_{iTCEP+mannose+BIA}$, titer after $i_{TCEP+mannose+BIA}$, were determined and the modification rate was calculated as ((titer before $_{iTCEP+BIA}$-titer after $_{iTCEP+BIA}$)/ titer before $_{iTCEP+BIA}$)-((titer before $_{iTCEP+mannose+BIA}$-titer after $_{iTCEP+mannose+BIA}$)/ titer before $_{iTCEP+mannose+BIA}$).

3.7. Selection of modified library against Con A

The procedure was similar as descried above. Briefly, one well of 96 well high-binding plate was coated with Con A (100 ug/ml, 100 µL) in CA buffer (10 mM HEPES, 150 mM NaCl, 1.0 mM $CaCl_2$, 1.0 $MnCl_2$, pH 7.4) overnight at 4°C. After washing and blocking

(0.5 % BSA in CA buffer), the modified library was incubated with coated ConA in CAT buffer (0.1 % Tween-20 in CA buffer) for 1 h at RT. Then the well was washed five times with CAT buffer. The bounded phages were eluted out with 100 µL glycine elution buffer (0.2 M glycine-HCl, pH 2.2, 1 mg/ml BSA) and immediately mixed with 15 µL 1 M Tris-HCl (pH 9.1) solution. The eluted phages were amplified and modified for the next round of panning. After phage-protein incubation, the well was washed ten times instead of 5 times for the round 2 and 3 panning.

3.8. Sequencing

20 phage colonies were picked randomly from the plate and incubated in 1 ml LB media for 4.5 h at 37°C with shaking. The culture was centrifuged at 14000 rpm for 10 min twice at 4°C to remove the E.coli. 500 µL of the supernatant was transferred to another tube and incubated with 200 µL of NaCl/PEG solution for 20 min at RT to precipitate the phage. The precipitated phages were pelleted after centrifuging at 14000 rpm for 10 min at 4°C, followed by incubation with 100 µL of Iodide Buffer and 250 µL ethanol for 20 min at RT. The DNA was then pelleted after spinning down at 14,000 rpm for 10 minutes at 4°C. After 2 times washes with cold 70 % ethanol, the DNA pellet was resuspended in 30 µL TE buffer. The solution for sequencing contained 2 µL of sample, 0.5 µL of 10 µM primer and 7.5 µL of water.

3.9. Phage Elisa

96-well high binding plate was coated with 100 µL 10 µg/ml ConA overnight at 4°C. After washing once with 200 µL CA buffer, the well was blocked with blocking buffer (2 % BSA in CA buffer) for 1 h at RT, then incubated with modified phage (5x10^8 pfu/ml) in CAT buffer for 1 h at RT followed by 3 times washes with CAT buffer. Then, anti-M13

antibody solution (1:1000) was added to the well and incubated for 1 h at RT. The well was washed three times with CAT buffer followed by the incubation with secondary anti-Rabbit-HRP (1:2000) for 1 h at RT. The well was then washed again with CAT buffer for three times. 100uL TMB substrates (1:1 mixture of A and B substrate) were added to the wells and incubated for 10 min. 50 µL of 2N H_2SO_4 was added to stop the reaction.

3.10. Selection of non-modified library against siglec-9

One well of 96 well high-binding plate was coated with siglec-9 (10 mg/ml, 100 µL) in $NaHCO_3$ solution (pH 8.6), or TBS (pH 7.4), overnight at 4°C. Next day, the well was washed once with 200 µL of $NaHCO_3$ solution or TBS and then blocked in 200 µL blocking buffer containing 0.5 % BSA in $NaHCO_3$ solution or TBS for 1 h at RT. After washing three times with the washing solution of 0.1 % (v/v) Tween-20 in TBS, 1 µL of Ph.D.-C7C phage library (10^{10} pfu) was mixed with 100 µL of washing buffer and added to the coated well for the 1 h - incubation at RT. Then the well was washed ten times with washing buffer. The bounded phages were eluted out with 100 µL glycine elution buffer (0.2 M glycine-HCl, pH 2.2, 1 mg/ml BSA) and immediately mixed with 15 µL 1 M Tris-HCl (pH 9.1) solution. The bounded phages were eluted and amplified as the input for the next round of panning after determination of the phage titer. The percentage of tween-20 was increased to 0.5 % in the washing buffer for the round 2 and 3 panning when use TBS for coating. For tittering, 10 µL diluted phage was mixed with 190 µL bacterial culture followed by the addition of 3 ml of melt top agar. The mixture was poured onto the LB/Xgal/IPTG agar plate and incubated overnight at 37°C incubator.

3.11. Phage Elisa/Competition assay

96-well high binding plate was coated with 100 µL 10 µg/ml ConA overnight at 4°C. After washing once with 200 µL CA buffer, the well was blocked with blocking buffer (2 % BSA in CA buffer) for 1 h at RT, then incubated with modified phage (5x10^8 pfu/ml) in CAT buffer for 1 h at RT followed by 3 times washes with CAT buffer. Various concentrations of mannose were co-incubated to compete with the modified phage. Then, anti-M13 antibody solution (1:1000) was added to the well and incubated for 1 h at RT. The well was washed three times with CAT buffer followed by the incubation with secondary anti-Rabbit-HRP (1:2000) for 1 h at RT. The well was then washed again with CAT buffer for three times. 100uL TMB substrates (1:1 mixture of A and B substrate) were added to the wells and incubated for 10 min. 50 µL of 2N H2SO4 was added to stop the reaction.

4. References

1 Smith, G. P. Filamentous fusion phage: novel expression vectors that display cloned antigens on the virion surface. *Science* **228**, 1315-1317 (1985). https://doi.org/10.1126/science.4001944

2 Henry, T. J. & Pratt, D. The proteins of bacteriophage M13. *Proceedings of the National Academy of Sciences of the United States of America* **62**, 800-807 (1969). https://doi.org/10.1073/pnas.62.3.800

3 Russel, M. & Model, P. Genetic analysis of the filamentous bacteriophage packaging signal and of the proteins that interact with it. *Journal of virology* **63**, 3284-3295 (1989).

4 Deyle, K., Kong, X. D. & Heinis, C. Phage Selection of Cyclic Peptides for Application in Research and Drug Development. *Accounts of chemical research* **50**, 1866-1874 (2017). https://doi.org/10.1021/acs.accounts.7b00184

5 Ven Chang, I., Tsutsumi, H. & Mihara, H. Screening for concanavalin A binders from a mannose-modified alpha-helix peptide phage library. *Molecular bioSystems* **13**, 2222-2225 (2017). https://doi.org/10.1039/c7mb00495h

6 Ng, S. *et al.* Genetically encoded fragment-based discovery of glycopeptide ligands for carbohydrate-binding proteins. *Journal of the American Chemical Society* **137**, 5248-5251 (2015). https://doi.org/10.1021/ja511237n

7 Green, N. M. Avidin. *Advances in protein chemistry* **29**, 85-133 (1975). https://doi.org/10.1016/s0065-3233(08)60411-8

8 Weber, P. C., Pantoliano, M. W. & Thompson, L. D. Crystal structure and ligand-binding studies of a screened peptide complexed with streptavidin. *Biochemistry* **31**, 9350-9354 (1992). https://doi.org/10.1021/bi00154a004

9 Katz, B. A. & Cass, R. T. In crystals of complexes of streptavidin with peptide ligands containing the HPQ sequence the pKa of the peptide histidine is less than 3.0. *The Journal of biological chemistry* **272**, 13220-13228 (1997). https://doi.org/10.1074/jbc.272.20.13220

10 Jafari, M. R. *et al.* Discovery of light-responsive ligands through screening of a light-responsive genetically encoded library. *ACS chemical biology* **9**, 443-450 (2014). https://doi.org/10.1021/cb4006722

11 Ng, S., Jafari, M. R., Matochko, W. L. & Derda, R. Quantitative synthesis of genetically encoded glycopeptide libraries displayed on M13 phage. *ACS chemical biology* **7**, 1482-1487 (2012). https://doi.org/10.1021/cb300187t

Appendix 2: Development of assays for the screening of 3CLp inhibitors and degraders

1. Introduction

Coronavirus disease 2019 (COVID-19) was caused by severe acute respiratory syndrome coronavirus 2 (SARS-CoV-2). SARS-CoV-2 contains a single-stranded positive-sense RNA (+ssRNA) encodes four structural proteins, at least six or seven accessory proteins and sixteen non-structural proteins (NSPs), which are responsible for viral genome replication and transcription[1]. NSPs were encoded by a large open reading frame 1 (ORF1) which was then translated into a polypeptide. This polypeptide was cleaved at various sites to produce different NSPs during proteolytic process which is mediated by 3-chymotrypsin-like protease (3CLp). It has been reported that SARS-CoV-2 3CLp shares over 70% sequence identity with several of its closest homologs and is 96% identical to SARS-CoV-1. The high degree of similarity and its critical role in viral replication make 3CLp an ideal target for COVID treatment. In this project, we aim to develop 3CLp-targeting PROTACs to degrade 3CLp and impede the viral replication process, with the ultimate goal of contributing to COVID-19 therapeutic strategies.

2. Results and Conclusion

2.1. Optimization on 293T and A549 cell transient transfection

I tried four different transfection methods, varying cell densities, the ratios of transfection reagent to plasmid, and components of the media for transfection in A549 cells. The transfection rate for A549 cells reached ~40% after optimization. In comparison, 293T cells demonstrated a higher transfection rate of around 90% (Fig. 1). During transfection, A549 cells should be maintained in serum-free media to enhance the

transfection efficiency, while 293T cells should be cultured in media without antibiotics to minimize the toxicity of transfection reagent.

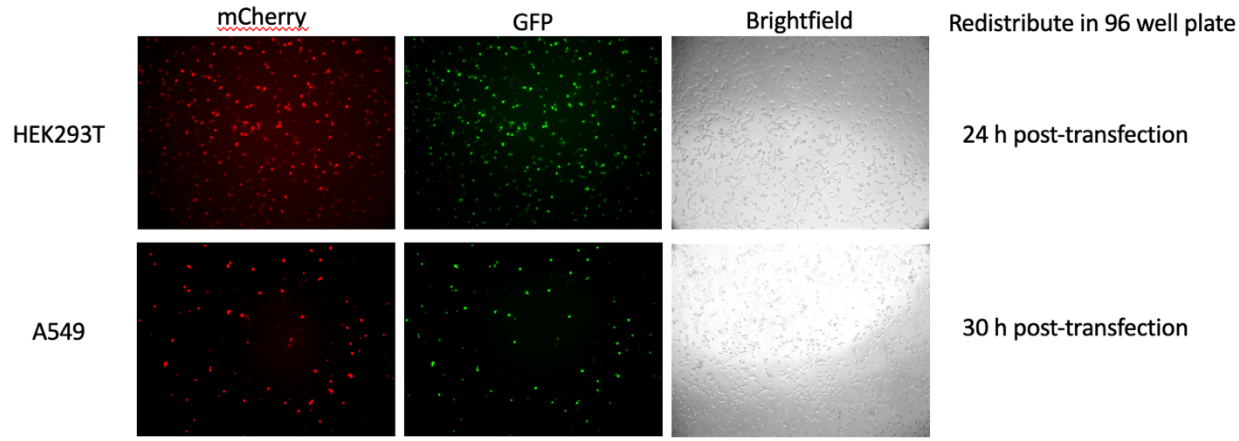

Figure 1. Transient transfection in 293T and A549 cells.

2.2. Generation of stable cell line

To generate 293t cells that stably express mCherry-3CLp, hygromycin B was used as the selection marker. The optimal concentration of hygromycin B that could kill most of the non-transfected cells was first determined by culturing cells in media containing 50, 100, 200, 250, 300, 400 μg/ml hygromycin B for 7 days. Concentrations above 200 μg/ml could kill 99% of 293t cells after 2-3 days. Interestingly, A549 cells were not killed by hygromycin B even at high concentration. After determining the desired concentration, 293t cells were transfected with the plasmid containing mCherry-3CLp following the transient transfection protocol in a 6 well plate. Cells were seeded in 3 wells corresponding to three hygromycin B concentrations (200, 250, 300 μg/ml) that would be used for selection. Transfected cells were replaced in a 60 mm petri dish 24 h post transfection. After 48 h post transfection, cells were maintained in the media

containing hygromycin B and the media was changed every three days. Most cells were killed after 2-3 days and the clones was observed after 2-3 weeks. The clones were collected to form polyclonal culture, which was frozen for storage after expansion and passage. Part of the culture was used for isolating the single clone by two diluting methods. 1) The cells were diluted into 0.8 cells per well and distributed into 4 96-well plates. 2) 2000 cells were seeded in the first well of 96 well plate and then diluted at 1 to 1 ratio in a row and column. The rest of the wells was diluted half of the previous well. The clone was detected after 7 days of culture. 16 clones were selected and transferred into 24 well plate. After removing the clones that didn't grow normally, 8 clones were finally selected. They were expanded into 6 well plate and the maintained in 60 mm petri dish. All the clones were verified by checking the 3CLp expression using western blot (Fig. 2).

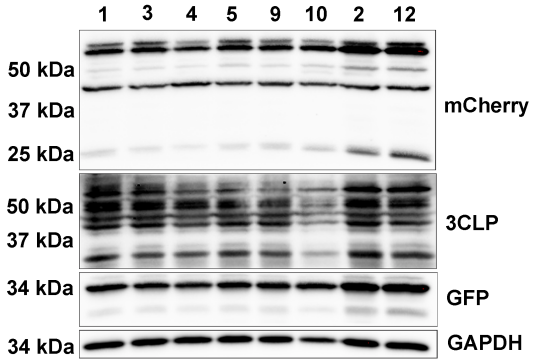

Figure 2. Verification of 3CLp expression in 8 clones.

2.3. 3CLp degradation

The degradation of 3CLp was first evaluated using transiently transfected 293t cell line. Totally 36 compounds were synthesized by Dr. Le Guo and I tested the degradation of

3CLP induced by these compounds at 1 and 10 μM. After 16 h of treatment, fluorescent signal was acquired to evaluate the degradation efficiency. The level of 3CLp was indicated by mCherry signal and GFP was used as a control for normalization. The results were presented as mCherry/GFP after being normalized to DMSO group. Unfortunately, no obvious degradation was observed for this batch of degraders (Fig. 3).

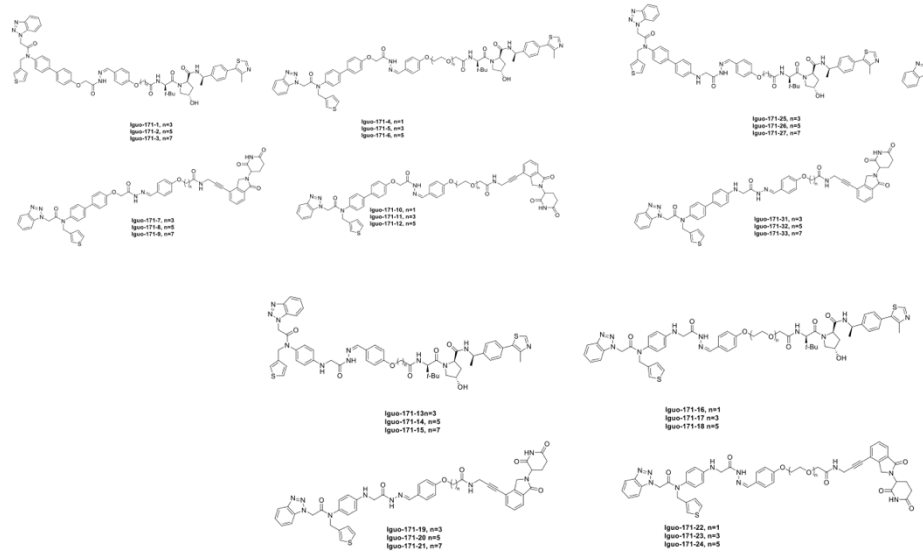

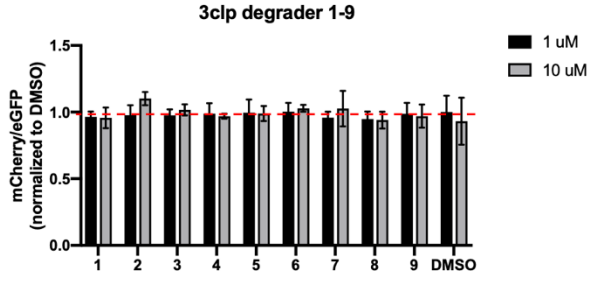

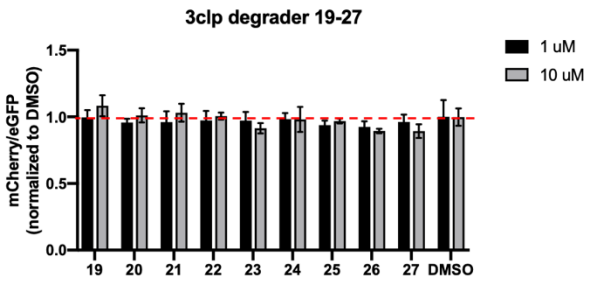

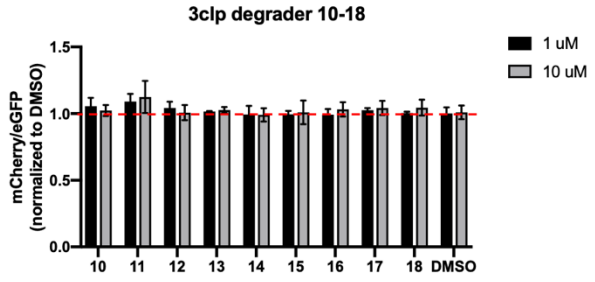

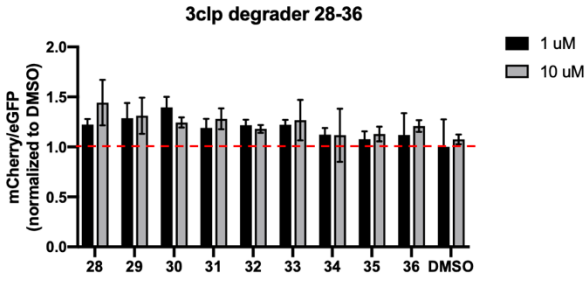

Figure 3. No obvious degradation of 1st batch of 3CLp degraders in transiently transfected 293T cells. Note: All the compounds were prepared by Dr. Le Guo.

Next, I tested the second batch of degraders synthesized by Dr. Le Guo in the established stable cell line. Compounds were tested at two different concentrations for a short and long treatment. Minimal degradation (~10%) was observed for some of the compounds. To verify the degradation, compound 3, 4, 8, 9,14, 16, 19, 21 were selected to evaluate the degradation efficiency by western blot. The results indicated that no significant degradation occurred in a 6 h treatment. I elongated the treatment time and tested two different cell seeding densities. However, those changes didn't enhance the degradation of 3CLp. Overall, no potential degrader was identified in the first two batches of degraders, likely due to the low binding affinity of the degraders to 3CLp (Fig.4,5).

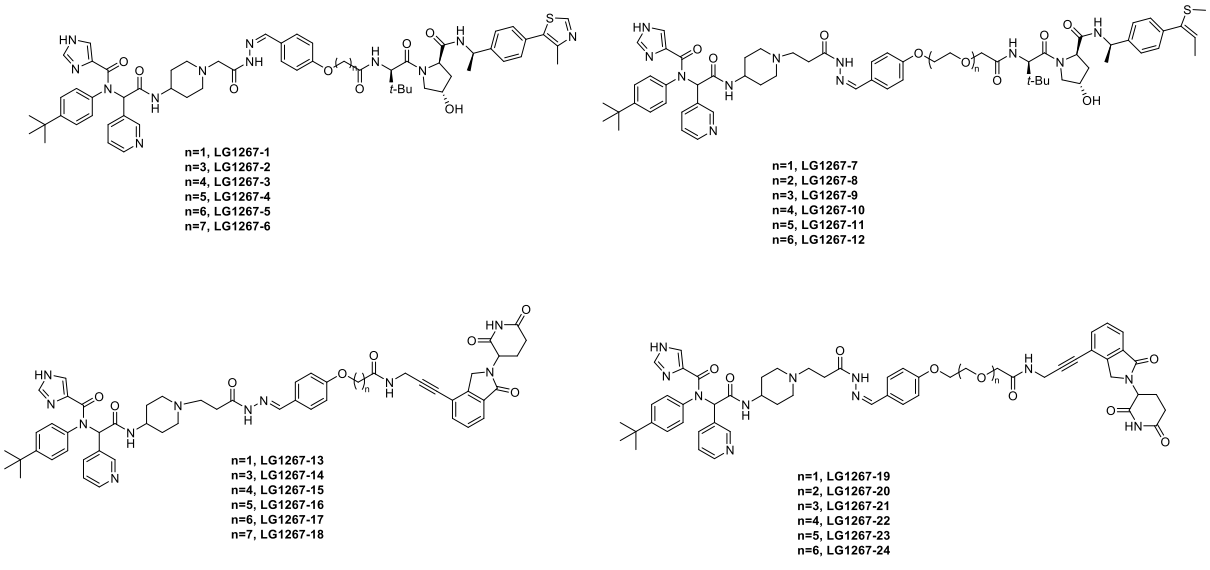

Figure 4. 2nd batch of 3CLp degraders. Note: All the compounds were prepared by Dr. Le Guo.

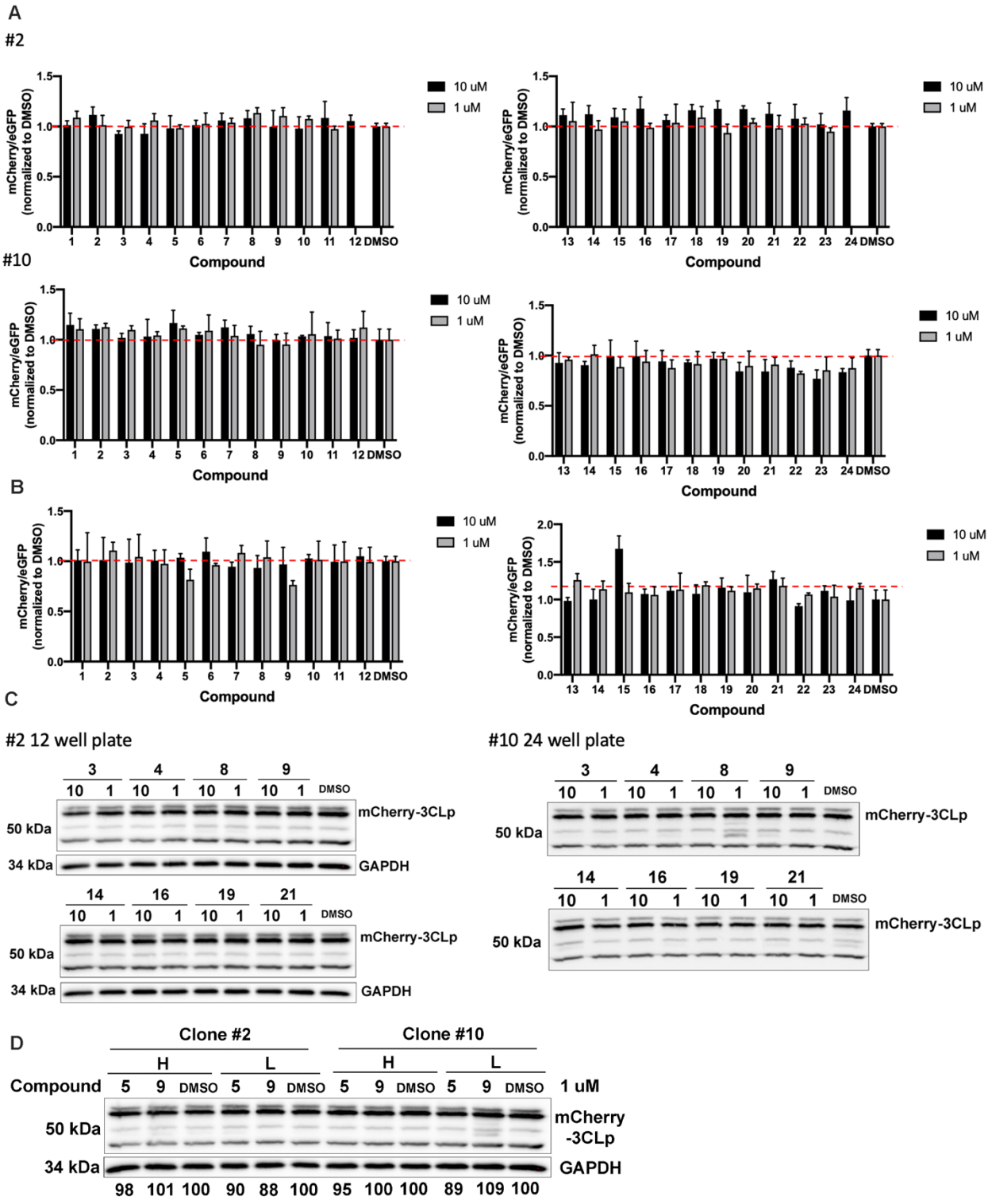

Figure 5. No obvious degradation of 2nd batch of 3CLp degraders in stably transfected 293T cells. A. First screening in clone 2 and 10 of a 6 h treatment. **B.** Second screening in clone 2 of a 16 h treatment. **C.** Western blot of selected degraders

of a 6 h treatment. **D.** Western blot of selected degraders of a 16 h treatment. H: 200,000 cells per well. L: 100,000 cells per well in a 24 well plate.

2.4. 3CLp degradation in stable cell line

I then tested the 3rd batch of 3CLp degraders synthesized by Dr. Le Guo in the established stable cell line (Fig. 6A). Compounds were tested at two different concentrations for a short and long treatment. Compound 1-5 showed significant downregulation of mCherry level after normalization when detected by plate reader (Fig. 6B). However, there was no 3CLp degradation when analyzed by western blot (Fig. 6C).

2.5. Development of Flip-GFP assay for high-throughput screening

A GFP-based protease reporter, Flip-GFP, was used to reflect 3CLp activity. Basically, GFP10-11 was flipped so that it cannot bind to GFP 1-9 when 3CLp is inactive, and thus no fluorescence is detected. Only in the presence of 3CLp, the GFP11 can flip back which results in the bright fluorescence. To establish the platform, I co-transfected 293t cells with plasmids expressing Flip-GFP-mCherry and wt 3CLp. I adjusted different parameters, including cell number, total plasmid amount, 3CLp/Flip-GFP ratio, transfection time and inhibitor treatment timepoint to obtain the optimal conditions for this assay. The plasmid encoding 3CLp from Sino Biological was initially used. However, the GFP signal is weak after 48 h of transfection, and background is high even after optimization (data not shown). Then I switched the plasmid to the one from Addgene, and the GFP signal was significantly increased. Three reported 3CLp inhibitors, Ethacridine lactate, X77, Boceprevir, were tested to validate this assay. The optimal conditions were determined as the following: 1) the ratio between 3CLp and Flip-GFP is 1 to 1; and 2) the inhibitors were treated 6 h post transfection. The fluorescence readout

from plate reader showed that the treatment of each inhibitor was able to decrease GFP signal in a dose-dependent manner after 24 h of transfection. The results were also confirmed by the fluorescent microscope imaging (Fig. 7).

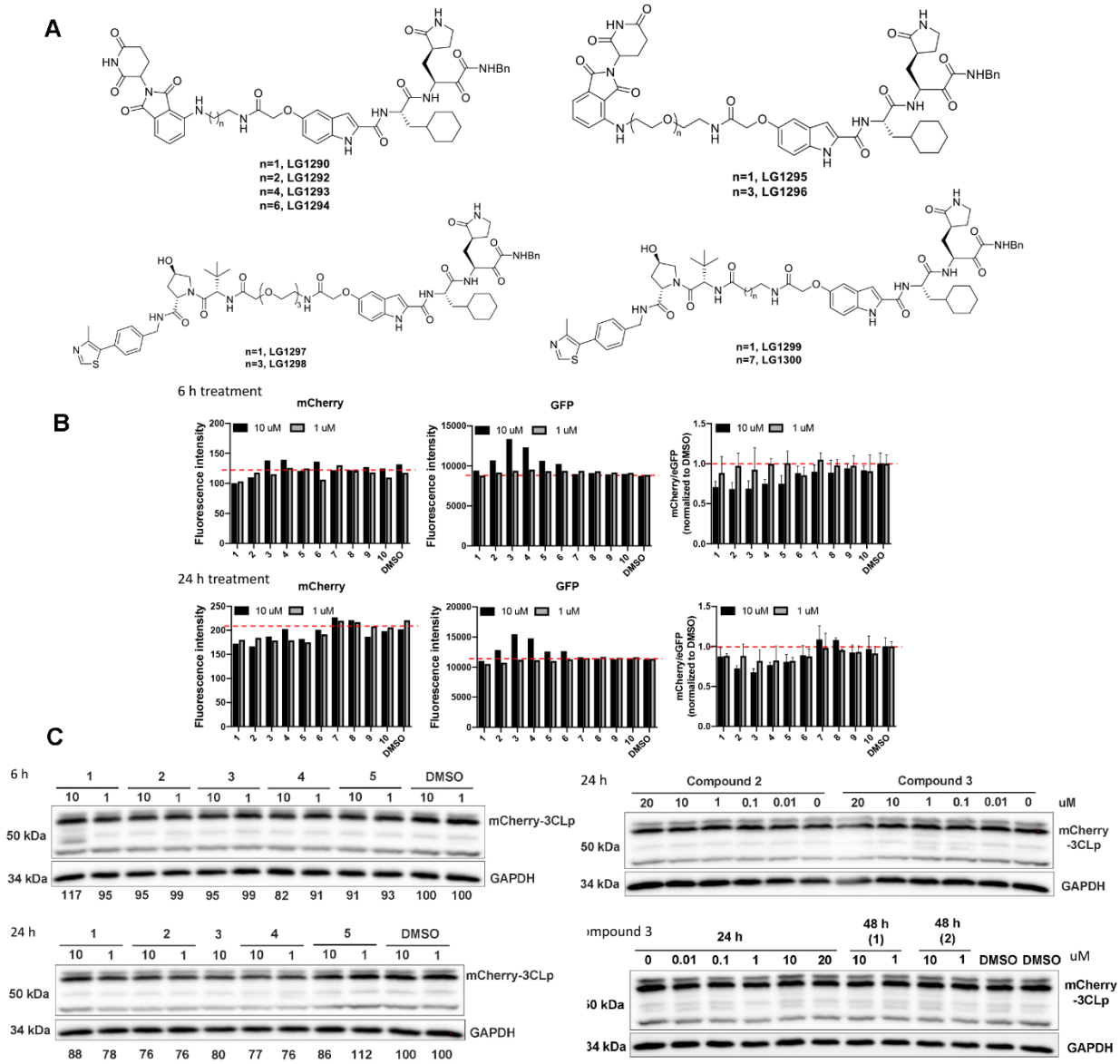

Figure 6. No obvious degradation of 3rd batch of 3CLp degraders in stably transfected 293T cells. A. 3CLp degraders synthesized by Dr. Le Guo. **B.** First round screening in clone 2 for a 6 or 24 h treatment. **C.** Western blot of selected degraders of a 6 or 24 h treatment. **Note:** All the compounds were prepared by Dr. Le Guo.

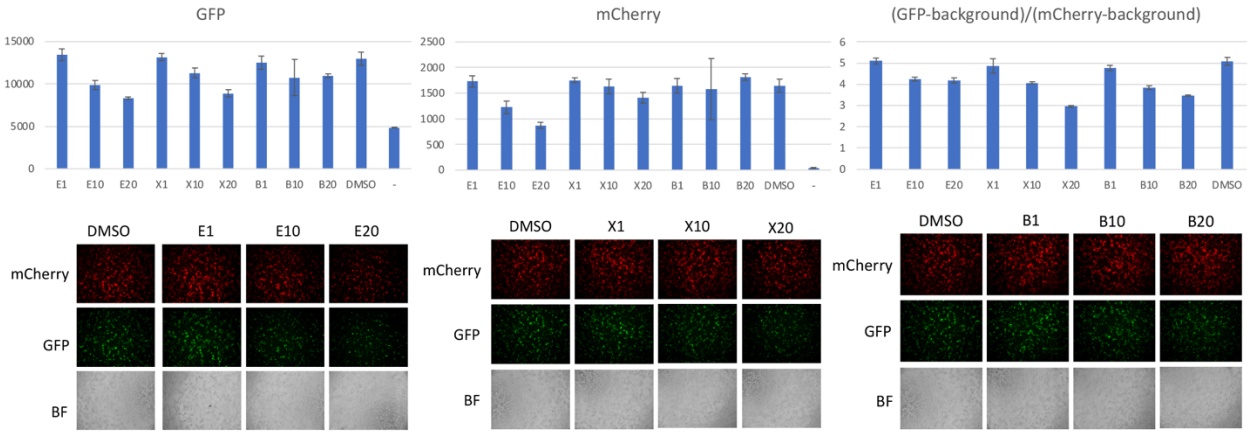

Figure 7. Optimization of Flip-GFP assay.

2.6. 3CLp inhibitor screening

3CLp inhibitors synthesized by Dr. Le Guo and Yu Zhao were screened using Flip-GFP assay under optimized conditions. Co-transfected 293t cells were treated with inhibitors at 10 and 20 μM for 18 h after 6 h of transfection. Nine compounds resulted in over 50% reduction of GFP signal and exhibited stronger effects than the known inhibitors (Fig. 8). I then confirmed the inhibition effects of these 9 compounds by treating cells with a broader range of concentrations. Both fluorescent readings and microscope image indicated that YZ3111 and YZ3141 had the highest enzyme inhibition activity (Fig. 9A). I then tested the effects of the top 4 hits selected from Flip-GFP assay together with another 5 compounds selected from biochemical assay on the cell growth inhibition in both 293t and Vero cells. The results showed that the compounds were less toxic for vero cells compared to 293t cells. LG1270, LG1288, YZ3086 had no obvious cytotoxic effect on vero cells but affected the cell viability of 293t cells at high concentrations.

YZ3111 and YZ3141 had the highest cytotoxicity with IC_{50} around 10 μM in 293t cells and 20 μM in vero cells (Fig. 9B).

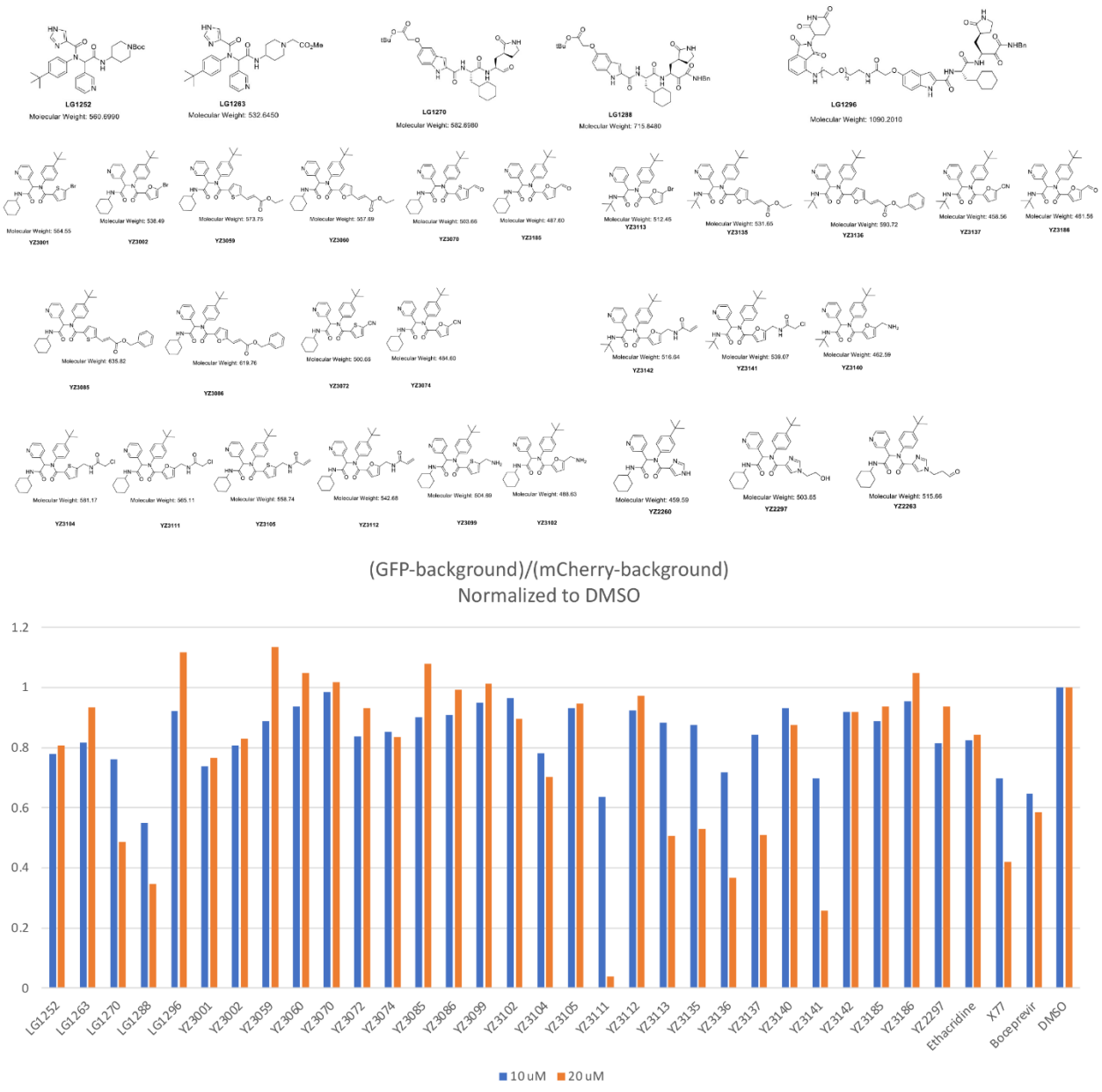

Figure 8. Screening of 3CLp inhibitors. Note: All the compounds were prepared by Dr. Le Guo and Yu Zhao.

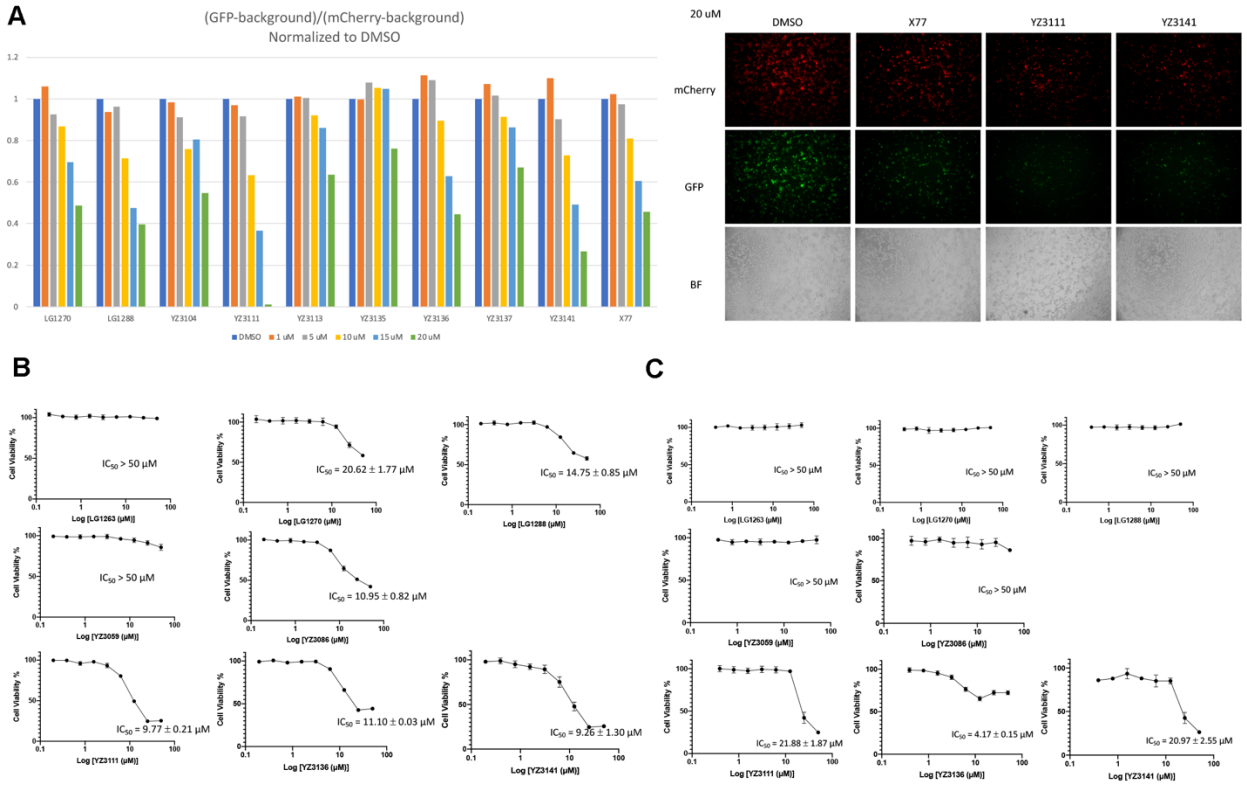

Figure 9. Verification of selected compounds. A. Enzyme inhibition effect analyzed by plate reader and fluorescent imaging. **B, C.** Anti-proliferation assay in 293 cells and vero cells. **Note:** All the compounds were prepared by Dr. Le Guo and Yu Zhao.

2.7. 3CLp degrader screening

Next, I expanded the application of the Flip-GFP assay to 3CLp degrader screening. Two batches of 3CLp degraders were prepared by Dr. Le Guo, which are noncovalent degrader based on X77 and covalent degraders based on covalent inhibitors, respectively. The screening was initially performed under the same conditions as the inhibitors. However, no obvious downregulation of the GFP signal was detected,

suggesting the 3CLp was not degraded. I then treated the cells with the degraders at the same time of transfection instead of 6 h post transfection to allow more time for the degradation. In addition, I detected the GFP signal at different time points. However, no degrader reduced the GFP signal, while the inhibitor positive control worked well. Surprisingly, some of the covalent degraders even increased the GFP signal. Overall, no degrader was successfully identified (Fig. 10).

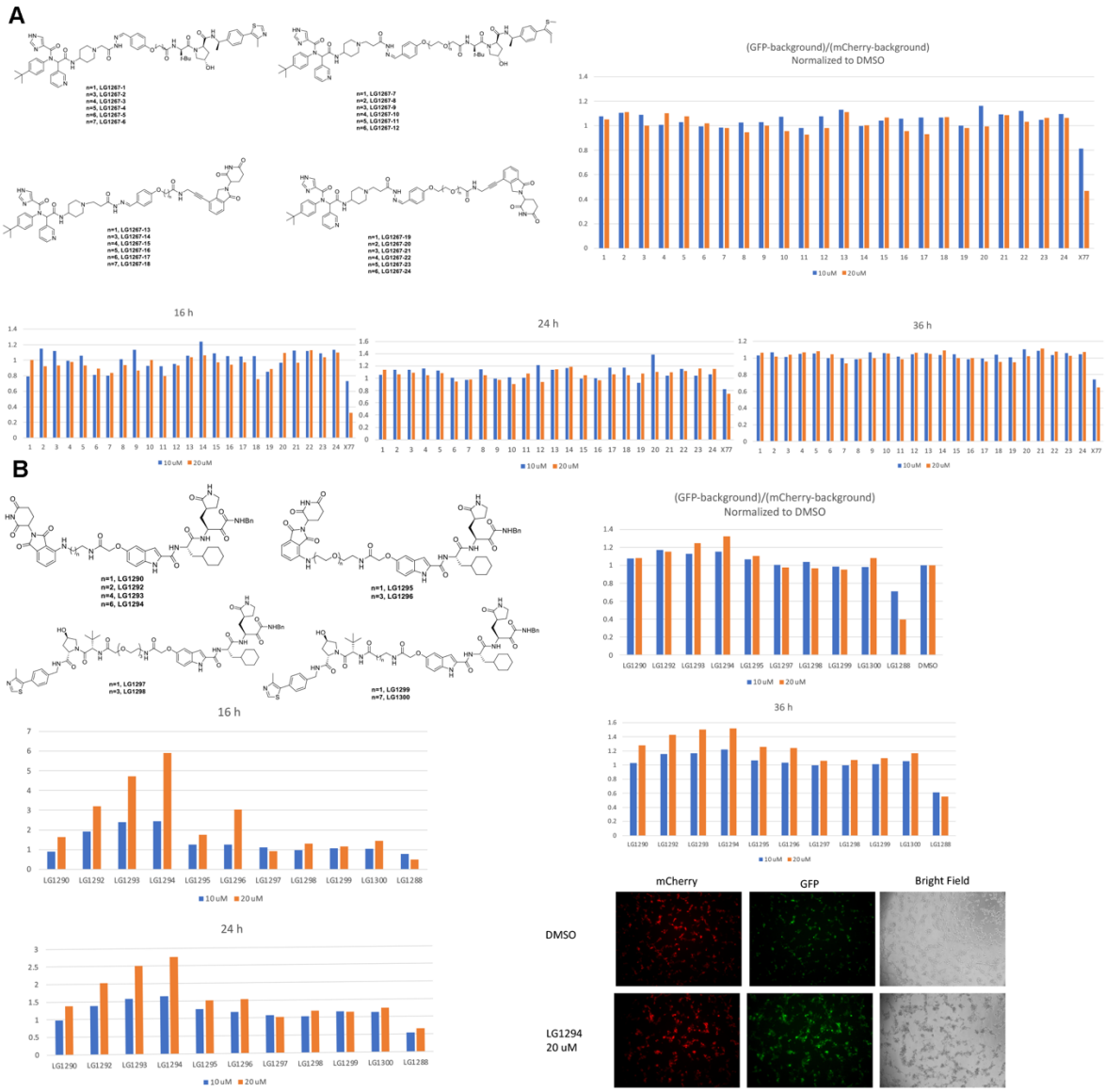

Figure 10. 3CLp degrader screening. A. X77-based non-covalent degrader. **B.** Covalent degrader. **Note:** All the compounds were prepared by Dr. Le Guo.

3. Methods

3.1. Transient transfection

A549 cells are seeded at 20,000 cells per well in a 24-well plate one day before transfection. Next day, cells were treated with 500 ng plasmid and transfected reagent at 1:5.5 ratio after changing the media into serum-free media. After 6h, media containing 20% FBS was added into the well and the cells were cultured for another 42 h treatment. 293T cells were seeded at 100,000 cells per well in a 24-well plate one day before transfection. Cells were maintained in antibiotic-free media during transfection. Next day, cells were treated with 500 ng plasmid and transfected reagent at 1:3.5 ratio and cultured for 48 h.

3.2. 3CLp degradation using transient cell line

293T cells were transfected in 6 well plate at a seeding density of 600,000 cells per well. 2.5 µg of plasmid was treated together with transfection reagent at 1:3.5 ratio. After 24 h of transfection, 20,000 cells were re-distributed into each well of a 96 well plate 6 h before treatment. Cells were then treated with 1 or 10 µM of degraders for 16 h followed by reading mCherry and GFP signal using plate reader.

3.3. 3CLp degradation using stable cell line

293T cells stably expressing mCherry-3CLp were seeded at 15,000 cells per well in a 96 well opaque or black side clear bottom plate and maintained in phenol red free media. 24 compounds were tested using two clones (#2 and 10) for a 6 h treatment at 1

μM and 10 μM. Compounds were also tested in #2 for 16 h. Fluorescent signal of mCherry and GFP were detected by plate reader and observed under microscope. For western blot, cells were seeded at 150,000 cells per well in a 12 well plate or 24 well plate and maintained in 1 ml or 500 μl of the media. Selected compounds were tested for 6 or 16 h treatment in two clones.

3.4. Flip-GFP assay

293t cells were seeded in phenol-red free media at 40,000 cells per well in black wall/clear bottom 96 well plate. Cells were transfected with 80 ng plasmid encoding 3CLp and 80 ng plasmid encoding Flip-GFP by Fugene. Inhibitors or degraders were treated after 6 h of transfection at indicated concentrations. The fluorescent signal in each well was read after 24 h of transfection. GFP intensity was determined at 480 nm excitation/520 nm emission and mCherry intensity was determined at 590 nm excitation/620 nm emission. Wells with cells only were set as blank control. The final readout was calculated as (GFP-blank)/(mCherry-blank).

3.5. Anti-proliferation assay

293t cells were seeded at the density of 5000 cell and vero cells were seeded at the density of 3000 cell per well in a 96-well plate. Next day, cells were treated with compounds at indicated concentrations and incubated in regular media for 3 days. Cell viability was measured using AlamarBlue assay by adding 10x AlamarBlue (0.5 mg/mL) to the well and incubated at 37 °C for 2 h. Fluorescent intensity was then determined at 650 nm excitation/680 nm emission and the percentage of cell viability was generated by normalizing to DMSO treated cells.

4. Reference

1 Alanagreh, L., Alzoughool, F. & Atoum, M. The Human Coronavirus Disease COVID-19: Its Origin, Characteristics, and Insights into Potential Drugs and Its Mechanisms. *Pathogens* **9** (2020). https://doi.org/10.3390/pathogens9050331